OPTIMAL DESIGN OF A HYBRID ELECTROLYSER/FUEL CELL SYSTEM TO PRODUCE POWER AND FRESHWATER FROM SEAWATER

WITS
UNIVERSITY

Melisha Singh

Master of Science in Engineering by Research:

"A dissertation submitted to the Faculty of Engineering and the Built Environment, University of the Witwatersrand, Johannesburg, in the fulfilment of the requirements for the degree of Master of Science in Engineering"

Supervisor: Professor Thokozani Majozi

Co-Supervisors: Doctor Peter Mukoma (CSIR) and Doctor Brian North (CSIR)

January 2022

Declaration

I, Melisha Singh, hereby declare that the dissertation entitled “Optimum Design of a Hybrid Electrolyser/Fuel Cell System to Produce Power and Freshwater from Seawater,” presented for the degree of Master of Science in Engineering is the result of my own unaided work. This dissertation is being submitted to the School of Chemical and Metallurgical Engineering at the University of the Witwatersrand under the guidance and supervision of Professor T. Majozi, University of the Witwatersrand, Johannesburg, South Africa, and Co-Supervision by P. Mukoma and B. North, Council of Scientific and Industrial Research, Pretoria, South Africa.

I am aware that plagiarism (the use of someone else’s work without their permission and/or acknowledging the original source) is wrong. Additionally, I have acknowledged all sources used in this dissertation and have cited these in the reference sections. I have followed the required conventions in referencing the thoughts and ideas of others.

Signature of Candidate 

Date: 26 JANUARY 2022

Abstract

Fossil fuels have earned a reputation as unsustainable sources of energy, due to the release of carbon emissions that are attributable to global warming. To overcome the extensive release of carbon emissions into the environment, different approaches are being explored to produce energy, by replacing non-renewable fuels with renewable energy. Additionally, many countries across the world are emerging as water-scarce countries due to the vulnerability of freshwater supply. This work, therefore, focuses on the design and synthesis of a hybrid electrolyser-fuel cell system to generate hydrogen and freshwater from seawater. The proposed system is designed to be integrated with a background process, such as a utility system, that requires both power and water. It has the potential to reduce the burden on freshwater sources and power requirements of background processes, with a significant reduction on carbon footprint. A one-dimensional, mathematical model is developed for a continuous hybrid seawater electrolyser-fuel cell system operated at steady state. The model determines the optimal operating conditions in terms of temperature, current density, electrode thickness and humidity, as well as the performance of the system through the activation overpotential, diffusion overpotential, ohmic overpotential and the open-circuit voltage. GAMS/BARON solver is used to optimise the hybrid system. Furthermore, a techno-economic evaluation is conducted to determine the viability of the system. Results indicate that an overall power conversion efficiency of 41.2 % and a freshwater recovery rate of 48.2 % is achieved. Freshwater produced is expected to have a purity of >99.9% based on the PEME which is assumed to produce pure hydrogen and oxygen. This indicates that the system shows promise of decentralising the production of electricity from fossil fuels, addressing the energy trilemma without straining freshwater bodies, and providing clean supplementary power to background processes. Furthermore, in addition to its environmental benefits, the HEFC system is economically viable presenting a positive net present value, 3.94-year payback period over a 20-year plant life and a 16.3% internal rate of return.

Publications

The work presented in this dissertation has been publication in the Journal of Cleaner Production (Pres ‘19 Special Issue):

Singh, M. *et al.* (2020) “Singh, M. *et al.* (2020) “A mathematical model for optimum design and synthesis of a hybrid electrolyser-fuel cell system: Production of hydrogen and freshwater from seawater,” *Journal of Cleaner Production*, 277.
doi: 10.1016/j.jclepro.2020.123899.”

Additionally, this work has been presented at the 22nd Conference on Process Integration for Energy Saving and Pollution Reduction (PRES ‘19) held in Agios Nikolaos, Greece. This work was included in the conference proceedings and as a poster presentation.

Acknowledgements

With boundless love and acknowledgement, I would like to express my profound gratitude and appreciation to the people who have assisted me in making my dreams of completing my master's degree a reality.

First and foremost, I would like to thank God for giving me the strength, knowledge, guidance and opportunity to undertake this master's research, and complete it to the best of my ability. This achievement would not have been possible without the blessings of Lord Ganesha.

Secondly, I would like to thank my supervisor and mentor, Professor Thokozani Majozi, for his guidance, patience and support throughout this journey. I deem myself extremely fortunate to have worked under his supervision. I cannot begin to express my sincere gratitude for the contributions and time he has taken to make this research a success. I would also like to thank Doctor Peter Mukoma and Doctor Brian North, my co-supervisors, who have been involved in this research from my undergraduate degree.

Thirdly, I would like to acknowledge my family, for all the love and support they have shown me throughout my studies. The constant encouragement and guidance has helped me explore new opportunities and experiences. I hope this achievement and the achievements to follow will continue making you proud.

This work would not have been possible without the financial support from the National Research Foundation (NRF) under the NRF/DST Chair in Sustainable Process Engineering in the School of Chemical and Metallurgical Engineering at the University of the Witwatersrand. In addition, I would like to acknowledge the University of Witwatersrand for awarding me the Postgraduate Merit Award and seeing the potential in me pursuing this degree.

Lastly, I would like to thank my colleagues from the Sustainable Process Engineering research office. Thank you for welcoming me and treating me as a member of the group from day one. I appreciate all the advice, insight and memories we shared.

Table of Contents

List of Figures

List of Tables

Nomenclature

Parameters

A_{H_2O}	Activity of water	-
α	Charge transfer coefficient	-
AI	Annual interest rate	-
C	Concentration	mol/m^3
CF	Cost factor	-
P_{cr}	Critical pressure	MPa
T_{cr}	Critical temperature	K
D_w	Diffusion coefficient	m^2/s
j_o	Exchange current density	A/m^3
F	Faraday's constant	C/mol
IR	Inflation rate	-
IF	Installation factor	-
δ_{mem}	Membrane thickness	μm
MW	Molar mass	kg/mol
$MW_{mem,dry}$	Molar mass of the dry membrane	kg/mol
n_{cell}	Number of cells	-
z	Number of electrons transferred	-
P	Pressure	MPa
P_{ref}	Reference pressure	MPa
T_{ref}	Reference temperature	K
R	Universal gas constant	J/$mol.K$
Tax_{rate}	Tax rate	-
D_w	Water diffusion coefficient	m^2/s
K_{darcy}	Water permeability coefficient	m^2
Y_{plant}	Plant life	yr
$Y_{purchase}$	Purchase year	-
Y_{rep}	Replacement year	-

Variables

$Cash$	Cash flow	USD
$Cost$	Cost	USD
C_{cap}	Capital cost	USD
I	Current	A
j	Current density	A/m^2
Dep	Depreciation	USD
D	Diffusion coefficient	m^2/s
DF	Discount factor	-
n_d	Electrostatic drag coefficient	-
FCI	Fixed capital investment	USD
D_{eff}	Effective diffusion coefficient	m^2/s
IRR	Internal rate of return	-
C_{main}	Maintenance cost	USD
$\dot{M}$	Mass flow rate	kg/hr
$\dot{N}$	Molar flow rate	mol/s
n	Molar flux	$mol/m^2.hr$
y	Molar fraction	-
Op_{hours}	Operating hours	hr
NPV	Net present value	USD
PAT	Profit after tax	USD
$PATPD$	Profit after tax plus depreciation	USD
PBT	Profit before tax	USD
PBP	Payback period	yr
$Power$	Power	kW
PV	Present value	USD
A	Reaction area	m^2
C_{rep}	Replacement cost	USD
Rev	Revenue	USD
P_{sat}	Saturation pressure	MPa
Rev	Revenue	USD
T	Temperature	K
TAC	Total annualised cost	USD
TDC	Total direct costs	USD
TIC	Total indirect costs	USD

TP	Total production	USD
V	Voltage or overpotential	V

Greek Symbols

α	Charge transfer coefficient	-
ρ	Density	kg/m^3
$\rho_{mem,dry}$	Density of dry membrane	kg/m^3
η	Efficiency	-
λ	Humidity degree	-
σ_{mem}	Membrane conductivity	$ohm^{-1}m^{-1}$
β	Partial pressure	MPa
ε_p	Percolation	-
ε	Porosity	-
δ	Thickness	m
μ	Viscosity	$kg.s/m^3$

Sets

M	Number of cells in electrolyser stack =1
N	Number of cells in fuel cell stack = 1,2, 3,…,25
P	Units = Electrolyser, Fuel cell
Q	Number of plant operating years = 1,2, 3,...,20

Subscripts

act	Activation
AL	Assembly labour
an	Anode
$annual$	Annual
BOP	Balance of Plant
cat	Cathode
cap	Capital
ch	Channel
ch, o	Channel at reference conditions
$construction$	Construction
$cons$	Consumed
cs	Control and sensors
$diff$	Diffusion

DC	Direct cost
dms	Delivery management system
DS	Distribution and selling
ED	Engineering and design
$elect$	Electrolyser
eo	Electro-osmotic drag
fc	Fuel cell
gms	Gas management system
H_2	Hydrogen
INS	Insurance
LC	Legal and contractor fees
$land$	Land
mem	Membrane
me	Membrane-electrode interface
me, o	Membrane-electrode interface at reference conditions
$MBOP$	Mechanical balance of plant
ohm	Ohmic
ocv	Open circuit voltage
$other$	Other
O_2	Oxygen
$other$	Other direct costs
PC	Project contingency
pe	Pressure effect
PR	Patents and royalties
$pelect$	Power electronics
$prod$	Produced
RD	Research and development
sw	Seawater
$stack$	Stack
sys	System
tms	Thermal management system
H_2O	Water
$H_2 - H_2O$	Hydrogen-water mixture
$O_2 - H_2O$	Oxygen-water mixture

CHAPTER 1

Introduction

1.1 Introduction

The 21st century is one of the most challenging times for humankind, as greenhouse gases pose huge concerns on the environment and human health. Although greenhouses gases cause detrimental harm to the environment and humans, these greenhouse gases are caused by human activities. These activities include deforestation, livestock farming and the combustion of fossil fuels for electricity generation, heating, transportation and industrial energy requirements (Environmental Protection Agency, 2021).

Energy is known to be the heart of all economic and social development in every nation. On that account, it is important to ensure a continuous supply of energy is maintained for the well-being of people, as well as countries collectively.

An ideal energy resource would be that which is readily available, affordable in terms of cost and environmentally friendly. This constitutes the so-called energy trilemma.(Rinkinen, Shove and Torriti, 2019). The energy trilemma is typically used to illustrate the balance between energy equity (accessibility and affordability), energy security (capacity to provide reliable energy) and environmental sustainability (transition towards a cleaner environment through decarbonisation and improvements in the efficiency of electricity generation, transmission, and distribution technology) (World Energy Council, 2022).

These variables are dependent on one another and cannot be thought of in isolation. A trade-off is required in which two variables may be addressed at the expense of the third (CarbonBrief, 2013).

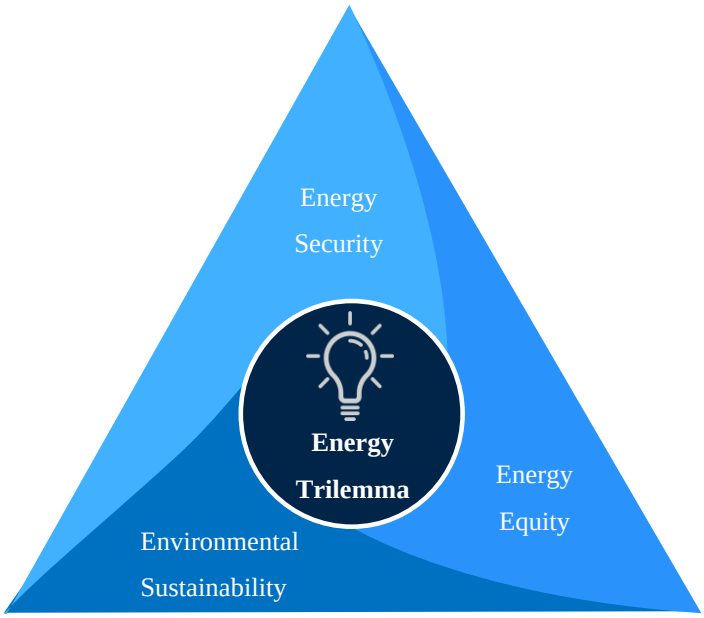

Figure 1.1: Energy Trilemma

Globally, 74.7% of the electricity generated is derived from fossil fuels which addresses the affordability and security goals of the energy trilemma (International Energy Agency, 2019). However, fossil fuels are incapable of meeting the environmental sustainability goal due to the emission of greenhouse gases, leading to the greenhouse effect. The greenhouse effect is defined as the natural increase of the earth's temperature, due to the presence of greenhouse gases caused by the combustion of fossil fuels (Anderson, Hawkins and Jones, 2016).

In relation to the developing world, energy security is largely dependent on the demand for energy, rate of population growth, rate of urbanisation and rate of economic growth and development (Department of Alternative Energy Development and Efficiency, 2015).

An increase in the energy demand will ultimately increase the consumption of fossil fuels and, therefore, lead to an increase in greenhouse gas emissions. Consequently, the combustion of fossil fuels for power generation, not only results in an increase in the greenhouse effect, but results in the depletion of non-renewable energy sources. Ultimately, resulting in a decrease in energy security.

Similarly, there is a direct correlation between population growth and energy security. An increase in the growth of a population results in an increase in energy demand, and therefore an increase in the combustion of fossil fuels and decrease in energy security.

Unlike, energy demand and the rate of population growth, the rate of urbanisation has been established to have a positive impact on energy security. An increase in industrialisation and urbanisation has been found to increase energy security and economic development due to improvements in energy efficiency(Li, Li and Strielkowski, 2019).

Figure 1.2 graphically illustrates the sources of energy used in the global production of electricity.

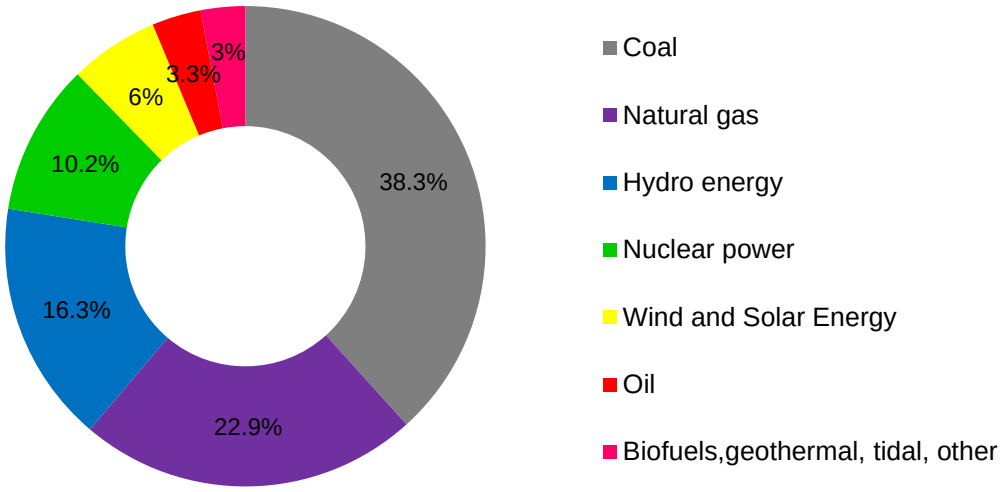

Figure 1.2: 2017 Global Electricity Production (International Energy Agency, 2019)

To address the environmental crisis, it is imperative for power generation utilities to pursue alternate avenues for energy production, which will lead to one of the biggest technological shifts experienced to date (Darras *et al.*, 2015). This could be attained by adopting the use of an energy system which harnesses energy from renewable energy sources, causes zero harm to the environment, is affordable and capable of securing the political, and the economic security of the nation (Kimura, Anbumozhi and Nishimura, 2019).

As such, hydrogen (H_2) produced from renewable energy through the use of electrolysers powered by hydro, solar, tidal and wind energy is gaining a substantial amount of attention as a promising substitute fuel, and an effective long-term energy storage mechanism. More specifically, electrolysis has been identified to be one of the most recognised methods of producing H_2 and oxygen (O_2) from freshwater and seawater.

However, through global warming, industrialisation and population growth, freshwater bodies across the world have become severely strained, due to the excessive demand for water, pollution of water bodies, as well as an increase in natural disasters such as droughts which are caused by the emission of greenhouse gases into the Earth's atmosphere. As seen in Figure 1.3, many countries across the world are experiencing water shortages due to the continuously declining average rainfall (Carylsue, 2016). It is, therefore, an obvious advantage to pursue saline sources of water when considering the production of hydrogen renewably, as seawater is an inexhaustible source of water, as opposed to freshwater which has become constrained.

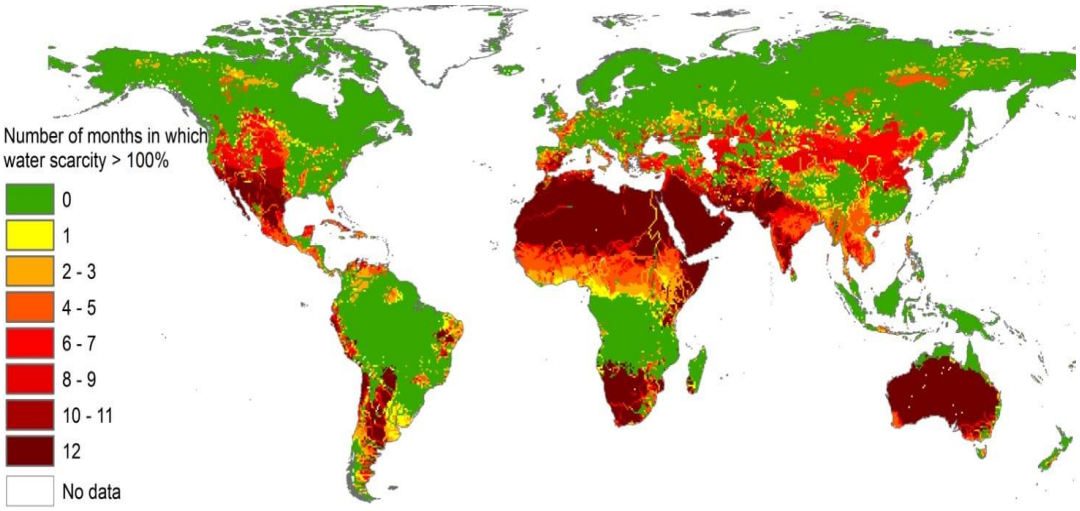

Figure 1.3: World Water Scarcity Map (Carylsue, 2016)

1.2 Research Motivation

According to the literature reviewed, many studies have been conducted on the development of individual mathematical models for freshwater Proton Exchange Membrane Electrolysers (PEMEs) and Proton Exchange Membrane Fuel Cells (PEMFCs). Additionally, numerous studies have been carried out on hybrid systems which couple various renewable energy sources and have been optimised in the Hybrid Optimisation Model for Electric Renewables (HOMER) software. Research on seawater electrolysis has been extensively carried out but has merely been focused on experimental work, such as investigating the performance of different electrocatalysts and electrodes for the evolution of O_2, as well as efficiency and viability of the seawater electrolyser.

However, to date, a comprehensive mathematical model for the optimal design of a one-dimensional seawater electrolyser has not yet been developed. Moreover, research on the development of a mathematical formulation for the optimum design of a hybrid electrolyser-fuel cell (HEFC) system, to produce H_2 and freshwater from seawater is limited. This work, therefore, aims to determine the optimal design parameters and operating conditions, as well as the economic viability of the HEFC system. The industrial applicability of this technology will provide insight into the feasibility of integrating a HEFC system into a background process, especially in energy and water constrained regions.

Consequently, the objective of this work is to tackle the water and energy crisis arising in many countries across the world, such as South Africa, which is the 30th driest country in the world (Gerbi, 2017), and where more than 90% of the electricity generated is sourced from coal (Ratshomo and Nembahe, 2016). It investigates whether a HEFC system can be conceptually applied, and whether it will be economically viable in the next 10-20 years. This is achieved by eliminating the strain on freshwater bodies, producing renewable energy, and eliminating environmental concerns by providing a green energy conversion and water purification system.

In this study, a background process is defined as a sub-process of a main process, e.g., a utility system. Integration of the proposed HEFC system with a background process allows for generated power and freshwater to be fed directly or indirectly to the process, thereby reducing freshwater and power requirements (Figure 1.4).

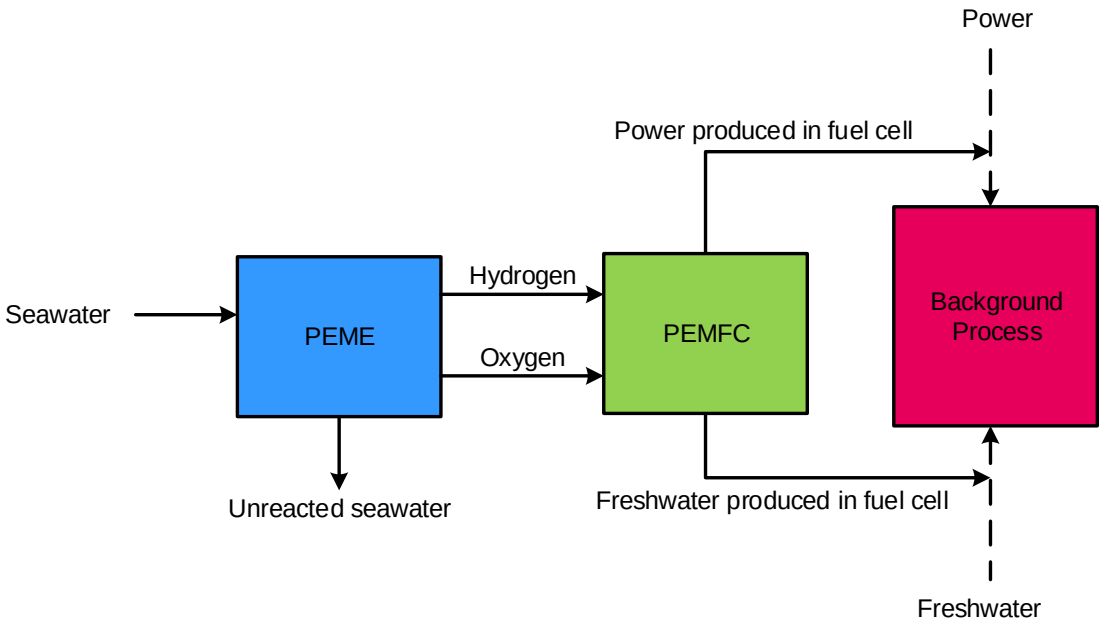

Figure 1.4: HEFC System Integrated with a Background Process

This research is focused on highlighting the value of utilising hydrogen as a renewable energy storage mechanism, and developing a mathematical model for the optimal design and synthesis of a HEFC system to produce hydrogen and freshwater from seawater. A nonlinear programming (NLP) formulation is presented. It determines the maximum power conversion efficiency achievable in the hybrid system. The model developed provides a framework to analyse the performance of the hybrid system, and a method of exploring variables that are difficult to measure in a physical system. Furthermore, an economic evaluation is carried out to determine the viability of the proposed system.

1.3 Scope of Research

In this research, a mathematical model of a hybrid electrolyser-fuel cell was developed to provide a systematic approach in solving the optimisation problem. It is expected that this work will contribute significantly to addressing the global energy and water crisis, particularly in South Africa. Moreover, a model of seawater electrolysis has not yet been developed and through this work, it is hoped that new avenues for future research will be inspired. This work also presents an optimisation approach for a hybrid electrolyser-fuel cell system which yields better results than those obtained from simulations. Additionally, the research conducted is purely of scientific value, but its industrial application in the future may be worth exploring.

1.4 Problem Statement

Many countries across the world are emerging as water-scarce countries, as well as experiencing an energy-crisis due to the increase in energy demand and greenhouse gas emissions. To alleviate pollution from fossil fuel-based energy production, the H_2 economy is explored. H_2 is a promising alternative energy carrier and a viable solution to decentralise the production of energy from oil and fossil fuels. Therefore, to tackle the energy and water crisis, a HEFC system is presented to produce H_2 and freshwater from seawater.

A mathematical model was developed for the optimum design and synthesis of a HEFC system and was formulated as an NLP optimisation problem. The advantages associated with integrating the HEFC system into background processes include the following:

(i) Reduced strain on freshwater bodies and feed water required
(ii) Supplementary power available for use within the background process
(iii) System is environmentally friendly with near-zero carbon emissions
(iv) In countries such as South Africa, where water and power are constrained, the current HEFC system will effectively utilise seawater to provide power and freshwater to processes
(v) Low-pressure operation (atmospheric) compared to membrane technology used in desalination
(vi) Reduced capital cost and limited seawater pre-treatment required
(vii) Onsite desalination and power production allows the chemical plant to operate off the grid

The problem being addressed in this work may be formally stated as follows:

Given:

(i) A set of units, *P*, composed of an electrolyser stack and fuel cell stack

(ii) A set of electrolyser cells, *M*, with a known number of cells in the electrolyser stack

(iii) A set of fuel cells, *N*, with a known number of cells in the fuel cell stack

(iv) A fixed flowrate of seawater entering the electrolyser stack, N_{H_2O}

(v) Source of energy used in the electrolyser

(vi) Type of electrolyser and fuel cell being used

The main objectives of this work are to:

(i) Highlight the importance of utilising hydrogen as a renewable energy storage mechanism

(ii) Model and optimise a hybrid electrolyser/fuel cell system to produce power and freshwater from seawater

(iii) Determine the optimal performance and design conditions that maximise the power conversion efficiency

(iv) Determine the techno-economic feasibility and viability of the system

1.5 Structure of the Dissertation

The structure that this dissertation follows is described below:

Chapter 1- Introduction: This chapter describes the background of the problem, provides the research motivation, defines the problem statement and states the research objectives.

Chapter 2-Literature Review: A comprehensive literature review is given on the global energy and water crisis, hydrogen economy, hydrogen production methods, different types of electrolysers, fuel cells and hybrid systems, as well as the mathematical models developed to describe each system. Additionally, literature associated with the economics of electrolysers and fuel cells is reviewed

Chapter 3 - Model Development: A detailed derivation of a seawater electrolyser and hydrogen fuel cell model from first principles is presented. This chapter describes the method and equations used to describe the development of superstructure-based hybrid electrolyser-fuel cell system model.

Chapter 4- Illustrative Example: The fourth section demonstrates the application of the HEFC mathematical model in an illustrative example. All the parameters, variables, economic data and assumptions are presented.

Chapter 5- Results and Discussion: In this chapter, the results obtained from the model developed are presented and discussed.

Chapter 6 – Limitations, Recommendations and Conclusion: The final chapter of this dissertation addresses the limitations of the model and suggests avenues worth pursuing in the future to improve the model. Finally, a summary of this research dissertation is given in the conclusion.

1.6 References

Anderson, T.R., Hawkins, E. and Jones, P.D. (2016) "CO2, the greenhouse effect and global warming: from the pioneering work of Arrhenius and Callendar to today's Earth System Models," *Endeavour*, 40(3), pp. 178–187. doi:10.1016/j.endeavour.2016.07.002.

CarbonBrief (2013) *Climate rhetoric: What's an energy trilemma?*, *Science*. Available at: https://www.carbonbrief.org/climate-rhetoric-whats-an-energy-trilemma (Accessed: January 22, 2022).

Carylsue (2016) *4 Billion People Face Water Scarcity*, *National Geographic*. Available at: https://blog.education.nationalgeographic.org/2016/02/15/4-billion-people-face-water-scarcity/ (Accessed: March 18, 2018).

Darras, C. *et al.* (2015) "Techno-economic analysis of PV/H2 systems," *International Journal of Hydrogen Energy*, 40(30), pp. 9049–9060. doi:10.1016/j.ijhydene.2015.05.112.

Department of Alternative Energy Development and Efficiency (2015) "Alternative Energy Development Plan : AEDP2015," 2579(September), p. 22.

Environmental Protection Agency (2021) *Sources of Greenhouse Gas Emissions*, *United States Environmental Protection Agency*. Available at: https://www.epa.gov/ghgemissions/sources-greenhouse-gas-emissions (Accessed: August 23, 2021).

Gerbi, G. (2017) *SA Ranked 30th Driest Country in the World*, *Eye Witness News*. Available at: http://ewn.co.za/2017/11/28/sa-ranked-30th-driest-country-in-the-world (Accessed: May 30, 2018).

International Energy Agency (2019) *Electricity Information: 2019*, *Statistics IEA*. Available at: https://www.iea.org/reports/electricity-information-2019 (Accessed: January 14, 2020).

Kimura, F., Anbumozhi, V. and Nishimura, H. (2019) *ASEAN VISION 2040 Volume III: Transforming and Deepening the ASEAN Community*. Jakarta.

Li, M., Li, L. and Strielkowski, W. (2019) “The impact of urbanization and industrialization on energy security: A case study of china,” *Energies*, 12(11). doi:10.3390/en12112194.

Ratshomo, K. and Nembahe, R. (2016) “South African Coal Sector Report Directorate : Energy Data Collection , Management and Analysis,” *Department of Energy*, pp. 1–34.

Rinkinen, J., Shove, E. and Torriti, J. (2019) *Energy Fables: Challenging Ideas in the Energy Sector*. 1st Edition, *Energy Fables: Challenging Ideas in the Energy Sector*. 1st Edition. London: Routledge. doi:10.4324/9780429397813.

World Energy Council (2022) *World Energy Trilemma Index*. Available at: https://www.worldenergy.org/transition-toolkit/world-energy-trilemma-index (Accessed: January 22, 2022).

CHAPTER 2

Literature Review

2.1 Introduction

The work in this dissertation focuses on the incorporation of electrolysers and fuel cells in a hybrid system for the production of power and freshwater. As a result, this chapter gives a detailed review of the relevant literature related to the work in this field. More specifically, this chapter will firstly present a background on the global water and global energy crisis, as well as the hydrogen economy and hydrogen production methods. Secondly, water electrolysers and fuel cells are introduced, followed by an overview and comparison between the different types of electrolyser and fuel cell technologies available to determine the best technology for this application. Thirdly, various optimisation approaches and models are discussed with their respective merits and limitations. Then, a detailed literature review is given on seawater electrolysis, hydrogen fuel cells and hybrid systems. Thereafter, an overview of mathematical modelling is given, followed by a review on the techno-economic evaluation of PEMEs and PEMFCs.

2.2 Global Water Crisis

Water is imperatively one of the most precious resources in the world. It is required by all living organisms including humans, flora, fauna, and micro-organisms in order to sustain life on earth. Earth is the only planet in the solar system whose surface is more than 70% covered with water (Teow and Mohammad, 2019). Water resources accessible to mankind are distributed across the atmosphere, hydrosphere and lithosphere.

Despite having over 70% of the earth's surface covered with water, only 3% of this water is available as freshwater, of which two-thirds of the freshwater is locked up in frozen glaciers or is unavailable for use. The rest of the water is saline and contains large amounts of dissolved solids and ions (Abdel-Aal, Zohdy and Kareem, 2010), which implies that it cannot be used directly for human consumption without prior treatment. Consequently, the treatment of saline water is associated with significant cost implications. Figure 2.1 illustrates Earth's water distribution.

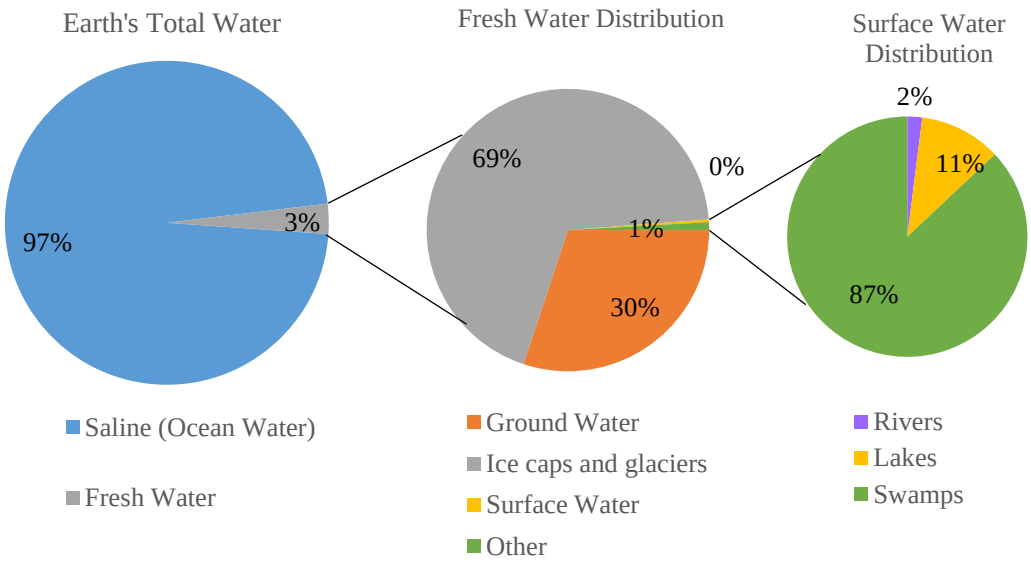

Figure 2.1: Earth's Water Distribution

The human population has successfully developed ways of utilising the world's natural waterways through dams, irrigation systems, and wastewater treatment plants. However, freshwater bodies across the world are drying up or are becoming severely strained due to pollution, agricultural demands, and population growth which have allowed civilisations to grow.

Water pollution is a serious issue affecting the quality and supply of available freshwater. Water pollution is caused by pesticides and fertilisers that are washed into rivers from farms, as well as untreated wastewater and industrial effluents that are pumped into streams, river, and lakes. More specifically, agricultural practices use approximately 70% of the worlds accessible freshwater to feed the population. However, majority (roughly 60%) of this is water is wasted due to inefficient application in irrigation systems, as well as poor cultivation techniques (Food and Agriculture Organization of the United Nations (FAO) and International Water Management Institute (IWMI), 2017).

Since over 70% of the surface of the world is covered with water, it is reasonable and practical to incorporate it into sustainable applications. As such, the production of hydrogen in the future will lie in the ability to pursue seawater electrolysis as opposed to freshwater which has become vulnerable in many countries across the world. Major concerns surrounding the production of hydrogen from the electrolysis of seawater include availability, cost of primary energy sources used in the electrolysis, location of the facility and availability of resources.

2.3 Global Energy Crisis

According to statistics, approximately 79.7 % of the energy consumed in the world is sourced from fossil fuels (World Bank, 2016). However, due to the increase in energy demand, the global fossil fuel supply is declining. Conventionally, electricity is generated from non-renewable resources such as coal, ethanol, methane, natural gas, and oil. This is achieved through various processes which include the combustion of coal, gasification of coal and steam reforming of ethanol, methane and natural gas. These processes are considered as greenhouse gas (GHG) emitting processes, as pollutant gases such as carbon dioxide, carbon monoxide, chlorofluorocarbons, methane, ozone, nitrous oxides and water vapour are released into the Earth's atmosphere.

The aforementioned gases have been correlated to have an impact on climate change, and as such have been found to have a detrimental effect on the environment if technologies such as filtering and carbon sequestration are not implemented (Saur, 2008). Consequently, these global warming effects contribute to the environmental concern regarding the increase in pollution levels, reduced energy security, and challenges associated with sustainability in the energy sector.

Over the last few years, nations have been shifting towards utilising renewable energy to meet the energy demand and reduce the release of carbon emissions. Adopting the use of renewable energy technologies for electricity generation, such as hydro, solar, wind and tidal energy will reduce the global dependency on fossil fuels and promote a sustainable energy sector for the foreseeable future. However, despite renewable energy being readily available, challenges related to the inherently intermittent supply, geographical limitations, seasonal variations, high capital cost, and reliability of these technologies are factors that need to be addressed (Sinha and Chandel, 2015).

To reduce the cost of renewable energy plants and ensure the steady supply of power, electrical energy storage devices such as batteries, flywheels, hydrogen fuel cells, and super-capacitors may be incorporated into the energy generation system (Wanjiku *et al.*, 2010). In particular, solar and wind energy hold a competitive advantage in many regions of the world due to their availability and inexhaustibility. Wind energy has proven to be a profitable and mature method of generating electricity. However, the quality and variability in wind supply has adverse effects on the grid (González, McKeogh and Gallachóir, 2004). Additionally, poor infrastructure associated with transportation and gridlines restrict the deployment of wind energy (Samaniego *et al.*, 2008).

To overcome these problems and promote the effective use of wind energy, electrical energy generated from wind farms can be stored in chemicals. In recent years, Power-to-Gas (PtG) storage systems have gained significant attention in storing large quantities of electricity. PtG systems convert electrical energy into chemical energy through the synthesis of hydrogen gas. This hydrogen may be used as a fuel for transportation, injected into the natural gas network or stored for deferred electricity generation (Gahleitner, 2013). These systems are geographically unconstrained and have high volumetric energy densities. which make storing electricity as a chemical fuel easier than storing it as potential or mechanical energy (Ferrero *et al.*, 2016).

Correspondingly, power-to-power systems are systems which use surplus electricity to synthesis and store hydrogen dissociated from water. In the instance of high-power demand, the stored hydrogen is converted back into power in fuel cells (Mura *et al.*, 2015; Ferrero *et al.*, 2016; Qolipour, Mostafaeipour and Tousi, 2017).

2.4 Hydrogen Economy

In recent years, the evolution of hydrogen as an energy carrier has been established as a promising alternative energy carrier, compared to the conventional use of fossil fuels. Hydrogen is prospectively a highly efficient energy carrier, and a viable solution to decentralise the production of energy from oil and other fossil fuels. Thus, offering a transition into a carbon-free future. Not only do these fossil fuels contribute significantly towards acid rain and the greenhouse effect, but they also coerce deforestation, social tension and sometimes war among countries. Implementing hydrogen into applications is favoured due to its future low-cost potential, versatility in applications, environmentally friendly properties in production, transportation, storage, and utilisation (classified as a clean fuel), as well as its efficient conversion into different forms of energy (Saebea *et al.*, 2017).

Moreover, hydrogen maintains the greatest gravimetric energy density compared to all other fuels (e.g., gravimetric density for hydrogen is 145 kJ/g and the gravimetric energy density for methane is 56 kJ/g) (Hussein, 1992). Despite, hydrogen's favourable chemical properties, it is not naturally present in its elemental form and must be produced in order to be used as energy (Barbir, 2005).

Currently, hydrogen is used in the production of ammonia, methanol, polymers, resins, metals (iron and steel), glass, semi-conductors, propellant fuel, hydrogenation of fats, cooling of generators, petroleum refineries, manufacturing of electronics, heating buildings and in the power generation sector (Smith and Newborougg, 2004; Turner *et al.*, 2007; Saur, 2008; IRENA, 2018).

2.5 Hydrogen Production Methods

Globally, approximately 70 million tonnes of hydrogen is annually produced (IEA, 2019). Technological advancement towards introducing a hydrogen economy will flourish globally in subsequent years, through supporting infrastructure pertaining to the production and storage of hydrogen. According to Genevieve Saur (2008), the rate of hydrogen production is expected to increase by 10% annually. As a result, the transition towards using hydrogen as a source of energy will reduce many countries' domestic dependence on international oil imports, and thus, increase local energy production.

According to published data, approximately 96% of the total hydrogen consumed in the world is currently being produced from fossil fuels (AlZahrani and Dincer, 2017). Among these fossil fuels are hydrocarbons such as coal, natural gas, and oil which are used as primary feedstock to produce H_2 through combustion, gasification, reforming processes and nuclear-powered water splitting (Ortiz, Zaragoza and Collins-Martínez, 2016). The process of steam and oxygen reforming is used to convert natural gas into carbon dioxide, hydrogen and carbon monoxide. A drawback to using coal and natural gas to obtain hydrogen is the large amount of carbon dioxide produced. It is worth noting that although less carbon dioxide is produced from natural gas than from the combustion of coal, this method is undesirable from an environmental point of view (Badea, Maior, *et al.*, 2007). Additionally, the production of hydrogen from fossil fuels has also been found to be infeasible due to the highly energy-intensive conversion processes required. Furthermore, hydrogen production from reforming processes do not produce 100% pure hydrogen. Traces of contaminants such as carbon monoxide are present, and if used in PEMFCs, detrimental effects will be observed on the performance of the fuel cell (Zamel and Li, 2011).

Alternatively, emerging technologies being implemented in the production of hydrogen include the following: water electrolysis, photolysis, photo-catalysis, photo-electrolysis, superficial water gasification, pyrolysis, thermo-chemical cycles, pyrolysis, steam reforming of biomass with/without carbon capture, utilisation and storage, and anaerobic digestion of biomass (Ni, Leung and Leung, 2006; Mohammad and Kaukhab, 2011; Colella *et al.*, 2014; IRENA, 2018).

Thermo-chemical cycles generate hydrogen through several chemical reactions used to split water into hydrogen gas and oxygen gas, at temperatures lower (~800-1000℃) than direct thermal dissociation (>2500℃). In comparison to conventional methods of producing hydrogen, photo-catalysis and thermo-chemical cycles are economically infeasible due to the low efficiencies achieved. Therefore, significant improvement will be required to make these processes viable in the future.

During the operation of water electrolysers, an electrical current is used to dissociate water molecules into gaseous hydrogen and oxygen, whereas photo-biological processes use solar energy, water and hydrogenase enzymes (algae and cyanobacteria) to produce hydrogen. For biomass gasification, biomass undergoes a process of incomplete combustion at approximately 1000 ℃ to produce hydrogen, carbon monoxide and traces of methane (Srivastava, 2013). In contrast, in the process of pyrolysis, biomass is heated to 350-600 ℃ in the absence of oxygen to produce hydrogen, methane, and a gaseous mixture consisting of carbon monoxide, carbon dioxide, and light hydrocarbons (Cheng, 2017).

2.6 Water Electrolysis

Water electrolysis was found to be the most practical and mature method of producing hydrogen renewably, achieving efficiencies of greater than 70% (Barbir, 2005). However, it had also been concluded that hydrogen production through water electrolysis is an energy-intensive process. To promote green energy, free of carbon dioxide emissions, renewable energy such as hydro, wind, photovoltaic, solar, geothermal, and tidal energy may be used as the primary source of energy to power electrolysers. However, some of the major limitations associated with renewable energy include intermittent availability and site-dependence.

It is for this reason that an extensive amount of research has been committed into making the production of hydrogen, via the electrolytic route more attractive. For the use of electrolysers to become more favourable, electrolysers need to be made cheaper by reducing the cost of the electricity being used in the process, and by reducing the consumption of energy (Stojić *et al.*, 2003).

On average 40 kWh of energy is required to produce 1 kilogram of hydrogen in a 100% efficient system. This value is derived from the higher heating value, and realistically energy systems operate with an efficiency in the range of 60-70% (Abdel-aal *et al.*, 2012). The higher heating value describes the efficiency of the system and includes the total thermal and electrical energy that is required to produce 1 kg of hydrogen at standard temperature and pressure. Some papers describe the efficiency of an electrolyser system with the lower heating value (LHV) which only takes into account the electrical input energy of 33.3 kWh/kg (Saur, 2008).

The water dissociation reaction is an endothermic reaction; this means that heat must be supplied to the system in order to split water into hydrogen and oxygen. The rate of enthalpy change is expressed in Equation (2.1).

$$\Delta H = \Delta G + Q = \Delta G + T\Delta S \qquad (2.1)$$

Where: ΔH = Change in enthalpy

ΔG = Change in Gibb's free energy

Q = Heat supplied to the system

ΔS = Change in entropy

Figure 2.2 graphically shows how the energy demand changes as temperature increases. It is apparent from Figure 2.2 that as temperature increases, the electrical demand (equivalent to Gibb's energy) decreases while the thermal energy increases (TΔS).

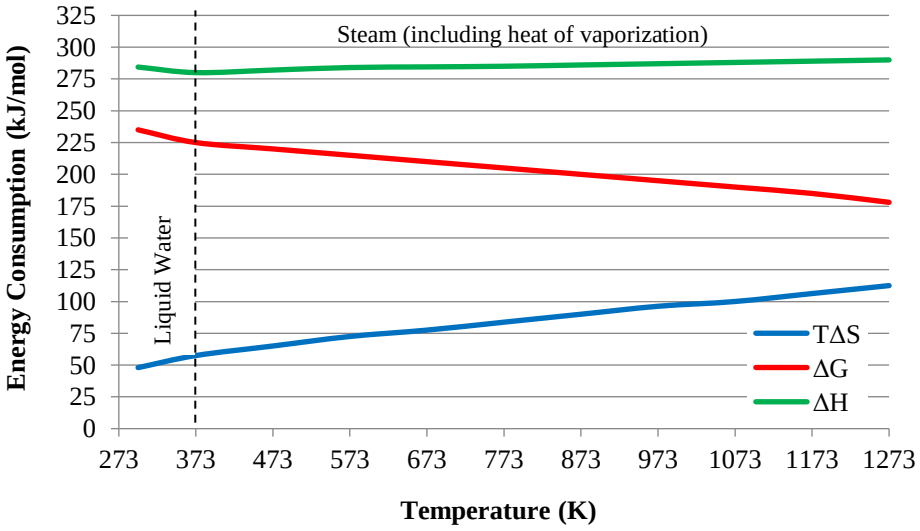

Figure 2.2: Energy Consumption of an Electrolyser Operating at 1 atmosphere (Ursúa et al., 2012)

There are several types of electrolysers used to dissociate water into H_2 and O_2, i.e., alkaline, proton exchange membrane electrolysers (PEME) and solid-oxide electrolysers (SOE). Each electrolyser is operated under different operating conditions and is selected based on the scale of operation and efficiencies required. The most common electrolyser used across the world is the alkaline electrolyser, which uses potassium hydroxide as an electrolyte. However, PEMEs are the most efficient electrolysers currently available.

In general, electrolysers are composed of a porous anode and porous cathode separated by an electrolyte. At the anode, water is fed to the electrolyser where it is broken down into hydrogen and oxygen ions. Oxygen gas is produced at the anode, whereas hydrogen gas is produced at the cathode. Electrons flow through an external circuit from the anode to the cathode. Figure 2.3 depicts a schematic diagram of a general electrolyser.

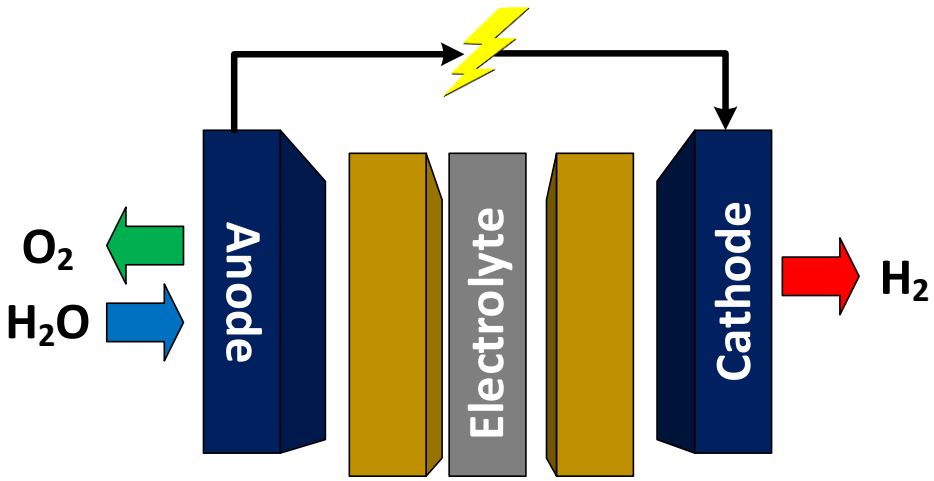

Figure 2.3: Electrolyser Schematic Diagram

2.7 Fuel Cells

As the world becomes more environmentally conscious, the necessity for new power generation technologies that address energy generation and environmental concerns is apparent. Fuel cells exhibit high efficiencies and extraordinary environmental quality. Additionally, due to the compatibility of coupling fuel cells with renewable energy sources, fuel cells have been recognised to improve the security of energy in countries, and increase sustainable development (Schaaf *et al.*, 2014). On the account of this, fuel cells have been found to be an excellent substitute source of clean energy for use in mobile and stationary applications. Such fuel cells have been largely used in the transport sector by NASA, for space travels, as well as to power hydrogen fuel cell vehicles for commercial use.

A fuel cell is an electrochemical device which directly converts gaseous hydrogen and oxygen into power and heat, and water is produced as a by-product. It uses chemical energy and converts it directly into electrical energy. This technology does not use the process of combustion, therefore, making it environmentally safe and free of pollution.

The technique of chemical conversion used within fuel cells provides high efficiencies for the effective use of hydrogen. Several types of fuel cells have been developed due to the variety of applications available. The most common fuel cells used include alkaline, PEM, solid-oxide, methanol and phosphoric acid fuel cells. Each type of fuel cell is operated under different operating conditions and are constructed from various electrolytes (Sharaf and Orhan, 2014). Consequently, hydrogen together with fuel cell technology shows promise of addressing the energy trilemma.

Typically, fuel cells contain a porous anode and porous cathode which are separated by an electrolyte. The electrolyte promotes the transfer of ions between the anode and cathode electrodes. An external circuit is used to connect the anode to the cathode. Generally, in fuel cells, gaseous hydrogen flows into the anode flow channel. The gaseous hydrogen molecules are broken down into electrons and ions. The electrons flow through an external circuit whereby an electric current is generated, while the ions are transferred through the electrolyte to the opposite electrode. This electric current is available in the form of direct current and will need to be converted to alternating current for practical use in applications. At the cathode, oxygen enters through the flow channel. The transfer of ions through the electrolyte produces water at the cathode. Figure 2.4 depicts a fuel cell schematic diagram.

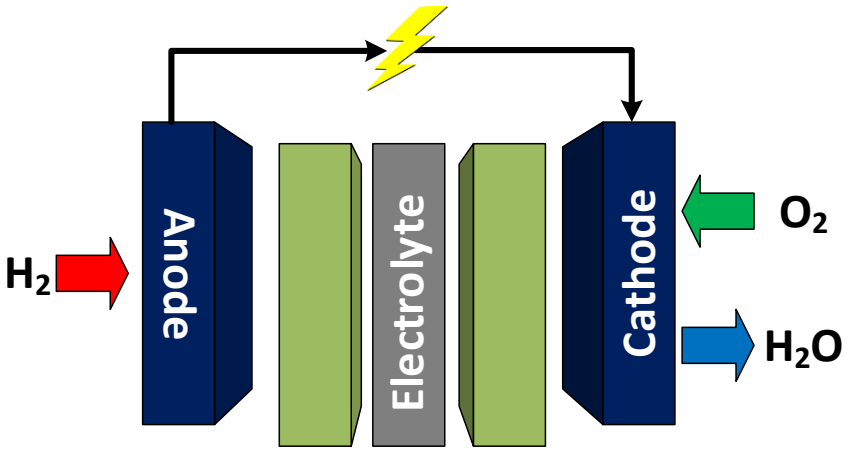

Figure 2.4: Fuel Cell Schematic Diagram

2.8 Types of Electrolysers and Fuel Cells

Hydrogen production through the electrolysis of water promises to be a viable solution for the generation of pure hydrogen. Water electrolysis was first introduced in 1800 by Nicholson and Carlistle, making it a well-established process for producing gaseous hydrogen and oxygen (Laguna-Bercero, 2012). However, it should be noted that production of hydrogen through water electrolysis has been found to be economically infeasible. This is due to the high costs related to the consumption of electricity generated in coal-fired power stations. Subsequently, renewable energy sources may be used to produce hydrogen inexpensively (Barbir, 2005).

Fuel cells had first been discovered by Professor Sir William Groove in 1839. During experiments conducted by Professor Groove, water had been discovered to dissociate into hydrogen and oxygen, achieved through the process of electrolysing dilute sulphuric acid over platinum electrodes. It had been observed that the reaction occurring within the circuit had been reversible, simple and did not cause pollution. As scientists attempted to scale up the fuel cell discovered by Professor Groove, the next 100 years proved to be unsuccessful. The failed attempts were due to the limitations in the materials available at the time. The 1950s and 1960s marked the beginning of the fuel cell era in which the Gemini and Apollo cells contributed towards the advances in the use of water to create an electrical current (Cameron, 1990).

There are several different types of electrolysers and fuel cells used in industries across the world. The main electrolysers and fuel cells include the following:

- Alkaline Electrolysers and Fuel Cells
- Proton Exchange Membrane Electrolysers and Fuel Cells
- Solid- Oxide Electrolysers and Fuel Cells

2.8.1 Alkaline Electrolysers and Fuel cells

Alkaline technology has been industrially available for large-scale operations since 1920 (Zhang *et al.*, 2015; Schmidt *et al.*, 2017). Typically, alkaline technology uses a potassium hydroxide (KOH) electrolyte. Additionally, the cathode in the cell is generally made from steel and the anode is made from nickel-plated steel (AlZahrani and Dincer, 2017). The process of selecting an electrolyte involves choosing an electrolyte, that has a maximum electrical conductivity and minimum corrosion rate on the materials from which the cell is constructed.

Alkaline electrolysers and fuel cells are expected to have a lifespan of between 20-30 years; however, maintenance will be required every 6 years (Mathiesen *et al.*, 2013). Zeng and Zhang (2010) proposed that improvements in the durability, reliability, and safety of the alkaline electrolyser and fuel cell technology, will make this electrolyser and fuel cell the most effective technology. Figure 2.5 illustrates the schematic diagram of an alkaline electrolyser.

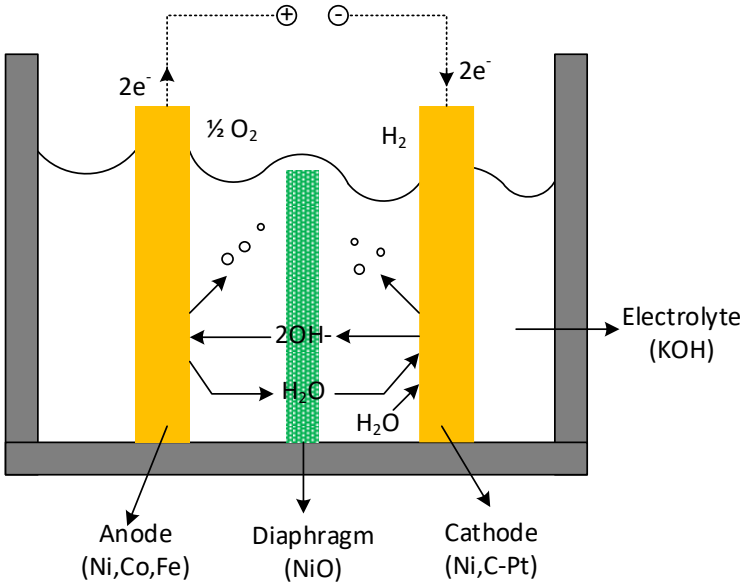

Figure 2.5: Alkaline Electrolyser Schematic Diagram (Ulleberg, 2003)

Commonly, alkaline electrolysers use freshwater with low salinity. Applying seawater electrolysis requires additional treatment processes to desalinate the water, which contributes to the cost of producing hydrogen. Alkaline electrolysers and fuel cells exhibit relatively low capital costs due to the absence of noble metal electrodes and catalysts, as well as mature stack components present (Zeng and Zhang, 2010; Carmo *et al.*, 2013; Schmidt *et al.*, 2017). However, the production cost of hydrogen is negatively affected by the size of the electrolyser and fuel cell, due to the low operating current density and pressures. Additionally, dynamic operation does not work well in alkaline electrolysers and fuel cells, therefore, exhibiting reduced efficiencies and product purities (Schmidt *et al.*, 2017). Alkaline electrolysers have the following disadvantages: electrode corrosion, low pressure, low efficiency, electrolyte contamination, inadequate scalability, and low working current density (Kalinci, Hepbasli and Dincer, 2015).

2.8.2 Proton Exchange Membrane and Fuel Cells

Proton exchange membrane technology was first invented in the early 1960s at General Electric (Rahimi *et al.*, 2014; Zhang *et al.*, 2015; Schmidt *et al.*, 2017). These electrolysers and fuel cells use a perfluorosulfonic acid polymer electrolyte, also known as Nafion (Carmo *et al.*, 2013). In proton exchange membrane electrolysers (PEMEs) and Proton exchange membrane fuel cells (PEMFCs), a proton exchange membrane (PEM) is used to separate hydrogen ions from water and oxygen. Typically, PEMEs and PEMFCs are operated at 20-100℃ and pressures up to 100 bar (Babic *et al.*, 2017).

PEMEs are the reverse technology of PEMFCs. Similarly, both PEMEs and PEMFCs contain the same components, namely, porous electrodes, a polymer membrane, current collectors, flow fields, bus plates, end plates, separator plates, and manifolds. The only differences between the two are the materials of construction and the type of catalyst used in each process.

Typically, carbon materials are used in the fuel cells to support the catalyst and electrode structures. However, due to corrosion, these materials cannot be used at the anode of the electrolyser, and cathode of the fuel cell as oxygen is present. To overcome the possibility of corrosion at the anode, porous metallic components are used, as well as platinum or platinum alloy catalysts.

The design of PEMEs and PEMFCs consists of multiple components as described below:

- Membrane Electrode Assembly (MEA) – this is the heart of all PEMEs and PEMFCs. It contains the membrane and is sandwiched between two electrodes (anode and cathode). The MEA enables the transfer of protons from the anode to the cathode, prevents the crossover of gases between the electrodes (ensuring high purity gases produced) and provides electrical isolation. The electrodes contain various electrocatalysts.
- Bipolar plates - are used to conduct electricity and are impermeable to gases.
- End Plates - serve as the electrode supporting structures and are used to provide uniform pressure distribution between the cell components
- Current collector - placed between the bipolar plate and MEA. It is used to transport electrical current from the bipolar plate to the electrode surface whereby water is split. Additionally, it is used to transport the produced gases from the electrodes to the flow channels of the bipolar plates to be extracted from the cell.

For many decades PEMEs were used to produce oxygen in space, as well as underwater. However, in the last few years PEMEs have been researched and explored more comprehensively for renewable hydrogen generation.

In comparison to alkaline electrolysers and fuel cells, PEMEs and PEMFCs have many advantages such as (Siracusano *et al.*, 2012; Zhang *et al.*, 2012; Dedigama *et al.*, 2014; Abdin, Webb and Gray, 2015; Han *et al.*, 2017; Habermeyer and Kurkela, 2018):

- Simple and compact design
- Absence of hazardous chemicals (no recirculation of caustic soda)
- High hydrogen purity (>99.99%) in electrolyser
- Excellent response to variable electricity input
- Higher current densities
- Fast charging and discharging

The key disadvantages of PEMEs and PEMFCs include the following (Schmidt *et al.*, 2017):

- Less mature than alkaline electrolysers and can only be used currently for small-scale operations
- Platinum and fluorinated materials used as catalysts are expensive
- High system complexity as a result of high-pressure operation
- Shorter lifetime compared to alkaline electrolysers
- Sizing variations due to intermittent energy supply

PEMEs contain two electrodes known as the anode and cathode. The anode splits water into oxygen, electrons, and protons at the anode of an electrolyser, by applying a direct current through the cell.

Present studies of hydrogen production through PEMEs have been extensively used in pilot plants and under laboratory-scale operations (<200kW), with a few electrolysers being commercialised (Grigoriev *et al.*, 2010). Future development and maturity in the technology used in the PEMEs and PEMFCs will improve efficiencies, lifespan, and costs. Table 2.1 shows the predicted lifetime of the PEME from 2017 to 2030.

Table 2.1: Predicted Lifetime of a PEME (Schmidt *et al.*, 2017)

System Lifetime (Hours)	2017	2020	2030
Minimum Lifetime	20,000	50,500	66,125
Maximum Lifetime	60,000	67,481	85,018

PEMEs may be operated as a single cell or may be operated as a stack, which is comprised of multiple cells. Therefore, based on the 'scale effect', the cost of the system is directly related to the size of the system. Increased operating temperatures of the PEME results in a reduced electrical energy input (Babic *et al.*, 2017). Pressurised systems allow PEME to reach temperatures above 100℃ while water remains in its liquid state. However, issues are encountered with the stability of the materials at temperatures above 100℃ (Habermeyer and Kurkela, 2018).

Applications for PEMEs include the following (Choi, Bessarabov and Datta, 2004; Görgün, 2006; Siracusano *et al.*, 2012):

- Oxygen for life support
- Military applications
- Space applications - onboard rocket fuel production
- Laboratory gas separators
- Sustainable energy systems
- H_2 corrosion control
- Gas chromatography sensors
- Metal formation and welding

2.8.3 Solid- Oxide Electrolysers and Fuel Cells

Solid oxide electrolysers (SOEs) were first developed in 1902 by Nerst, who used ZrO_2 with a 15% Y_2O_3 high-temperature electrolyte (Laguna-Bercero, 2012). Since then, SOE technology has been undergoing extensive research and development for commercial use but is still the least developed technology compared to alkaline and PEM technology. SOEs and solid oxide fuel cells (SOFCs) are generally operated at high temperatures (800℃-1000℃) and has been found to exhibit higher conversions and lower energy consumption rates. Operating at elevated temperatures reduces the electricity demand (cell voltage), and simultaneously increases the heat demand. In theory, an electrical efficiency of above 100% is achievable when these electrolysers are operated in endothermic mode. Furthermore, high-temperature electrolysers were found to attain higher efficiencies than low-temperature electrolysers due to the reduced electrical energy required by the water dissociation reaction(Habermeyer and Kurkela, 2018).

In SOEs, hydrogen and oxygen are produced by feeding water in the form of steam to the cathode. The oxygen ions migrate from the cathode through a solid ion-conducting ceramic electrolyte, Yttria-stabilised Zirconia (YSZ), to the anode to produce oxygen (Schmidt *et al.*, 2017). The catalyst used at the anode is a Perovskite-type lanthanum strontium manganese (LaO.8Sr0.2mNo3) stabilised on YSZ, and the catalyst used at the cathode is a Ni/YSZ catalyst (Habermeyer and Kurkela, 2018).

Key advantages associated with SOEs and SOFCs include (Schmidt *et al.*, 2017):

- High electrical efficiency
- Ability to operate in reverse mode (electrolyser/fuel cell mode)
- Low material cost

Although SOEs are capable of achieving high efficiencies due to the lower electrical energy required, and higher temperatures which cause lower internal resistances, some of the disadvantages include:

- Impure product stream consisting of hydrogen and steam- this results in further processing which increases the investment and operating costs
- The system is not very flexible when there are variations in load due to the temperature changes. This reduces the lifetime of the electrolyser and fuel cell. The lifetime is reduced as a result of microcracks present on the ceramic (Habermeyer and Kurkela, 2018)
- Start-up time occurs over several hours (Mathiesen *et al.*, 2013)
- Higher capital costs than alkaline and PEMEs
- Shorter lifetime compared to PEMEs
- Membrane degradation due to operation at elevated temperatures

In comparison to alkaline and PEMEs, SOEs are not restricted to converting H_2O to H_2, the SOE is capable of operating with a CO_2 feed or a mixture of CO_2 and H_2O. Figure 2.6 graphically illustrates the schematic diagram of an SOE.

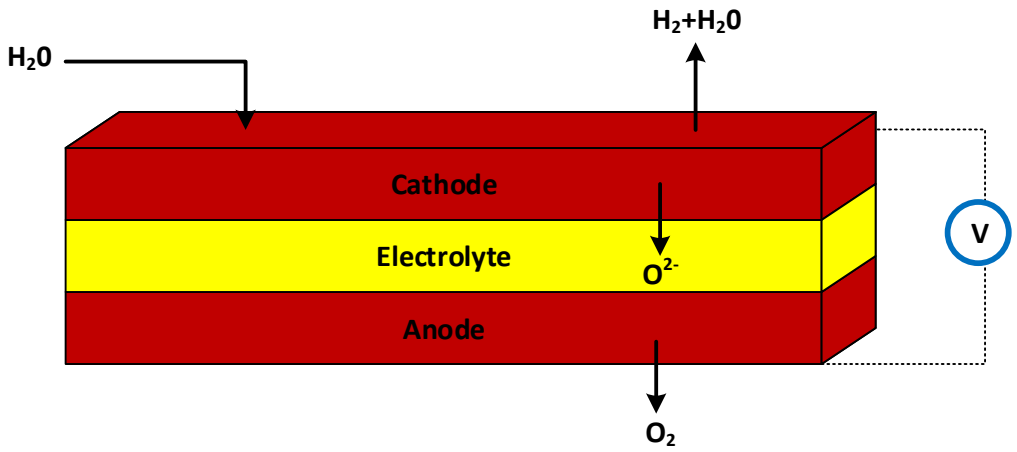

Figure 2.6: Schematic Diagram of a Solid-Oxide Electrolyser (Laguna-Bercero, 2012)

2.9 Seawater Electrolysis

Seawater is a solution of salts, organic and inorganic substances which are dissolved in water, and is the most common source of water found naturally on earth. Oceanic water or seawater plays a pivotal role in managing climate across the globe. It has a constant composition and contains more than 70 different elements. However, only 6 elements make up >99% of the solution. Table 2.2 summarises the composition of the 6 main elements that make up seawater.

Table 2.2: Composition of Seawater (Badea, Caraban, *et al.*, 2007)

Element	Composition (wt. %)
Chloride Ions (Cl^-)	55.04
Sodium Ions (Na^+)	30.61
Sulphate Ions (SO_4^{2-})	7.68
Magnesium Ions ($Mg^{2+)}$	3.69
Calcium Ions (Ca^{2+})	1.16
Potassium Ions (K^+)	1.10
Other	0.72

To produce hydrogen renewably, water electrolysis is considered. Unfortunately, the availability of freshwater in many countries is limited due to the effect of global warming. Thus, seawater electrolysis provides merit from an environmentally sustainable perspective. Table 2.3 below expresses the advantages and disadvantages of seawater electrolysis (Badea, Caraban, *et al.*, 2007; Mohammad and Kaukhab, 2011).

Table 2.3: Advantages and Disadvantages Associated with Seawater Electrolysis

Advantages	Disadvantages
Inexhaustible	Energy-intensive
Accessible around the coastal regions	Precipitation of magnesium hydroxide and calcium carbonate on the cathode
Environmentally friendly	Evolution of chlorine-may be toxic
Produces hydrogen	Presence of other minerals can cause unforeseen problems in the investigation

2.9.1 Seawater Electrolysis Methods

There are two main types of seawater electrolysis (Abdel-Aal, Zohdy and Kareem, 2010), namely the direct and the indirect method.

In the indirect method, a two-step process is followed and involves complete removal of the ions dissolved in seawater, followed by alkaline electrolysis, or hydrolysis to produce hydrogen and oxygen as the main products. This method requires additional capital costs to produce distilled water and causes environmental problems due to the disposal of salt. Despite these disadvantages, the indirect method favours the promotion of using the well-established commercialised freshwater electrolysis technology.

The direct method is a one-step process which directly converts seawater to hydrogen and chlorine as the main products. However, caustic soda may also be formed in some instances. Some drawbacks of using this method include the occurrence of electrode corrosion, contamination problems and the evolution of undesirable chlorine. Despite these shortcomings, the direct method offers lower capital costs, recovery of metals from seawater and the elimination of brine through natural means.

The chlorine produced at the anode may be:

- Dissolved into the ocean
- Collected and sold as a commercial product
- Suppressed by optimising the electrodes

2.9.2 Basic Chemistry of Electrolysis

Electrolysis of water is the process of splitting a water molecule into hydrogen and oxygen. This is achieved by passing an electric current through the electrolyte. An electrolyte is a solution used to conduct electricity. In an electrolysis cell, a pair of electrodes are immersed into the electrolyte which contains dissolved water. A diaphragm or membrane is generally used to separate the products formed at the anode and the cathode.

In freshwater hydrogen/oxygen is produced in a 2:1 ratio when used in electrolysis. Consequently, in seawater electrolysis, hydrogen/chlorine is produced in a 1:1 ratio (Hussein, 1992). Based on the study conducted by (Bennett, 1980), it had been concluded that the production of chlorine is promoted at a current density in the range of 1-1000 mA/cm^2.

If seawater electrolysis is to be considered for hydrogen production, oxygen evolution should be promoted at the anode over chlorine evolution. This is due to the excessive amounts of chlorine that will be generated which will exceed the market demand (Kuang *et al.*, 2019). Reactions (2.2)-(2.4) describe the reactions that occur at the electrodes during seawater electrolysis (Bennett, 1980; Badea, Caraban, *et al.*, 2007; Amikam, Nativ and Gendel, 2018).

Hydrogen evolution at the cathode:

$$2H_2O + 2e^- \rightarrow H_2 + 2OH^- \quad (2.2)$$

Oxygen or chlorine evolution at the anode:

$$6H_2O \rightarrow O_2 + 4H_3O^+ + 4e^- \quad (2.3)$$

$$2Cl^- \rightarrow Cl_2 + 2e^- \quad (2.4)$$

To determine the appropriate conditions to ensure that oxygen evolution takes precedence over the chlorine evolution reaction, the electrolyser should be operated either below 1 mA/cm^2 or above 1000 mA/cm^2. However, practically operating the electrolysis system below 1 mA/cm^2 would result in large electrode areas, making the electrolyser impractical. Furthermore, using current densities greater than 1000 mA/cm^2 would result in greater energy required which would result in higher operating costs. Alternatively, implementing electrocatalysts or selecting electrodes constructed from a material that inhibits the evolution of chlorine, and favours oxygen evolution should be endorsed. Furthermore, coating the anode with a cationic exchange membrane material to suppress chlorine evolution at the anode may also be used.

In the early 1980s, Bennet (1980) conducted a study to examine the variables and conditions that affect the evolution of chlorine and oxygen in seawater electrolysis. That work also proposed techniques to enhance the selectivity of oxygen evolution over chlorine. Based on that work, the oxygen evolution reaction was found to be thermodynamically favoured at the anode and had a lower equilibrium potential compared to chlorine. However, the chlorine evolution reaction is simpler compared to the oxygen evolution reaction, and this generally promotes the generation of chlorine instead of oxygen at the anode.

2.9.3 Challenges Associated with Seawater Electrolysis

Despite seawater electrolysis being highly favourable as a source for renewable hydrogen production, there are a few drawbacks which need to be addressed. The main bottleneck hindering the development and commercialisation of seawater electrolysis include the evolution of undesirable chlorine, cathode precipitation and corrosion at the anode. Under normal seawater electrolysis operation, a large quantity of undesirable chlorine will be generated in the large-scale production of hydrogen.

Discharging brine from the electrolysis of seawater into the ocean may cause inherent harm to marine ecosystems due to the increase in temperature of the water, as well as an increase in the salinity of the water compared to the salinity of natural seawater. To put this into perspective, reverse osmosis plants typically discharge brine at 1.3-1.7 times the concentration of natural seawater (Shim, Jeong and Park, 2017). Consequently, chlorine has been identified as toxic and harmful to humans and animals. According to EPA, chlorine cannot be directly released into the environment without being pre-treated. Chlorine can cause acute effects in animals and humans at low concentrations of 0.014 ppm. Additionally, at high concentrations of 46 ppm, human and animal health may be affected by toxic pneumonitis and pulmonary edema. Additionally, converting the chlorine back to chlorides is an expensive process to pursue (Bennett, 1980)

Precipitation at the cathode occurs due to the formation of insoluble precipitates on the surface of the cathode. This is due to the presence of Mg^{+} and Ca^{+} ions in seawater which results in fouling, reduced electrode active surface area which leads to higher overpotentials, and additional power required for the generation of hydrogen (Badea, Caraban, *et al.*, 2007). The precipitation reactions of Ca^{+2} and Mg^{+2} are described in Equation (2.5) and Equation (2.6).

$$Ca^{+2} + OH^{-} + HCO_3^{-} \rightarrow CaCO_3 + H_2O \tag{2.5}$$

$$Mg^{+2} + 2OH^{-} \rightarrow Mg(OH)_2 \tag{2.6}$$

Calcium carbonate was found to form at a lower pH than magnesium hydroxide. Generally, magnesium hydroxide forms at the cathode surface when the pH is greater than 9, but Kirk (1982) and Bennett (1980) had specifically reported the formation of magnesium hydroxide occurs at a pH of 10.7 and 11, respectively. On the account of the synthesis of magnesium hydroxide at the cathode, the electrode gap may become clogged. To minimise the formation of calcium carbonate and magnesium hydroxide precipitation, the turbulence of the seawater may be increased, the correct current density must be applied, and an adequate cathode surface must be selected (Hussein, 1992).

Moreover, in the electrolysis of seawater, the anode is susceptible to corrosion due to oxidation. A linear relationship is present between the current supplied to the electrolysis cell and corrosion. In electrolysis, corrosion may not only take the form of rust, but the anode may develop cracks and lose strength. In addition, the process of electrolysis is hindered by the presence of salts and impurities. These impurities may foul the catalyst present, resulting in catalyst deactivation, as well as damage and blockage in components of the system. As a result, the performance of the electrolyser may be reduced due to higher voltages required and reduced efficiencies in the electrolyser.

2.9.4 Disposal and Uses of Chlorine, Brine and Sodium Chloride

To deal with the evolution or presence of chlorine in the process of seawater electrolysis, several disposal and handling methods may be implemented. This includes (Bockris, 1976):

- Performing electrolysis and storing chlorine deep within the ocean. The chlorine evolved may be reacted with alkali hydroxides and released into the ocean.
- Collecting chlorine at the surface of the ocean and reacting it with water at a temperature of 650℃. This method imposes additional costs in the production of hydrogen.

- If chlorine gas production at the anode is eliminated through the evolution of oxygen, chlorine will leave the system as a liquid with brine. The discharged product will have a higher salinity compared to the salinity of seawater.

In the event that chlorine is present as a liquid, it will be converted to hypochlorite which is preferred compared to chlorine gas. Hypochlorite may be used as an anti-fouling agent in coastal power stations and ships, to inhibit the growth of micro-organisms which damage equipment. It may also be used in to sterilise wastewater (Bennett, 1980). Moreover, it may be safely disposed of into the environment as a non-toxic compound. Although chlorine is found to be very toxic, it is used in many applications, such as disinfecting water, treating wastewater and sewage, as well as industrial effluent streams.

Any sodium chloride and oxygen formed may be sold off into the market. Sodium chloride is used in industrial plants to protect the equipment against organic fouling. As opposed to the use of commercial hypochlorite, sodium hypochlorite prevents the build-up of hard deposits when alkaline substances are dissolved in water. Furthermore, the risks of transporting, storing and handling chlorine are eliminated when sodium hypochlorite is present (De Nora, 2015).

Conventionally, waste brine produced from desalination processes may be used to produce an economical material used in the construction industry. The brine undergoes a process of electrolysis to facilitate its conversion into an alkaline solution, which serves as an alkali activator (Shim, Jeong and Park, 2017).

2.9.5 Performance Studies

Over recent years, several performance studies have been conducted for seawater electrolysis to determine the viability, efficiency, and use of effective electrodes and catalysts to promote H_2 and O_2 evolution. More specifically, Abdel-Aal et al. (2010) presented an experimental study to determine the rate of hydrogen and chlorine evolution from the electrolysis of seawater. El-bassuoni et al. (1982) reviewed the production of hydrogen and investigated an electrochemical method, to simultaneously produce hydrogen and freshwater from seawater. That system included a set of electrodes and selectively permeable membranes. When a direct current was applied to the seawater, cations migrated towards the cation and passed through the cation-selective membrane where it had been trapped. Similarly, the anions migrated towards the anion and passed through the anion-selective membrane, where the anions were trapped. It had been observed that as the seawater salinity increased, more electrical power was required. Additionally, it has been found that an increase in the concentration of brine resulted in a decrease in the resistance of the cell, and a decrease in the coulombs required.

Badea et al. (2007) investigated the amount of energy consumed and the electric tension for the electrolysis of seawater obtained from the Black Sea in Constanta, Romania, and compared it to a solution of 15% $NaOH$. The two samples (seawater from the Black Sea and the 15% $NaOH$ solution) were exposed to the same conditions. The seawater electrolysis cell used in the experiment contained a graphite anode and a stainless-steel cathode. The results showed that electrical tension was dependent on current density. Seawater had a higher electrical tension and smaller conductivity than the sodium hydroxide mixture, therefore, leading to a higher energy consumption rate. Additionally, it had been concluded that operating the electrolysis cell at elevated temperatures, reduced the electrical tension, increased the conductivity of seawater and ultimately reduced the overall quantity of energy consumed.

In 2015, Hsu et al. (2015) investigated the effect of process conditions of deep ocean water (DOW) on the generation of chlorine and storage stability. The results showed that a small electrode gap reduced the required cell potential to electrolyse seawater, thus, resulting in higher energy efficiencies. Moreover, the optimal electrode distance was found to be dependent on the concentration of chlorine in DOW.

Another study performed by Hsu et al. (2017) was conducted to study the effect of electrolysis time and cell potential on the efficiency of chlorine generation in DOW. Results showed that current density was significantly affected by the potential of the cell, whereas time was not as significant. Additionally, the temperature of the electrolyte increased as the cell potential increased, whilst time had no effect. This increase in temperature was largely dependent on the conversion of electrical energy into heat and the dissipation of heat to the electrolyte from the electrodes. Additionally, current efficiency was found to be significantly affected by the electrolysis time.

More recently, Srisiriwat and Pirom (2017) conducted a feasibility study on the electrolysis of seawater for a photovoltaic-fuel cell (PV/FC) hybrid system. An experiment was performed to investigate the parameters of the system when a 10kW fuel cell was used. Based on that work, the production rate of hydrogen generated in the electrolyser could be determined, as well as the rate of hydrogen consumption in the fuel cell. The PV/FC hybrid system contained PV arrays, a seawater electrolyser, hydrogen storage and a fuel cell. According to the results from that work, hydrogen from the seawater electrolyser was produced at a rate of 1 litre.hr^{-1} with a 9.6 W power demand, and an efficiency of 41.7% was achieved. The seawater electrolyser was operated at 26℃ and required an input voltage of 3V.

Moreover, that study showed that technical challenges evolved in the PV/FC hybrid system when the cost, safety, storage, efficiency and production in real-time was considered. Srisiriwat and Pirom (2017) had proposed to later obtain an optimal design of the system they had experimentally developed in 2017. This system was proposed to be simulated into HOMER (Hybrid Optimisation Model for Electric Renewable) as future work.

2.9.6 Seawater Electrolysis Electrocatalysts

Conventionally, in seawater electrolysis, platinum has commonly been used in the production of hydrogen. However, platinum catalysts were found to be expensive and less abundant. This led to the exploration of alternative electrocatalysts to make seawater electrolysis more feasible. Iridium oxide and Ruthium oxide electrocatalysts are typically used commercially but were found to have high costs and had insufficient stabilities over long periods of time for large scale operation (Hsu *et al.,* 2018). As such, transition metal carbides such as tungsten carbide (WC) and molybdenum carbide (Mo_2C) have been explored and were identified as suitable substitutes to platinum catalysts, due to their similarity in behaviour, activity levels and stability properties to that of platinum.

Liu et al. (2015) developed a nickel molybdenum sulfide anode catalyst for seawater electrolysis. The catalyst was found to decrease the voltage required to produce hydrogen, and promoted hydrogen and oxygen evolution, as well as suppressed the evolution of chlorine.

In 2017, an experimental study was conducted by Ma et al. (2017) to identify a highly efficient low-cost and stable electrocatalyst for the evolution of hydrogen. A cobalt molybdenum phosphide nanocrystal (CoMoP@C) electrocatalyst coated with layers of N-doped carbon shells was demonstrated, as an adequate alternative catalyst for the hydrogen evolution reaction (HER). Results indicated that the catalyst exhibited outstanding performance with regards to the HER, and showed superior stability compared to platinum/carbon (Pt/C) electrocatalysts.

The catalyst also demonstrated a high Faraday's efficiency of 92.5%. The superior stability of the CoMoP@C electrocatalysts was due to the presence of the N-doped carbon shell, which protected the electrocatalyst against agglomeration, etching, and poisoning (due to interactions with the transition metal ion). Additionally, the activity performance of the CoMoP@C catalyst was greater than Pt/C electrocatalysts in seawater. This was due to the layer of protection provided by the N-doped carbon shell.

In a different study, Cheng et al. (2017) investigated the use of a Co-Fe layered double hydroxide (Co-Fe LDH) electrocatalyst for the oxidation of seawater under near-neutral conditions. It had been concluded that the Co-Fe LDH electrocatalyst loaded onto a titanium mesh electrode exhibited high activity, good stability and durability for the oxygen evolution reaction (OER) at moderate overpotentials, in the presence of seawater only. No additional buffered electrolytes were required. Moreover, the catalyst proposed was low-cost and did not contain any noble metals. Therefore, exhibiting properties for practical application in seawater electrolysis.

Lei et al. (2018) studied the electrochemical activity and stability of a nano-tungsten carbide composite electro-catalyst (AuPdPt-WC/W) in seawater for the HER. The AuPdPt-WC/C nanocomposite catalyst was prepared via a direct chemical reduction method. The study evaluated the electrochemical activity and the stability of the prepared catalyst in simulated seawater solution. From the experiment, it had been found that as pH was increased, the electrolysis current had decreased. It had also been concluded that as the temperature of the electrolyser was increased, the currently density also increased. Furthermore, the AuPdPt-WC/W nanocomposite catalyst had better stability properties compared to commercial Pt/C electrocatalyst.

In 2018, Hsu et al. (2018) carried out an experimental study on a highly efficient electrocatalyst fabricated from earth-abundant elements to favour the oxygen evolution reaction (OER). In that study, metal hexacyanomettalates (MHCM) were introduced and were constructed into a core-shell nano-architecture in which the core was made of basic cobalt carbonate (BCC). The MCHM-z-BCC catalyst was used with a NiMoS electrocatalyst for the production of hydrogen and oxygen from seawater. Experimental results indicated that the MHCM-z-BCC and NiMoS catalysts achieved a nearly 100% faradaic efficiency for oxygen and hydrogen production. Additionally, the MHCM-z-BCC electrocatalyst showed good stability, negligible degradation, and no traceable quantities of chlorine was generated. The electrolyser was powered by a photovoltaic cell and achieved an overall of 17.9% solar-to-hydrogen efficiency.

In a similar study, Yu et al. (2019) presented an experimental study on a 3-D core-shell metal nitride catalyst which was constructed from NiFeN nano-particle on NiMoN nanorods supported on nickel foam. The proposed NiMoN@NiFeN electrocatalyst was investigated to promote the OER and was used in an alkaline seawater electrolyser. It had been combined with a NiMoN electrocatalyst for the evolution of hydrogen. The electrolyser attained current densities of 500 and 1000 mA/cm^2 at voltages of 1.608 and 1.709V. The two-electrode electrolyser was operated at a temperature of 60℃. Excellent durability was exhibited and illustrated significant development for large-scale production of hydrogen and oxygen from the electrolysis of seawater. The above study was similar to the experimental study conducted by the Hsu et al. (2018), in which a core-shell structure was used for the OER electrocatalysts. However, the OER and HER electrocatalyst used were different. Hsu et al. (2018) used an MCHM-z-BCC and NiMoS for the OER and HER electrocatalysts, respectively, whereas Yu et al. (2019) used a NiMoN@NiFeN and a NiMoN for the OER and HER electrocatalysts, respectively. Both studies proposed electrocatalysts that were highly efficient, durable, had good stability and good conductivity, and could be attained at low-cost.

2.9.7 Oxygen Evolution Electrodes

Previously in the chlor-alkali industry, ruthenium-titanium dioxide/titanium anode had been developed for the evolution of chlorine at low current densities. This, however, required large anodes. As a result of the impracticality of utilising these electrodes, research moved towards developing oxygen selective electrodes. High current densities were achieved in the evolution of hydrogen from the direct electrolysis of seawater in a non-diaphragm cell. Typically, chlorine is generated at the anode in the form of sodium hypochlorite and is the dominant reaction under normal conditions where seawater electrolysis, reaction kinetics, and mass transfer limitations play a major role in promoting the evolution of chlorine.

To promote oxygen evolution, electrodes coated with manganese dioxide have been used and are capable of achieving a 99% efficiency in seawater (Bennett, 1980; Abdel Ghany *et al.*, 2002; El-Deab *et al.*, 2007). The reason for this selectivity towards oxygen is uncertain but may be due to the diffusion barrier layer of the MnO_2 film which limits the movement of chloride ions.

Fujimura et al. (1999) investigated the evolution efficiency of oxygen when a manganese-molybdenum oxide anodic electrode was used. In a similar study, El-Moniem(2011) presented a study on an Mn-Mo-W electrode deposited on a Ti/IrO_2 net to promote the OER. A two-compartment electrolyser and current density of 100 mA/cm^2 was used. The results reported that an efficiency of 99% was achieved.

Balaji et al. (2009) dedicated their research towards promoting the evolution of oxygen, whilst suppressing the evolution of chlorine in the electrolysis of seawater. In that study, an electrostatic repulsive force was applied to prevent chloride ions from gaining access to the electrode surface. This was achieved by introducing a cation-selective coating (perfluorosulfonic acid membrane) to the electrode surface. Iridium oxide-coated titanium anodes, Nafion solution-coated iridium oxide titanium ($NS/IrO_2/Ti$) anodes and Nafion membrane-coated iridium oxide titanium ($NM/IrO_2/Ti$) anodes were compared.

It had been found that the IrO_2/Ti electrode operated at a higher current density than the NS/IrO_2/Ti and NM/IrO_2/Ti. This was due to the gas evolution resistance offered by the polymer film on the electrode surface. Additionally, the oxygen evolution efficiency was greater in both NS/IrO_2/Ti and NM/IrO_2/Ti, compared to the IrO_2/Ti electrode which exhibited an oxygen evolution of 28.7% at 100 mA/cm^2. This could have been attributed to the mass transport limitations of the chloride ions and the availability of water for oxygen evolution (since water was readily available, oxygen evolution increased). Furthermore, due to the presence of microcracks and the surface morphology of NS/IrO_2/Ti, a lower oxygen evolution efficiency and higher current density was observed compared to NM/IrO_2/Ti. This was due to the transfer of chloride ions that had been transported to the electrode surface through the cracks. Consequently, the NM/IrO_2/Ti anode was found to be uniform, did not contain cracks and only facilitated the transport of water.

Similarly, to the research conducted by Balaji et al. (2009), Ravichanran et al. (2011) focused their research on employing selectively permeable electrodes, constructed from a material that was cationically selective towards oxygen evolution in the electrolysis of seawater. Sulfonated polystyrene-block-(ethylene-ran-butylene)-block-polystyrene (SPSEBS) membrane on an IrO_2 electrode were used to repel chlorine ions for the electrolysis of seawater. This was achieved by using electrostatic repulsive forces to prevent chloride ions from interacting with the anode surface. The results showed that the SPSEBS/ IrO_2/ Ti electrode hindered the transport of chloride ions, whilst water was allowed to be transported through the SPSEBS film and was oxidised at the anode to produce oxygen. As a result, a 95% oxygen efficiency was achieved, compared to an oxygen efficiency of 25.6% when an IrO_2/Ti electrode was used at a current efficiency of 100 mA/cm^2. An oxygen evolution of 100% could not be achieved due to the morphology of the SPSEBS electrode, which had a lower mechanical strength and formed micro-cracks during the process of seawater electrolysis.

Mohammad and Kaukhab (2011) investigated the use of sulfur electrodes and sulfur powder to promote the evolution of oxygen, by preventing the evolution of chlorine and formation of magnesium hydroxide precipitation on the cathode. Furthermore, they had investigated the formation of H_2SO_4 in an exploratory experimental study. In that study, a $MgCl_2$ solution was used to represent seawater, and platinum, graphite and carbon-felt electrodes were used with either sulfur powder or sulfur electrodes. A single-compartment cell and a double-compartment cell were used. The results from the exploratory experimental study showed that when sulfur powder was introduced into the anode compartment and stirred, the powder remained afloat on the surface of the solution. Hence, the sulfur electrode was found to be a more practical and an efficient alternative in the prevention of magnesium hydroxide precipitation. The double-compartment cell was found to be inefficient because the sulphuric acid took longer to diffuse through the frit and into the cathode compartment. Additionally, whilst this was occurring, $Mg(OH)_2$ was being deposited onto the cathode. Therefore, it had been concluded that the single-compartment cell was more practical. Consequently, it had been reported that both sulfur powder and the sulfur electrodes were both favourable in preventing the formation of $Mg(OH)_2$ and evolution of chlorine.

In a more recent study, Kuang et al. (2019) developed a hierarchical anode with corrosion-resistant and oxygen evolution properties. The anode was fabricated from a nickel-iron hydroxide electrocatalyst coated uniformly on nickel sulfide layer which had been developed on porous nickel foam. According to the results obtained, the nickel-iron electrocatalyst was highly selective towards the OER. The electrolyser developed was found to be highly stable and corrosion-resistive and experienced no degradation or activity loss when subjected to a 1000 hr stability test.

Yan et al. (2019) conducted an investigation on improving the O_2 evolution efficiency and stability of various transition metals such as manganese, manganese+molybdenum, manganese+molybdenum+vanadium and manganese+iron+vanadium oxide coated electrodes, that were prepared on a titanium substrate, and contained an iridium dioxide (IrO_2) intermediate layer. The experiment was carried out at a temperature of 90 ℃ in a simulated seawater solution. According to the results obtained, the manganese oxide electrode exhibited the lowest oxygen efficiency of 42.27%, whereas the highest efficiency was presented in the manganese+molybdenum+vanadium oxide electrode (99.78%) and the manganese+iron+vanadium oxide electrode (99.99%) at 1000 A/m^2. This indicated that the addition of vanadium, molybdenum and iron improved the morphology of the electrode and crystal structure, as well as enhanced the efficiency of oxygen evolution.

2.9.8 Seawater Electrolysis Models

In contrast to all the experimental work, Yang et al. (2019) presented a performance model for seawater electrolysis in an undivided cell (no membrane between anolyte and catholyte). Semi-empirical models were developed for current density, cell voltage, total residual oxidant and energy consumption. This included a current efficiency model, total residual oxidant (TRO) model, energy consumption model and a cell voltage model. The effects of varying current density and the salinity of seawater on the electrolyser performance had also been investigated. Additionally, it had been observed that increasing the current density, increased the total residual oxidant (TRO) concentration, as well as the voltage of the cell. The effect of salinity on the performance of the cell indicated that increasing the salinity of seawater, increased the TRO concentration, whereas the cell voltage decreased.

This was due to the electrolyte conductivity and the electrode reaction kinetics. It should be noted that although some work has been conducted in modelling the performance of a seawater electrolyser, the above-mentioned model was limited to seawater electrolysis in an undivided cell. Additionally, the model did not take into account diffusion overpotential, and optimisation of the seawater electrolyser was not performed.

2.10 Types of Mathematical Models

In recent years various types of models have been developed to predict the performance, reproduce the behaviour of real systems and investigate the balance of the PEME and PEMFC systems operated in either steady-state or dynamic state. Moreover, the models found in literature vary in levels of complexity based on the type of model presented. As such, analytical, empirical and semi-empirical have been formulated.

Analytical models are effective in illustrating the effect of different variables on electrolyser and fuel cell performance through simplified physical law equations and are associated with a physical meaning. However, some equations may be computed and correlated to empirical equations.

Empirical models are useful in predicting the behaviour of the electrolyser and fuel cell, as a function of pressure and temperature through empirical equations. These models are restricted to a range of operating conditions in which they have been studied and can only be applied for that specific design. Moreover, these models are dependent on parametric equations, and the parameters obtained from the model do not contain any physical implications. Semi-empirical models can be validated and provide a basis for quick modelling and engineering applications.

Mechanistic models are theoretical models that are dependent on the electrochemistry, fluid dynamics and thermodynamics of s system. Typically, these models are solved through various numerical methods and are comprised of algebraic and differential equations. These equations are acquired from the electrolyser and fuel cell electrochemical phenomena. Mechanistic models provide accurate predictions due to the extensive calculations performed, resulting in long computational times, and are usually difficult to validate.

Additionally, depending on the purpose of the model; steady-state and dynamic models have been reported. Dynamic models may be further broken down into static models which are derived from lumped parameter models that are based on ordinary differential equations, algebraic equations, and distributed parameter dynamic models which contain Partial Differential Equations (PDEs).

2.11 PEM Electrolyser Models

Due to the dynamic issues associated with connecting an electrolyser to an intermittent electrical source such as PV-arrays, modelling is an important tool to use for understanding the transport phenomena and electrochemical behaviour, sizing the equipment, applying adequate control and optimising the system.

An appropriate way of understanding the phenomena of water electrolysis is to perform experimental studies on the electrolysis cell, and analyse the data received. However, this process is time-consuming, and expansion towards using computational methods such as, modelling has been promoted. Modelling supports the investigation into the design of the system, as well as the effect of different operating conditions and design parameters on the performance and durability of the cell. Ultimately, saving time, effort and experimental costs. The development of computational electrolysis modelling began in the 1990s; however, this had been limited to alkaline technology. It was only in the early 2000s when computational modelling of PEME technology was initially explored (Olivier, Bourasseau and Bouamama, 2017). Numerous models have been developed based on the objectives that need to be achieved, and the approaches followed will determine the multi-physics and dynamic considerations that need to be taken into account. Although, PEME modelling has developed at a fast pace, it is not as developed as the state of the art of PEMFC models. As a result, an extensive literature review was conducted by Falcão and Pinto (2020) on the various types of models that have been developed to predict the performance of a PEME.

2.11.1 Zero-Dimensional Models

Since research into PEME modelling is a newly explored field; it is not surprising that work in the comprehensive modelling of PEM water electrolysis is scarce. Zero-dimensional (O-D) and one-dimensional (1-D) models formed the early modelling approaches followed and were steady-state, isothermal, approximation models. Typically, 0-D models are used to investigate the Butler-Volmer electrode kinetics and ohmic overpotential present in the PEME. However, it should be noted, that these models neglected the effects of mass transport (Ojong *et al.*, 2017).

A simple O-D analytical solid polymer electrolyte membrane model was developed by Choi et al, (2004). The above-mentioned model was based primarily on the Butler-Volmer kinetics and membrane transport resistances. The cell voltage was calculated from the summation of the activation overpotential, ohmic overpotential and open-circuit voltage (OCV). A relationship between the applied terminal voltage and the current density was established. The model proved that the cathode reduction kinetics were relatively fast, whilst the anodic overpotential contributed largely to the voltage drop. IrO_2 was added to platinum (Pt) and the evolution of oxygen at the anode occurred at a reduced cell potential. This indicated better cell potential, as well as efficiencies. Additionally, it had been established that the aforementioned model did not consider the diffusion overpotential, as it had been assumed that there were no mass transport limitations.

Similarly, Ni et al (2006) developed an electrochemical model to analyse the relationship between current density and voltage in PEMEs. The model took into account the OCV, activation overpotential, and the ohmic overpotential in the form of a parametric analysis but did not evaluate the effect of the diffusion overpotential. This was due to negligible gas transport limitations present in thin electrodes operated under normal conditions.

The model found that between the activation overpotential and ohmic overpotential, activation overpotential contributed significantly to the overall voltage loss. This was attributed to the slow kinetics of the anode oxidation reaction. This correlated with the results obtained from Choi et al. (2004) Additionally, it had been concluded that an increase in temperature resulted in a decrease in cell potential and therefore, electrolyser performance.

Marangio et al. (2009) presented a detailed 0-D, steady-state, theoretical electrochemical model to evaluate the characteristics of a PEME stack operated under high pressures. Gibbs free energy had been used to calculate the OCV subject to non-standard temperatures and pressures. The model investigated in detail the flow of water into the anode and cathode, water transport due to the concentration difference, pressure difference, electro-osmotic drag, and the water that had been consumed due to the chemical reaction. In addition, the ohmic overpotential term took into account the resistance caused by the electrodes, plates and the membrane. Results from that study indicated that temperature and pressure was significantly affected by the hydrogen ion diffusion coefficient and cathode exchange current density. Based on the results obtained from the model, temperature was found to be directly related to the cathode exchange current density. More specifically, the cathode exchange current density was found to increase with an increase in temperature. Correspondingly, this increased the hydrogen ion diffusion coefficient, which was linked to the membrane conductivity, and ultimately the ohmic overpotential. The model was limited to the traditional nafion membrane and neglected the effect of temperature on other membrane material. It should also be noted that the detailed evaluation of the electrostatic drag coefficient had not been conducted and that a numerical model could yield more accurate results.

2.11.2 Semi-Empirical Models

Among the various modelling approaches available for PEMEs, empirical and semi-empirical models are considered as one of the simplest approaches present. Semi-empirical models are based on physical laws and are obtained from empirical correlations, whereas empirical models are dependent on parametric equations obtained from experimental data that have been used to generate model parameters. Harrison et al. (2006) developed a 0-D, steady-state, semi-empirical model to determine the performance of a cell stack. The anode exchange current density, cathode exchange current density and membrane conductivity were attained from experimental data. Non-linear curve fitting methods were used to predict the relationship between current and voltage.

Similarly, Dale et al. (2008) developed a non-isothermal, semi-empirical model of a PEME that took into account the reversible cell voltage. Curve fitting methods were also used to determine the model parameters and fit the experimental results. The results indicated that a directly proportional relationship was present between the exchange current density and temperature.

In a different study Biaku et al. (2008) investigated the effect of temperature on the anode charge transfer coefficient through a semi-empirical model, whereas Santarelli et al. (2009) presented a 0-D, steady-state, non-isothermal, regression model to analyse the effect of temperature, water feed rate and pressure on the operation of the PEME.

In the works of Garćia-Valverde et al. (2012) an atmospheric electrochemical water PEME model was developed. The proposed model was divided into three sub-models, namely: the electrochemical model in which non-linear fitting and statistical analysis were used to investigate the effects on the polarisation curve. Secondly, a hydrogen production model was included, and lastly, a lumped thermal capacitance sub-model based on semi-empirical equations was presented.

Auxiliary cooling units were not modelled. The Arrhenius Equation was used to model the membrane conductivity and exchange current density. Furthermore, the aforementioned work was different compared to other literature, due to the incorporation of a dynamic model and lumped thermal capacitance model for the production of hydrogen.

Zhang et al. (2012) discussed and presented a mathematical model to determine the efficiency and design configuration of a PEME. The model was based on semi-empirical equations, and a thermal model was included to account for heat in the system. A thermodynamic-empirical model was developed to take into consideration the main energy consumption processes, as well as utilise waste heat produced. Results from that study demonstrated that increasing the operating temperature, increased the current density, decreased the inlet water flow rate and increased the efficiency of the PEME.

2.11.3 Dynamic Models

Dynamic models consider the intermittent behaviours of renewable energy and variable sources of power that may be used to power PEMEs. This inclusion significantly increases the complexity of the model, as these models use Ordinary Differential Equations (ODEs) or Partial Differential Equations (PDEs) to carry out system control analysis, sizing, and design of chemical and thermal processes. As such, in the works of Görgün (2006), the first dynamic PEME in MATLAB-Simulink was presented. That model was a 0-D model operated under isothermal conditions. The model was based on anode and cathode mole balances. It incorporated the transportation of water through the membrane, which was dependent on the electro-osmotic drag and diffusion. However, it should be noted that the model had not been corroborated with any experimental data, but the authors verified that the aforementioned PEME model could accurately describe and replicate the transient behaviour.

Awasthi et al. (2011) presented an analytical dynamic model that was operated under varying conditions to investigate the performance of a PEME. The model was simulated as a 0-D model in MATLAB/Simulink and had been divided up into four sections: anode, cathode, membrane and voltage section. That model also considered water transport through the membrane, and it had been observed that majority of the water transport across the membrane was due to the electro-osmotic drag. However, the model did not consider the transportation of water in detail and did not consider a thermal model.

In another study, Kim et al. (2013) demonstrated a high pressure, 1-D dynamic model of a water electrolyser. In that work, unsteady state mass and energy balance equations were considered. To simplify the model, the flow of water and gas were assumed to flow simultaneously. Moreover, it had been concluded that the proposed model was not validated with experimental data.

In the works of Lee et al. (2013) a dynamic control-oriented simulation model of a PEME was presented in Simulink. That work was based on an anode mole balance, cathode mole balance and Butler-Volmer kinetics. Additionally, the effects of temperature and water flow rate had been studied. The model neglected the flow of water through the membrane due to the pressure effect.

2.11.4 Atmospheric and High-Pressure PEM Electrolyser Models

In 2004, Onda et al. (2004) presented a study to investigate the electrical power required for the production of hydrogen under high pressure water electrolysis. In that study, electrolysis under atmospheric and high pressures were considered. It should be noted that the study did not take into account the effects of overpotential on cell voltage and performance. This was due to the limited experimental data available for water electrolysis under high pressure operation. According to the results obtained, at high pressures of 70 MPa, a power saving of up to 6% was achieved, as opposed to the compression of hydrogen after atmospheric water electrolysis was performed.

It had also been concluded that the output voltage decreased with increasing temperature and increased with increasing cell pressure. Ultimately, it was concluded that high-pressure water electrolysis saved more power than compressing hydrogen after atmospheric water electrolysis was carried out. This was applicable when hydrogen and oxygen are required to be stored and supplied at high pressures.

Saebea et al. (2017) proposed an electrochemical simulation model of a PEME operated at high pressures in the absence of a compressor. Hydrogen permeation was accounted for in the model. The effect of membrane thickness and cathode pressure had been evaluated and the electrochemical model was modelled into MATLAB. Unbalanced pressures between the anode and the cathode were applied. As a result, hydrogen was found to be transferred from the cathode side to the anode side, which reduced the electrolyser performance. The performance of the electrolyser was also found to decrease with increasing cathode pressure. This was mainly due to an increase in cell potential when the cathode pressure was increased. Additionally, it had been concluded that an increase in pressure, resulted in an increase in hydrogen concentration at the anode. This was due to the pressure gradient present between the anode and the cathode, which promoted the permeation of hydrogen from the cathode to the anode. This relationship was intensified at elevated pressures. Furthermore, electrolyser performance was improved by using thinner membranes when the electrolyser was operated under high pressure. However, hydrogen was found to permeate more easily through thinner membranes.

Lebbal and Lecoeuche (2009) proposed an electrical steady-state model integrated with a dynamic thermal model to investigate, identify and observe the efficiency and safety of a PEME. Model parameters had been identified through curve-fitting techniques obtained from experimental data. The model developed was based on electrochemical equations and physical laws. This included algebraic expressions between current, voltage and temperature. In the electrical model, parameters were identified using the non-linear least-squares method.

The algorithm presented was used to illustrate, detect and isolate faults on the electrolyser, actuators and sensors. Consequently, the model was also capable of avoiding electrode destruction, membrane dehydration and the melting of the membrane.

Ni et al. (2008) presented an integrated thermodynamic-electrochemical model to analyse the energy and exergy for hydrogen production in a PEME. The model investigated the design and operating conditions on the cell performance, as well as the production of heat. The results showed that as temperature increased, the thermal energy demand increased, whilst the electrical energy demand decreased. This translated to a reduced activation overpotential (due to increased exchange current density) and ohmic overpotential (due to increased membrane conductivity), and increased cell performance. The efficiency of the PEME was found to decrease with increased membrane thickness. This was due to higher ohmic overpotential. It should be noted that the limitations of the model included the exclusion of solar cells and wind turbine performance characteristics.

In the work of Dedigama et al. (2014), the effect of various overpotentials were analysed and presented in an electrochemical model. The model developed was a simple model and was based on species transport, mass balances and reaction kinetics which described the relationship between current and voltage. According to the model developed in MATLAB, activation and ohmic overpotentials were the dominating overpotentials present. Water flow rate due to the effect of pressure was not taken into account as pressure remained constant in the electrolyser. That work also assumed that the diffusion overpotential (mass transport limitations neglected) was negligible due to the cell being operated at current densities of up to 1 A/cm^2.

In addition, the results presented in the study aligned with the results obtained from Awasthi et al. (2011). Although that model was a dynamic model, the results revealed that the output voltage was controlled by the anode activation overpotential and that ohmic overpotential increased linearly with current density. Furthermore, the model presented by Dedigama et al. (2014) proved to be sensitive to cathode exchange current density, charge transfer coefficients and water diffusivity.

2.11.5 One-Dimensional Models

The work of Fritz et al. (2014) took into account the effect of the gas-phase on mass transportation in the development of a 1-D isothermal model. However, in that model, the special distribution of the dissolved gases and total gas phase volume had not been considered. Additionally, the model did not address heat and water management, and was limited to operations under $3A/cm^2$, limiting its application to industrial hydrogen production.

Chanderis et al. (2015) developed a 1-D numerical model to analyse the effect of temperature and current density on the degradation of the proton exchange membrane. They concluded that the degradation of the membrane was worse at the cathode and temperature had a significant impact.

Han et al. (2015) developed a comprehensive 1-D, computational, ohmic loss model of a PEME to determine the influence of varying operating conditions, and design parameters on the performance of the cell. This included investigating the effects of operating temperature, pressure, electrode thickness, membrane thickness, exchange current density and internal resistance on the performance of the electrolytic cell. Results from the study emphasised that internal resistance between the electrode and the membrane had a significant impact on the overpotential and performance of the electrolyser. Additionally, the thickness of both the electrolyser and the membrane affected the performance of the cell, due to their contribution to increased diffusion and ohmic overpotentials.

It had also been identified that increasing the temperature reduced the electrolyser overpotential, but an increase in pressure resulted in an increase in electrolyser overpotential. Pressure was found to be controlled by the OCV of the cell. Smaller exchange current densities were also found to exhibit favourable results in cell voltages and translated to improved cell performance. The model was similar to the work done by Dedigama et al. (2014) and Awasthi et al. (2011) except in the model presented by Han et al. (2015), diffusion overpotential and interfacial resistances had been taken into account.

Tijani and Rahim (2016) conducted a study on the numerical modelling of PEMEs, to determine the effect of varying operating conditions on Faraday's efficiency. In that work, temperature, pressure and membrane thickness were evaluated to determine the performance of PEMEs. According to the results, temperature had no effect on Faraday's efficiency. On the contrary, a linear relationship was found between current density and Faraday's efficiency. Additionally, it was observed that Faraday's efficiency decreased with increasing membrane thickness. It should be pointed out that an increase in current density led to an increase in the quantity of water dissociated into hydrogen and oxygen and, thus, an increase in cell voltage. Unbalanced pressure operation in the electrolyser cell also led to gas-cross over which reduced the faradaic efficiency. Moreover, it had been established that the PEME operated under isobaric conditions of 1 atm, presented the highest efficiency in comparison to other pressures. However, the scope of the study did not include the effects of a compressor required in the faradaic efficiency calculation.

2.11.6 Two-Phase Flow Models

Although PEMEs and PEMFCs share similar properties and challenges, only a few two-phase models have been developed for PEMEs. Implementing two-phase fuel cell models to PEMEs provides numerous challenges such as issues with model validation, gas bubble dynamics, interfacial effects, equivalent resistance modelling, performance, and efficiency modelling, as well as issues with coupling two-phase flow models.

Compared to the research conducted on the transport properties within PEMFC, research into the water transport properties in PEMEs is fairly new. Wang et al. (2001) studied two-phase water phenomena by employing a multi-phase mixture model. In 2008, a three-dimensional (3-D) mathematical model was developed by Wang (2008) to simulate two-phase flow, and the electrochemical performance of the gas diffusion layer (GDL) at the anode and cathode.

More recently, Han et al. (2017) developed a two-phase mathematical model which explored the transport properties within the liquid/GDLs, as well as investigated the effect of the transport properties on the electrolyser voltage and efficiency. Liquid water distribution inside the liquid-gas distribution layer was investigated at the anode. Additionally, the electrochemical model was coupled with a resistance model to determine the effects of physical parameters on the efficiency and performance of the cell. The aforementioned model was developed in Fortran 90 compiler. Limitations of the model included the exclusion of the effects of temperature gradients and micro-scale flow through the electrolyser porous media.

2.12 Fuel Cell Models

In the energy generation sector, emphasis was put on PEMFCs, due to the advantages, efficiency and purity obtained from this type of fuel cell. Fuel cells are devices which convert chemical energy into electrical energy and will provide an important role in providing electrical energy to future generations. Several models of fuel cells focus on determining the optimum operating conditions and cell potential, as a function of the cell's current density have been proposed in literature. In addition, existing models and experimental data presented in literature are only valid under specific operating conditions and assumptions, which cannot be applied to general models.

In 2004, Haraldsson and Wipke (2004) presented a study on evaluating PEMFC models. In their study, the selection criteria for choosing an appropriate model was presented. The criterion demonstrated the selection process of state-of-the-art models available commercially and in literature. Fuel cell models played an integral role in designing fuel cells.

In the work of Amphlett et al. (1995), a parametric steady-state model was presented for a single cell PEMFC. The 1-D model followed a mechanistic methodology. To gather empirical data for the model, a Ballard Mark IV single cell was used. The anode side of the membrane was assumed to have a relative humidity of 50%, whereas the cathode was assumed to be fully hydrated.

Mann et al. (2000) published a paper on a mechanistic steady-state electrochemical model of a PEMFC which had been an extension of the work conducted by Amphlett et al.(1995) The generalised model considered the gas feed rates of the anode and cathode, temperature, pressure, anode and cathode compositions, and current density, as well as the active reaction area and membrane thickness. In addition, the model took into account membrane ageing.

The results from that study reflected that the model could be applied to fuel cells with any specific membrane thickness and active area and could be operated at high current densities. The model, however, could not determine if sufficient removal of water was achieved.

2.12.1 One-Dimensional Models

Notable contributions were presented by Bernardi and Verbrugge (1992) and Springer et al. (1991,1993) whose models formed the basis for multi-dimensional PEMFC modelling. These models were among the earliest studies of PEMFCs, dating back to the early 1990s. Later, researchers developed new models and made modifications to existing models to investigate the effects of membrane dehydration (Z. Yang *et al.*, 2019), membrane flooding (Mammar, Saadaoui and Laribi, 2019), and H_2O transport through the membrane (Lee *et al.*, 2019).

Springer et al. (1991) presented an isothermal, 1-D, steady-state model of a complete PEMFC. The model employed the use of water diffusion coefficients, water isotherms, electro-osmotic drag coefficients and membrane conductivities, all of which were a function of water content in the membrane. That model mainly predicted the transportation of water through the entire PEMFC, as well as the performance of the cell. It also experimentally investigated the protonic conductivity of the membrane on the transport of water and cell performance. One of the discrepancies found in the model was that the model was unable to predict the cathode humidification at high current densities, whilst experimentally it had been found that the cell performed the best in well-humidified cathode streams. Moreover, applying thinner membranes was found to alleviate membrane resistance when the PEMFC was operated at high current densities. Since the model developed was 1-D, the effect of water transport due to pressure was also neglected.

In 1992, Bernardi and Verbrugge (1992) developed a 1-D, mathematical model to investigate the factors that affected cell performance, as well as the species transportation in the gas, liquid and solid phases of the cell. The model presented made use of a pseudo-homogenous catalyst approach. The influence of the electrode porosity and membrane properties were also investigated. The results showed that the inefficient transportation of unreacted hydrogen and oxygen through the membrane did not affect the current density. However, dissolved gases limited the effective use of the catalyst.

The limitations of their model included the following:

- The model was only valid when fully hydrated membranes were used.
- The electrostatic drag of water molecules through the membrane was not taken into account
- At high current densities, the polarisation curve obtained from the model diverged from the experimental results.

Weisbrod et al. (1996) presented an isothermal, 1-D PEMFC model operated under steady-state conditions. Similarly, to the work conducted by Bernadi et al. (1992), a pseudo-homogenous catalyst layer modelling approach was followed. In that work, the effect of catalyst layer loading, cathode pressure, cell temperature, water balance of backing layers and platinum loading were investigated on the cell performance. The model, however, neglected the catalyst layer kinetic resistance at the anode.

In 1998, Eikerling et al. (1998) demonstrated a steady-state 1-D model of a PEMFC operated under isothermal conditions. In their study, the effects of membrane parameters were evaluated on cell performance and had been compared with convection and diffusion membrane models. Their main conclusion was that the transportation of water through the membrane was mainly attributable to convection. However, their model did not take into account the electrode gas transport limitations and assumed that the membrane water content was only affected by capillary forces.

Mawardi et al. (2005) developed a 1-D, numerical model to optimise the operating conditions of a PEMFC and maximise the power density, whilst being subjected to various process constraints. In that optimisation model, the results obtained illustrated the effects of electrode thickness, membrane thickness, CO concentration and process constraints on the optimum operating conditions.

In the works of Marr and Li (1998), the model developed by Bernardi and Verbrugge (1991, 1992) was adapted and used to improve the formulation of the catalyst layer, as well as the gas flow channel. Variable pressure was allowed to flow through the channel. It should be noted that 1-D flow was assumed in the model. Additionally, the catalyst layer model was also adapted from Bernardi and Verbrugge (1991, 1992). In the model, the void space had been used to accommodate liquid water present, as well as the PEM electrolyte.

Falcão et al. (2009) presented a single-cell 1-D, steady-state, mathematical model of a PEMFC that accounted for the effects of heat and mass transfer. MATLAB and Microsoft Excel were used as the software tools to develop the model. The results indicated that as the current density increased, the water content decreased. Furthermore, water transport due to the concentration gradient was identified as the main water transport responsible for keeping the membrane hydrated. According to the temperature profile, higher temperatures were observed at higher current densities, and the highest temperature occurred at the cathode of the PEMFC. This was a result of the exothermic reaction responsible for the formation of water.

Cong and Xinghu (2010) developed a 1-D steady-state model for a PEMFC that was based on semi-empirical equations. A new method of calculating the output voltage of the PEMFC was introduced. Based on the results obtained, increasing the pressure and stoichiometric ratio of oxygen entering the cathode, improved the performance of the fuel cell by increasing the reactant partial pressures.

Suh and Park (2012) investigated the distribution of overpotential in the MEA, as well as transport phenomena of PEMFCs in a steady-state, non-isothermal, 1-D model. The model took into account two-phase flow, and some of the major assumptions included negligible pressure drop in GDL. Additionally, the capillary effect was assumed to be responsible for the removal of liquid water.

Kumar and Khare (2011) simulated a 1-D, steady-state model of a PEMFC, to investigate membrane diffusion, membrane hydration and water transport through the membrane. The model was simulated in MATLAB and was based on a theoretical electrochemical model. The results indicated that the largest potential loss was due to the transport of ions through the membrane. Additionally, it had been concluded that the thickness of the membrane was related to the ohmic losses in the fuel cell. In particular, increasing membrane thickness resulted in larger ohmic overpotential losses due to an increase in local conductivity.

Beicha et al. (2013) developed a 1-D electrochemical model to predict output power as a function the operating parameters (temperature, membrane humidity and partial pressure) and the efficiency of a PEMFC. A mass transport model was also included to evaluate the effect of water through the membrane. At high current densities, the increase in the formation of water and excess humidification resulted in a blockage on the reaction sites. As a result, the transportation of oxygen ions to the cathode reaction sites was restricted. A nonlinear least-squares method was used to fit experimental data for the current and cell voltage. It had been found that increasing the amount of platinum loaded on the electrodes, increased the exchange current density. This was attributed to the greater presence of active sites available for hydrogen adsorption. It was indicative from the study, that increasing the temperature of the cell from 298 K to 353 K increased the cell voltage by 28%.

Ferreira et al. (2015) presented a 1-D PEMFC simulation model with two-phase flow. The model was developed as a steady-state, analytical model and was validated with experimental results. That model considered the effect of liquid water on the cell performance. The results from the model predicted more accurate results than single-phase flow models at high current densities. A boundary between single and two-phase flow was found and was used to provide operating conditions to prevent PEMFC performance deterioration.

In a similar study, Li and Lv (2018) presented a model on the combined effects of water transport on the performance of PEMFCs. As with the model presented by Ferreira et al. (2015), a 1-D, two-phase flow, steady-state model was developed. However, in that work, the cell performance was investigated under varying operating conditions and had been based on water transport. The model results obtained from the aforementioned model correlated to the results obtained from Ferreira et al. (2015). More specifically, an increase in temperature was found to improve cell performance, due to an increase in membrane conductivity. Membrane resistance was found to decrease with increasing temperature. The model also predicted better cell performance at high hydrogen humidities and low air relative humidities. Finally, the performance of the cell increased with increased air pressure due to the increase in oxygen concentration and decrease in membrane resistance. Overall, the study showed positive effects on membrane hydration. However, the cathode experienced a negative effect of flooding.

In another study, Salva et al. (2016) presented a 1-D analytical PEMFC model to investigate and optimise the operating conditions required to provide maximum and minimum power output. In order to be competitive with available power generation systems, PEMFCs need to overcome technological barriers such as cost, volume and weight. A maximum power performance polarisation curve was obtained to determine the operating conditions at varying currents. The model was developed in Engineering Equation Solver (EES) V. 9.705-3D.

EES is software that solves non-linear and algebraic differential equations. It is different compared to traditional methods, in which constant operating conditions are used. The model used variable operating conditions that was dependent on the current of the PEMFC.

More recently, Adbin et al. (2016) developed a 1-D mathematical model of a PEMFC in MATLAB-Simulink. The model was developed based on physical parameters with the main aim of predicting the performance of the cell beyond empirical means. The influence of temperature, pressure, humidification and reactant partial pressures were evaluated with regards to the performance of the PEMFC. However, the model did not calculate the membrane water uptake as a function of feed gas relative humidity and cell temperature.

2.12.2 Two-Dimensional Models

Although 1-D models have been extensively studied, the developments of two-dimensional (2-D) models have become an area of interest in fuel cell research and development for heat and water analysis. Gurau et al. (1998) presented a 2-D, non-isothermal model of a PEMFC to investigate the concentrations of water, hydrogen and oxygen within the fuel cell. That work considered the effects of temperature, porosity and rates of airflow through the GDL on the cell performance. The approach followed was a mechanistic multi-domain approach. The model had assumed that feed gas flow channels contained negligible amounts of water in liquid phase, the flow through the cell was laminar, and the cell was operated under steady-state conditions. According to the results obtained, the current density of the cell was affected by the non-uniform distribution of the reactants.

In the works of Singh et al. (1999) an isothermal 2-D model was developed to investigate cell performance, improve heat and water management, and alleviate transport limitations. The results from the model indicated that the cathode voltage loss was due to slow cathode kinetics in the PEMFC, dominant at practical current densities.

Um et al. (2000) extended the work conducted by Gurau et al. (1998). The model presented a simulated transient operation of fuel cells, and the assumptions made were similar to that of Gurau et al. (1998). The model was applied to determine the effect of hydrogen dilution present along the flow channel of the anode. Results from the study indicated that the mass transport limitations during high current density operation were mainly due to the increased hydrogen consumption rate.

Grujicic and Chittajallu (2004) presented a mathematical model on the design and optimisation of a PEMFC. The model developed was a nonlinear, steady-state 2-D electrochemical model, and was modelled in FEMLAB using the finite element method. Mechanical design optimisation and design analysis was included to determine the optimal design of a PEMFC. MATLAB was used to optimise the mechanical design of the PEMFC and was solved using the optimisation function fmincon (). The results from the study showed that an increase in air pressure, increased the airflow of oxygen to the reaction sites and reduced the diffusion layer. As a result, a higher current density at constant cell voltage was achieved.

The works of Secanell et al. (2010) demonstrated a computational model for the optimisation of a PEMFC membrane electrode assembly. The model presented was a single-phase MEA model incorporated into a 2-D isobaric and isothermal model. It had been concluded that the MEA performance was enhanced by improved MEA composition.

In another study, Belkhiri et al. (2011) developed a 2-D mathematical model of a PEMFC to investigate the effect of temperature and water content on the performance of a PEMFC. The model developed considered the flow of hydrogen, oxygen and water through the GDL, electrodes and the PEM. The results indicated that the performance of the PEMFC was dependent on temperature and membrane water content. An increase in temperature was found to not only increase the reaction and mass transfer rates, but also decreased the ohmic overpotential due to an increase in membrane conductivity. As such, more water was produced, and the membrane was better hydrated. Additionally, it had been concluded that as the MEA became dry, the activation overpotential losses increased.

2.12.3 Three-Dimensional Models

Three-dimensional models are useful in understanding and identifying the detailed behaviour of different elements in the fuel cell. It provides an insightful tool in the process optimisation of fuel cell systems and performance enhancements. Particularly, Natarajan and Nyugen (2003) presented a 3-D numerical model that took into account the effects of flow rate, humidity and temperature on cathode flooding. Similarly, Meng and Wang (2005) developed a non-isothermal, single-phase model that predicted and studied various heat generation mechanisms. In addition, a thermal model was integrated with electrochemical and mass transport models to provide a comprehensive evaluation of heat and water management.

Other sophisticated 3-D models were applied to investigate different fuel cell behaviour. Kahroba et al. (2009) presented a single-phase, isothermal, 3-D model of a PEMFC to determine the influence of membrane thickness on the operation of the PEMFC. The model was developed and solved in a computational fluid dynamics (CFD) package. According to the results obtained from that model, cell performance was found to increase with decreasing membrane thickness. In addition, the deviations at high current densities were caused water present in the GDLs and the catalyst layers.

Obayopo et al. (2013) developed a steady-state 3-D numerical model to investigate the design parameters and operating conditions (reactant flow rates, GDL porosity, flow orientation and geometric configurations) on the performance of a single channel PEMFC. The computational model also took into account the anode and cathode flow channels and the membrane electrode assembly. CFD was used to numerically solve continuity, energy, momentum and species conservation equations. The results indicated that the optimal flow channel width, reactant flow rate and GDL porosity contributed towards enhanced fuel cell performance leading to maximum power output. In addition, it had been established that the effects of design parameters and operating conditions are more distinguished at low operating voltages compared to high operating voltages.

Kahveci and Taymaz (2014) investigated the effect of varying the GDL porosity from 0.3-0.6 on the PEMFC performance. A 3-D, isothermal, single-phase, steady-state model was developed in Fluent 14.0 CFD code software to investigate the effect of the GDL parameters on the cell performance. The results from that study indicated that an increase in GDL porosity improved the hydrogen and oxygen diffusion transport across the membrane. Furthermore, during stationary operation, narrow width channels were found to allow water to diffuse easily through the channel to the membrane, where the performance of the cell increased, and the membrane was effectively hydrated.

Carton and Olabi (2017) demonstrated a unique 3-D dynamic model which was derived from computational fluid dynamics. The proposed model was an electrochemical model developed for open-pore cellular foam flow plates. The open-pore cellular foam plate was compared to double channel flow plates. According to the results obtained, the open-pore cellular foam flow plate was found to evenly distribute hydrogen and oxygen across the fuel cell and had outperformed the double channel fuel cells experimentally and in numerical simulations.

2.12.4 Optimisation Models

In fuel cell systems, a few attempts have been made on the optimisation of the system. Mo et al. (2006) demonstrated an electrochemical steady-state model to determine the optimal parameters for PEMFCs using a hybrid genetic algorithm (HGA). The HGA used the output stack voltage, stack current and the anode and cathode pressure. It merged Nelder-Mead's simplex method and Niche techniques with the original genetic algorithm. The niche techniques are used to control the diversity of the population in order to prevent premature convergence, whereas the Nelder-Mead's simplex method was used to enhance the local search capacities. Results from the model developed in MATLAB indicated that the HGA model converged, provided a global optimisation solution and was more accurate than a simple genetic algorithm model. In that model, membrane thickness and maximum current density were set as parameters. As such, the model could not determine the optimal current density and membrane thickness.

Shimpalee et al. (2007) numerically studied the impact of the cross-sectional channel and rib dimensions of serpentine flow-fields, on the PEMFC performance when subjected to automotive and stationary conditions. The CFD model developed incorporated a control volume technique and used the STAR-CD 3.26 solver, which is a commercial flow solver, to solve the model. In comparison to the stationary conditions, operating the PEMFC under automotive conditions showed a higher overall performance.

Mert et al. (2015) conducted a complete exergo-economic analysis and multi-objective study on four types of fuel cell systems to determine the maximum power production capacities, minimum costs and exergy efficiency. This was achieved with the Genetic Algorithm (GA) method derived from the natural selection process that mimics biological evolution. The fuel cells investigated were PEMFCs, direct methanol fuel cells (DMFCs), solid-oxide fuel cells (SOFCs) and molten carbonate fuel cells (MCFCs).

These fuel cells were modelled in MULOP (Multi-objective Optimiser) and were parametrically studied with varying operating conditions. From the study, it had been concluded that higher efficiencies were obtained when high-temperature fuel cells were used.

Bednarek and Tsotridis (2017) highlighted the issues and limitations associated with computational fluid dynamics (CFD) when modelling PEMFCs. All numerical simulations presented in the study were simulated in the Fluent Fuel Cell and Electrolysis Module. Their research showed that a convergence method was necessary for steady-state operations due to numerical instabilities present. Moreover, hydrogen was found to diffuse faster, whereas limitations in oxygen diffusion were present at the cathode, due to the slower rate of oxygen diffusion and lower oxygen concentrations. At low current densities, the membrane water content was well distributed, and it was indicative that the membrane was well humidified.

2.13 Hybrid Systems

Hybrid energy systems integrate several sources of energy into one system for energy generation. In most instances, the issue of intermittent energy production from renewable energy has led to several combinations of renewable energy technologies being integrated into the energy system. More specifically, several combinations of solar, wind, hydrogen, battery, biogas, battery, electrolyser, fuel cell and diesel have been incorporated into hybrid systems.

Most island states across the world utilise hybrid systems to meet energy demands and reduce their dependency on fossil fuels, as well as reduce the costs of sourcing energy from the mainlands. Renewable energy usage is emerging in islands, as it has the potential to increase the security of energy supply, as well as encourage a self-sufficient and sustainable economy (Kalinci, Hepbasli and Dincer, 2015). Some hybrid systems currently being used are summarised in Table 2.4.

Correspondingly, a seawater electrolyser was coupled with fuel cells to produce several products. Ju-Hyung (2013) presented a patent on an integrated hybrid system to simultaneously produced caustic soda, PCV, urea, and ammonia whilst generating electricity using fuel cells based on a seawater electrolyser.

Publications on the mathematical modelling and optimisation of hybrid systems in recent years has increased significantly, due to improved computational power and reduced computational time. Dokkar et al. (2013) focused on the optimisation of a photovoltaic-hydrogen power system for application in a mobile phone station. The proposed system included a photovoltaic field, water electrolyser and two fuel cells. The model applied a Genetic Algorithm (GA) coupled with the Quasi-Newton Method to determine the optimal operating conditions for the fuel cells.

Table 2.4: Hybrid Energy Systems used in Islands Across the World

Island Name	Country	Hybrid System Present	Reference
St Martin Island	Bangladesh	PV/wind/battery/diesel	(Mahmud, Hassan and Rahman, 2013)
Hainan Island	China	Wind/PV/NG/hydro/ grid	(Ye *et al.*, 2012)
Kinmen Island	China	Wind/PV/biogas/ tidal	(Liu and Wu, 2010)
Rhodes Island	Greece	Wind-powered pumped storage system with a diesel system	(Katsaprakakis and Christakis, 2014)
Pulau Ubin Island	Singapore	Micro-turbine/PV/biomass/SOFC	(Chua *et al.*, 2014)
Corvo Island	Portugal	Wind/hydro/pump	(Duić, Krajačić and da Graça Carvalho, 2008)
Sicilia Island	Italy	Pump/turbine	(Ciapessoni *et al.*, 2013)
El Hierro	Spain	Wind/pump/turbine	(Pezic and Cedres, 2013)
Porto Santo Island	Portugal	Electrolyser/H_2 storage/fuel cell and Wind	(Mendoza-Vizcaino *et al.*, 2016)
Saint Vincente	Cape Verde	Desalination and hydro water	(Segurado *et al.*, 2011)
Metlalaka	Alaska	Hydroelectric system with a diesel generator and battery storage	(Komor and Glassmaire, 2012)

In a similar study, Clarke et al. (2015) conducted a study to simultaneously investigate size optimisation and Power Management Strategies for stand-alone hybrid systems, to meet both electrical and water loads. In that model, Particle Swarm Optimisation (PSO) was modelled in MATLAB/Simulink and was compared to HOMER which had also been used to model the system. Multi-objective functions were incorporated into minimising the net present value (NPV) and carbon dioxide emissions.

The aforementioned model was different to the model presented by Dokkar et al. (2013) because it used PSO and HOMER to size and optimise the energy system instead of GA. Additionally, it did not take into account the optimal operating conditions for the system. The study also did not investigate the incorporation of different energy storage mechanisms, sensitivity of different initial operating conditions, level of metal hydride or battery charge.

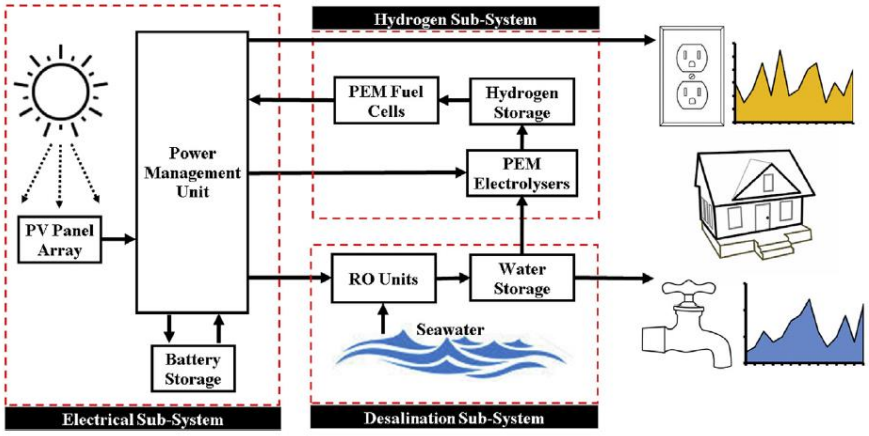

Figure 2.7: Hybrid Stand-Alone System Consisting of Three Sub-Systems (Clarke, Al-Abdeli and Kothapalli, 2015)

HOMER was developed by the National Renewable Energy Laboratory (NREL) and is used to model grid-connected systems or stand-alone systems. The inputs required include load data, renewable source data, component specifications, costs and other parameters required for optimisation (Kalinci, Hepbasli and Dincer, 2015).

In 2015, Lin et al. (2015) developed a generic mathematical model to analyse the temporary operational flexibility of a solar/wind/PEM fuel cell/battery hybrid system. The energy input rates into the photovoltaic cell, fuel cell and wind turbine were considered to be time-dependent and uncertain. Therefore, discrepancies between the power supply and demand were buffered with the operation of a battery.

The results illustrated that the flexibility of the above-mentioned system was enhanced with the inclusion of the battery. Additionally, it had been concluded that the optimal size of the battery was required for variations in power supply and demand.

Recently, the incorporation of electrolysers and fuel cells into hybrid systems has increased significantly, due to the increase in environmental consciousness and exploration of alternate sources of energy generation. More specifically, Sharifian and Harasek (2015) developed a dynamic mathematical model of a PV system coupled with an alkaline water electrolyser, to simulate the generation of hydrogen from renewable energy. TRNSYS was used as the modelling tool for dynamic simulation. The simulation model that was developed, modelled the electrolyser with several cells connected in series and with two power modes: constant or variable.

In a different study, Shedid and Elshokary (2015) presented an experimental study on a PV/alkaline electrolyser hybrid system. That study was applied to the weather conditions in Egypt, and the electrolytes used included seawater, water extracted from the Nile River and a potassium hydroxide solution. The results indicated that increasing the input voltage of the electrolyser, increased the hydrogen production flow rate until a maximum was reached. Thereafter, the hydrogen production flow rate decreased with increased voltage. This was due to sulphate and magnesium salt precipitate deposits present on the electrode surface. As a result, there was an increase in the resistivity of ion flow to and from the electrodes, as well as reduced electrode surface contact.

A novel 100% renewable energy system comprised of a photovoltaic array, wind generator, fuel cell, seawater electrolysis plant, hydrogen tank, compressor and a battery energy storage system (BESS) was presented by Tobaru et al. (2017). In that work, a real-time pricing model was included to limit the output variations of the renewable energy systems.

Mixed-integer linear programming (MILP) was used to minimise the difference between the cost of equipment and the revenue generated (objective function) from the chemicals produced from seawater electrolysis. However, it should be noted that the model did not take into account the influence of the scale of the system, structure, heat of electrolysis and the electrolysis processing flow rate.

Similar to the research conducted by Tobaru et al. (2017), Prieto-Prado et al. (2018) presented a system that coupled wind, photovoltaic energy technology, electrolysers, fuel cells and hydrogen storage tanks, as well as a reverse osmosis plant to provide water to the Gran Canaria island in Spain. However, instead of storing surplus energy in batteries Prieto-Prado et al. (2018) used the surplus energy in a reverse osmosis plant to make potable water, and conducted the research for islands located in Spain, instead of Japan. The study conducted by Prieto-Prado(2018) used the HOMER simulation software to determine the economic and technical feasibility of the power system. More specifically, the aim of the study was to determine whether the system could meet the energy demands of the island using renewable energy and provide a self-sufficient system by meeting the population's water demands. Additionally, the reverse osmosis plant was simulated in the Reverse Osmosis System Analysis design software (ROSA). ROSA was created by Dow Chemical and is used to design reverse osmosis plants according to the water treatment specifications that are required. Furthermore, the system was found to be similar to the system presented by Clarke et al. (2015).

Demir and Dincer (2017) proposed a system which consisted of a gas turbine sub-system that was powered by solar energy, PEME, latent heat storage system, multi-stage flash distillation system and a thermo-electric generator to produce electricity and hydrogen. The proposed system was used to determine the energy and exergy for each component in the hybrid renewable energy system. COMSOL Multiphysics software package was used to numerically model the thermo-electric generator, whereas all other components were analysed in the Engineering Equation Solver.

Kabir and Matin Bhuiyan (2017) presented a study on the design and simulation of a hybrid green power system that produced hydrogen from seawater. That system consisted of a PV panel, wind turbine generator, controller, PEME, hydrogen storage tanks, gas turbine generator and an AC load. The simulation was simulated in HOMER. The results from that work indicated that the system was environmentally friendly due to the system being completely green and emitted no carbon emissions. It was also established that the abovementioned research was similar to the research conducted by Srisiriwat and Pirom (2017), with the exception that the research conducted by Kabir and Matin Bhuiyan (2017) was simulated in HOMER and that Srisiriwat and Pirom (2017) performed an experimental study which was later proposed to be validated in HOMER. Figure 2.8 visually illustrated the system proposed by Kabir and Matin Bhuiyan.

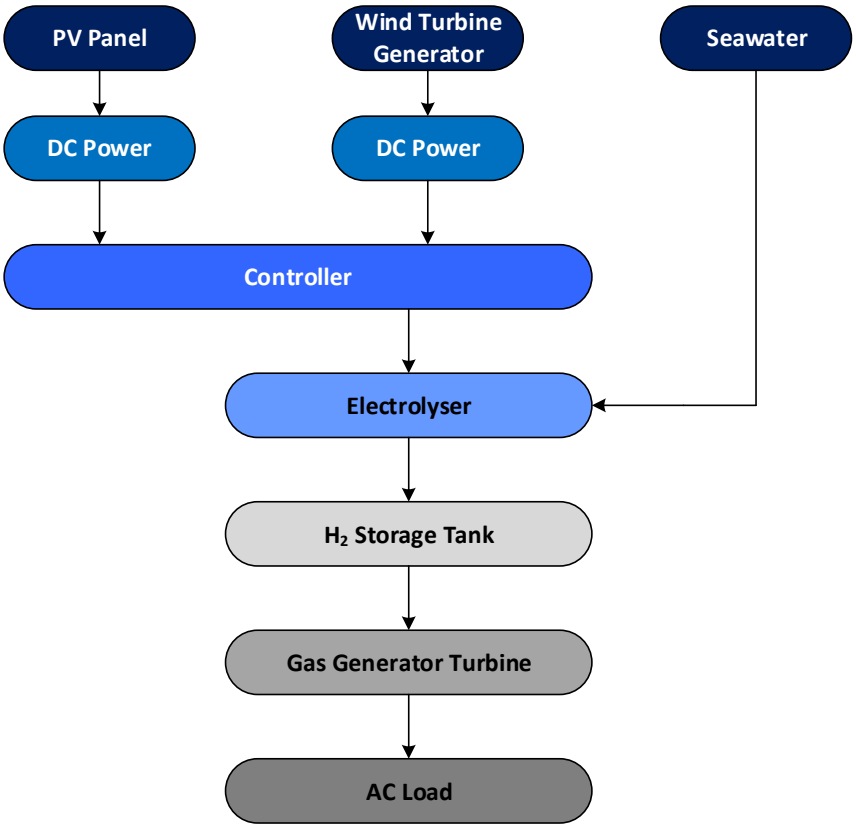

Figure 2.8: HOMER Green Hybrid Renewable Energy System (Kabir and Matin Bhuiyan, 2017)

In 2018, Espinosa-Lȯpez et al. (2018) developed a semi-empirical, steady-state electrochemical model coupled with a lumped capacitance, dynamic, thermal model of a 46-kW high-pressure PEME. The electrolyser was installed in a MYRTE platform (real-scale demonstrator). MATLAB-Simulink was used to develop and validate the model. PSO was also used to identify the parameters in the electrochemical model. The abovementioned hybrid system was comprised of a PV-array, electric inverters, storage tanks, a PEMFC and a PEMEC. Results from the simulation indicated that low pressures and high temperatures maximised the electrolyser efficiency in the system. To size the equipment installed in the MYRTE platform, ORIENTE was used. ORIENTE is a numerical optimisation and simulation code which had been developed by the University of Corsica.

In a different study, Paul and Andrews (2017) conducted a review on the state-of-the-art Unitised Regenerative Fuel Cell (URFC), which is essentially an individual cell that operates as an electrolyser and fuel cell. The review evaluated regenerative fuel cells which could be divided up into discrete regenerative fuel cells (DRFC) and URFC. In DRFCs separate units were used for electrolysis and fuel cell operations. The study investigated the main challenges associated with these hybrid systems and found that URFCs were more economical and technologically viable.

A mathematical model for the design and optimisation of various hybrid renewable energy systems that included solar-wind-reverse osmosis desalination systems, coupled with either a battery or hydrogen energy storage was demonstrated by Maleki (2018). A metaheuristic optimisation technique known as the bee's algorithm was proposed for the optimal design of the hybrid renewable energy systems. The objective function of the model was to minimise the total life cycle cost of the hybrid energy systems.

The results indicated that a hybrid renewable energy system coupled with a battery was more cost-effective than a hybrid renewable energy system coupled with a hydrogen storage system. Additionally, the hybrid solar-wind-reverse osmosis desalination-battery system was the most reliable in terms of increasing the availability of freshwater and satisfying the load demand.

In contrast, Liu et al. (2019) developed a model of a novel integrated energy system of a multiple decentralised energy generation systems, integrated with a centralised energy generation system to provide a stable supply of electricity. The capacity of the proposed hybrid energy system was optimised through the use of a superstructure based MINLP model. General Algebraic Modeling System (GAMS) was used to model the optimisation problem and BARON was used as the solver. Energy for the decentralised energy system was harnessed from solar, wind and biomass energy, whereas the centralised energy generation system was powered by fossil fuels. In that work two objective functions were calculated; the first objective function was to minimise the overall cost of the system and the second objective function was to maximise the systems operational efficiency.

2.14 Mathematical Modelling and Optimisation

Engineering disciplines and research and development operations across the world utilise mathematical modelling, and optimisation techniques to determine the best solution to a problem. Mathematical models are used to explain and analyse the physical behaviour of the scientific world through the use of mathematics (Snyman and Wilke, 2018). Mathematical models translate physical system problems into mathematical formulations. From these formulations, the results obtained from the numerical and theoretical analysis are used to provide insight and guidance into the physical behaviour of the system. This is described through mathematical relationships in the form of equations, equalities, inequalities and logical expressions. Some of the benefits associated with mathematical modelling include analysing the viability of a system and relationships within the system without conducting experiments. This is vital in chemical engineering, as in some instances, conducting experiments may be undesirable due to high costs and time constraints. Furthermore, it may not be physically possible to explore changes to the system through experimentation, due to contamination of products, damage to equipment, safety risks and raw material wastage. Typical techniques used in engineering mathematical modelling include computational fluid dynamics (CFD), computer-aided design and finite element modelling and analysis.

2.14.1 Mathematical Optimisation

Over the last few years, mathematical optimisation has gained a lot of attention, as many businesses are looking into optimally using resources, maximising performance and minimising costs. It involves finding the optimal solution to a mathematical problem which may be subjected to various constraints. As the world becomes more developed and more technologically advanced, optimisation methods may be used to solve complex, large-scale problems in diverse fields.

Extensive reviews have been presented by Biegler and Grossman (2004) and Grossman and Harjunkoski (2019) on the various types and uses of mathematical modelling used in process systems engineering to date. Optimisation problems may be classified according to discrete or continuous variables. Optimisation in engineering is necessary in order to minimise costs and maximise performance and profit. This is achieved through obtaining the optimal solution in a predefined domain, subject to various equality and inequality constraints (Snyman and Wilke, 2018)

All optimisation problems contain at least one objective function, equality constraints and inequality constraints. These problems may either be constrained or unconstrained. The objective function may either be maximised or minimised. Equations (2.10)-(2.14) describe the general structure of a constrained optimisation problem (Sun and Yuan, 2006).

$$\min_{x \in R^n} \quad f(x) \tag{2.10}$$

$$\text{s.t.} \qquad c_i(x) = 0, i \in E, \tag{2.11}$$

$$c_i(x) \geq 0, i \in I, \tag{2.12}$$

$$x^L \leq x \leq x^U \tag{2.13}$$

$$x_i \in \mathbb{Z} \tag{2.14}$$

Where E and I are the index set of equality and inequality constraints, respectively. Equation (2.13) describes the bounds of a variable, *x*, where x must be less than or equal to x^U, but greater than or equal to x^L. Equation (2.14) expresses a constraint which states that x_i must be an integer value.

An unconstrained optimisation is written as follows:

$$\min_{x \in R^n} \quad f(x) \tag{2.15}$$

Based on the mathematical model, a solution will be given. Different types of solutions are summarised below:

- Feasible solution – This solution is obtained when all variables satisfy the constraints present in the optimisation problem.
- Optimal solution – This solution is the best feasible solution among all feasible solutions in the feasible region.
- No solution- This solution is obtained if the variables in the model cannot satisfy the constraints in the optimisation problem.

2.14.2 Model Classification

The variables used in mathematical modelling may either be classified into two types of variables, namely: continuous and integer variables. Continuous variables are found to be more generic compared to integer variables and may be identified as any real number. According to the structure of the optimisation model, the model may be classified as a linear programming (LP) model, nonlinear programming (NLP) model, mixed-integer linear programming (MILP) model or a mixed-integer nonlinear programming (MINLP) model (Chong and Zak, 2013). A mathematical model is classified as an LP model when the constraints of the model and the objective function are all linear functions.

In the event that one of the constraints or the objective function is found to contain a nonlinear equation or term, the model is then classified as an NLP model. NLP models are generally more difficult to solve than LP models, which are the simplest models.

NLP models may, therefore, be linearised to facilitate solving the model faster and reducing the computational complexity of the model. Nonlinear models are formed from the product of two continuous variables (Zamora and Grossmann, 1998). When nonlinear terms in NLP and MINLP models are linearised it may not only lead to a globally optimal solution but will also accelerate model convergence.

Mixed-integer programming models are models which are comprised of both continuous and integer variables. It may be further classified as being either linear or nonlinear functions, thus, forming either MILP models or MINLP models (Samsatli and Samsatli, 2018). Figure 2.9 graphically illustrates the different classes of optimisation problems.

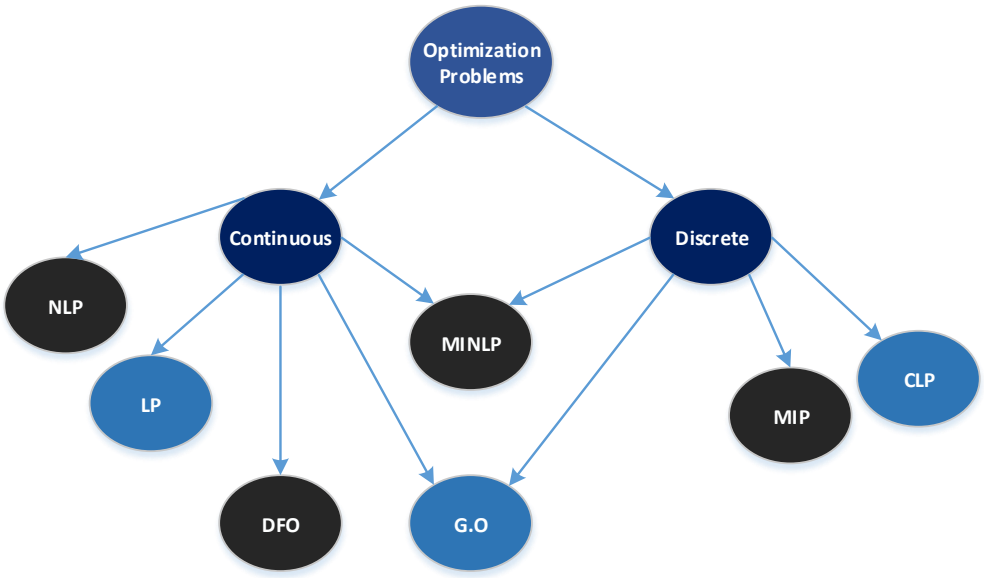

Figure 2.9: Classes of Optimisation Problems (Biegler and Grossmann, 2004)

2.14.3 Convexity

Typically, superstructure-based models have been found to behave in a nonlinear nature, due to a large number of economic, environmental, physical and mass balance constraints present. Convexity is used to determine the number of optimal solutions in a feasible region of a mathematical optimisation problem. Functions may either be classified as being either convex or concave functions. A model that is convex in nature is described as having an arbitrary line constructed between two points in a feasible region, and all the values lie above the region. If a function is concave the arbitrary line has values below the curve (Ruzhansky, Dutta and Agarwal, 2018). These observations are best observed in Figure 2.10.

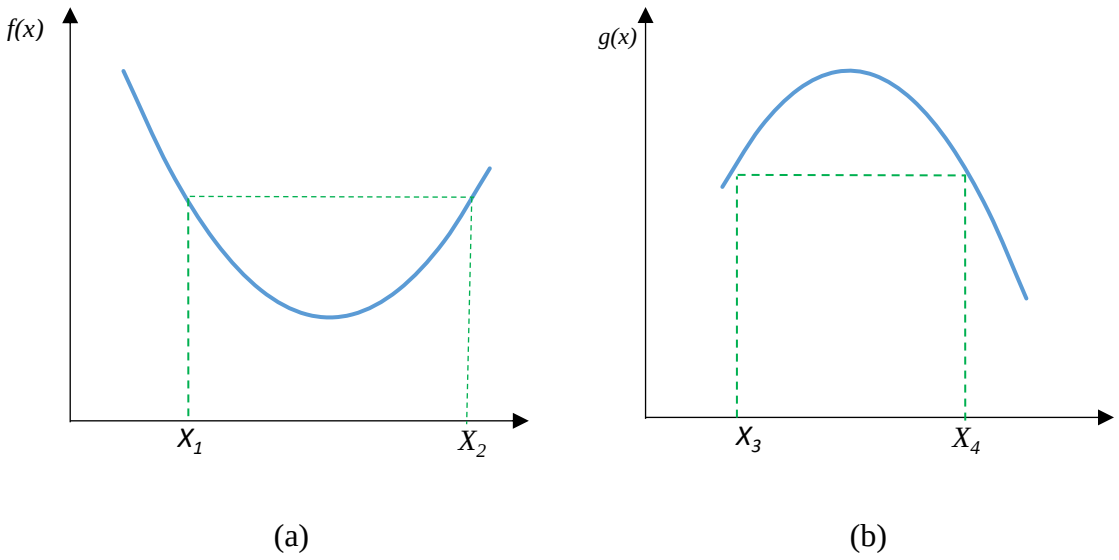

Figure 2.10: Convex and Concave Functions

As seen in Figure 2.10a, all the points in a convex function must be less than or equal to the points on the arbitrary line, whereas in a concave function all points on an on the curve must be greater than or equal to the points on the arbitrary line (Figure 2.10b). Furthermore, it should be noted that convexity is used to determine whether a maximum or minimum solution is obtained, and if the solution is a local or global solution.

In engineering, mathematical optimisation is used to determine the global optimal solution or local optimal solution. The global optimal solution is defined as the best solution for a given function among all other feasible solutions, whereas a locally optimal solution is defined as the best solution within a small range of possible solutions. Convex and concave functions guarantee a single optimal solution for the optimisation problem. However, non-convex functions provide multiple locally optimal solutions.

Global optimal solutions may be classified as either a global maximum solution or global minimum solution, and local optimal solutions may be classified as either a local maximum solution or a local minimum solution. Figure 2.11 illustrates the different types of optimal solutions found in optimisation problems.

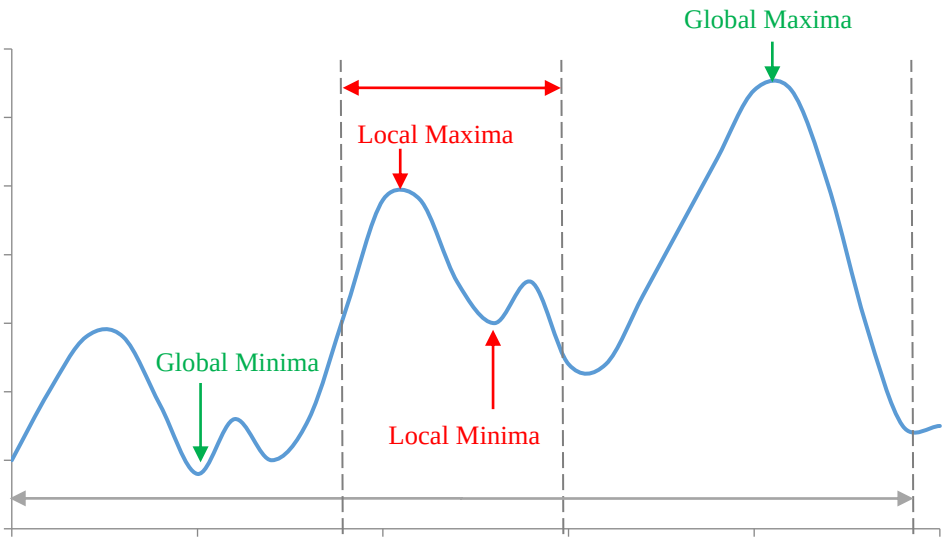

Figure 2.11: Types of Solutions in Mathematical Optimisation Problem

Lundell and Westerlund(2012) stated that the only way to guarantee a globally optimal solution is achieved, is by ensuring a convex function is used. Covexification is, therefore, the technique used to make nonconvex problems convex. This is obtained through convexification methods such as Glover transformations, McCormick (1976) over and under estimators, reformulation-linearisation, piecewise linearization methods and other nonlinear transformations.

2.14.4 Optimisation Techniques

Direct linearisation, global (deterministic) optimisation methods, generating a good starting point and using sequential solution procedures may be used to assist NLP models in locating the global optimisation technique. Given below is a brief description of the different techniques used in optimisation:

- Direct linearisation- Direct linearisation involves linearising nonlinear equations present in a mathematical model.
- Good starting point method - The good starting point method is a linearisation technique which uses a good starting point to solve non-convex problems. The starting point may be obtained from linearisation or stochastic optimisation methods
- Sequential solution procedures- Sequential solution procedure is a linearisation technique which uses an iterative approach in linearising an NLP model. It essentially breaks down the problem into smaller sub-problems which are solved progressively until an optimal solution is obtained. This method is computationally demanding due to the variety of iterative procedures and does not guarantee global optimality.
- Stochastic optimisation
- Deterministic optimisation

2.14.5 Stochastic

Stochastic optimisation is a method of optimisation which uses the theory of probability to optimise a system. Stochastic optimisation models use probability distribution to describe variables, as such unique variables are not included, and a degree of randomness is present. Examples of stochastic optimisation methods include genetic algorithms, particle swarm optimisation and simulated annealing (Rao, 2019). This method cannot guarantee global optimality due to the convergence of the model in a finite amount of iterations (Zamora and Grossmann, 1998).

Particle Swarm Optimisation is a metaheuristic computational optimisation technique based on improving candidate solutions through the use of successive iterations. This technique mimics the behaviour of birds flocking, bees swarming and fish schooling. In this optimisation technique, a population of solutions also referred to as particles are randomly dispersed into a search space at random velocities and random positions. At each iteration, the objective function is evaluated, and the best solution is selected, and used to improve all the particles positions and velocities. This optimisation technique is similar to the Genetic Algorithm optimisation technique, with additional features such as enhanced computational efficiencies (Espinosa-López *et al.*, 2018).

Genetic algorithm is known as an evolutionary optimisation technique and is based on Darwin's principle of "survival of the fittest". This technique was developed by Holland in 1975 and was later modified by several authors. The genetic algorithm uses four principles namely, crossover, mutation, reproduction and selection. A set of solutions called a population undergo GA functions whereby the values are modified until the values converge to an optimal solution. (Rao, 2019).

2.14.6 Deterministic Optimisation

In deterministic optimisation, all the variables in the model are determined from parameters and previous variable values. This approach is designed to achieve a globally optimal solution or prove that a solution does exist. Examples of deterministic optimisation methods include branch and bound, cutting plane methods, outer-approximation, and difference of convex and concave methods, primal-dual methods and piece-wise linearisation methods (Lin, Tsai and Wang, 2012; Castro, Castillo and Mahalec, 2017; Muts, Nowak and Hendrix, 2020).

2.14.7 Branch and Bound

Branch and bound is an optimisation algorithm which is used for discrete programming and solves most NLP and MINLP problems. It is composed of an enumeration of solutions in a search space. More specifically, the candidate solutions form a rooted tree. The feasible region, also known as the search space, is broken down into smaller LP sub-models, whereby the objective function is applied to each sub-model and solved. This is known as branching. The subset solutions represent the branches of the tree. The branch of the algorithm is examined against the lower and upper limits of the solution, and the branch is discarded if a better solution than the previous solution can be obtained (Rao, 2019).

Minimisation models use the lower bound of the solution to determine the solution though the relaxation into an LP problem. This is achieved by treating the variables as continuous variables, and different branching rules are applied. At each branch, an LP solution is obtained at the lower bound. If a feasible solution is obtained, an upper bound is found.

This branching process continues until the lower bound is equal to the upper bound at a specified tolerance. It should be noted that the branch and bound optimisation method is known for eliminating infeasible branches within the tree enumeration. To elaborate further, if there is no solution to the problem or the lower bound is worse than the upper bound, the entire branch is deleted. Thus, reducing the search space (Ryoo and Sahinidis, 1996).

There are two branching approaches, namely the depth-first approach and the breadth-first approach. The depth-first approach evaluates the entire branch from the first node to the next node, before seeking a better solution in the next branch (Ryoo and Sahinidis, 1996). This is illustrated in Figure 2.12. On the contrary, the breadth-first approach follows the node with the best solution and expands to the next node/branch. Figure 2.13 depicts the breadth-first approach.

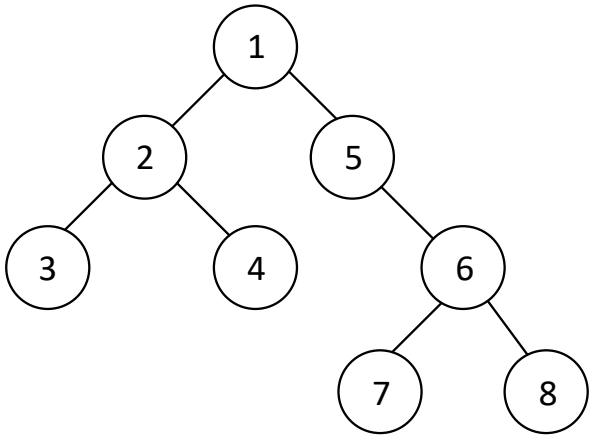

Figure 2.12: Branch and Bound Depth-First Approach

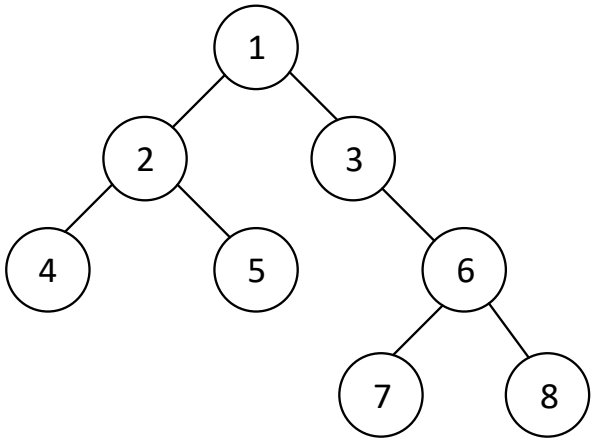

Figure 2.13: Branch and Bound Breadth-First Approach

Branch and Reduce Optimisation Navigator (BARON) is an NLP and MINLP solver used to achieve globally optimal solutions. It was first developed at the University of Illonis by Nikolaos Sahindis. It uses the Branch and Bound algorithm to solve optimisation problems (Kronqvist *et al.*, 2018).

2.15 Techno-Economic Evaluation of PEMEs and PEMFCs

In order to adopt hydrogen as a future fuel source, the cost would need to be competitive to the cost of fossil-fuel derived energy. Fossil fuels are widely used globally and, therefore, have a significant presence in the economic market. Alkaline electrolysers were developed in 1920 (Zhang *et al.*, 2015; Schmidt *et al.*, 2017) and have low capital costs and high maintenance costs. This is attributed towards the electrolyte's corrosive nature and circulation required (Habermeyer and Kurkela, 2018). As PEM technology becomes more mature and commercialised, the cost of PEMEs and PEMFCs will decrease. Additionally, improvement in the efficiency of PEMEs and PEMFCs is predicted to promote greater market penetration in the renewable energy sector, as well as reduce the operating costs of the PEME and PEMFC stack (Saur, 2008; Thomas, 2018).

Saur (2008) performed a study to analyse the economic cost of electrolyser components being commercially developed. The effect of the cost of hydrogen was evaluated on various system sizes. This analysis used the standard H2A production model to simulate different scenarios. In the study, the capital cost of the stack was identified as the costliest component in the electrolyser. For small systems (10 kg/day-100 kg/day) the cost of hydrogen significantly influenced the capital cost of the system. The cost of those systems could be reduced by introducing a simpler electrolyser design with fewer components, as well as an increasing the volume of hydrogen produced. Secondly, power electronics had been identified as the second most costly component in electrolysers. In larger systems (100kg/day-1000kg/day hydrogen production) it has been established that greater electrolyser efficiency reduced the amount of input electricity required, which ultimately reduced the hydrogen production cost.

In the work of Samaniego et al. (2008), a hybrid wind/electrolyser/storage/fuel cell system used to provide continuous electrical generation was presented. More specifically, an economic evaluation was carried out on the system to determine its viability. The economic evaluation was simulated in TRNSYS 15, and different scenarios were investigated. Scenario one presented an electrolyser that was operated in a non-constant mode (operated when excess energy was available), whereas in the Scenario two, batteries were included to guarantee a constant electrolyser operation mode. The results indicated that the system which used the non-constant electrolyser mode had a lower initial investment and maintenance cost. This was due to the presence of batteries in the constant electrolyser operation mode. However, both modes expressed excessively long payback periods, as a result of high capital costs. Therefore, improvements in the individual components, as well as evolution of the various technologies, will improve the competitiveness of hybrid systems.

The work of Corsini et al. (2009) investigated the use of a hydrogen system and desalination system, to effectively use surplus renewable energy present on the Ventotene Island. The proposed systems were examined and functioned as a seasonal buffering system. As a result, the systems contributed towards an oil saving of more than 60%, thereby reducing costs.

In 2013, Bezmalinovic et al. (2013) performed a techno-economic evaluation of a PEMFC integrated with a hybrid PV-system for application in remote telecommunication base stations. The system studied consisted of PV/diesel/ generator/battery and PV/PEMFC/battery. The authors reported that the use of hydrogen was appealing, even though the cost and application of hydrogen storage provided various challenges. At the time at which the analysis was conducted, the system with the diesel generator realised a lower levelised cost of electricity (approximately 15% lower) compared to the system with the PEMFC.

Rahimi et al. (2014) worked on a techno-economic evaluation of a hybrid system comprised of an electrolyser, wind turbine, hydrogen storage tank and a PEMFC. All components were modelled, and an energy, exergy and economic evaluation was conducted. The analysis was done on five Iranian cities and a positive net present value was realised in all the investigated cities.

Kalinci et al. (2015) conducted a techno-economic analysis of a wind turbine/PV/electrolyser/converter/hydrogen tank/fuel cell system for Bozcaada Island located in Turkey. HOMER was used to optimise the system based on the island's available geographical and meteographic data. In that work, the net present cost (NPC) method was used to rank the suitability of the system. Additionally, the total annualised cost (TAC) and the cost of energy (COE) was calculated to give an indication of the economic viability of the system. To optimise the equipment sizes, HOMER considered the operating conditions and technical specifications of each component, as well as minimised the system's NPC.

In another study, Felgenhauer et al. (2015) investigated the economic feasibility of power-to-hydrogen systems, with alkaline and proton exchange membrane electrolysers used in mobility applications. Based on their research, alkaline electrolysers were found to competitively supply hydrogen at costs ranging from \$4.96-\$5.78/kg. Conversely, Hosseinalizadeh et al. (2016) conducted a feasibility study on a hybrid system containing wind turbines, PVs and fuel cells. The investigation was conducted for regions in Iran and used the meteographic data of those regions which included solar radiance and average wind speeds.

Ferrero et al. (2016) investigated PtG systems for renewable energy storage in gaseous hydrogen. The study included a cost assessment for hydrogen used for electricity generation, grid injection and mobility applications. The cost assessment was conducted for the years 2013-2030. Additionally, a case study for the Italian electricity and mobility sectors was presented to determine the influence of energy storage in hydrogen.

The results indicated that in 2013, alkaline and PEMFCs presented the most cost-effective PtP systems, and will be able to compete with battery-electric energy systems.

A dynamic PtG model was presented by Parra and Patel (2016) to determine the levelised cost, performance and value of PtG systems. The model also took into account electrolyser ageing. The results from that work indicated that a 35.1% internal rate of return was obtained in a 1 MW PtG system that sold electricity and hydrogen. The levelised cost of PEME under kW scale operation was found to be 15% greater than the levelised cost of alkaline electrolysers. This was attributed towards greater initial stack costs, as well as component degradation which limited the life of the electrolyser and increased the rate of power consumption.

Schmidt et al. (2017) presented an expert elicitation study on alkaline, PEM and SOEC water electrolysis cells to predict the prospective capital costs, efficiencies and lifetimes expected over the next 20 years. In the elicitation study, ten experts (five academic experts and five industry experts) were contracted, interviewed, and asked to complete a questionnaire. Based on the results obtained, alkaline electrolysers were identified to be the most dominant electrolysers in 2020, whereas PEMEs in 2030. Additionally, increased research and development funding is capable of reducing the capital cost by 0-24%, whilst production scale-up has a 17-30% impact on the capital cost. This was due to improved manufacturing processes, an increase in operational experience and automation of the electrolysers.

In general, capital costs for PEMEs were found to the range for 1860-2320 €/kW, compared to alkaline electrolysers with a capital cost of 1000-1200 € /kW (Schmidt *et al.*, 2017; Habermeyer and Kurkela, 2018). Schmidt et al. (2017) identified the platinum catalyst and the fluorinated membrane as the key cost drivers for the high PEME capital costs.

In order to reduce capital costs, current developments are focused on targeting less expensive catalysts and simplifying the manufacturing process. Furthermore, Schmidt et al. (2017) elicited cost development predictions from electrolyser experts and found that most experts estimated that the capital cost of PEMEs will drop in the price range of 700-1200 €/kW in 2020 and 500-1200 €/kW in 2030. Another study conducted by Andrews and Shabani (2012) assumed a capital cost of 1500 €/kW and estimated a price drop to 1000 €/kW in 2030.

In a different report conducted by IRENA, the PEME was expected to have a stack capital cost of 1200 €/kW in 2017, and this was expected to decrease to 700 €/kW in 2025. The stack replacement cost was found to be 420 €/kW in 2017 and reduced to 210 €/kW in 2025 (IRENA, 2018). Figure 2.14 and Figure 2.15 graphically illustrates the PEME and alkaline capital costs predicted from 1990 to 2030 extracted from the work done by Saba et al. (2018).

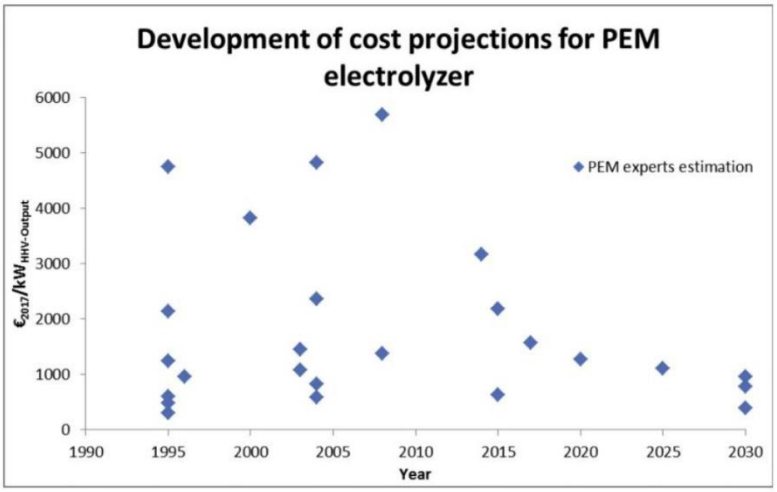

Figure 2.14: PEME Capital Cost Trends Based on Expert Estimations (Saba *et al.*, 2018)

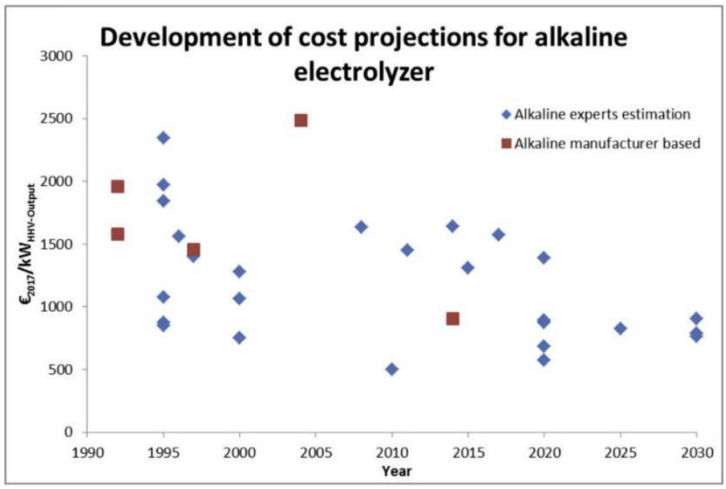

Figure 2.15: Alkaline Electrolysis Capital Cost Trends Based on Expert Estimations (Saba *et al.*, 2018)

In order for PEMEs to become more economically favourable in the future, the following drivers contribute towards the cost reduction:

- The more exposure the electrolysers have in the market, the greater the demand and higher the volume of electrolysers produced. This will, therefore, result in a reduction in the cost.
- Costs will reduce if more industries supply electrolysers, eliminating the monopoly effect on the economy and consumers.
- Higher competition results in reduced margins and lower prices
- As the electrolysers become more mature, better quality of products may be produced, resulting in higher efficiencies and improved lifetimes.

In contrast, SOEs were found to have a higher capital cost in comparison to alkaline and PEMEs. Current SOEs are available at a capital cost of >2000 €/kW. Despite the high costs associated with SOEs, this type of technology is the most recently developed electrolyser, therefore, there is potential for a price reduction when alternative materials of construction are found. Furthermore, high material degradation is present in SOEs, due to the elevated temperatures at which the electrolysers are operated.

To reduce the capital cost in the future, research in finding a more stable material is required, or the temperature at which the electrolysis takes place must be reduced. According to the study conducted by Schmidt et al (2017), the capital cost is predicted to drop to 1300-3000 €/kW in 2020 and to 500-1000 €/kW in 2030. This makes the SOE a competitive option for future application.

2.16 References

Abdel Ghany, N.A. *et al.* (2002) "Oxygen evolution anodes composed of anodically deposited Mn-Mo-Fe oxides for seawater electrolysis," *Electrochimica Acta*, 48(1), pp. 21–28. doi:10.1016/S0013-4686(02)00539-X.

Abdel-aal, H. *et al.* (2012) "Feasibility study for a solar-energy stand-alone system," *Smart Grid and Renewable Energy*, 3(3), pp. 204–206. doi:10.4236/sgre.2012.33028.

Abdel-Aal, H.K., Zohdy, K.M. and Kareem, M.A. (2010) "Hydrogen production using sea water electrolysis," *The Open Fuel Cells Journal*, 3, pp. 1–7. doi:10.2174/1875932701003010001.

Abdin, Z., Webb, C.J. and Gray, E.M. (2015) "Modelling and simulation of a proton exchange membrane (PEM) electrolyser cell," *International Journal of Hydrogen Energy*, 40(39), pp. 13243–13257. doi:10.1016/j.ijhydene.2015.07.129.

Abdin, Z., Webb, C.J. and Gray, E.M.A. (2016) "PEM fuel cell model and simulation in Matlab–Simulink based on physical parameters," *Energy*, 116, pp. 1131–1144. doi:10.1016/j.energy.2016.10.033.

AlZahrani, A.A. and Dincer, I. (2017) "Thermodynamic and electrochemical analyses of a solid oxide electrolyzer for hydrogen production," *International Journal of Hydrogen Energy*, 42(33), pp. 21404–21413. doi:10.1016/j.ijhydene.2017.03.186.

Amikam, G., Nativ, P. and Gendel, Y. (2018) "Chlorine-free alkaline seawater electrolysis for hydrogen production," *International Journal of Hydrogen Energy*, 43(13), pp. 6504–6514. doi:10.1016/j.ijhydene.2018.02.082.

Amphlett, J.C. and J. C. Amphlett, R. M. Baumert, R. F. Mann, B. A. Peppley, and P.R.R. (1995) "Performance modeling of the Ballard Mark IV solid polymer electrolyte fuel cell," *Journal of The Electrochemical Society*, 142(1), pp. 9–15. doi:10.1149/1.2043959.

Andrews, J. and Shabani, B. (2012) “Dimensionless analysis of the global techno-economic feasibility of solar-hydrogen systems for constant year-round power supply,” *International Journal of Hydrogen Energy*, 37(1), pp. 6–18. doi:10.1016/j.ijhydene.2011.09.102.

Awasthi, A., Scott, K. and Basu, S. (2011) “Dynamic modeling and simulation of a proton exchange membrane electrolyzer for hydrogen production,” *International Journal of Hydrogen Energy*, 36(22), pp. 14779–14786. doi:10.1016/j.ijhydene.2011.03.045.

Babic, U. *et al.* (2017) “Critical Review—Identifying Critical Gaps for Polymer Electrolyte Water Electrolysis Development,” *Journal of The Electrochemical Society*, 164(4), pp. F387–F399. doi:10.1149/2.1441704jes.

Badea, G.E., Caraban, A., *et al.* (2007) “Hydrogen generation by electrolysis of seawater,” *Fascicle of Management and Technological Engineering*, VI(XVI).

Badea, G.E., Maior, I., *et al.* (2007) “The cathodic evolution of hydrogen on nickel in artificial seawater,” *Revue Roumaine de Chimie*, 52(12), pp. 1123–1130.

Balaji, R. *et al.* (2009) “An alternative approach to selective sea water oxidation for hydrogen production,” *Electrochemistry Communications*, 11(8), pp. 1700–1702. doi:10.1016/j.elecom.2009.06.022.

Barbir, F. (2005) “PEM electrolysis for production of hydrogen from renewable energy sources,” *Solar Energy*, 78(5), pp. 661–669. doi:10.1016/j.solener.2004.09.003.

Bednarek, T. and Tsotridis, G. (2017) “Issues associated with modelling of proton exchange membrane fuel cell by computational fluid dynamics,” *Journal of Power Sources*, 343, pp. 550–563. doi:10.1016/j.jpowsour.2017.01.059.

Beicha, A. and Zaamouche, R. (2013) “Electrochemical model for proton exchange membrane fuel cells systems,” *Journal of Power Technologies*, 93(1), pp. 27–36. Available at: http://papers.itc.pw.edu.pl/index.php/JPT/article/view/307.

Belkhiri, Z. *et al.* (2011) “Effect of temperature and water content on the performance of PEM fuel cell,” *Revue des Energies Renouvelables*, 14(1), pp. 121–130.

Bennett, J.E. (1980) “Electrodes for generation of hydrogen and oxygen from seawater,” *International Journal of Hydrogen Energy*, 5(4), pp. 401–408. doi:10.1016/0360-3199(80)90021-X.

Bernardi, D.M. and Verbrugge, M.W. (1991) “Mathematical model of a gas diffusion electrode bonded to a polymer electrolyte,” *AIChE Journal*, 37(8), pp. 1151–1163. doi:10.1002/aic.690370805.

Bernardi, D.M. and Verbrugge, M.W. (1992) “A Mathematical Model of the Solid-Polymer-Electrolyte Fuel Cell,” *Journal of The Electrochemical Society*, 139(9), pp. 2477–2491. doi:10.1149/1.2221251.

Bezmalinović, D., Barbir, F. and Tolj, I. (2013) “Techno-economic analysis of PEM fuel cells role in photovoltaic-based systems for the remote base stations,” *International Journal of Hydrogen Energy*, 38(1), pp. 417–425. doi:10.1016/j.ijhydene.2012.09.123.

Biaku, C.Y. *et al.* (2008) “A semiempirical study of the temperature dependence of the anode charge transfer coefficient of a 6 kW PEM electrolyzer,” *International Journal of Hydrogen Energy*, 33(16), pp. 4247–4254. doi:10.1016/j.ijhydene.2008.06.006.

Biegler, L.T. and Grossmann, I.E. (2004) “Retrospective on optimization,” *Computers and Chemical Engineering*, 28(8), pp. 1169–1192. doi:10.1016/j.compchemeng.2003.11.003.

Bockris, J.O. (1976) “Energy: The Solar Hydrogen Alternative,” *Journal of The Electrochemical Society*, 123(8). doi:10.1149/1.2133054.

Cameron, D.S. (1990) “World developments of fuel cells,” *International Journal of Hydrogen Energy*, 34(1), pp. 26–35. doi:10.1016/0360-3199(90)90148-R.

Carmo, M. *et al.* (2013) “A comprehensive review on PEM water electrolysis,” *International Journal of Hydrogen Energy*, 38(12), pp. 4901–4934. doi:10.1016/j.ijhydene.2013.01.151.

Carton, J.G. and Olabi, A.G. (2017) “Three-dimensional proton exchange membrane fuel cell model: Comparison of double channel and open pore cellular foam flow plates,” *Energy* [Preprint]. doi:10.1016/j.energy.2016.02.010.

Castro, P.M., Castillo, P.C. and Mahalec, V. (2017) “Deterministic global optimization algorithm using piecewise relaxations and bound tightening with dynamic partitioning,” in *Computing and Systems Technology Division 2017 - Core Programming Area at the 2017 AIChE Annual Meeting*.

Chandesris, M. *et al.* (2015) “Membrane degradation in PEM water electrolyzer: Numerical modeling and experimental evidence of the influence of temperature and current density,” *International Journal of Hydrogen Energy*, 40(3), pp. 1353–1366. doi:10.1016/j.ijhydene.2014.11.111.

Cheng, J.J. (2017) *Biomass to renewable energy processes*. 2nd edn, *Biomass to Renewable Energy Processes, Second Edition*. 2nd edn. Boca Raton: CRC Press. doi:10.1201/9781315152868.

Choi, P., Bessarabov, D.G. and Datta, R. (2004) “A simple model for solid polymer electrolyte (SPE) water electrolysis,” *Solid State Ionics*, 175(1–4), pp. 535–539. doi:10.1016/j.ssi.2004.01.076.

Chong, E.K.P. and Zak, S.H. (2013) *An Introduction To Optimization*. Fourth, *Journal of Chemical Information and Modeling*. Fourth. Available at: Wiley.

Chua, K.J. *et al.* (2014) “Sustainable energy systems for a remote island community,” *Applied Energy*, 113, pp. 1752–1763. doi:10.1016/j.apenergy.2013.09.030.

Ciapessoni, E. *et al.* (2013) “Renewable power integration in Sicily: Frequency stability issues and possible countermeasures,” *2013 IREP Symposium Bulk Power System Dynamics and Control - IX Optimization, Security and Control of the Emerging Power Grid*, pp. 1–7. doi:10.1109/IREP.2013.6629350.

Clarke, D.P., Al-Abdeli, Y.M. and Kothapalli, G. (2015) “Multi-objective optimisation of renewable hybrid energy systems with desalination,” *Energy*, 88, pp. 457–468. doi:10.1016/j.energy.2015.05.065.

Colella, W.G. *et al.* (2014) *Techno-economic analysis of PEM electrolysis for hydrogen production*. Colorado. Available at: https://www.energy.gov/sites/prod/files/2014/08/f18/fcto_2014_electrolytic_h2_wkshp_colella1.pdf.

Cong, Z. and Xinghu, L. (2010) “A new one dimensional steady state model for PEM fuel cell,” *World Electric Vehicle Journal*, 4, pp. 000437–0000443.

Corsini, A. *et al.* (2009) “Assessment of H2- and H2O-based renewable energy-buffering systems in minor islands,” *Renewable Energy*, 34(1), pp. 279–288. doi:10.1016/j.renene.2008.03.005.

Dale, N.V., Mann, M.D. and Salehfar, H. (2008) “Semiempirical model based on thermodynamic principles for determining 6kW proton exchange membrane electrolyzer stack characteristics,” *Journal of Power Sources*, 185(2), pp. 1348–1353. doi:10.1016/j.jpowsour.2008.08.054.

Dedigama, I. *et al.* (2014) “An experimentally validated steady state polymer electrolyte membrane water electrolyser model,” *International Journal of Electrochemical Science*, 9(5), pp. 2662–2681.

Demir, M.E. and Dincer, I. (2017) “Development of a hybrid solar thermal system with TEG and PEM electrolyzer for hydrogen and power production,” *International Journal of Hydrogen Energy*, 42(51), pp. 30044–30056. doi:10.1016/j.ijhydene.2017.09.001.

Dokkar, B. *et al.* (2013) “Optimization of PEM fuel cells for PV-Hydrogen power system,” *Energy Procedia*, 36, pp. 798–807. doi:10.1016/j.egypro.2013.07.092.

Duić, N., Krajačić, G. and da Graça Carvalho, M. (2008) “RenewIslands methodology for sustainable energy and resource planning for islands,” *Renewable and Sustainable Energy Reviews*, 12(4), pp. 1032–1062. doi:10.1016/j.rser.2006.10.015.

Eikerling, M. *et al.* (1998) “Phenomenological theory of electro-osmotic effect and water management in polymer electrolyte proton-conducting membranes,” *Journal of The Electrochemical Society*, 145(8), pp. 2684–2699. doi:10.1149/1.1838700.

El-Bassuoni, A.M.A., Sheffield, J.W. and Vezirogl'u, T.N. (1982) “Hydrogen and fresh water production from sea water,” *International Journal of Hydrogen Energy*, 7(12), pp. 919–923. doi:10.1016/0360-3199(82)90159-8.

El-Deab, M.S. *et al.* (2007) “Enhanced water electrolysis: Electrocatalytic generation of oxygen gas at manganese oxide nanorods modified electrodes,” *Electrochemistry Communications*, 9(8), pp. 2082–2087. doi:10.1016/j.elecom.2007.06.011.

El-Moneim, A.A. (2011) “Mn-Mo-W-oxide anodes for oxygen evolution during seawater electrolysis for hydrogen production: Effect of repeated anodic deposition,” *Fuel and Energy Abstracts*, 36(21), pp. 13398–13406. doi:10.1016/j.ijhydene.2011.07.100.

Espinosa-López, M. *et al.* (2018) “Modelling and experimental validation of a 46 kW PEM high pressure water electrolyzer,” *Renewable Energy*, 119, pp. 160–173. doi:10.1016/j.renene.2017.11.081.

Falcão, D.S. *et al.* (2009) “Water transport through a PEM fuel cell: A one-dimensional model with heat transfer effects,” *Chemical Engineering Science*, 64(9), pp. 2216–2225. doi:10.1016/j.ces.2009.01.049.

Falcão, D.S. and Pinto, A.M.F.R. (2020) “A review on PEM electrolyzer modelling: Guidelines for beginners,” *Journal of Cleaner Production*. doi:10.1016/j.jclepro.2020.121184.

Felgenhauer, M. and Hamacher, T. (2015) “State-of-the-art of commercial electrolyzers and on-site hydrogen generation for logistic vehicles in South Carolina,” *International Journal of Hydrogen Energy* [Preprint]. doi:10.1016/j.ijhydene.2014.12.043.

Ferreira, R.B. *et al.* (2015) “A one-dimensional and two-phase flow model of a proton exchange membrane fuel cell,” *Journal of Chemical Technology and Biotechnology*, 90(9), pp. 1547–1551. doi:10.1002/jctb.4651.

Ferrero, D. *et al.* (2016) “Power-to-Gas Hydrogen: Techno-economic Assessment of Processes towards a Multi-purpose Energy Carrier,” *Energy Procedia*, 101, pp. 50–57. doi:10.1016/j.egypro.2016.11.007.

Food and Agriculture Organization of the United Nations (FAO) and International Water Management Institute (IWMI) (2017) *Water pollution from agriculture: a global review, FAO and IWMI*. doi:http://www.fao.org/3/a-i7754e.pdf.

Fritz, D.L., Mergel, J. and Stolten, D. (2014) “PEM Electrolysis Simulation and Validation,” *ECS Transactions*, 58(19), pp. 1–9. doi:10.1149/05819.0001ecst.

Gahleitner, G. (2013) “Hydrogen from renewable electricity: An international review of power-to-gas pilot plants for stationary applications,” *International Journal of Hydrogen Energy*, pp. 2039–2061. doi:10.1016/j.ijhydene.2012.12.010.

García-Valverde, R., Espinosa, N. and Urbina, A. (2012) “Simple PEM water electrolyser model and experimental validation,” *International Journal of Hydrogen Energy*, 37(2), pp. 1927–1938. doi:10.1016/j.ijhydene.2011.09.027.

González, A., McKeogh, E. and Gallachóir, B.Ó. (2004) “The role of hydrogen in high wind energy penetration electricity systems: The Irish case,” *Renewable Energy*, 29(4), pp. 471–489. doi:10.1016/j.renene.2003.07.006.

Görgün, H. (2006) “Dynamic modelling of a proton exchange membrane (PEM) electrolyzer,” *International Journal of Hydrogen Energy*, 31(1), pp. 29–38. doi:10.1016/j.ijhydene.2005.04.001.

Grigoriev, S.A. *et al.* (2010) “Mathematical modeling of high-pressure PEM water electrolysis,” *Journal of Applied Electrochemistry*, 40(5), pp. 921–932. doi:10.1007/s10800-009-0031-z.

Grossmann, I.E. and Harjunkoski, I. (2019) “Process systems Engineering: Academic and industrial perspectives,” *Computers and Chemical Engineering*, 126, pp. 474–484. doi:10.1016/j.compchemeng.2019.04.028.

Grujicic, M. and Chittajallu, K.M. (2004) “Design and optimization of polymer electrolyte membrane (PEM) fuel cells,” *Applied Surface Science*, 227(2004), pp. 56–72. doi:10.1016/j.apsusc.2003.10.035.

Gurau, V., Liu, H. and Kakaç, S. (1998) “Two-dimensional model for proton exchange membrane fuel cells,” *AIChE Journal*, 44(11), pp. 2410–2422. doi:10.1002/aic.690441109.

Habermeyer, F. (DLR) and Kurkela, M. (VTT) (2018) *Flexible combined production of power, heat and transport fuels from renewable energy sources*.

Han, B. *et al.* (2015) “Electrochemical performance modeling of a proton exchange membrane electrolyzer cell for hydrogen energy,” *International Journal of Hydrogen Energy*, 40(22), pp. 7006–7016. doi:10.1016/j.ijhydene.2015.03.164.

Han, B. *et al.* (2017) “Modeling of two-phase transport in proton exchange membrane electrolyzer cells for hydrogen energy,” *International Journal of Hydrogen Energy*, 42(7), pp. 4478–4489. doi:10.1016/j.ijhydene.2016.12.103.

Haraldsson, K. and Wipke, K. (2004) “Evaluating PEM fuel cell system models,” *Journal of Power Sources*, 126(1–2), pp. 88–97. doi:10.1016/j.jpowsour.2003.08.044.

Harrison, K.W. *et al.* (2006) “Semiempirical model for determining PEM electrolyzer stack characteristics,” *Journal of Fuel Cell Science and Technology*, 3(2), pp. 220–223. doi:10.1115/1.2174072.

Hosseinalizadeh, R. *et al.* (2016) “Economic sizing of a hybrid (PV-WT-FC) renewable energy system (HRES) for stand-alone usages by an optimization-simulation model: Case study of Iran,” *Renewable and Sustainable Energy Reviews* [Preprint]. doi:10.1016/j.rser.2015.09.046.

Hsu, G.S.W., Hsia, C.W. and Hsu, S.Y. (2015) “Effects of electrode settings on chlorine generation efficiency of electrolyzing seawater,” *Journal of Food and Drug Analysis* [Preprint]. doi:10.1016/j.jfda.2015.06.007.

Hsu, G.S.W., Lu, Y.F. and Hsu, S.Y. (2017) “Effects of electrolysis time and electric potential on chlorine generation of electrolyzed deep ocean water,” *Journal of Food and Drug Analysis*, 25(4), pp. 759–765. doi:10.1016/j.jfda.2016.07.001.

Hsu, S.H. *et al.* (2018) “An Earth-Abundant Catalyst-Based Seawater Photoelectrolysis System with 17.9% Solar-to-Hydrogen Efficiency,” *Advanced Materials*, 30(18). doi:10.1002/adma.201707261.

Hussein, I.A. (1992) *Hydrogen Production by The Electrolysis of Saline Water*. Hhahran, Saudi Arabia.

IEA (2019) *The Future of Hydrogen*. Available at: https://www.iea.org/reports/the-future-of-hydrogen (Accessed: April 10, 2020).

IRENA (2018) *Hydrogen from Renewable Power : Technology Outlook for the Energy Transition*. Available at: https://www.irena.org/-/media/Files/IRENA/Agency/Publication/2018/Sep/IRENA_Hydrogen_from_renewable_power_2018.pdf.

Ju-Hyung, L. (2013) “Fuel cell using seawater electrolyzer, methods for producing caustic soda, ammonia, urea and pvc using the seawater electrolyzer and integrated system thereof.” Korea: United States Patent Application Publication.

Kabir, K.M. and Matin Bhuiyan, M.A. (2017) “Design & simulation of hydrogen based hybrid green power system using sea water for Cox’s Bazar,” *Cogent Engineering*, 4(1), pp. 1–14. doi:10.1080/23311916.2017.1347029.

Kahroba, P., Mirzaee, I. and Shirvani, H. (2009) “The influence of membrane thickness on the PEM fuel cell operation,” in *h2fc2009*.

Kahveci, E.E. and Taymaz, I. (2014) “An investigation of GDL porosity on PEM fuel cell performance,” *Chemical Engineering Transactions*, 42, pp. 37–42. doi:10.3303/CET1442007.

Kalinci, Y., Hepbasli, A. and Dincer, I. (2015) “Techno-economic analysis of a stand-alone hybrid renewable energy system with hydrogen production and storage options,” *International Journal of Hydrogen Energy*, 40(24), pp. 7652–7664. doi:10.1016/j.ijhydene.2014.10.147.

Katsaprakakis, D. Al and Christakis, D.G. (2014) “Seawater pumped storage systems and offshore wind parks in islands with low onshore wind potential. A fundamental case study,” *Energy* [Preprint]. doi:10.1016/j.energy.2014.01.021.

Kim, H., Park, M. and Lee, K.S. (2013) “One-dimensional dynamic modeling of a high-pressure water electrolysis system for hydrogen production,” *International Journal of Hydrogen Energy*, 38(6), pp. 2596–2609. doi:10.1016/j.ijhydene.2012.12.006.

Kirk, D.W. and Ledas, A.E. (1982) “Precipitate formation during sea water electrolysis,” *International Journal of Hydrogen Energy*, 7(12), pp. 925–932. doi:10.1016/0360-3199(82)90160-4.

Komor, P. and Glassmaire, J. (2012) “Electricity storage and renewables for island power,” *IRENA* [Preprint].

Kronqvist, J. *et al.* (2018) “A review and comparison of solvers for convex MINLP,” *Optimization and Engineering*, 20, pp. 397–455. doi:10.1007/s11081-018-9411-8.

Kuang, Y. *et al.* (2019) “Solar-driven, highly sustained splitting of seawater into hydrogen and oxygen fuels,” *Proceedings of the National Academy of Sciences of the United States of America*, 116(14), pp. 6624–6629. doi:10.1073/pnas.1900556116.

Kumar, N. and Khare, P.S. (2011) “One Dimensional Steady State Model for Studying Hydration of Membrane in Proton Exchange Membrane Fuel Cell,” *International Journal of Applied Physics and Mathematics* [Preprint]. doi:10.7763/ijapm.2011.v1.18.

Laguna-Bercero, M.A. (2012) “Recent advances in high temperature electrolysis using solid oxide fuel cells: A review,” *Journal of Power Sources*, 203, pp. 4–16. doi:10.1016/j.jpowsour.2011.12.019.

Lebbal, M.E. and Lecœuche, S. (2009) “Identification and monitoring of a PEM electrolyser based on dynamical modelling,” *International Journal of Hydrogen Energy*, 34(14), pp. 5992–5999. doi:10.1016/j.ijhydene.2009.02.003.

Lee, B., Park, K. and Kim, H.M. (2013) “Dynamic simulation of PEM water electrolysis and comparison with experiments,” *International Journal of Electrochemical Science*, 8, pp. 235–248.

Lee, D. *et al.* (2019) “Transport of water through polymer membrane in proton exchange membrane fuel cells,” *Korean Chemical Engineering Research*, 57(3), pp. 338–343. doi:10.9713/KCER.2019.57.3.338.

Lei, D. *et al.* (2018) “Properties of AuPdPt-WC/C nanocomposite catalyst in simulated seawater solution for hydrogen evolution,” *Materials Research Innovations*, 22(4), pp. 183–186. doi:10.1080/14328917.2017.1287491.

Li, Y. and Lv, H. (2018) “The combined effects of water transport on proton exchange membrane fuel cell performance,” *Chemical Engineering Transactions*, 65(2015), pp. 691–696. doi:10.3303/CET1865116.

Lin, M. *et al.* (2015) “Flexible Photovoltaics / Fuel Cell / Wind Turbine (PVFCWT) Hybrid Power System Designs,” *Chemical Engineering Transactions*, 45, pp. 559–564. doi:10.3303/CET1545094.

Lin, M.-H., Tsai, J.-F. and Wang, P.-C. (2012) “Solving Engineering Optimization Problems by a Deterministic Global Optimization Approach,” *Applied Mathematics & Information Sciences*, 6(3), pp. 1101–1107. Available at: http://www.naturalspublishing.com/files/published/lrk6a1j779a881.pdf.

Liu, H.Y. and Wu, S. De (2010) “An assessment on the planning and construction of an island renewable energy system - A case study of Kinmen Island,” *Renewable Energy*, 35(12), pp. 2723–2731. doi:10.1016/j.renene.2010.04.021.

Liu, W.H. *et al.* (2019) “Development and optimization of an integrated energy network with centralized and decentralized energy systems using mathematical modelling approach,” *Energy*, 183, pp. 617–629. doi:10.1016/j.energy.2019.06.158.

Lundell, A. and Westerlund, T. (2012) “Finding an optimized set of transformations for convexifying nonconvex MINLP problems,” *Computer Aided Chemical Engineering*, 31. doi:10.1016/B978-0-444-59506-5.50130-9.

Ma, Y.Y. *et al.* (2017) “Highly efficient hydrogen evolution from seawater by a low-cost and stable CoMoP@C electrocatalyst superior to Pt/C,” *Energy and Environmental Science*, 10(3). doi:10.1039/c6ee03768b.

Mahmud, N., Hassan, A. and Rahman, M.S. (2013) “Modelling and cost analysis of hybrid energy system for St. Martin Island using HOMER,” in *2013 International Conference on Informatics, Electronics and Vision, ICIEV 2013*. doi:10.1109/ICIEV.2013.6572678.

Maleki, A. (2018) “Design and optimization of autonomous solar-wind-reverse osmosis desalination systems coupling battery and hydrogen energy storage by an improved bee algorithm,” *Desalination*, 435, pp. 221–234. doi:10.1016/j.desal.2017.05.034.

Mammar, K., Saadaoui, F. and Laribi, S. (2019) “Design of a PEM fuel cell model for flooding and drying diagnosis using fuzzy logic clustering,” *Renewable Energy Focus*, 30(11), pp. 123–130. doi:10.1016/j.ref.2019.06.001.

Mann, R.F. *et al.* (2000) “Development and application of a generalized steady-state electrochemical model for a PEM fuel cell,” *Journal of Power Sources*, 86(1–2), pp. 173–180. doi:10.1016/S0378-7753(99)00484-X.

Marangio, F., Santarelli, M. and Calì, M. (2009) “Theoretical model and experimental analysis of a high pressure PEM water electrolyser for hydrogen production,” *International Journal of Hydrogen Energy*, 34(3), pp. 1143–1158. doi:10.1016/j.ijhydene.2008.11.083.

Marr, C. and Li, X. (1998) “An engineering model of proton exchange membrane fuel cell performance,” *ARI - An International Journal for Physical and Engineering Sciences*, 50, pp. 190–200. doi:10.1007/s007770050014.

Mathiesen, B.V. *et al.* (2013) “Aalborg Universitet Technology data for high temperature solid oxide electrolyser cells, alkali and PEM electrolysers,” *Technology data for high temperature solid oxide electrolyser cells, alkali and PEM* [Preprint]. Available at: http://vbn.aau.dk/ws/files/80222058/Technology_data_for_SOEC_alkali_and_PEM_electrolysers.pdf.

Mawardi, A., Yang, F. and Pitchumani, R. (2005) “Optimization of the operating parameters of a proton exchange membrane fuel cell for maximum power density,” *Journal of Fuel Cell Science and Technology*, 2(2), p. 121. doi:10.1115/1.1867978.

Mendoza-Vizcaino, J. *et al.* (2016) “Renewable technologies for generation systems in islands and their application to Cozumel Island, Mexico,” *Renewable and Sustainable Energy Reviews*, 64, pp. 348–361. doi:10.1016/j.rser.2016.06.014.

Meng, H. and Wang, C.Y. (2005) “Model of two-phase flow and flooding dynamics in polymer electrolyte fuel cells,” *Journal of the Electrochemical Society*, p. A1733. doi:10.1149/1.1955007.

Mert, S.O., Ozcelik, Z. and Dincer, I. (2015) “Comparative assessment and optimization of fuel cells,” *International Journal of Hydrogen Energy*, 40(24), pp. 7835–7845. doi:10.1016/j.ijhydene.2014.11.050.

Mo, Z.J. *et al.* (2006) “Parameter optimization for a PEMFC model with a hybrid genetic algorithm,” *International Journal of Energy Research* [Preprint]. doi:10.1002/er.1170.

Mohammad, M. and Kaukhab, M. (2011) “Prospects of Sea Water Electrolysis for the Production of Hydrogen: An Exploratory Study on the Electrolysis of Magnesium Chloride Solution in the Presence of Sulfur,” *Journal of the Chemical Society of Pakistan*, 32(2), pp. 166–170.

Mura, P.G. *et al.* (2015) “An energy autonomous house equipped with a solar PV hydrogen conversion system,” *Energy Procedia*, 78, pp. 1998–2003. doi:10.1016/j.egypro.2015.11.392.

Muts, P., Nowak, I. and Hendrix, E.M.T. (2020) “The decomposition-based outer approximation algorithm for convex mixed-integer nonlinear programming,” *Journal of Global Optimization*, 77, pp. 75–96. doi:10.1007/s10898-020-00888-x.

Natarajan, D. and van Nguyen, T. (2003) “Three-dimensional effects of liquid water flooding in the cathode of a PEM fuel cell,” *Journal of Power Sources*, 115, pp. 60–80. doi:10.1016/S0378-7753(02)00624-9.

Ni, M., Leung, M.K.H. and Leung, D.Y.C. (2006) “Electrochemistry Modeling of Proton Exchange Membrane (PEM) Water Electrolysis for Hydrogen Production,” *WHEC*, 16, pp. 13–16.

Ni, M., Leung, M.K.H. and Leung, D.Y.C. (2008) “Technological development of hydrogen production by solid oxide electrolyzer cell (SOEC),” *International Journal of Hydrogen Energy*, 33(9), pp. 2337–2354. doi:10.1016/j.ijhydene.2008.02.048.

De Nora (2015) *Seawater Electrochlorination Systems*.

Obayopo, S.O., Bello-Ochende, T. and Meyer, J.P. (2013) “Three-dimensional optimisation of a fuel gas channel of a proton exchange membrane fuel cell for maximum current density,” *International Journal of Energy Research*, 37(3). doi:10.1002/er.1935.

Ojong, E.T. *et al.* (2017) “Development of an experimentally validated semi-empirical fully-coupled performance model of a PEM electrolysis cell with a 3-D structured porous transport layer,” *International Journal of Hydrogen Energy* [Preprint]. doi:10.1016/j.ijhydene.2017.08.183.

Olivier, P., Bourasseau, C. and Bouamama, P.B. (2017) “Low-temperature electrolysis system modelling: A review,” *Renewable and Sustainable Energy Reviews*, 78, pp. 280–300. doi:10.1016/j.rser.2017.03.099.

Onda, K. *et al.* (2004) “Prediction of production power for high-pressure hydrogen by high-pressure water electrolysis,” *Journal of Power Sources*, 132(1–2), pp. 64–70. doi:10.1016/j.jpowsour.2004.01.046.

Ortiz, A.L., Zaragoza, M.J.M. and Collins-Martínez, V. (2016) “Hydrogen production research in Mexico: A review,” *International Journal of Hydrogen Energy*, 41(48), pp. 23363–23379. doi:10.1016/j.ijhydene.2016.07.004.

Parra, D. and Patel, M.K. (2016) “Techno-economic implications of the electrolyser technology and size for power-to-gas systems,” *International Journal of Hydrogen Energy*, 41(6), pp. 3748–3761. doi:10.1016/j.ijhydene.2015.12.160.

Paul, B. and Andrews, J. (2017) “PEM unitised reversible/regenerative hydrogen fuel cell systems: State of the art and technical challenges,” *Renewable and Sustainable Energy Reviews*, 79, pp. 585–599. doi:10.1016/j.rser.2017.05.112.

Pezic, M. and Cedres, V.M. (2013) “Unit commitment in fully renewable, hydro-wind energy systems,” in *International Conference on the European Energy Market, EEM*. Stockhom,Swedan: IEEE. doi:10.1109/EEM.2013.6607331.

Prieto-Prado, I. *et al.* (2018) “Water and energy self-supply in isolated areas through renewable energies using hydrogen and water as a double storage system,” *Desalination*, 430, pp. 1–14. doi:10.1016/j.desal.2017.12.022.

Qolipour, M., Mostafaeipour, A. and Tousi, O.M. (2017) “Techno-economic feasibility of a photovoltaic-wind power plant construction for electric and hydrogen production: A case study,” *Renewable and Sustainable Energy Reviews*, 78, pp. 113–123. doi:10.1016/j.rser.2017.04.088.

Rahimi, S. *et al.* (2014) “Techno-economic analysis of wind turbine-PEM (polymer electrolyte membrane) fuel cell hybrid system in standalone area,” *Energy*, 67, pp. 381–396. doi:10.1016/j.energy.2014.01.072.

Rao, S.S. (2019) *Engineering Optimization Theory and Practice*. Fifth, *Engineering Optimization Theory and Practice*. Fifth. Edited by John Wiley & Sons. doi:10.1002/9781119454816.

Ravichanran, S. *et al.* (2011) “Sulfonated polystyrene-block-(ethylene-ran-butylene)-block-polystyrene (SPSEBS) membrane for sea water electrolysis to generate hydrogen,” in *ECS Transactions*. doi:10.1149/1.3565511.

Ruzhansky, M., Dutta, H. and Agarwal, R.P. (2018) *Mathematical Analysis and Applications*. Chennai: Wiley.

Ryoo, H.S. and Sahinidis, N. v. (1996) “A branch-and-reduce approach to global optimization,” *Journal of Global Optimization*, 8, pp. 107–138. doi:10.1007/bf00138689.

Saba, S.M. *et al.* (2018) “The investment costs of electrolysis – A comparison of cost studies from the past 30 years,” *International Journal of Hydrogen Energy*, pp. 1209–1223. doi:10.1016/j.ijhydene.2017.11.115.

Saebea, D. *et al.* (2017) “Analysis of unbalanced pressure PEM electrolyzer for high pressure hydrogen production,” *Chemical Engineering Transactions*, 57. doi:10.3303/CET1757270.

Salva, J.A. *et al.* (2016) “Optimization of a PEM fuel cell operating conditions: Obtaining the maximum performance polarization curve,” *International Journal of Hydrogen Energy* [Preprint]. doi:10.1016/j.ijhydene.2016.03.136.

Samaniego, J. *et al.* (2008) “Economic and technical analysis of a hybrid wind fuel cell energy system,” *Renewable Energy*, 33(5), pp. 839–845. doi:10.1016/j.renene.2007.09.023.

Samsatli, S. and Samsatli, N.J. (2018) “A general mixed integer linear programming model for the design and operation of integrated urban energy systems,” *Journal of Cleaner Production*, 191, pp. 458–479. doi:10.1016/j.jclepro.2018.04.198.

Santarelli, M., Medina, P. and Calì, M. (2009) “Fitting regression model and experimental validation for a high-pressure PEM electrolyzer,” *International Journal of Hydrogen Energy*, 34(6), pp. 2519–2530. doi:10.1016/j.ijhydene.2008.11.036.

Saur, G. (2008) *Wind-To-Hydrogen Project: Electrolyzer Capital Cost Study*. doi:10.2172/944892.

Schaaf, T. *et al.* (2014) “Methanation of CO2 - storage of renewable energy in a gas distribution system,” *Energy, Sustainability and Society*, 4(2). doi:10.1186/s13705-014-0029-1.

Schmidt, O. *et al.* (2017) “Future cost and performance of water electrolysis: An expert elicitation study,” *International Journal of Hydrogen Energy*, 42(52), pp. 30470–30492. doi:10.1016/j.ijhydene.2017.10.045.

Secanell, M. *et al.* (2010) “Optimization of a proton exchange membrane fuel cell membrane electrode assembly,” *Structural and Multidisciplinary Optimization*, 40(1–6), pp. 563–583. doi:10.1007/s00158-009-0387-z.

Segurado, R. *et al.* (2011) “Increasing the penetration of renewable energy resources in S. Vicente, Cape Verde,” *Applied Energy*, 88(2), pp. 466–472. doi:10.1016/j.apenergy.2010.07.005.

Sharaf, O.Z. and Orhan, M.F. (2014) “An overview of fuel cell technology: Fundamentals and applications,” *Renewable and Sustainable Energy Reviews*, 32(C), pp. 810–853. doi:10.1016/j.rser.2014.01.012.

Sharifian, S. and Harasek, M. (2015) “Renewable Energy Sources,” 45, pp. 409–414. doi:10.3303/CET1545069.

Shedid, M.H. and Elshokary, S. (2015) “Hydrogen Production from an Alkali Electrolyzer Operating with Egypt Natural Resources,” *Smart Grid and Renewable Energy*, 6(01), pp. 14–25. doi:10.4236/sgre.2015.61002.

Shim, J.H., Jeong, J.Y. and Park, J.Y. (2017) “SWRO brine reuse by diaphragm-type chlor-alkali electrolysis to produce alkali-activated slag,” *Desalination*, 413, pp. 10–18. doi:10.1016/j.desal.2017.02.019.

Shimpalee, S. and van Zee, J.W. (2007) “Numerical studies on rib & channel dimension of flow-field on PEMFC performance,” *International Journal of Hydrogen Energy*, 32(7), pp. 842–856. doi:10.1016/j.ijhydene.2006.11.032.

Singh, D., Lu, D.M. and Djilali, N. (1999) “A two-dimensional analysis of mass transport in proton exchange membrane fuel cells,” *International Journal of Engineering Science*, 37, pp. 431–452. doi:10.1016/s0020-7225(98)00079-2.

Sinha, S. and Chandel, S.S. (2015) “Review of recent trends in optimization techniques for solar photovoltaic-wind based hybrid energy systems,” *Renewable and Sustainable Energy Reviews*, pp. 755–769. doi:10.1016/j.rser.2015.05.040.

Siracusano, S. *et al.* (2012) “An electrochemical study of a PEM stack for water electrolysis,” *International Journal of Hydrogen Energy*, 37(2), pp. 1939–1946. doi:10.1016/j.ijhydene.2011.06.019.

Smith, A.F.G. and Newborougg, M. (2004) “Low-Cost Polymer Electrolysers and Electrolyser Implementation Scenarios for Carbon Abatement,” *Carbon* [Preprint].

Snyman, J.A. and Wilke, D.N. (2018) *Practical Mathematical Optimization*. Second, *Practical Mathematical Optimization*. Second. Springer. doi:10.1007/b105200.

Springer, T.E., Zowodzinski, T.A. and Gottesfeld, S. (1991) “Polymer Electrolyte Fuel Cell Model,” *Journal of the Electrochemical Society*, 138(8). doi:10.1149/1.2085971.

Srisiriwat, A. and Pirom, W. (2017) “Feasibility Study of Seawater Electrolysis for Photovoltaic/Fuel Cell Hybrid Power System for the Coastal Areas in Thailand,” *IOP Conference Series: Materials Science and Engineering*, 241(1). doi:10.1088/1757-899X/241/1/012041.

Srivastava, T. (2013) “Renewable Energy (Gasification),” *Advance in Electronic and Electric Engineering*, 3(9), pp. 1243–1250.

Stojić, D.L. *et al.* (2003) “Hydrogen generation from water electrolysis - Possibilities of energy saving,” *Journal of Power Sources*, 118(1–2), pp. 315–319. doi:10.1016/S0378-7753(03)00077-6.

Suh, D.M. and Park, S. (2012) “Transport phenomena in proton exchange membrane fuel cells and over-potential distribution of membrane electrode assembly,” *International Journal of Thermal Sciences*, 51(1), pp. 31–41. doi:10.1016/j.ijthermalsci.2011.08.013.

Sun, W. and Yuan, Y.-X. (2006) *Optimization Theory and Methods - Nonlinear Programming*. 1st edn. Springer Science & Business Media.

Teow, Y.H. and Mohammad, A.W. (2019) “New generation nanomaterials for water desalination: A review,” *Desalination*, 451, pp. 2–17. doi:10.1016/j.desal.2017.11.041.

Thomas, D. (2018) *Cost Reduction Potential for Electrolyser Technology, EY P2G Platform*. Berlin. Available at:https://www.humsterlandenergie.nl/resources/LInks-duurzaam/Linkpagina/20180619_Hydrogenics_EU-P2G-Platform_for-distribution.pdf (Accessed: September 15, 2018).

Tijani, A.S. and Rahim, A.H.A. (2016) "Numerical Modeling the Effect of Operating Variables on Faraday Efficiency in PEM Electrolyzer," *Procedia Technology*, 26, pp. 419–427. doi:10.1016/j.protcy.2016.08.054.

Tobaru, S., Conteh, F. and Senjyu, T. (2017) "Novel 100% renewable energy power system considering real-time pricing," *2017 IEEE 3rd International Future Energy Electronics Conference and ECCE Asia, IFEEC - ECCE Asia 2017*, pp. 1047–1052. doi:10.1109/IFEEC.2017.7992186.

Turner, J. *et al.* (2007) "Renewable hydrogen production," *International Journal of Energy Research*, 32(5), pp. 379–407. doi:10.1002/er.1372.

Um, S., Wang, C.-Y. and Chen, K.S. (2000) "Computational Fluid Dynamics Modeling of Proton Exchange Membrane Fuel Cells," *Journal of The Electrochemical Society*, 147(12), p. 4485. doi:10.1149/1.1394090.

Ursúa, A., Gandía, L.M. and Sanchis, P. (2012) "Hydrogen production from water electrolysis: Current status and future trends," *Proceedings of the IEEE*, 100(2), pp. 410–426. doi:10.1109/JPROC.2011.2156750.

Wang, Y. (2008) "Modeling of two-phase transport in the diffusion media of polymer electrolyte fuel cells," *Journal of Power Sources*, 185(1), pp. 261–271. doi:10.1016/j.jpowsour.2008.07.007.

Wang, Z.H., Wang, C.Y. and Chen, K.S. (2001) "Two-phase flow and transport in the air cathode of proton exchange membrane fuel cells," *Journal of Power Sources*, 94(1), pp. 40–50. doi:10.1016/S0378-7753(00)00662-5.

Wanjiku, J.G. *et al.* (2010) "Analytical sizing of an electrolyser for a small scale wind electrolysis plant," *2010 IEEE International Energy Conference*, pp. 10–15. doi:10.1109/ENERGYCON.2010.5771658.

Weisbrod, K.R., Vanderborgh, N.E. and Grot, S.A. (1996) *Modeling of gaseous flows within proton exchange membrane fuel cells*. Orlando: Fuel Cell Seminar Organizing Committee. doi:10.2172/460311.

World Bank, T. (2016) *Fossil fuel energy consumption (% of total)*. Available at: Development and optimization of an integrated energy network with%0Acentralized and decentralized energy systems using mathematical%0Amodelling approach (Accessed: March 30, 2020).

Yan, Z. *et al.* (2019) "Oxygen evolution efficiency and chlorine evolution efficiency for electrocatalytic properties of MnO2 -based electrodes in seawater," *Journal Wuhan University of Technology, Materials Science Edition*, 34, pp. 69–74. doi:10.1007/s11595-019-2016-z.

Yang, S. *et al.* (2019) "Performance modelling of seawater electrolysis in an undivided cell: Effects of current density and seawater salinity," *Chemical Engineering Research and Design*, 143, pp. 79–89. doi:10.1016/j.cherd.2019.01.009.

Yang, Z. *et al.* (2019) "Effects of operating conditions on water and heat management by a transient multi-dimensional PEMFC system model," *Energy*, 183, pp. 462–476. doi:10.1016/j.energy.2019.06.148.

Ye, B. *et al.* (2012) "Feasibility study of renewable energy powered Island-Hainan," *Proceedings - 2012 International Conference on Computer Distributed Control and Intelligent Environmental Monitoring*, pp. 330–333. doi:10.1109/CDCIEM.2012.85.

Yu, L. *et al.* (2019) "Non-noble metal-nitride based electrocatalysts for high-performance alkaline seawater electrolysis," *Nature Communications*, 10(1). doi:10.1038/s41467-019-13092-7.

Zamel, N. and Li, X. (2011) "Effect of contaminants on polymer electrolyte membrane fuel cells," *Progress in Energy and Combustion Science*, 37(3), pp. 292–329. doi:10.1016/j.pecs.2010.06.003.

Zamora, J.M. and Grossmann, I.E. (1998) “Continuous global optimization of structured process systems models,” *Computers and Chemical Engineering*, 22(12), pp. 1749–1770. doi:10.1016/S0098-1354(98)00244-0.

Zeng, K. and Zhang, D. (2010) “Recent progress in alkaline water electrolysis for hydrogen production and applications,” *Progress in Energy and Combustion Science*, 36(3), pp. 307–326. doi:10.1016/j.pecs.2009.11.002.

Zhang, H. *et al.* (2012) “Efficiency calculation and configuration design of a PEM electrolyzer system for hydrogen production,” *International Journal of Electrochemical Science*, 7(5), pp. 4143–4157.

Zhang, X. *et al.* (2015) “Towards a smart energy network: The roles of fuel/electrolysis cells and technological perspectives,” *International Journal of Hydrogen Energy*, 40(21), pp. 6866–6919. doi:10.1016/j.ijhydene.2015.03.133.

CHAPTER 3

Model Approach and Development

3.1 Introduction

The mathematical model that was developed in this dissertation integrated the design and synthesis of a PEME system and a PEMFC system. This chapter explains the method followed and the development of the hybrid electrolyser-fuel cell (HEFC) system optimisation model. A comprehensive mathematical formulation that aims to simultaneously produce hydrogen and freshwater from seawater is presented, and is used to determine the optimal performance, design conditions, parameters and economic viability of the system. The aforementioned concept was achieved with seawater electrolysers and hydrogen fuel cells. The development of the model incorporated a superstructure approach in which all possible sources of renewable energy were considered to power the seawater electrolyser. Firstly, in this chapter, the systematic approach followed in modelling the hybrid system is presented. Secondly, the mathematical expressions for the voltage component and the membrane component are described. The mass balance constraints are then given, followed by the overall system performance. Finally, an economic evaluation is carried out to determine the viability of the proposed system.

3.2 Systematic Approach

To develop the optimisation model for the HEFC system, the approach illustrated in Figure 3.1 was followed. Firstly, a superstructure of the system was developed. The NLP model was based on the superstructure and was used to explore all the possible combinations for the optimisation problem. After the development of the superstructure, the hybrid system was divided into two sub-models, viz. the seawater electrolyser and the H_2 fuel cell. The overall superstructure for the HEFC system is given in Figure 3.2.

As illustrated in Figure 3.2, a set of units, *P*, composed of an electrolyser stack and fuel cell stack are used to produce H_2 and freshwater from seawater. The energy required to power the electrolyser may be supplied by solar, wind, tidal or hydro energy. This power is supplied to a set of electrolyser cells, *M*, with a known number of cells in the electrolyser stack, where it is consumed and used to split seawater molecules into H_2 and O_2. All the H_2 and O_2 formed in the electrolyser stack are then sent to a set of fuel cells, *N*, with a known number of cells in the fuel cell stack, where the H_2 and O_2 react to form freshwater. Electrons flow through an external circuit from the anode to the cathode. This transfer of electrons generates power. Unreacted H_2 and O_2 in one fuel cell flows into the next cell in the stack, where they are reacted until all the reactants are consumed.

In developing a mathematical model for the HEFC, the system was broken down into three components, viz. voltage, membrane and material balance. All potential losses present in the electrolyser and fuel cell were modelled in the voltage component. H_2O concentration and transport were modelled in the membrane component for each of the sub-models. The mass and molar balance for H_2, O_2 and H_2O in the electrolyser and the fuel cell were modelled in the material balance component. Thereafter, performance equations for the seawater electrolyser and hydrogen fuel cell sub-model were given in the formulation of system constraints.

It should be noted that the seawater electrolyser was initially modelled as a freshwater electrolyser. Modifications were made by altering the parameters to suit the electrolysis of seawater. The seawater electrolyser model with the objective function of minimising power consumed was solved to determine the feasibility of the model.

In contrast, the H_2 fuel cell sub-model with the objective function of maximising power produced was solved to determine the feasibility of the model. Lastly, once each sub-model had been modelled, solved and deemed feasible, mass balance constraints were included to integrate the seawater electrolyser sub-model and fuel cell sub-model. This integrated model was then solved and the optimal design parameters were obtained and used to size the internal components of the HEFC system. This was followed by the techno-economic evaluation of the HEFC system based on the optimal variables obtained from the optimised integrated HEFC system model. For the techno-economic evaluation, the annual cash flow, net present value, payback period and internal rate of return were calculated to determine the viability of the proposed system.

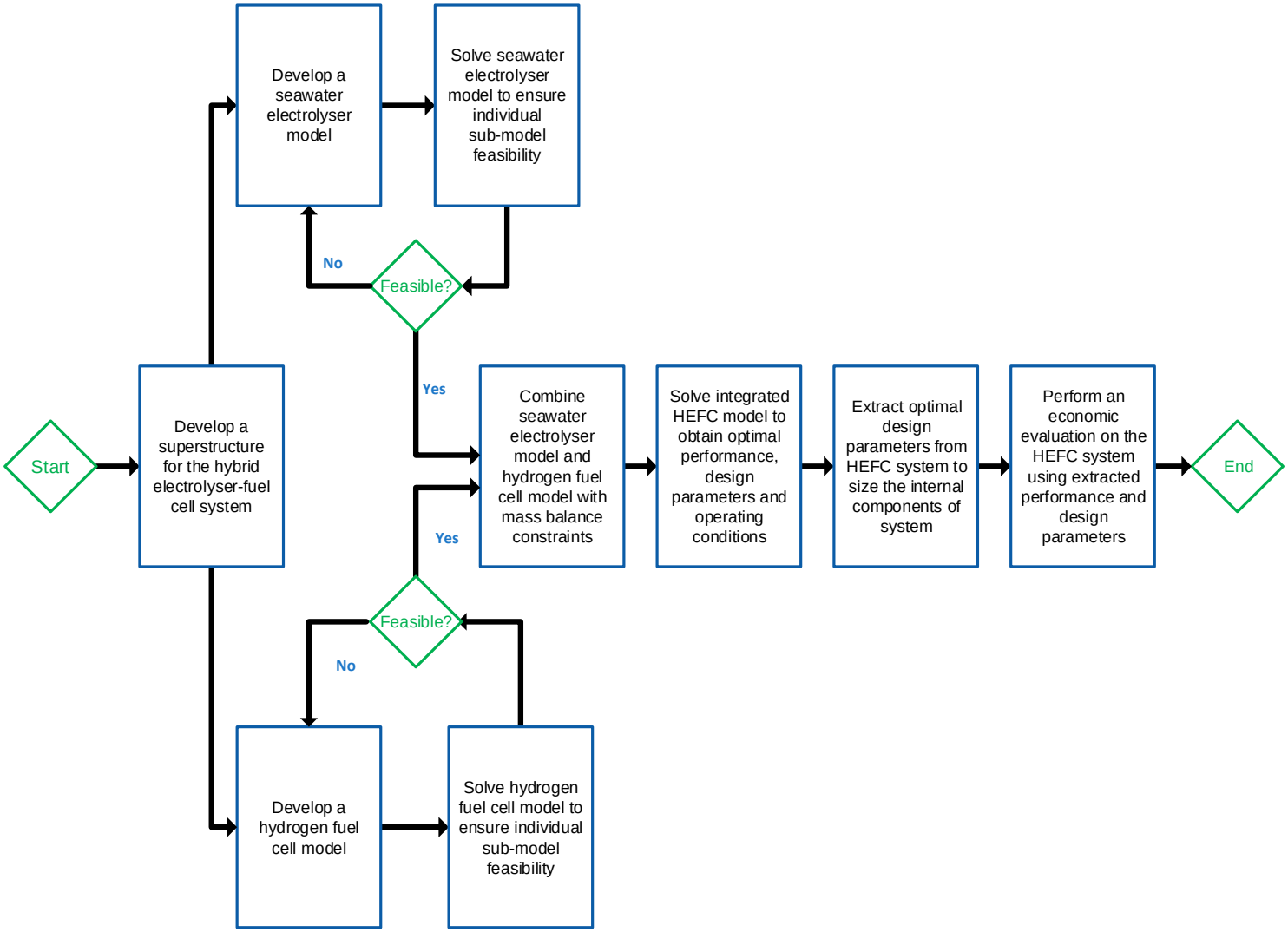

Figure 3.1: HEFC System Schematic Approach

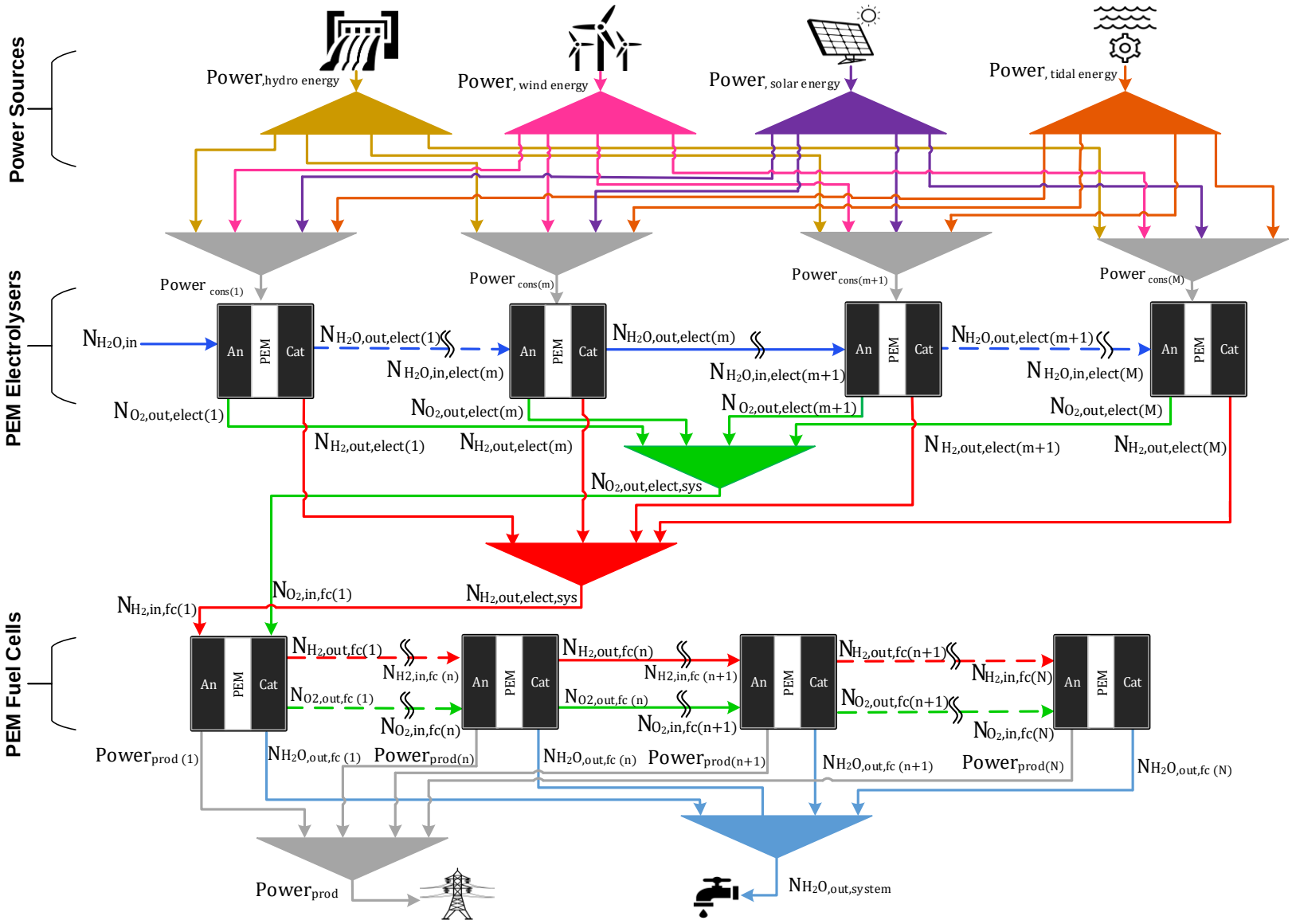

Figure 3.2: Superstructure for a Hybrid Electrolyser Fuel Cell System

3.3 Electrolyser and Fuel Cell Operation

In the electrolyser, seawater is fed to the anode where it is oxidised to form O_2. H^+ ions flow from the anode through a Nafion electrolyte membrane to a platinum cathode where H_2 gas is formed. In seawater electrolysis, chlorine evolves at the anode instead of O_2. However, in this model, the evolution of O_2 was promoted with a nano-tungsten carbide electro-catalyst and a magnesium hydroxide anode. Chlorine leaves the electrolyser as a solution with the brine and excess seawater. Reactions (3.1)-(3.2) describe the reactions that take place in the seawater electrolyser. A schematic diagram of a PEME is shown in Figure 3.3 (Han *et al.*, 2015).

Anode: $$H_2O \rightarrow \frac{1}{2}O_2 + 2e^- + 2H^+ \quad (3.1)$$

Cathode: $$2H^+ + 2e^- \rightarrow H_2 \quad (3.2)$$

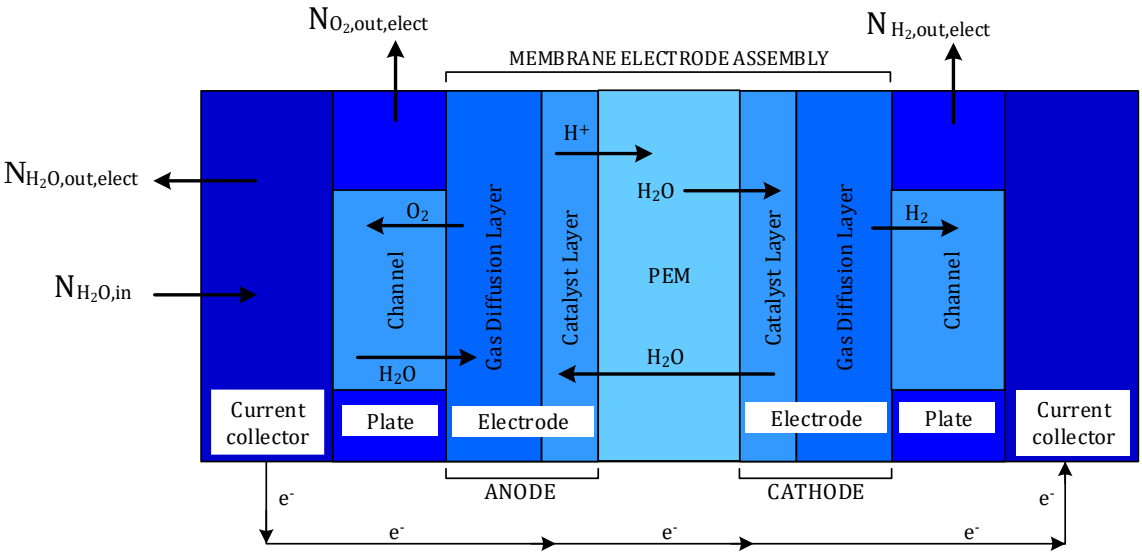

Figure 3.3: Schematic Diagram of a PEME

In the fuel cell, H_2 fed to the anode is oxidised and the O_2 fed to the cathode is reduced to form freshwater. Figure 3.4 illustrates a schematic diagram of a PEMFC (Abdin, Webb and Gray, 2015).

Anode: $$H_2 \rightarrow 2H^+ + 2e^- \quad (3.3)$$

Cathode: $$\frac{1}{2}O_2 + 2e^- + 2H^+ \rightarrow H_2O \quad (3.4)$$

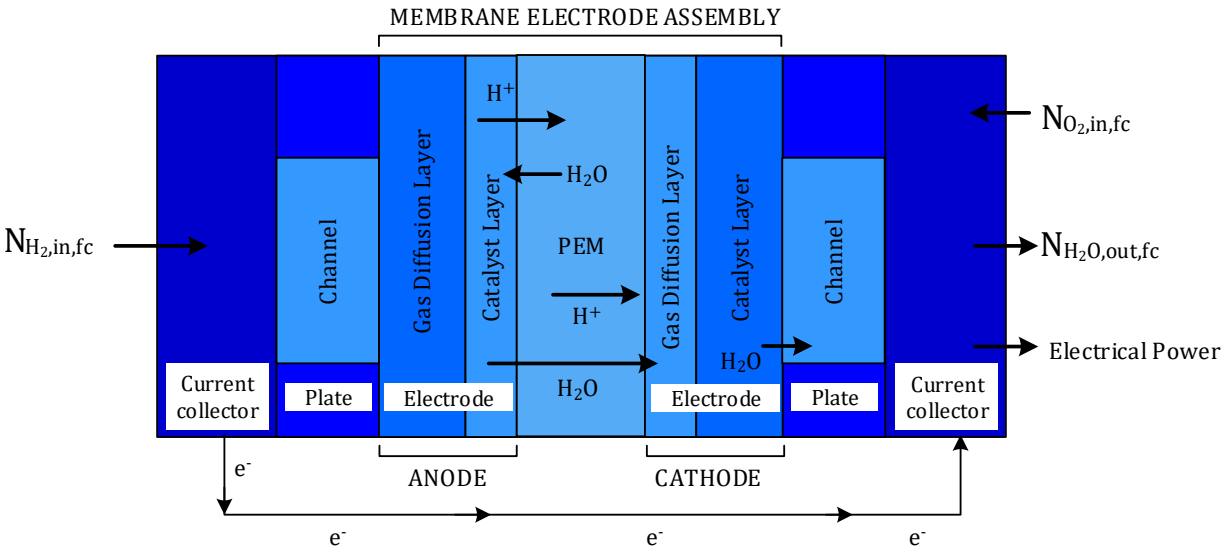

Figure 3.4: Schematic Diagram of a PEMFC

3.4 Voltage Component

The seawater electrolyser model was adapted from the models developed by Marangio et al. (2009) and Han et al. (2015). Modifications were made to these models by altering the current density, charge transfer coefficient, exchange current density and the input voltage required to suit seawater electrolysis. Additionally, the H_2 fuel cell modelled in this system was adapted from the model proposed by Abdin et al. (2016). Most of the mathematical expressions presented in the electrolyser models are identical to the expressions in the fuel cell, with the exception that H_2 is present in the anode and O_2 in the cathode of the fuel cell, as opposed to the electrolyser where H_2 is present in the cathode and O_2 in the anode. Adjustments are made to take this into account.

The performance of the electrolyser and the fuel cell are measured via the current and voltage of each unit. Since the cells are connected in series, the current in each cell of the electrolyser and fuel cell stacks remain the same. This assumption also holds for the fuel cell stack. Subsequently, this section describes the voltage component of the HEFC system.

3.4.1 Current

Current in the electrolyser and fuel cell stack is dependent on the reaction area and the current density. Where I is current, A is the reaction area and j is the current density.

$$I(p) = A(p) * j(p) \qquad \forall\, p \in P \tag{3.5}$$

3.4.2 Open Circuit Voltage

The open-circuit voltage (OCV) is theoretically known as the minimum voltage when all other overpotentials are not taken into consideration. The reversible voltage describes the voltage obtained if the system experiences no voltage losses, and all Gibbs free energy could be converted to electrical energy (Han *et al.*, 2015). Equation (3.6) describes the OCV derived from the Nernst equation at standard pressure. *T* is the operating temperature in Kelvin, *R* is the gas constant, z is the number of electrons transferred during the reaction, F is Faraday's constant (96 485 mol/C) and β_i is the partial pressure of species *i*.

$$V_{OCV}(p) = 1.229 - 0.9 * 10^{-3}[T(p) - 298] + \frac{RT(p)}{zF}\ln\left(\frac{\beta_{H_2}\beta_{O_2}^{0.5}}{\beta_{H_2O}}\right) \qquad \forall\, p \in P \tag{3.6}$$

3.4.3 Activation Overpotential

Activation overpotential is derived from the Butler-Volmer equation and is defined as the potential loss due to the electrochemical reaction. It is the voltage used to drive the chemical reaction at the anode and cathode and determines the rate at which the electrochemical reactions take place at the surface of the electrode. It is influenced by chemical and physical parameters, viz. temperature, pressure, active reaction site, catalyst property and electrode morphology.

$$V_{act}(p) = \frac{RT(p)}{\alpha_{an}F} * ln\left[\left(\left(\frac{j\,(p)}{2j_{o,an(p)}}\right) + \sqrt{\left(\frac{j(p)}{2j_{o,an(p)}}\right)^2 + 1}\right)\right] + \frac{RT(p)}{\alpha_{cat}F} * ln\left[\left(\left(\frac{j(p)}{2j_{o,cat(p)}}\right) + \sqrt{\left(\frac{j(p)}{2j_{o,cat(p)}}\right)^2 + 1}\,)\right)\right] \qquad \forall\, p \in P, p = electrolyser \tag{3.7}$$

$$V_{act}(p) = \left[\frac{RT(p)}{\alpha_{an}F} * ln\left(\frac{j\,(p)}{j_o, an(p)}\right)\right] + \left[\frac{RT(p)}{\alpha_{cat}F} * ln\left(\frac{j(p)}{j_o, cat(p)}\right)\right] \qquad \forall\, p \in P, p = fuel\ cell \tag{3.8}$$

$$V_{act}(p) = V_{act,an}(p) + V_{act,cat}(p) \qquad \forall\, p \in P \qquad (3.9)$$

Where α_{an} and α_{cat} are the anode and cathode charge transfer coefficients. $j_{o,an}$ and $j_{o,cat}$ are the exchange current densities of the anode and cathode. $V_{act,an}$, $V_{act,cat}$ and V_{act} are the anode, cathode and overall activation overpotentials.

3.4.4 Diffusion Overpotential

The diffusion overpotential is also known as the concentration overpotential and is defined as the potential loss due to the mass transport limitations within the membrane-electrode interface. The mass transport of H_2, O_2 and H_2O through the porous electrode is governed by Fick's law. Typically, diffusion overpotential plays a major role in electrolysers when the surface of the membrane becomes heavily populated with O_2 gas bubbles, and the rate of the reaction is reduced. Similarly, in fuel cells, O_2 bubbles present prevent the flow of H^+ ions to the cathode. This hinders the H_2O formation reaction and consequently reduces the performance of the fuel cell (Abdin, Webb and Gray, 2016).

Equations (3.10)-(3.12) describe the anode, cathode and total diffusion overpotential in the electrolyser. In fuel cells, the anode of the electrolyser becomes the cathode and vice versa.

$$V_{diff,an}(p) = \frac{R\,T(p)}{4F} ln \frac{C_{O_2,me}(p)}{C_{O_2,me,o}(p)} \qquad \forall\, p \in P, p = electrolyser \qquad (3.10)$$

$$V_{diff,cat}(p) = \frac{R\,T(p)}{2F} ln \frac{C_{H_2,me}(p)}{C_{H_2,me,o}(p)} \qquad \forall\, p \in P, p = electrolyser \qquad (3.11)$$

$$V_{diff}(p) = V_{diff,an}(p) + V_{diff,an}(p) \qquad \forall\, p \in P \qquad (3.12)$$

Where $C_{O_2,me}$ and $C_{H_2,me}$ are the concentration of O_2 and H_2 at the electrode-membrane interface. $C_{O_2,me,o}$ and $C_{H_2,me,o}$ are the concentrations of O_2 and H_2 at the electrode-membrane interface at reference conditions. $V_{diff,an}$, $V_{diff,cat}$ and V_{diff} are the anode, cathode and overall diffusion overpotentials.

3.4.5 Ohmic Overpotential

The ohmic overpotential is the resistance due to the transfer of electrons through the membrane, electrodes, plates and interconnectors present in the electrolyser and the fuel cell. Typically, the ohmic overpotential is comprised of two resistances, viz. electrical and ionic. The electrical resistance is due to the flow of electrons through an electrically conductive component. In contrast, the ionic resistance is caused by the flow of H^+ ions in the membrane. Bernardi and Verbrugge (1991) found that ionic resistances contributed significantly to the ohmic overpotential.

Due to a large number of unknowns in the electrodes and bipolar plates, the ohmic overpotential in this dissertation only takes into account ionic resistances. The protonic conductivity of the membrane is calculated as a function of H_2O content. It is expressed in the empirical equation proposed by Springer et al. (1993). σ_{mem} is the membrane conductivity, V_{ohm} is the ohmic overpotential, δ_{mem} is the thickness of the membrane and λ_{mem} is the membrane humidity degree.

$$\sigma_{mem}(p) = (0.5139\lambda_{mem}(p) - 0.326)\exp\left(1268\left(\frac{1}{303} - \frac{1}{T(p)}\right)\right) \quad \forall\, p \in P \tag{3.13}$$

$$V_{ohm}(p) = \delta_{mem}(p)\left[\frac{I(p)}{A(p)\,\sigma_m(p)}\right] \qquad \forall\, p \in P \tag{3.14}$$

3.4.6 Total Voltage

The input voltage of the electrolyser cell is expressed in Equation (3.15) as the sum of the open-circuit voltage, activation, diffusion and ohmic overpotentials. In contrast, the output voltage of the fuel cell stack is expressed in Equation (3.16) as the difference between the open-circuit voltage, activation, diffusion and ohmic overpotentials.

$$V(p) = V_{OCV}(p) + V_{act}(p) + V_{diff}(p) + V_{Ohm}(p)$$
$$\forall\, p \in P,\ p = electrolyser \tag{3.15}$$

$$V(p) = V_{OCV}(p) - V_{act}(p) - V_{diff}(p) - V_{Ohm}(p)$$
$$\forall\, p \in P, p = fuel\ cell \tag{3.16}$$

3.4.7 Seawater Density and Viscosity

The density and viscosity of seawater are taken as a function of temperature and salinity. An equation of state and experimental data adapted from the study conducted by El-Dessouky and Ettouney (2002), was used to determine the density and viscosity of seawater in the temperature range of 10-180℃, and salinity from 0-160 ppt (parts per thousand). Equation (3.17) expresses the density of seawater, where ρ_w is the density of H_2O, and D_i and F_i are constants. Equation (3.18) gives the viscosity of seawater, where μ_{H_2O} is the viscosity of H_2O, μ_r is the relative viscosity of H_2O and μ_{sw} is the viscosity of seawater

$$\rho_w = (D_1F_1 + D_2F_2 + D_3F_3 + D_4F_4) * 1000 \tag{3.17}$$

$$\mu_{sw} = \left(\mu_{H_2O}\right)(\mu_R) * 10^{-3} \tag{3.18}$$

3.4.8 Concentration in the Anode-Membrane and Cathode-Membrane Interface

To determine the concentration gradient present on either side of the membrane, the concentration is taken as a function of H_2O content. The H_2O activity, anode and cathode humidity degree, and the electrode concentration expressions are derived from the model presented by Shimpalee and Van Zee (2007). Equations (3.19) and (3.20) describe the activity of H_2O in the anode-membrane interface and cathode-membrane interface. Where $A_{H_2O.an}$ and $A_{H_2O,cat}$ are the H_2O activities in the anode and cathode. y_{H_2O} is the H_2O molar composition, P is the operating pressure and P_{sat} is the saturated vapour pressure.

$$A_{H_2O.an}(p) = \frac{y_{H_2O,an}(p) * P(p)}{P_{sat}(p)} \qquad \forall\, p \in P \tag{3.19}$$

$$A_{H_2O.cat}(p) = \frac{y_{H_2O,cat}(p) * P(p)}{P_{sat}(p)} \qquad \forall\, p \in P \tag{3.20}$$

Equation (3.21) expresses the saturated vapour pressure of H_2O, which is a function of temperature (Tiwary and Williams, 2018).

$$P_{sat}(\mathrm{p}) = 611e^{\frac{19.65(\mathrm{T(p)}-273.15)}{\mathrm{T(p)}}} \qquad \forall\, p \in P \tag{3.21}$$

The molar compositions of H_2O at the anode and cathode of the electrolyser are given in Equations (3.22) and (3.23). Where $n_{H_2O,an}$ is the molar flux of H_2O at the anode, $n_{H_2O,cat}$ is the molar flux of H_2O at the cathode, n_{O_2} is the molar flux of O_2 and n_{H_2} is the molar flux of H_2.

$$y_{H_2O,an}(p) = \frac{n_{H_2O,an}(p)}{n_{H_2O,an}(p) + n_{O_2}(p)} \qquad \forall\, p \in P,\ p = electrolyser \tag{3.22}$$

$$y_{H_2O,cat}(p) = \frac{n_{H_2O,cat}(p)}{n_{H_2O,cat}(p) + n_{H_2}(p)} \qquad \forall\, p \in P, p = electrolyser \tag{3.23}$$

Equations (24) and (25) express the molar composition of H_2O at the anode and cathode of the fuel cell.

$$y_{H_2O,an}(p) = \frac{n_{H_2O,an}(p)}{n_{H_2O,an}(p)+n_{H_2}(p)} \qquad \forall\, p \in P,\ p = fuel\ cell \qquad (3.24)$$

$$y_{H_2O,cat}(p) = \frac{n_{H_2O,cat}(p)}{n_{H_2O,cat}(p)+n_{O_2}(p)} \qquad \forall\, p \in P,\ p = fuel\ cell \qquad (3.25)$$

The molar flux of H_2O at the anode and cathode of the electrolyser are given in Equations (3.26) and (3.27), whereas the molar flux of H_2O in the fuel cell are given in Equations (3.28) and (3.29).

$$n_{H_2O,an}(p) = \frac{\dot{N}_{H_2O,cons}+\dot{N}_{H_2O.mem}(p)}{A(p))} \qquad \forall\, p \in P,\ p = electrolyser \qquad (3.26)$$

$$n_{H_2O,cat(p)} = \frac{\dot{N}_{H_2O.mem}(p)}{A(p)} \qquad \forall\, p \in P,\ p = electrolyser \qquad (3.27)$$

$$n_{H_2O,an}(p) = \frac{\dot{N}_{H_2O.mem}(p)}{A(p))} \qquad \forall\, p \in P, p = fuel\ cell \qquad (3.28)$$

$$n_{H_2O,cat(p)} = \frac{\dot{N}_{H_2O,prod}-\dot{N}_{H_2O.mem}(p)}{A(p)} \qquad \forall\, p \in P, p = fuel\ cell \qquad (3.29)$$

Equations (3.30) and (3.31) express the molar flux of H_2 and O_2 in the electrolyser.

$$n_{H_2}(p) = \frac{\dot{N}_{H_2,prod}}{A(p)} \qquad \forall\, p \in P, p = electrolyser \qquad (3.30)$$

$$n_{O_2(p)} = \frac{\dot{N}_{O_2,prod}}{A(p)} \qquad \forall\, p \in P, p = electrolyser \qquad (3.31)$$

The H_2 and O_2 molar flux of the fuel cell are described in Equations (3.32) and (3.33).

$$n_{H_2}(p) = \frac{\dot{N}_{H_2,cons}}{A(p)} \qquad \forall\, p \in P,\ p = fuel\ cell \qquad (3.32)$$

$$n_{O_2(p)} = \frac{\dot{N}_{O_2,cons}}{A(p)} \qquad \forall\, p \in P,\ p = fuel\ cell \qquad (3.33)$$

The humidity of H_2O at the anode and the cathode under different H_2O activity conditions are given in Equations (3.34) -(3.37).

$$\lambda_{an}(p) = 14 + 1.4\,(A_{H_2O,an}(p) - 1) \quad 1 \le A_{H_2O,an} \le 3 \quad \forall\, p \in P \qquad (3.34)$$

$$\lambda_{cat}(p) = 14 + 1.4\,(A_{H_2O,cat}(p) - 1) \quad 1 \le A_{H_2O,cat} \le 3 \quad \forall\, p \in P \qquad (3.35)$$

$$\lambda_{an}(p) = 0.043 + 17.8 * A_{H_2O,an}(p) - 39.65 * A_{H_2O,an}(p)^2 + 36 * A_{H_2O,an}(p)^3$$
$$0 \le A_{H_2O,an} \le 1 \qquad \forall\, p \in P \qquad (3.36)$$

$$\lambda_{cat}(p) = 0.043 + 17.8 * A_{H_2O,cat}(p) - 39.65 * A_{H_2O,cat}(p)^2 + 36 * A_{H_2O,cat}(p)^3 \qquad 0 \le A_{H_2O,cat} \le 1 \qquad \forall\, p \in P \qquad (3.37)$$

Where λ_{an} and λ_{cat} are the anode and cathode humidity degrees. Equation (3.38) describes the membrane humidity degree as the average anode and cathode humidity degree.

$$\lambda_{mem}(p) = \frac{\lambda_{an}(p) + \lambda_{cat}(p)}{2} \qquad \forall\, p \in P \qquad (3.38)$$

Equations (3.39)-(3.40) describe the concentration of H_2O at the membrane-electrode interface of the anode and the cathode in the electrolyser. $\rho_{mem,dry}$ is the dry density of the membrane and $MW_{mem,dry}$ is the molecular mass of the dry membrane.

$$C_{H_2O,me,an}(p) = \frac{\rho_{m,dry}}{MW_{mem,dry}} \lambda_{an}(p) \quad \forall\, p \in P,\ p = electrolyser \tag{3.39}$$

$$C_{H_2O,me,cat}(p) = \frac{\rho_{m,dry}}{MW_{mem,dry}} \lambda_{cat}(p) \ \ \forall\, p \in P, p = electrolyser \tag{3.40}$$

The concentration of H_2O at the membrane-electrode interface of the anode and cathode of the fuel cell are given in Equations (3.41) and (3.42). δ_{an} and δ_{cat} are the anode and cathode thickness. $D_{eff,an}$ and $D_{eff,cat}$ are the anode and cathode effective diffusion coefficients. MW_{H_2O} is the molecular weight of water.

$$C_{H_2O,me,an}(p) = \left(\frac{\rho_{H_2O}{}^{*}T_{(p)}}{MW_{H_2O}}\right) - \left(\frac{\delta_{an}(p)*n_{H_2O,an}(p)}{D_{eff,an}}\right) \quad \forall\, p \in P, p = fuel\ cell \tag{3.41}$$

$$C_{H_2O,me,cat}(p) = \left(\frac{\rho_{H_2O}{}^{*}T_{(p)}}{MW_{H_2O}}\right) + \left(\frac{\delta_{cat}(p)*n_{H_2O,cat}(p)}{D_{eff,cat}}\right) \ \forall\, p \in P, p = fuel\ cell \tag{3.42}$$

Equations (3.43) and (3.44) give the H_2 and O_2 channel concentration of the electrolyser. $C_{H_2,ch}$ and $C_{O_2,ch}$ are the concentrations of H_2 and O_2 at the channel. $y_{H_2,ch}$ and $y_{O_2,ch}$ are the molar compositions of H_2 and O_2 at the channel.

$$C_{H_2,ch}(p) = \frac{P_{cat}(p)* y_{H_2,ch}(p)}{RT(p)} \qquad \forall\, p \in P, p = electrolyser \tag{3.43}$$

$$C_{O_2,ch}(p) = \frac{P_{an}(p)* y_{O_2,ch}(p)}{RT(p)} \qquad \forall\, p \in P, p = electrolyser \tag{3.44}$$

The concentration of H_2 and O_2 at the channel of the fuel cell is given in Equations (3.45) and (3.46).

$$C_{H_2,ch}(p) = \frac{P_{an}(p) * y_{H_2,ch}(p)}{RT(p)} \qquad \forall\, p \in P, p = fuel\ cell \qquad (3.45)$$

$$C_{O_2,ch}(p) = \frac{P_{cat}(p) * y_{O_2,ch}(p)}{RT(p)} \qquad \forall\, p \in P, p = fuel\ cell \qquad (3.46)$$

At reference conditions, the H_2 and O_2 molar concentrations at the membrane and channel of the electrolyser are given by Equations (3.47)-(3.50). $C_{H_2,me,o}$ and $C_{O_2,me,o}$ are the concentrations of H_2 and O_2 at the membrane under reference conditions. $C_{H_2,ch,o}$ and $C_{O_2,ch,o}$ are the concentrations of H_2 and O_2 at the channel under reference conditions. T_{ref} and P_{ref} are the reference temperature and pressure.

$$C_{O_2,me,o}(p) = C_{O_2,ch,o}(p) + \frac{\delta_{an}(p) * n_{O_2}(p)}{D_{eff,an}(p)} \qquad \forall\, p \in P, p = electrolyser \qquad (3.47)$$

$$C_{H_2,me,o}(p) = C_{H_2,ch,o}(p) + \frac{\delta_{cat}(p) * n_{H_2}(p)}{D_{eff,cat}(p)} \qquad \forall\, p \in P, p = electrolyser \qquad (3.48)$$

$$C_{O_2,ch,o}(p) = \frac{P_{ref} y_{O_2,ch(p)}}{RT_{ref}} \qquad \forall\, p \in P, p = electrolyser \qquad (3.49)$$

$$C_{H_2,ch,o}(p) = \frac{P_{ref} y_{H_2,ch(p)}}{RT_{ref}} \qquad \forall\, p \in P, p = electrolyser \qquad (3.50)$$

In the fuel cell, the molar concentrations of H_2 and O_2 at the membrane and the channel are described in Equations (3.51)-(3.54).

$$C_{H_2,me,o}(p) = C_{H_2,ch,o}(p) + \frac{\delta_{an}(p) * n_{H_2}(p)}{D_{eff,an}(p)} \qquad \forall\, p \in P, p = fuel\ cell \qquad (3.51)$$

$$C_{O_2,me,o}(p) = C_{O_2,ch,o}(p) + \frac{\delta_{cat}(p) * n_{O_2}(p)}{D_{eff,cat}(p)} \quad \forall\, p \in P,\ p = fuel\ cell \qquad (3.52)$$

$$C_{H_2,ch,o}(p) = \frac{P_{ref} y_{H_2,ch(p)}}{RT_{ref}} \qquad \forall\, p \in P, p = fuel\ cell \qquad (3.53)$$

$$C_{O_2,ch,o}(p) = \frac{P_{ref} y_{O_2,ch(p)}}{RT_{ref}} \qquad \forall\, p \in P, p = fuel\ cell \qquad (3.54)$$

Equations (3.55)-(3.58) describe the molar composition of H_2 and O_2 at the channel of the electrolyser and the fuel cell.

$$y_{H_2,ch}(p) = \frac{n_{H_2}(p)}{n_{H_2O,cat}(p) + n_{H_2}(p)} \qquad \forall\, p \in P, p = electrolyser \qquad (3.55)$$

$$y_{O_2,ch}(p) = \frac{n_{O_2}(p)}{n_{H_2O,an}(p) + n_{O_2}(p)} \qquad \forall\, p \in P, p = electrolyser \qquad (3.56)$$

$$y_{H_2,ch}(p) = \frac{n_{H_2}(p)}{n_{H_2O,an}(p) + n_{H_2}(p)} \qquad \forall\, p \in P, p = fuel\ cell \qquad (3.57)$$

$$y_{O_2,ch}(p) = \frac{n_{O_2}(p)}{n_{H_2O,cat}(p) + n_{O_2}(p)} \qquad \forall\, p \in P, p = fuel\ cell \qquad (3.58)$$

According to Equation (3.59) and Equation (3.60), the effective diffusion coefficients of the H_2-H_2O mixture and O_2-H_2O mixture are functions of porosity, percolation and diffusion coefficient of the mixture. Equations (3.61) and (3.62) give the diffusion coefficients for the H_2-H_2O mixture and the O_2-H_2O mixture.

$$D_{eff,H_2-H_2O}(p) = D_{H_2-H_2O}(p)\varepsilon\left(\frac{\varepsilon - \varepsilon_p}{1 - \varepsilon_p}\right)^{\tau} \qquad \forall\, p \in P \qquad (3.59)$$

$$D_{eff,O_2-H_2O}(p) = D_{O_2-H_2O}(p)\varepsilon\left(\frac{\varepsilon-\varepsilon_p}{1-\varepsilon_p}\right)^{\tau} \qquad \forall\, p \in P \qquad (3.60)$$

$$D_{H_2-H_2O}(p) = a\left(\frac{T(p)}{\sqrt{T_{cr,H_2}T_{cr,H_2O}}}\right)^{b}\left(P_{cr,H_2}P_{cr,H_2O}\right)^{\frac{1}{3}}\left(T_{cr,H_2}T_{cr,H_2O}\right)^{\frac{5}{12}}\left(\frac{1}{MW_{H_2}}+\frac{1}{MW_{H_2O}}\right)^{\frac{1}{2}}$$
$$\forall\, p \in P \qquad (3.61)$$

$$D_{O_2-H_2O}(p) = a\left(\frac{T}{\sqrt{T_{cr,O_2}T_{cr,H_2O}}}\right)^{b}\left(P_{cr,O_2}P_{cr,H_2O}\right)^{\frac{1}{3}}\left(T_{cr,O_2}T_{cr,H_2O}\right)^{\frac{5}{12}}\left(\frac{1}{MW_{O_2}}+\frac{1}{MW_{H_2O}}\right)^{\frac{1}{2}}$$
$$\forall\, p \in P \qquad (3.62)$$

Where $D_{H_2-H_2O}$ and $D_{O_2-H_2O}$ are the diffusion coefficients of the H_2-H_2O mixture and the O_2-H_2O mixture. ε is the electrode porosity, ε_p is the Percolation threshold (0.11), τ is the empirical coefficient (τ = 0.785), a and b are the empirical coefficients ($a = 3.64 \times 10^{-4}$ and $b = 2.334$), P_{cr} is the critical pressure, T_{cr} is the critical temperature and MW_{H_2} and MW_{O_2} are the molecular weights of hydrogen and oxygen.

3.5 Membrane Component

Mass transport plays a fundamental role in the membrane and is responsible for the formation of H_2, O_2 and H_2O. The driving force in the membrane is due to the flow of H_2O. It occurs in three forms as described below and illustrated in Figure 3.5 (Han *et al.*, 2015).

(i) Flow due to the electro-osmotic drag

(ii) Flow due to the pressure gradient across the PEM from the cathode to the anode

(iii) Flow due to the concentration difference

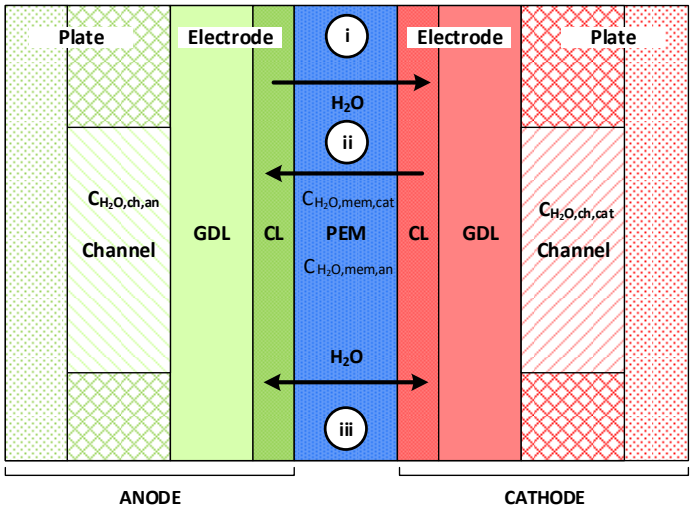

Figure 3.5: Water Transport through the PEM

The flow of H_2O due to the concentration gradient across the PEM is calculated in Equation (3.63). $\dot{N}_{H_2O,grad}$ is the molar flow rate of H_2O due to the concentration gradient and D_w is the diffusion coefficient of H_2O inside the membrane.

$$\dot{N}_{H_2O,grad}(p) = \frac{A(p)D_w}{\delta_{mem}(p)}\left[C_{H_2O,me,cat}(p) - C_{H_2O,me,an}(p)\right] \quad \forall\, p \in P \qquad (3.63)$$

The electro-osmotic drag is the transportation of H_2O molecules from the anode to the cathode, as a result of the flux of hydrated protons flowing through the membrane. It is a potential-driven flow which is caused by the attraction between the polar water molecules and protons. $\dot{N}_{H_2O,eo}$ is the molar flow rate due to the electro-osmotic drag and n_d is the electro-osmotic drag coefficient.

$$\dot{N}_{H_2O,eo}(p) = n_d(p) * \frac{I(p)}{F} \qquad \forall\, p \in P \tag{3.64}$$

The H_2O flow rate due to the pressure difference across the membrane is expressed in Equation (3.65) and is driven from the high-pressure side to the low-pressure side. $\dot{N}_{H_2O,pe}$ is the molar flow rate due to the pressure effect and K_{darcy} is the permeability coefficient of H_2O. ρ_{H_2O}, μ_{H_2O} and MW_{H_2O} are the density, viscosity and molecular weight of H_2O.

$$\dot{N}_{H_2O,pe}(p) = K_{darcy} \frac{A(p)\rho_{H_2O}}{\mu_{H_2O} MW_{H_2O} \delta_{mem}(p)} \qquad \forall\, p \in P \tag{3.65}$$

The net flow rate of H_2O through the membrane is expressed in Equation (3.66). It describes the flow rate of H_2O that is transported through the membrane ($\dot{N}_{H_2Omem}$), as the flow of H_2O due to the concentration gradient, electro-osmotic drag and the pressure effect.

$$\dot{N}_{H_2O,mem}(p) = \dot{N}_{H_2O,grad}(p) + \dot{N}_{H_2O,eo}(p) - \dot{N}_{H_2O,pe}(p) \quad \forall\, p \in P \tag{3.66}$$

3.6 Material Balance Constraints

3.6.1 Water Balance

As seen in Figure 3.6a, seawater enters at the electrolyser at the anode where it is consumed. In a similar manner, the fuel cell system (Figure 3.6b) works in a reverse way; H_2O is produced in the cathode. In both the electrolyser and fuel cell, H_2O flows through the PEM to keep the membrane hydrated.

(3.6a)

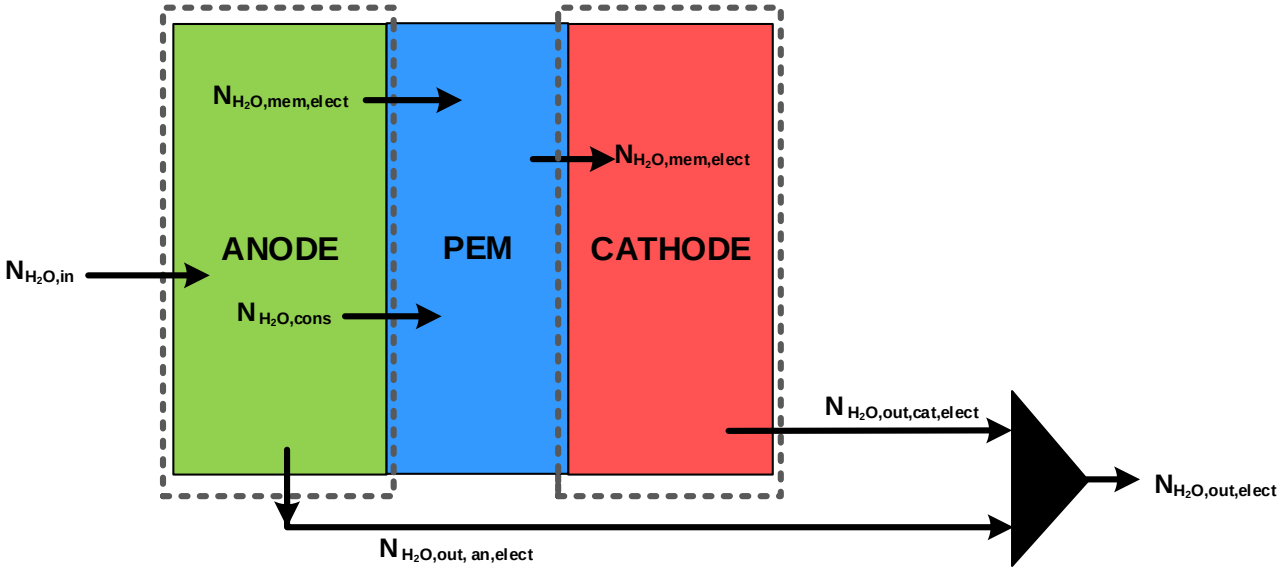

(3.6b)

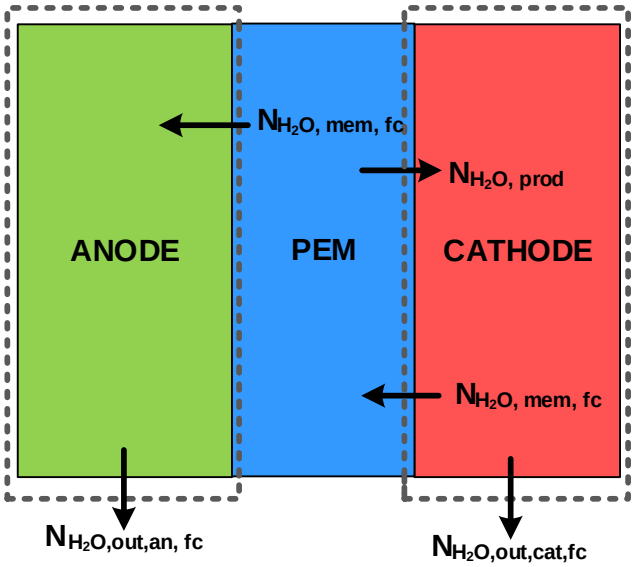

Figure 3.6: H_2O Balance Across the Electrolyser (a) and Fuel Cell (b)

Equation (3.67) states that the molar flow rate of seawater entering the electrolyser is equal to the H_2O entering the anode of the first electrolyser cell. The molar flow rate of H_2O consumed ($\dot{N}_{H_2O,cons}$) is given in Equation (3.68).

$$\dot{N}_{H_2O,in} = \dot{N}_{H_2O,in,an,elect}(m) \qquad \forall\, m \in M, m = 1 \tag{3.67}$$

$$\dot{N}_{H_2O,cons} = \frac{I(p)}{2F} \qquad \forall\, p \in P, p = electrolyser \tag{3.68}$$

Equation (3.69) states that the molar flow rate of H_2O leaving the anode of the electrolyser is equal to the difference between the molar flow rate of H_2O entering the anode, being consumed and the amount of H_2O flowing through the membrane.

$$\dot{N}_{H_2O,out,an,elect}(m) = \dot{N}_{H_2O,in,an,elect}(m) - \dot{N}_{H_2O,cons} - \dot{N}_{H_2O,mem,elect} \qquad \forall\ m \in M \tag{3.69}$$

Equation (3.70) gives the flowrate of H_2O leaving the cathode of the electrolyser cell.

$$\dot{N}_{H_2O,out,cat,elect}(m) = \dot{N}_{H_2O,mem,elect} \qquad \forall\, m \in M \tag{3.70}$$

The total flow rate of H_2O leaving a cell in the electrolyser is given in Equation (3.71)

$$\dot{N}_{H_2O,out,elect}(m) = \dot{N}_{H_2O,out,an,elect}(m) + \dot{N}_{H_2O,out,cat,elect}(m) \qquad \forall\ m \in M \tag{3.71}$$

Equation (3.72) describes the molar flow rate of H_2O entering the next anode cell as the molar flow rate of H_2O leaving the previous cell.

$$\dot{N}_{H_2O,in,an,elect}(m) = \dot{N}_{H_2O,out,elect}(m-1) \qquad \forall\ m \in M, m > 1 \qquad (3.72)$$

Equation (3.73) describes the total molar flow rate leaving the electrolyser system.

$$\dot{N}_{H_2O,out,elect,sys} = \sum \dot{N}_{H_2O,out,elect}\,(m) \qquad \forall\, m \in M \qquad (3.73)$$

The molar flow rate of H_2O produced in the fuel cell is given in Equation (74).

$$\dot{N}_{H_2O,prod} = \frac{I(p)}{2F} \qquad \forall\, p \in P, p = fuel\ cell \qquad (3.74)$$

Equation (3.75) and Equation (3.76) express the molar flow rate of H_2O leaving the anode and cathode of the fuel cell.

$$\dot{N}_{H_2O,out,an,fc}(n) = \dot{N}_{H_2O,mem,fc} \qquad \forall\, n \in N \qquad (3.75)$$

$$\dot{N}_{H_2O,out,cat,fc}(n) = \dot{N}_{H_2O,prod} - \dot{N}_{H_2O,mem,fc} \qquad \forall\, n \in N \qquad (3.76)$$

Equation (3.77) gives the overall mass balance for the PEME system.

$$\dot{M}_{H_2O,in} = \dot{M}_{H_2O,out,elect,sys} + \dot{M}_{H_2,out,elect,sys} + \dot{M}_{O_2,Oout,elect,sys} \qquad (3.77)$$

Equation (3.78) describes the mass balance for the PEMFC system and states that the mass of H_2O, H_2 and O_2 leaving the fuel cell must equal the mass of H_2 and O_2 entering the fuel cell.

$$\dot{M}_{H_2O,out,fc,sys} + \dot{M}_{H_2,out,fc,sys} + \dot{M}_{O_2,out,fc,sys} = \dot{M}_{H_2,in,fc}(n) + \dot{M}_{O_2,in,fc}(n)$$

$$\forall\, n \in N, n = 1 \tag{3.78}$$

Equation (3.79) states that the total mass of H_2O leaving the electrolyser and fuel cell systems must be equal to the mass of seawater entering.

$$\dot{M}_{H_2O,in} = \dot{M}_{H_2O,out,elect,sys} + \dot{M}_{H_2O,out,fc,sys} \tag{3.79}$$

3.6.2 Oxygen Balance

The PEM only allows protons to flow through the membrane. Therefore, all hydroxide and O^{2-} ions remain within the anode compartment of the electrolyser. In electrolysers, O_2 is formed and leaves from the anode. No O_2 is found within the cathode. On the contrary, in fuel cells, O_2 enters the fuel cell at the cathode, where it reacts to form H_2O. Figure 3.7 graphically illustrates the O_2 balance in the electrolyser (a) and fuel cell(b).

(3.7a)

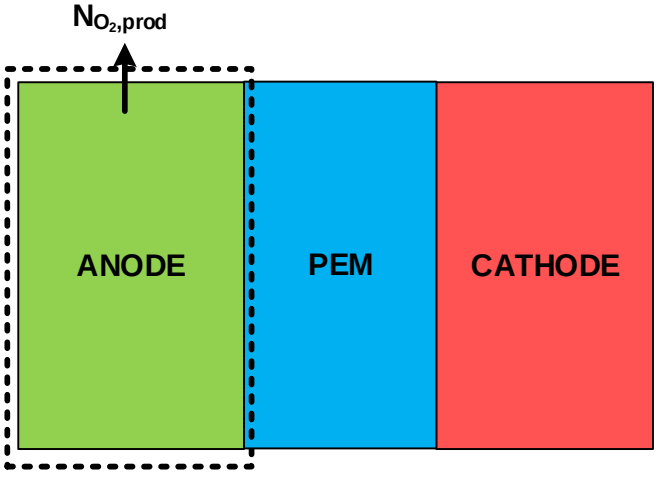

(3.7b)

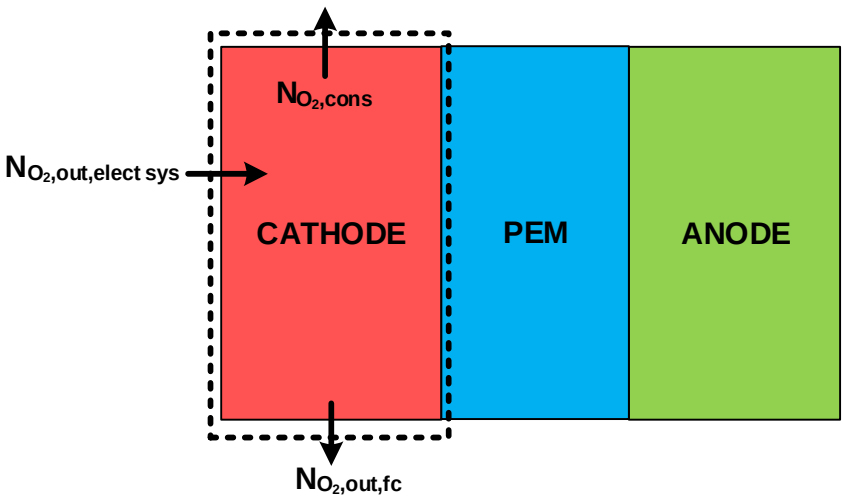

Figure 3.7: O_2 Balance Across the Electrolyser (a) and Fuel Cell (b)

Equation (3.80) expresses the molar flow rate of O_2 produced in the electrolyser. Equations (3.81) describes the molar flow rate of O_2 leaving the anode of a cell in the electrolyser stack. Equation (3.83) gives the total O_2 leaving the electrolyser system.

$$\dot{N}_{O_2,prod} = \frac{I(p)}{4F} \qquad \forall\, p \in P, p = electrolyser \qquad (3.80)$$

$$\dot{N}_{O_2,out,an,elect}(m) = \dot{N}_{O_2,prod} \qquad \forall\, m \in M \qquad (3.81)$$

$$\dot{N}_{O_2,out,elect}(m) = \dot{N}_{O_2,out,an,elect}(m) \qquad \forall\ m \in M \qquad (3.82)$$

$$\dot{N}_{O_2,out,elect,sys} = \sum \dot{N}_{O_2,out,elect}(m) \qquad \forall\ m \in M \qquad (3.83)$$

Equation (3.84) states that the total molar flow rate of O_2 leaving the electrolyser system is equal to the molar flow rate of O_2 entering the first cell of the fuel cell.

$$\dot{N}_{O_2,out,elect,sys} = \dot{N}_{O_2,in,fc}(n) \qquad \forall\, n \in N, n = 1 \tag{3.84}$$

The molar flow rate of O_2 consumed is given in Equation (3.85)

$$\dot{N}_{O_2,cons} = \frac{I(p)}{4F} \qquad \forall\, p \in P, p = fuel\ cell \tag{3.85}$$

Equation (3.86) states that the molar flow rate of O_2 leaving a cell is equal to the difference between the molar flow rate of O_2 entering the fuel cell, and the amount of O_2 consumed.

$$\dot{N}_{O_2,out,fc}(n) = \dot{N}_{O_2,in,fc}(n) - \dot{N}_{O_2,cons} \qquad \forall\ n \in N \tag{3.86}$$

Equation (3.87) states that the molar flow rate of O_2 in the cell *n* is equal to the molar flow rate of O_2 in the previous cell, i.e., *n*-1, of the fuel cell system.

$$\dot{N}_{O_2,in,fc}(n) = \dot{N}_{O_2,out,fc}(n-1) \qquad \forall\, n \in N, n > 1 \tag{3.87}$$

Equation (3.88) states that the molar flow rate of O_2 leaving the last cell in the fuel cell stack must be equal 0 to demonstrate that all O_2 produced in the electrolyser system is consumed.

$$\dot{N}_{O_2,out,fc}(n) = 0 \qquad \forall\, n \in N, n = |N| \tag{3.88}$$

3.6.3 Hydrogen Balance

The PEM is designed to allow H^+ ions to transfer from the anode to the cathode. Moreover, since the model being formulated is one-dimensional, no cross-permeation occurs. This means that the flow of H_2 into the anode compartment of the electrolyser is assumed to be negligible. H_2 in the fuel cell sub-system enters through the anode and is transferred through the membrane into the cathode, where H_2O is formed. Figure 3.8 graphically illustrates the H_2 balance across the electrolyser (a) and fuel cell (b).

(3.8a)

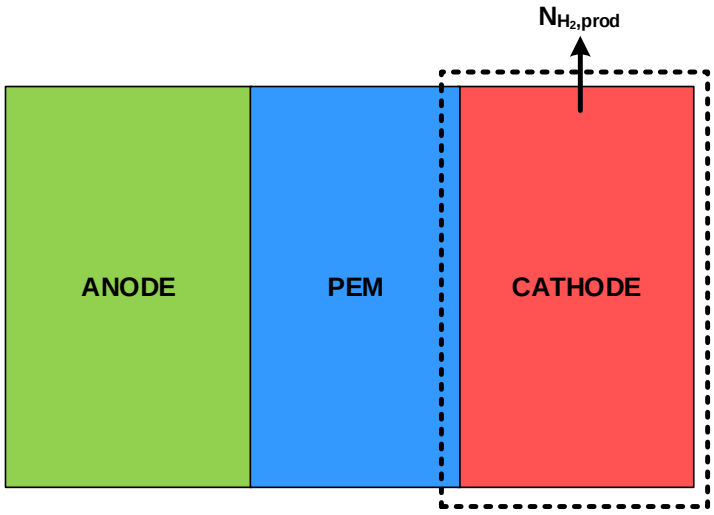

(3.8b)

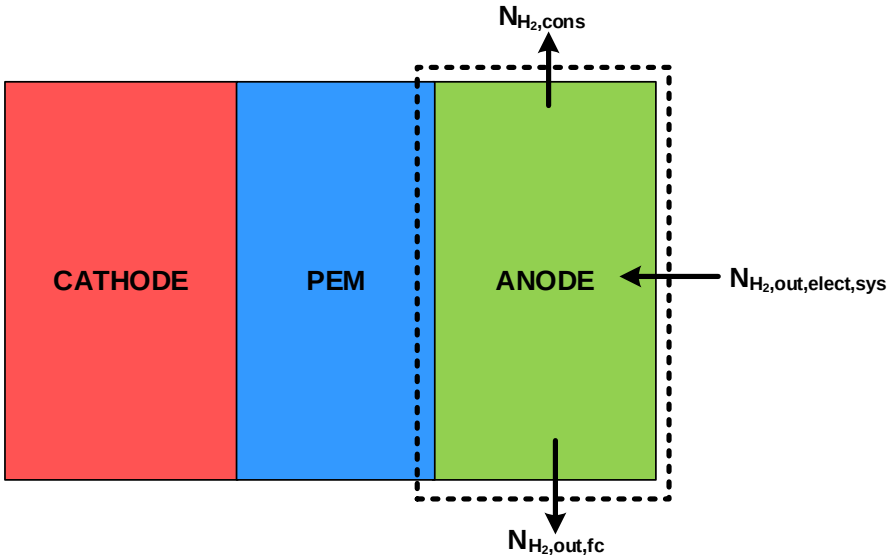

Figure 3.8: H_2 Balance Across the Electrolyser (a) and the Fuel Cell (b)

The molar flow rate of H_2 produced in the electrolyser is given in Equation (3.89).

$$\dot{N}_{H_2,prod} = \frac{I(p)}{2F} \qquad \forall\, p \in P, p = electrolyser \tag{89}$$

Equation (3.90) states that the molar flow rate of H_2 leaving the cathode of the electrolyser is equivalent to the molar flow rate of H_2 produced. It should be noted that the molar flow rate of H_2 entering the cathode of the electrolyser is assumed to be zero since H_2 is produced in the cathode.

$$\dot{N}_{H_2,out,cat,elect}(m) = \dot{N}_{H_2 prod} \qquad \forall\ m \in M \tag{3.90}$$

The molar flow rate of H_2 leaving the electrolyser is given in Equation (3.91) and is equal to the molar flow rate of H_2 leaving the cathode of the electrolyser.

$$\dot{N}_{H_2,out,elect}\ (m) = \dot{N}_{H_2,out,cat,elect}(m) \qquad \forall\ m \in M \tag{3.91}$$

Equation (3.92) describes the total molar flow rate of H_2 leaving the system as the sum of all hydrogen molar flowrates leaving the electrolyser system.

$$\dot{N}_{H_2,out,elect,sys} = \sum \dot{N}_{H_2,out,elect}(m) \qquad \forall\, m \in M \tag{3.92}$$

The total molar flow rate of H_2 consumed is given in Equation (93).

$$\dot{N}_{H_2,cons} = \frac{I(p)}{2F} \qquad \forall\, p \in P, p = fuel\ cell \tag{3.93}$$

Equation (3.94) states that the total molar flow rate of H_2 leaving the electrolyser system is equal to the molar flow rate of H_2 entering the first cell of the fuel cell.

$$\dot{N}_{H_2,out,elect,sys} = \dot{N}_{H_2,in,fc}(n) \qquad \forall\, n \in N, n = 1 \tag{3.94}$$

Equation (3.95) expresses the molar flow rate of H_2 as the difference between the molar mass of H_2 entering the fuel cell and being consumed.

$$\dot{N}_{H_2,out,fc}(n) = \dot{N}_{H_2,in,fc}(n) - \dot{N}_{H_2,cons} \qquad \forall\, n \in N \tag{3.95}$$

Equation (3.96) states that the molar flow rate of H_2 in the next cell is equal to the molar flowrate H_2 in the previous cell of the fuel cell system stack.

$$\dot{N}_{H_2,in,fc}(n) = \dot{N}_{H_2,out,fc}(n-1) \qquad \forall\, n \in N, n > 1 \tag{3.96}$$

Equation (3.97) states that the molar flow rate of H_2 leaving the last cell in the fuel cell stack must be equal 0, to demonstrate that all H_2 produced in the electrolyser system is consumed.

$$\dot{N}_{H_2,out,fc}(n) = 0 \qquad \forall\, n \in N, n = |N| \tag{3.97}$$

3.7 Overall System Performance

3.7.1 Total Power

The total power consumed and produced in the electrolyser and fuel cell systems are given in Equations (3.98) and (3.99). n_{cell} is the number of cells in the stacks.

$$Power_{cons} = \frac{V(p)*I(p)*n_{cell,elect}}{1{,}000} \qquad \forall\, p \in P, p = electrolyser \qquad (3.98)$$

$$Power_{prod} = \frac{V(p)*I(p)*n_{cell,fc}}{1{,}000} \qquad \forall\, p \in P, p = fuel\ cell \qquad (3.99)$$

3.7.2 Freshwater Recovery Rate

Equation (3.100) expresses the freshwater recovery rate in the HEFC system. It describes the percentage of seawater recovered as freshwater. FRR is the freshwater recovery rate.

$$FRR = \frac{N_{H_2O,prod}*n_{cell,fc}}{N_{H_2O,in,elect}} * 100 \qquad (3.100)$$

3.7.3 Objective Function

The objective function in the HEFC system is to maximise the power conversion efficiency, which comprises of the power consumed, power produced and system efficiency. It is described in Equation (3.101).

$$\begin{aligned} obj &= \max\ (power\ conversion\ efficiency) \\ &= \max\left(\frac{Power_{prod}}{Power_{cons}} * \eta_{system}\right) \end{aligned} \qquad (3.101)$$

3.8 Economic Evaluation

The purpose of the economic evaluation is to determine the economic feasibility and viability of pursuing the development of the HEFC system. The model provides the system component sizes which are used to calculate the fixed capital investment and the working capital of the system. This is used to determine the total annualised capital cost, total production cost, total revenue generated, annual cash flows, discounted cash flow, net present value and the payback period. To conduct the economic evaluation, the fixed capital investment, replacement cost, maintenance cost and total annualised cost (TAC) equations are derived from the work done by Rahimi et al. (2014).

3.8.1 Fixed Capital Investment

The initial capital cost also known as fixed capital investment, is the amount of capital required to establish a chemical plant or business venture. It is comprised of the total direct capital cost and the total indirect capital cost. Equation (3.102) expresses the total direct capital cost required for the HEFC system, where $Cost_{stack}$ is the capital cost of the stack, $Cost_{BOP}$ is the capital cost of the balance of the plant, IF is the installation factor and CF_{land} is the land cost factor. Equations (3.103)-(3.104) give the cost of the stack and cost of the balance of the plant. CF_{stack} is the stack cost factor and CF_{BOP} is the balance of the plant cost factor. It should be noted that the capital cost of the electrolyser ($Cost_{cap,elect}$) and fuel cell ($Cost_{cap,fc}$) were extrapolated from the research conducted by Thomas (2018), whereby a graph had been constructed and a polynomial function obtained. The polynomial function obtained for the electrolyser and fuel cell are shown in Equations (3.105) and (3.106). Equation (3.107) gives the total capital cost ($Cost_{cap}$) for the HEFC system.

$$Cost_{TDC} = [(Cost_{stack} + Cost_{BOP}) * (1 + IF)] + (Cost_{cap} * CF_{land}) \quad (3.102)$$

$$Cost_{stack} = Cost_{cap} * CF_{stack} \tag{3.103}$$

$$Cost_{BOP} = Cost_{cap} * CF_{BOP} \tag{3.104}$$

$$Cost_{cap,elect} = \left(4.6 * Y_{purchase}{}^{2} - 18{,}658.2\, Y_{purchase} + 18{,}920{,}787\right) Power_{cons} \tag{3.105}$$

$$Cost_{cap,fc} = \left(4.6 * Y_{purchase}{}^{2} - 18{,}658.2\, Y_{purchase} + 18{,}920{,}787\right) Power_{prod} \tag{3.106}$$

$$Cost_{cap} = Cost_{cap,elect} + Cost_{cap,fc} \tag{3.107}$$

Equation (3.108) expresses the BOP cost factor. It is made up of the anode gas management system ($CF_{gms,an}$), cathode gas management system ($CF_{gms,cat}$), water delivery management system (CF_{dms,H_2O}), thermal management system (CF_{tms}), power electronics (CF_{pelect}), controls and sensors (CF_{cs}), mechanical BOP (CF_{MBOP}), other direct costs (CF_{other}) and assembly labour (CF_{AL}) cost factors.

$$CF_{BOP} = \begin{pmatrix} CF_{gms,an} + CF_{gms,cat} + CF_{dms,H_2O} + CF_{tms} \\ +CF_{pelect} + CF_{cs} + CF_{MBOP} + CF_{other} + CF_{AL} \end{pmatrix} \tag{3.108}$$

The indirect capital cost of the HEFC system is made up of the construction, engineering and design, project contingency, and the legal and contractor costs. Equation (3.109) describes the total indirect capital cost (C_{TIC}) of the HEFC system. $CF_{construction}$, CF_{ED}, CF_{PC} and CF_{LC} are the construction, engineering and design, project contingency, and legal and contractor fee cost factors.

$$C_{TIC} = \left[(CF_{construction} + CF_{PC} + CF_{LC})Cost_{TDC} + \left(CF_{ED} * Cost_{cap}\right)\right] \tag{3.109}$$

Equation (3.110) expresses the fixed capital investment (FCI) required for the HEFC system.

$$FCI = C_{TDC} + C_{TIC} \tag{3.110}$$

3.8.2 Total Annualised Cost

The total annualised cost (TAC) describes the annual cost of owning, maintaining and operating the HEFC system over the lifetime of the plant. It comprises of the annualised capital cost($C_{Cap,annual}$), annualised replacement cost ($C_{Rep,annual}$) and the annualised maintenance cost ($C_{Main,annual}$). Equation (3.111) expresses the TAC of the HEFC system.

$$TAC\ (q) = C_{Cap,annual} + C_{rep,annual} + C_{main,annual} \qquad \forall\, q \in Q \tag{3.111}$$

Equation (3.112) describes the total annualised capital cost of the system ($C_{Cap,annual}$). Y_{plant} is the plant lifetime and AI is the annual interest rate.

$$C_{Cap,annual} = \frac{(FCI*AI)(1+AI)^{Y_{plant}}}{(1+AI)^{Y_{plant}-1}} \tag{3.112}$$

Similarly, to the direct capital cost of the PEME and the PEMFC, the replacement cost is extrapolated from the research conducted by Thomas (2018). Equations (3.113) and (3.114) express the polynomial function used to describe the replacement cost of the electrolyser and fuel cell. Where Y_{rep} is the year of replacement, $Cost_{rep,elect}$ is the replacement cost of the electrolyser and $Cost_{rep,fc}$ is the replacement cost for the fuel cell. Equation (3.115) gives the total replacement cost ($Cost_{rep}$) for the HEFC system. The annualised replacement cost is shown in Equation (3.116)

$$Cost_{rep,elect} = \left(4.6 * {Y_{rep}}^2 - 18{,}658.2\, Y_{rep} + 18{,}920{,}787\right) Power_{cons} \quad (3.113)$$

$$Cost_{rep,fc} = \left(4.6 * {Y_{rep}}^2 - 18{,}658.2\, Y_{rep} + 18{,}920{,}787\right) Power_{prod} \quad (3.114)$$

$$Cost_{rep} = (Cost_{rep,elect} + Cost_{rep,fc})(1 + \mathrm{IF}) \quad (3.115)$$

$$C_{rep\,,annual} = \frac{Cost_{rep}}{Y_{plant}} \quad (3.116)$$

The annualised maintenance cost is considered to remain constant every year. In this dissertation, the annualised maintenance cost is taken as 2.5% of the initial capital cost.

3.8.3 Revenue and production costs

To determine the total revenue generated from the HEFC system, the income generated from the sale of freshwater and electricity are considered. Equation (3.117) states that the total income generated from the sale of water (Rev_{H_2O}) is equal to the mass flow rate of water ($M_{H_2O,out,fc,sys}$) multiplied by the cost of water ($Cost_{H_2O}$) and plant operating hours (Op_{hours}). Similarly, the sale of electricity (Rev_{elect}) is given in Equation (3.118).

$$Rev_{H_2O} = \left(\frac{M_{H_2O,out,fc,sys}}{\rho_{H_2O}}\right) * Cost_{H_2O} * Op_{hours} \tag{3.117}$$

$$Rev_{elect} = Power_{prod} * Cost_{elect} * Op_{hours} \tag{3.118}$$

Equation (3.119) gives the total revenue generated from the sale of water and electricity produced (Rev). In Equation (3.120) it is assumed that the revenue generated will annually increase at the same rate as the interest rate.

$$Rev(q) = Rev_{H_2O} + Rev_{elect} \qquad \forall\, q \in Q, q = 1 \tag{3.119}$$

$$Rev(q) = \left(Rev_{H_2O} + Rev_{elect}\right) * (1 + AI)^q \qquad \forall\, q \in Q, q > 1 \tag{3.120}$$

Equation (3.121) expresses the total production costs incurred in the HEFC system. CF_{PR}, CF_{DS}, CF_{RD} and CF_{INS} are the patent and royalty, selling and distribution, research and development, and insurance cost factors.

$$C_{TP}(q) = [(CF_{PR} + CF_{DS} + CF_{RD}) * Rev(q) + (FCI * CF_{INS})] \qquad \forall\, q \in Q \tag{3.121}$$

3.8.4 Cash Flow

The cash flow over the lifetime of the HEFC system is calculated in Equations (3.122) – (3.127). Equation (3.122) describes the depreciation(Dep) of the system and is calculated using the straight-line method. Equation (3.123) gives the profit before tax (PBT). Equation (3.124) indicates the amount of tax payable to the government (TAX). The profit after tax (PAT), profit after tax plus depreciation ($PATPD$) and annual cash flow ($CASH$) are given in Equations (3.125) - (3.127).

$$Dep\ (q) = \frac{FCI + Cost_{rep}}{Y_{plant}} \qquad \forall\ q \in Q \qquad (3.122)$$

$$PBT(q) = Rev(q) - C_{TP}(q) - Dep(q) \qquad \forall\ q \in Q \qquad (3.123)$$

$$TAX(q) = PBT(q) * Tax_{rate} \qquad \forall\ q \in Q \qquad (3.124)$$

$$PAT(q) = PBT(q) - TAX(q) \qquad \forall\ q \in Q \qquad (3.125)$$

$$PATPD(q) = PAT(q) + Dep(q) \qquad \forall\ q \in Q \qquad (3.126)$$

$$CASH(q) = PATPD(q) - TAC(q) \qquad \forall\ q \in Q \qquad (3.127)$$

3.8.5 Net Present Value

The net present value (NPV) gives the current value of operating the HEFC system over the lifetime of the plant. The discount factor (DF) is expressed in Equation (3.128) and is used to determine the present value of future cash flows. Equations (3.129) and (3.130) describe the present value (PV) and NPV of the proposed system.

$$DF(q) = \frac{1}{(1+AI)^{q-1}} \qquad \forall\, q \in Q \qquad (3.128)$$

$$PV(q) = CASH(q) * DF(q) \qquad \forall\, q \in Q \qquad (3.129)$$

$$NPV = \sum PV(q) \qquad \forall\, q \in Q \qquad (3.130)$$

3.8.6 Payback Period

Equation (3.131) gives the payback period of the plant, which states that the payback period is equal to the FCI multiplied by the plant life divided by the total revenue generated over the plant life.

$$PBP = \frac{FCI * Y_{plant}}{\sum Rev(q)} \qquad \forall\, q \in Q \qquad (3.131)$$

3.9 References

Abdin, Z., Webb, C.J. and Gray, E.M. (2015) "Modelling and simulation of a proton exchange membrane (PEM) electrolyser cell," *International Journal of Hydrogen Energy*, 40(39), pp. 13243–13257. doi:10.1016/j.ijhydene.2015.07.129.

Abdin, Z., Webb, C.J. and Gray, E.M.A. (2016) "PEM fuel cell model and simulation in Matlab–Simulink based on physical parameters," *Energy*, 116, pp. 1131–1144. doi:10.1016/j.energy.2016.10.033.

Bernardi, D.M. and Verbrugge, M.W. (1991) "Mathematical model of a gas diffusion electrode bonded to a polymer electrolyte," *AIChE Journal*, 37(8), pp. 1151–1163. doi:10.1002/aic.690370805.

El-Dessouky, H.T. and Ettouney, H.M. (2002) *Fundamentals of Salt Water Desalination*. First. Amsterdam: Elsevier Science B.V. doi:10.1016/B978-0-444-50810-2.X5000-3.

Han, B. *et al.* (2015) "Electrochemical performance modeling of a proton exchange membrane electrolyzer cell for hydrogen energy," *International Journal of Hydrogen Energy*, 40(22), pp. 7006–7016. doi:10.1016/j.ijhydene.2015.03.164.

Marangio, F., Santarelli, M. and Calì, M. (2009) "Theoretical model and experimental analysis of a high pressure PEM water electrolyser for hydrogen production," *International Journal of Hydrogen Energy*, 34(3), pp. 1143–1158. doi:10.1016/j.ijhydene.2008.11.083.

Rahimi, S. *et al.* (2014) "Techno-economic analysis of wind turbine-PEM (polymer electrolyte membrane) fuel cell hybrid system in standalone area," *Energy*, 67, pp. 381–396. doi:10.1016/j.energy.2014.01.072.

Shimpalee, S. and van Zee, J.W. (2007) "Numerical studies on rib & channel dimension of flow-field on PEMFC performance," *International Journal of Hydrogen Energy*, 32(7), pp. 842–856. doi:10.1016/j.ijhydene.2006.11.032.

Springer, T.E., Wilson, M.S. and Gottesfeld, S. (1993) “Modeling and Experimental Diagnostics in Polymer Electrolyte Fuel Cells,” *Journal of the Electrochemical Society*, 1140(12). doi:10.1149/1.2221120.

Thomas, D. (2018) *Cost Reduction Potential for Electrolyser Technology*, *EY P2G Platform*. Berlin. Available at: https://www.humsterlandenergie.nl/resources/LInks-duurzaam/Linkpagina/20180619_Hydrogenics_EU-P2G-Platform_for-distribution.pdf (Accessed: September 15, 2018).

Tiwary, A. and Williams, I. (2018) *Air Pollution Measurement, Modelling and Mitigation*. Fourth Edition. Boca Raton: CRC Press.

CHAPTER 4

Illustrative Example

4.1 Introduction

This chapter demonstrates the application of the HEFC system that is presented in Chapter 3. The model is applied to an illustrative example based on data extracted from literature. This chapter provides all the assumptions, parameters, constraints and cost factors used in the HEFC system model.

4.2 Seawater Electrolyser and Fuel Cell Parameters

To accurately model the HEFC system, an extensive literature review was conducted to extract modelling parameters for each subsystem. Table 4.1 summarises all the parameters used in the seawater electrolyser model. Table 4.2 gives all the parameters used in the hydrogen fuel cell model, and Table 4.3 demonstrates the general parameters used to model both the seawater electrolyser and hydrogen fuel cell. The critical temperatures, pressures and molecular weights of the key components present in the HEFC system are given in Table 4.4.

Table 4.1: Seawater Electrolyser Parameters

	Value	Reference
Inlet flowrate of seawater (mol/s)	0.01	-
Salinity (parts per thousand)	35	(Dresp *et al.*, 2019)
Anode charge transfer coefficient	0.5	(Tijani *et al.*, 2019)
Cathode charge transfer coefficient	0.5	(Nafchi *et al.*, 2019)
Anode exchange current density (A/m^2)	13	(Bennett, 1980)
Cathode exchange current density (A/m^2)	900	(Han *et al.*, 2015)
Membrane thickness (μm)	178	(Webster and Bode, 2019)

Table 4.2: Hydrogen Fuel Cell Parameters

	Value	Reference
Anode charge transfer coefficient	0.5	(Tijani *et al.*, 2019)
Cathode charge transfer coefficient	1	(Chowdhury, Genc and Toros, 2018)
Anode exchange current density (A/m^2)	2000	(Shimpalee and van Zee, 2007)
Cathode exchange current density (A/m^2)	200	(Shimpalee and van Zee, 2007)
Membrane thickness (μm)	178	(Saebea *et al.*, 2017)

Table 4.3: General HEFC System Parameters

	Value	Reference
Universal gas constant ($J/mol.K$)	8.314	(Vuppala *et al.*, 2019)
Pressure (atm)	1	-
Reference temperature (K)	298.15	(Dresp *et al.*, 2019)
Reference pressure (atm)	1	(Chowdhury, Genc and Toros, 2018)
Faraday's constant	96 485	(Tijani *et al.*, 2019)
Water diffusion coefficient (m^2/s)	1.28×10^{-10}	(Liso *et al.*, 2018)
Water permeability (m^2)	1.58×10^{-18}	(Abdin, Webb and Gray, 2016)
Dry membrane density (kg/m^3)	2 000	(Lee *et al.*, 2019)
Membrane dry equivalent weight (kg/mol)	1.1	(Ferreira *et al.*, 2017)
Electrode porosity	0.3	(Han *et al.*, 2015)
Percolation threshold	0.11	(Tijani *et al.*, 2019)
Number of electrons transferred	2	(Liso *et al.*, 2016)
Empirical coefficient	0.785	(Han *et al.*, 2015)
Empirical coefficient for a	3.64×10^{-4}	(Liso *et al.*, 2018)
Empirical coefficient for b	2.334	(Liso *et al.*, 2018)

Table 4.4: Critical Values for Substances in the PEME and PEMFC Sub-Systems

Substance	Critical Temperature (K)	Critical Pressure (MPa)	Molecular Weight (kg/kmol)
Water	647.3	22.12	0.018
Hydrogen	33.3	1.297	0.002
Oxygen	154.4	5.036	0.032

4.3 Economic Data and Cost Factors

The economic data used to perform the economic evaluation are based on the optimal design parameters obtained from the HEFC model and are presented in Tables 4.5 - 4.7. Table 4.5 and Table 4.6 summarises the cost factors used to determine the direct and indirect costs (Colella *et al.*, 2014), whereas Table 4.7 gives other economic data and rates used in the techno-economic evaluation.

Table 4.5: Direct Cost Factors used in the HEFC System

Direct Costs	Cost Factor
Stack	38%
Hydrogen gas management system	6%
Oxygen gas management system	2%
Water delivery management system	5%
Thermal management	5%
Power electronics	26%
Controls and sensors	6%
Mechanical balance of the plant	5%
Other direct costs	2%
Assembly labour	5%
Land	4%
Installation factor	10%

Table 4.6: Indirect Cost Factors used in the HEFC System

Indirect Costs	Cost Factor
Construction costs	2%
Engineering and design	8%
Project contingency	15%
Legal and contractor	15%

Table 4.7: Other Economic Data and Rates

Other factors	Value	Reference
Working capital	20%	(Turton, 2013)
Annual interest rate	6.75%	(Trading Economics, 2019)
Inflation rate	4.5%	(SA Stats, 2020)
Maintenance factor	2.5%	(Colella *et al.*, 2014)
Purchase year	2019	-
Replacement year (10 years after purchase)	2029	(Colella *et al.*, 2014)
Project life (years)	20	-
Tax rate	28%	(South African Revenue Services, 2020)
Price of electricity ($/kWh)	0.09	(City Power Johannesburg, 2019)

4.4 Model Variable Bounds

The lower and upper bounds for the variables used in the HEFC system are given in Table 4.8. The internal HEFC component size constraints are given in Table 4.9.

Table 4.8: Model Constraints

Variable	Electrolyser range	Fuel cell range	Reference
Temperature (℃)	25-90	25-90	(Atyabi *et al.*, 2019; Nafchi *et al.*, 2019)
Current density (A/m^2)	>10,000 -50,000	-	(Abdel-Aal, Zohdy and Kareem, 2010; Yan *et al.*, 2019)
Voltage (V)	2.1-6	-	(Abdel-Aal, Zohdy and Kareem, 2010)
Humidity degree	14-25	14-25	(Han *et al.*, 2015)
Electro-osmotic drag coefficient	>0.2	> 0.2	-
System efficiency	67-82	67-82	(Valiollahi *et al.*, 2019)
Power produced (kW)	-	1	-
Reaction area (cm^2)	50-400	50-400	-
Anode and cathode thickness (μm)	50-6250	50-6250	-

Table 4.8: Model Constraints (Continued)

Variable	Electrolyser range	Fuel cell range	Reference
Activity of water	1-3	1-3	(Shimpalee and van Zee, 2007)
Distribution and selling factor (%)	0-7	0-7	(Sari and Kolmetz, 2014)
Research and development factor (%)	2-5	2-5	(Peters, Timmerhaus and West, 2003)

Table 4.9: Internal Component Size Constraints

Variable	Electrolyser range	Fuel cell range	Reference
Anode channel width (mm)	1.00-1.25	1.00-1.25	(Kahveci and Taymaz, 2014; Ahmadi *et al.*, 2016)
Cathode channel width (mm)	1.00-1.25	1.00-1.25	(Dedigama *et al.*, 2014; Kahveci and Taymaz, 2014)
Anode GDL width (mm)	0.21-0.30	0.21-0.30	(Obayopo, Bello-Ochende and Meyer, 2010; Bednarek and Tsotridis, 2017)
Cathode GDL width (mm)	0.21-0.30	0.21-0.30	(Obayopo, Bello-Ochende and Meyer, 2010; Bednarek and Tsotridis, 2017)
Anode CL width (mm)	0.01-0.02	0.01-0.02	(Liu, Li and Wang, 2013; Bednarek and Tsotridis, 2017)
Cathode CL width (mm)	0.01-0.02	0.01-0.02	(Bednarek and Tsotridis, 2017; Ebrahimzadeh, Khazaee and Fasihfar, 2018)

4.5 Assumptions

To model the HEFC system, the following assumptions are made:

i. The system operates in a continuous one-dimensional flow
ii. The system operates under steady-state, isothermal and isobaric conditions
iii. PEME produces pure H_2 and O_2
iv. All H_2O is present in the liquid phase
v. Solar and wind energy are used to power the PEME
vi. Cells are connected in series (current remains the same) and current is distributed uniformly
vii. Gases behave as ideal gases
viii. The pressure gradient between the anode and cathode is negligible
ix. Uniform H_2O activity across the membrane
x. No H_2O enters the PEMFC
xi. No H_2 leaves the anode of the PEME and enters the cathode of the PEMFC
xii. No O_2 leaves the cathode of the PEME and enters the anode of the PEMFC
xiii. Chlorine leaves as a solution with excess seawater
xiv. Auxiliary units such as heat exchangers, pumps and valves are not modelled. Therefore, the power consumed by these units are not considered
xv. System is operated for 8000 hours/annum

4.6 References

Abdel-Aal, H.K., Zohdy, K.M. and Kareem, M.A. (2010) "Hydrogen production using sea water electrolysis," *The Open Fuel Cells Journal*, 3, pp. 1–7. doi:10.2174/1875932701003010001.

Abdin, Z., Webb, C.J. and Gray, E.M.A. (2016) "PEM fuel cell model and simulation in Matlab–Simulink based on physical parameters," *Energy*, 116, pp. 1131–1144. doi:10.1016/j.energy.2016.10.033.

Ahmadi, N. *et al.* (2016) "Study of the effect of gas channels geometry on the performance of polymer electrolyte membrane fuel cell," *Periodica Polytechnica Chemical Engineering*, 62(1), pp. 97–105. doi:10.3311/PPch.9369.

Atyabi, S.A. *et al.* (2019) "Effects of assembly pressure on PEM fuel cell performance by taking into accounts electrical and thermal contact resistances," *Energy*, 179, pp. 490–501. doi:10.1016/j.energy.2019.05.031.

Bednarek, T. and Tsotridis, G. (2017) "Issues associated with modelling of proton exchange membrane fuel cell by computational fluid dynamics," *Journal of Power Sources*, 343, pp. 550–563. doi:10.1016/j.jpowsour.2017.01.059.

Bennett, J.E. (1980) "Electrodes for generation of hydrogen and oxygen from seawater," *International Journal of Hydrogen Energy*, 5(4), pp. 401–408. doi:10.1016/0360-3199(80)90021-X.

Chowdhury, M.Z., Genc, O. and Toros, S. (2018) "Numerical optimization of channel to land width ratio for PEM fuel cell," *International Journal of Hydrogen Energy*, 43(23), pp. 10798–10809. doi:10.1016/j.ijhydene.2017.12.149.

City Power Johannesburg (2019) *Schedule of Approved Electricity Tariffs for FY2019 /20*. Johannesburg. Available at: 15/01/2022Schedule of Approved Electricity Tariffs for FY2019 /20.

Colella, W.G. *et al.* (2014) *Techno-economic analysis of PEM electrolysis for hydrogen production*. Colorado. Available at: https://www.energy.gov/sites/prod/files/2014/08/f18/fcto_2014_electrolytic_h2_wkshp_colella1.pdf.

Dedigama, I. *et al.* (2014) "An experimentally validated steady state polymer electrolyte membrane water electrolyser model," *International Journal of Electrochemical Science*, 9(5), pp. 2662–2681.

Dresp, S. *et al.* (2019) "Direct electrolytic splitting of seawater: opportunities and challenges," *ACS Energy Letters*, 4(4), pp. 933–942. doi:10.1021/acsenergylett.9b00220.

Ebrahimzadeh, A.A., Khazaee, I. and Fasihfar, A. (2018) "Numerical investigation of dimensions and arrangement of obstacle on the performance of PEM fuel cell," *Heliyon*, 4(11). doi:10.1016/j.heliyon.2018.e00974.

Ferreira, R.B. *et al.* (2017) "1D + 3D two-phase flow numerical model of a proton exchange membrane fuel cell," *Applied Energy*, 203, pp. 474–495. doi:10.1016/j.apenergy.2017.06.048.

Han, B. *et al.* (2015) "Electrochemical performance modeling of a proton exchange membrane electrolyzer cell for hydrogen energy," *International Journal of Hydrogen Energy*, 40(22), pp. 7006–7016. doi:10.1016/j.ijhydene.2015.03.164.

Kahveci, E.E. and Taymaz, I. (2014) "An investigation of GDL porosity on PEM fuel cell performance," *Chemical Engineering Transactions*, 42, pp. 37–42. doi:10.3303/CET1442007.

Lee, D. *et al.* (2019) "Transport of water through polymer membrane in proton exchange membrane fuel cells," *Korean Chemical Engineering Research*, 57(3), pp. 338–343. doi:10.9713/KCER.2019.57.3.338.

Liso, V. *et al.* (2016) "Modeling and experimental validation of water mass balance in a PEM fuel cell stack," *International Journal of Hydrogen Energy*, 41(4), pp. 3079–3092. doi:10.1016/j.ijhydene.2015.10.095.

Liso, V. *et al.* (2018) “Modelling and experimental analysis of a polymer electrolyte membrane water electrolysis cell at different operating temperatures,” *Energies*, 11(12). doi:10.3390/en11123273.

Liu, H., Li, P. and Wang, K. (2013) “Optimization of PEM fuel cell flow channel dimensions - Mathematic modeling analysis and experimental verification,” *International Journal of Hydrogen Energy*, 38(23), pp. 9835–9846. doi:10.1016/j.ijhydene.2013.05.159.

Nafchi, F.M. *et al.* (2019) “A parametric study of polymer membrane electrolyser performance, energy and exergy analyses,” *International Journal of Hydrogen Energy*, 44(34). doi:10.1016/j.ijhydene.2018.11.081.

Obayopo, S.O., Bello-Ochende, T. and Meyer, J.P. (2010) “Thermodynamic optimization of PEM fuel cell stack gas channel for optimal thermal performance,” in *2010 14th International Heat Transfer Conference, IHTC 14*. doi:10.1115/IHTC14-22233.

Peters, M.S., Timmerhaus, K.D. and West, R.E. (2003) *Plant Design and Economics for Chemical Engineers 5th edition*. 5th edn, *McGraw-Hill*. 5th edn. McGraw-Hill Europe.

SA Stats (2020) *Inflation edges up to 4,6%*. Available at: http://www.statssa.gov.za/?p=13127 (Accessed: March 23, 2020).

Saebea, D. *et al.* (2017) “Analysis of unbalanced pressure PEM electrolyzer for high pressure hydrogen production,” *Chemical Engineering Transactions*, 57. doi:10.3303/CET1757270.

Sari, R.M. and Kolmetz, K. (2014) “General Process Plant Cost Estimating (Engineering Design Guideline),” *KLM Technology Group* [Preprint].

Shimpalee, S. and van Zee, J.W. (2007) “Numerical studies on rib & channel dimension of flow-field on PEMFC performance,” *International Journal of Hydrogen Energy*, 32(7), pp. 842–856. doi:10.1016/j.ijhydene.2006.11.032.

South African Revenue Services (2020) *Companies, trusts and small business corporations (SBC)*. Available at: https://www.sars.gov.za/Tax-Rates/Income-Tax/Pages/Companies-Trusts-and-Small-Business-Corporations.aspx (Accessed: July 15, 2020).

Tijani, A.S. *et al.* (2019) "Electrochemical characteristics of (PEM) electrolyzer under influence of charge transfer coefficient," *International Journal of Hydrogen Energy*, 44(50), pp. 27177–27189. doi:10.1016/j.ijhydene.2019.08.188.

Trading Economics (2019) *South Africa Interest Rate*. Available at: https://tradingeconomics.com/south-africa/interest-rate.

Turton, R. (2013) *Analysis, Synthesis, and Design of Chemical Processes*. Fourth, *Journal of Chemical Information and Modeling*. Fourth. Ann Arbor: Prentice Hall. doi:10.1017/CBO9781107415324.004.

Valiollahi, R. *et al.* (2019) "Electrochemical hydrogen production on a metal-free polymer," *Sustainable Energy and Fuels*, 12. doi:10.1039/c9se00687g.

Vuppala, R.K.S.S. *et al.* (2019) "Optimization of membrane electrode assembly of PEM fuel cell by response surface method," *Molecules*, 24(17). doi:10.3390/molecules24173097.

Webster, J. and Bode, C. (2019) "Implementation of a Non-Discretized Multiphysics PEM Electrolyzer Model in Modelica," in *Proceedings of the 13th International Modelica Conference, Regensburg, Germany, March 4–6, 2019*. doi:10.3384/ecp19157833.

Yan, Z. *et al.* (2019) "Oxygen evolution efficiency and chlorine evolution efficiency for electrocatalytic properties of MnO2 -based electrodes in seawater," *Journal Wuhan University of Technology, Materials Science Edition*, 34, pp. 69–74. doi:10.1007/s11595-019-2016-z.

CHAPTER 5

Results and Discussion

5.1 Introduction

This chapter analyses and discusses the results obtained from the illustrative example presented in Chapter 4. The results and discussion chapter is divided into 8 sections. Firstly, the model is validated with published literature. Secondly, the optimal number of cells required for the PEMFC is given. Thirdly, the HEFC performance results are presented and discussed. Thereafter, the design and operating conditions are given and analysed. The mass and molar balance results are then presented. This is followed by the system's internal component sizes and the overall results of the HEFC system. Lastly, the techno-economic evaluation data is presented and discussed.

The mathematical model of the HEFC system is implemented in GAMS 24.8.5 to maximise power conversion efficiency. BARON is used to solve the NLP optimisation problem. All results for the mathematical model were solved using a computer with the following specifications: Intel i7 processor on a Windows 7 Professional, 64-bit operating system with 8 GB of RAM.

5.2 Model Validation

Since the HEFC system incorporates a seawater electrolyser and to the best of our knowledge, no mathematical models have been developed for a seawater electrolyser, validating the entire model proved to be challenging. Therefore, each sub-system was validated separately. To validate the seawater electrolyser, according to Zuttel et al. (2010), the minimum theoretical energy required at ambient conditions is 39.7 kWh/kg H_2. In this model, an energy requirement of 56.8 kWh/kg H_2 was achieved in the seawater electrolysis sub-system. This showed that the model was in fair agreement with the theoretical minimum energy requirement. Any deviations present may be attributed to the uncertainty in the type of electrolyser and water source used.

The present fuel cell model was validated with the simulation model developed by Adbin et al. (2016). As seen in Figure 5.1, the present model results were in fair agreement with the model developed by Adbin et al. (2016). However, the discrepancy at low current densities was large and may be due to the effect of the activity of H_2O, and the humidity degree of the anode-membrane and cathode-membrane interface, as well as the optimisation of the fuel cell in the HEFC system. In this model, the H_2O activity and the humidity degree expressions were adapted from Shimpalee and Van Zee (2007). At high current densities and low membrane humidity degrees, the ohmic overpotential was greater which means that there was a greater resistance for electrons to transfer through the membrane. As a result, the discrepancy between the two models was reduced. Additionally, the activation overpotential contributed to greater potential losses in the fuel cell. This may be due to the natural logarithmic function present in the activation overpotential, which was linearised in the proposed model. As a result, this reduced the output voltage of the fuel cell and led to the nonlinear model presented by Abdin et al. (2016).

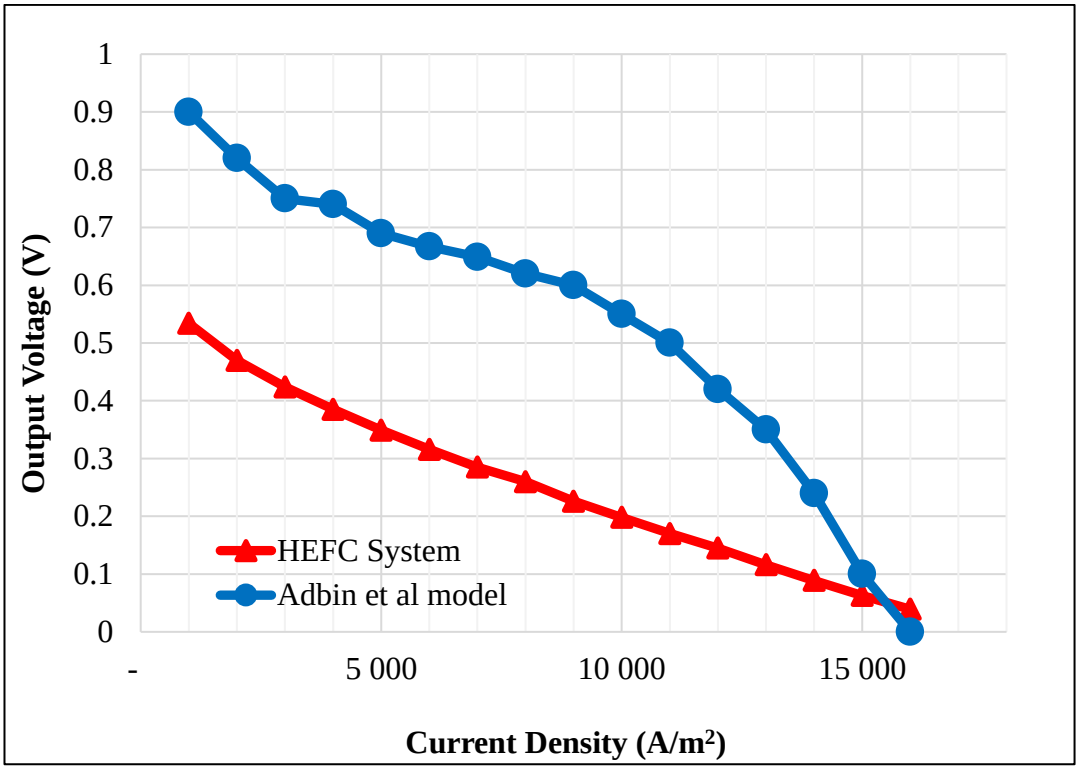

Figure 5.1: Fuel Cell Model Validation

5.3 Optimal Number of Cells in the PEMFC

To determine the optimal number of cells in the fuel cell stack, the relationship between power conversion efficiency and the number of cells was evaluated. According to Figure 5.2, which was constructed from the current HEFC model, the optimal number of cells to maximise power conversion efficiency was 12 cells. The results reported hereafter will be based on a model formulated with 1 cell PEME cell and 12 PEMFC cells. Evidently, there is also an inverse relationship present between power conversion efficiency and the water recovery rate.

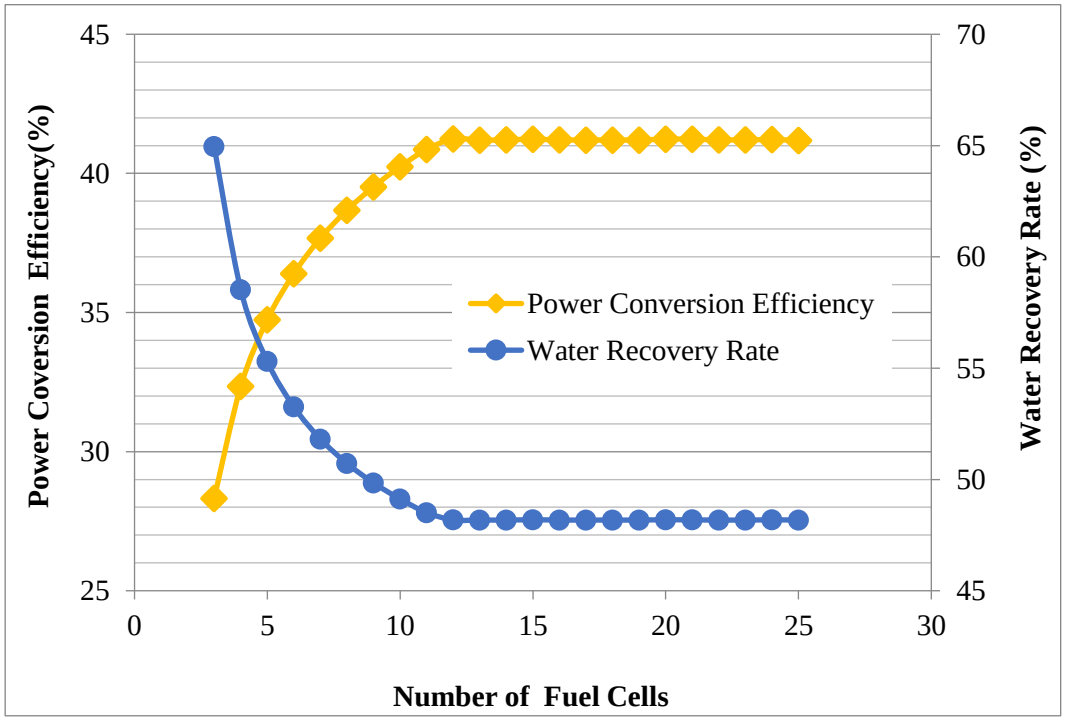

Figure 5.2: Relationship between Power Conversion Efficiency, Freshwater Recovery Rate and Number of Cells in the Fuel Cell Stack

5.4 HEFC System Performance Results and Discussion

Seawater is a solution of salts composed mainly of chloride, sodium, sulphate, magnesium, calcium, and potassium ions dissolved in H_2O. Since O_2 evolution was promoted over chlorine evolution, chlorine leaves the system as a solution with brine. This was achieved by operating the seawater electrolyser at current densities either below 1 mA/cm^2 which would require large electrode areas, or greater than 1,000 mA/cm^2 which would require more energy. In this study, current densities greater than 1,000 mA/cm^2 were used, as the cost required to power the electrolyser was not considered. This was based on solar and wind energy being readily available. The dissolved chlorine will take the form of hypochlorite, which is preferred compared to chlorine gas due to its non-toxic characteristics.

One of the major concerns facing seawater electrolysis is the deposition of magnesium hydroxide and calcium carbonate on the cathode. This generally occurs due to the rise in pH caused by the generation of H_2. Consequently, if precipitation deposits are not removed it will build-up and prevent the efficient transfer of ions, which affects cell performance and efficiency (Badea *et al.*, 2007). To account for this, precipitation removal costs were considered in the techno-economic evaluation. Furthermore, to overcome corrosion, platinum and nickel electrodes which are highly corrosion resistant were used to protect the electrode.

The activation overpotential was found to be the main contributor to the voltage losses in the electrolyser and fuel cell. In the fuel cell, the slow kinetics of the oxygen reaction was responsible for the large cathode activation overpotential. Evidently, Table 5.1 indicates that the overpotential in the cathode is greater than the overpotential in the anode which is seen to have a negligible effect on performance.

Conversely, in PEMEs the kinetics of the anode is responsible for limiting the performance of the PEME. This was due to the slower rate of the OER compared to the HER.

Due to the resistance in the flow of H^+ ions through the membrane, the ohmic overpotential was the second-largest source of potential loss. It should be noted that in PEMFC, as the water content in the membrane was increased, the ohmic overpotential decreased. This was due to the increase in proton conductivity. As such, it may be deduced that the opposite occurs in the electrolyser due to the consumption of water in the formation of hydrogen and oxygen gas.

From the results in Table 5.1, it can be seen that the diffusion overpotential had no effect on the performance of both the electrolyser and the fuel cell. This was due to the presence of the PEM electrolyte and insignificant gas transport limitations present in the thin electrodes. Furthermore, the input voltage of the electrolyser was found to be two times greater than the output voltage of the fuel cell. This was attributed towards the greater losses present in the electrolyser, as opposed to the potential losses in the fuel cell.

Table 5.1: Optimal Performance Results for Each Cell

	Electrolyser	Fuel cell
Current density (A/m^2)	23 266	2 000
Current (A)	930.6	77.47
Open circuit voltage (V)	1.162	1.175
Anode activation overpotential (V)	0.456	0
Cathode activation overpotential (V)	0.198	0.067
Total activation overpotential (V)	0.654	0.067
Anode diffusion overpotential (V)	0	0
Cathode diffusion overpotential (V)	0	0
Total diffusion overpotential (V)	0	0
Ohmic overpotential (V)	0.323	0.031
Input voltage (V)	2.136	-
Output voltage (V)	-	1.076

5.5 Design and Operating Conditions

The optimal design and operating conditions for the HEFC system are summarised in Table 5.2. Table 5.2 shows that the optimal operating temperature when the electrolyser and fuel cell were operated under atmospheric pressure was 80.1 ℃ and 66.7 ℃. In literature, high temperatures (40-80℃) were found to improve the performance of both the PEME and PEMFC (Han *et al.*, 2015). The optimal temperatures obtained from the model were in agreement with the observations made by Han et al. (2015), indicating that the electrolyser and fuel cell performed better at elevated temperatures. This was due to the increase in the reaction rate, as well as the mass transfer rate. However, in this model the temperature of the electrolyser and fuel cell were limited to temperatures in the range of 25-90℃, to prevent the degradation of the membrane, as well as sustain the ionic conductivity of the electrolyte. Additionally, as temperature was increased, the conductivity of the membrane increased, this resulted in an increase in the amount of hydrogen ions diffusing through the membrane leading to reduced ohmic overpotentials and greater water production rates in the fuel cell.

The humidity degree describes the amount of H_2O present in the membrane. Typically, a range of 14-25 is given, where 14 describes a fully saturated membrane and 25 is for a supersaturated membrane. From the results, the optimal humidification degrees were 14.4 and 14.6 in the electrolyser and fuel cell. This shows that adequate water management is required to prevent membrane dehydration and cathode flooding. If there is too little H_2O present in the membrane, membrane dehydration will occur and lead to a lower performance. Additionally, cathode flooding will occur if there is excess H_2O present in the membrane. This will ultimately increase the resistance of the electrode. Consequently, it is apparent that the humidification degree is critical to the performance of the electrolyser and the fuel cell.

According to literature, it had been observed that an increase in membrane thickness resulted in an increase in diffusion and ohmic overpotentials (Han *et al.*, 2015). This led to reduced performance and efficiency in the PEME and PEMFC. In this model, the membrane thickness was assumed to remain constant at 178 μm. Subsequently, the effect of different membrane thicknesses on the performance of the electrolyser and fuel cell may be investigated in the future.

Optimal electrolyser electrode thickness of the anode and cathode was found to be 237 mm and 238 mm respectively, compared to the PEMFC in which the optimal anode and cathode thickness was 270 mm. Similarly, to membrane thickness, an increase in electrode thickness resulted in an increase in diffusion and ohmic losses.

Table 5.2: Optimal Design and Operating Conditions

	Electrolyser	Fuel cell
Temperature (℃)	80.1	66.7
Anode membrane humidity	14.8	14.0
Cathode membrane humidity	14.0	15.3
Humidity degree	14.4	14.6
Density of seawater / freshwater (kg/m^3)	997.3	979.1
Viscosity of seawater/ freshwater (MPa.s)	0	0
Electro-osmotic drag coefficient	1.64	0.20
Anode water activity	1.56	1.00
Cathode water activity	1.00	1.91
Membrane conductivity	12.8	11.3
Anode thickness (μm)	237	270
Cathode thickness (μm)	238	270
Reaction area (cm^2)	400	390

5.6 Mass and Molar Balance Results and Discussion

In Table 5.3, the mass and molar balance results for hydrogen, oxygen and water are given. It should be noted that the mass flow rate of hydrogen and oxygen produced and consumed, as well as water consumed and produced is primarily dependent on current. As the current of the electrolyser increases, the consumption and production rate of water, hydrogen and oxygen is increased. Similarly, in fuel cells, as current increases, more water is produced at the cathode due to the presence of the electrochemical reactions taking place, as well as the electro-osmotic drag. As this takes place the water vapour pressure exceeds the saturation pressure leading to the formation of liquid water. Thus, indicating the importance of the performance of the electrolyser and fuel cell on the quantity of freshwater produced and seawater consumed.

The transportation of water within the membrane of the PEME and PEMFC is largely dependent on the flow due to electro-osmotic drag, flow due to concentration gradient and flow due to the pressure effect across the membrane. In this model, the flow due to the effect of pressure was found to be negligible, as both the electrolyser and fuel cell are operated under isobaric conditions. Additionally, the flow due to the concentration gradient was also found to have no effect on the flow of water through the membrane. As a result, in this model, the membrane water transport was largely dependent on the electro-osmotic drag. It describes the diffusion mechanism followed in dragging water molecules and protons through the membrane from the anode to the cathode in the electrolyser, and from the cathode to the anode in the fuel cell. It is also responsible for preventing damage to the membrane and ensuring that the membrane is hydrated. Adequate water management is required in the PEME and PEMFC to prevent the PEME and PEMFC from flooding. If flooding occurs the water molecules will inhibit and slow down the hydrogen-oxygen reaction at the catalyst layer. Thus, reducing the performance of the system.

Table 5.3: Mass and Molar Flowrate Results

	Electrolyser	Fuel cell
Mass flowrate of water consumed/produced (kg/hr)	0.312	0.026
Mass flowrate of hydrogen produced/consumed (kg/hr)	0.035	0.003
Mass flowrate of oxygen produced/consumed (kg/hr)	0.277	0.023
Molar flow rate of water in the membrane (mol/s)	0.005	0.0002

5.7 Optimal Size of the Internal Components in the HEFC System

The optimal size of the internal components in the HEFC system is given in Table 5.4. According to the results, the cells of the proposed electrolyser and fuel cell stacks were compact in size. The seawater electrolyser cell had the following dimension 240mm (L) x 240mm (H) x 5mm (W) whereas a PEMFC cell was slightly smaller with dimensions of 236mm x 236 mm x 5mm. Thus, indicating that the PEMFC cell is 1.67% smaller than the PEME. As seen in Figure 5.3, the current collectors and channels were found to occupy the greatest percentage of the total width of the PEME and PEMFC. In the electrolyser the current collectors and channels occupy 89.2% of the PEME whereas in the PEMFC the combined current collector and channel contribution is only 88.2%.

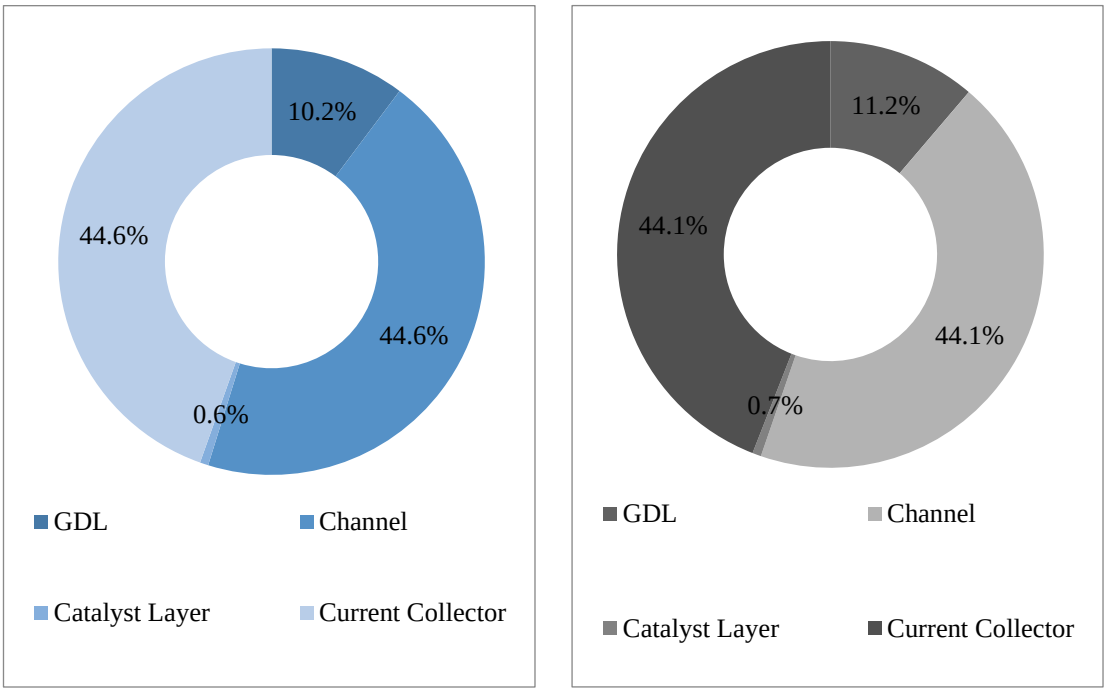

(a) (b)

Figure 5.3: Percentage Contribution of Each Internal Component Width to the Total Width of the Electrolyser (a) and Fuel Cell (b)

Table 5.4: Internal Component Sizes

	Electrolyser size (mm)	Fuel cell size (mm)
Anode GDL width	0.22	0.255
Cathode GDL width	0.24	0.255
Anode channel width	1.00	1.00
Cathode channel width	1.00	1.00
Anode catalyst layer width	0.01	0.02
Cathode catalyst layer width	0.01	0.02
Anode current collector width	1.00	1.00
Cathode current collector width	1.00	1.00
Total anode width	2.23	2.00
Total cathode width	2.25	2.00
Total width	4.48	5.00
GDL length	200	197
Channel length	240	236
Catalyst layer length	200	197
Total length	240	236
GDL height	200	197
Channel height	240	236
Catalyst layer height	200	197
Total height	240	236

5.8 Overall Results

Table 5.5 describes the overall results for the hybrid system. As seen, the power conversion efficiency of the system was 41.2 % and was produced from 100% green energy with near-zero carbon emissions. Furthermore, 48.2 % of the seawater fed to the electrolyser was recovered as freshwater in the fuel cell. This H_2O recovered may be sent to the background process. By integrating the HEFC system with a background process, energy and H_2O can be produced on-site.

Table 5.5: Overall Results

Power conversion efficiency (%)	41.2
Freshwater recovery rate (%)	48.2
System Efficiency (%)	81.9
CPU Time (s)	0.03

5.9 Economic Evaluation

Since in most instances, both good solar and wind resources are available, the power consumed in the electrolyser could be supplied by solar and wind energy. Recently, the cost-competitiveness of renewable energy shows a remarkable transformation in the electricity generation sector. Typically, fossil fuel-derived power costs 0.04-0.14 USD /kWh, compared to electricity generated from wind, which costs 0.04 USD /kWh in the absence of financial support. Similarly, in the solar and PV power generation industry, utility-scale electricity generation costs 0.069 USD /kWh (Strielkowski, 2020). Conversely, in another report, it has been reported that solar PV auction prices of 0.03 USD/kWh are currently available (IRENA, 2020). In this work, the cost for renewable energy consumed was not taken into account, as the model was developed primarily for the optimal design and synthesis of the HEFC system. As such, the purpose of the model was to investigate the operational feasibility of the proposed system in terms of power conversion efficiency. Therefore, no additional costs were assumed to be incurred to break down H_2O molecules, since the cost of electricity for the electrolyser was deemed negligible for the purposes of this study.

The basic cost factors used to breakdown the direct and indirect capital costs of various components in the HEFC system are obtained from Colella et al. (2014). Based on that work, the forecourts cost factors were used because the current HEFC system was modelled to have a 1 kW power production capacity. As a result, using the centralised production facility (CPF) cost factors would be inaccurate due to the large size variance between the HEFC system and the CPF.

The overall capital cost of the PEME was extrapolated from the research conducted by Thomas (2018). Based on that research, Figure 5.4 was constructed, and a polynomial function was obtained. The PEME capital cost is expected to decrease over time, due to greater market uptake, higher production volumes, improved efficiencies, and cheaper catalysts and electrodes.

It is important to note that Figure 5.4 was also used to determine the capital cost of PEMFCs, as PEMFC and PEME are constructed from similar components.

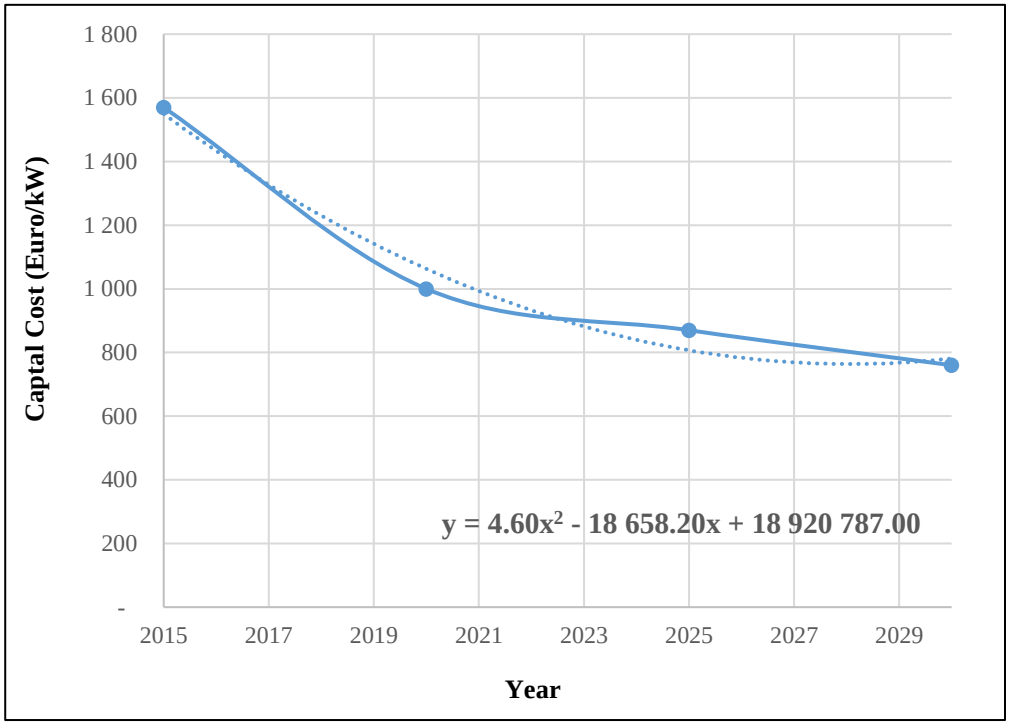

Figure 5.4: PEME and PEMFC Capital Cost from 2015-2030

Table 5.6 gives the installed direct capital costs of the auxiliary components for the PEME and the PEMFC. As seen, the capital costs of the PEME were greater than the PEMFC. This was attributable to the greater size of electrolyser required compared to the size of the PEMFC. The cost of power electronics was found to be the largest contributor to the balance of the plant cost in both the PEME and PEMFC. To avoid membrane degradation, proper feed hydrogen, oxygen and water control is required to ensure and maintain the efficient flow of reactants to the electrolyser and fuel cell. As such, this had been considered through the anode and cathode gas management capital costs presented in Table 5.6. As seen, the cathode gas management cost in the PEMFC is small in comparison to the PEME. This was due to the presence of liquid water in the PEMFC cathode, as opposed to the PEME cathode which is comprised mainly of gaseous hydrogen.

Additionally, to maintain the temperature of the PEME and PEMFC, as well ensure that the membrane is hydrated to prevent membrane degradation, the cost for an adequate water delivery system and thermal management system was included into the total capital cost of the system.

Table 5.6: Installed Direct Capital Costs (USD)

	PEME Capital Cost	PEMFC Capital Cost
Direct capital cost	2772	1394
Stack cost	1053	529.8
Balance of plant	1718	864.4
Anode gas management	55.43	83.65
Cathode gas management	166.3	27.88
Water reactant delivery	138.6	69.71
Thermal management system	138.6	69.71
Power electronics cost	720.6	362.5
Control and sensors	166.3	83.65
Mechanical balance of plant	138.6	69.71
Other direct costs	55.43	27.88
Assembly labour cost	138.6	69.71

According to Table 5.7, the legal and contractor costs, as well as the project contingency costs were the greatest indirect costs incurred in the HEFC system. A high contingency was assumed to compensate and budget for unanticipated market changes, scheduling delays, extended lead times, currency effects, natural disasters, weather-related problems and changes in the size of the system, as well as subcontractor faults. These costs are once-off costs generally incurred to erect the plants. Collectively, the total indirect cost of the HEFC system was 1715 USD.

Table 5.7: Indirect Costs (USD)

Construction costs	86.35
Engineering and design costs	333.3
Legal and contractor costs	647.6
Project contingency costs	647.6
Total indirect cost	1 715

Table 5.8: Other Economic Indicators

Total direct costs (USD)	4 317
Total indirect costs (USD)	1 715
Fixed capital investment (USD)	6 032
Working capital (USD)	1 206
Annualised capital cost (USD)	558.4
Annualised replacement cost (USD)	140.1
Annualised maintenance cost (USD)	94.68
Total annualised cost (USD)	793
Water revenue (USD)	0.002
Electricity revenue (USD)	720.0
Depreciation	441.7

The total direct cost of the HEFC system was calculated as 4 317 USD and included the cost of installation. Collectively, the total direct capital costs and the total indirect capital costs make up the fixed capital investment of the system, which was 6 032 USD. The working capital was taken as 20% of the fixed capital cost and describes the capital required to carry out the daily operations of the plant. The working capital of the plant is used to describe the plant's liquidity, efficiency and overall health. Adequate management is required to ensure the working capital is utilised in an efficient manner to ensure the needs of the plant are met, and that future expansion plans are fulfilled.

The annualised capital cost, annualised maintenance cost and annualised replacement cost describe the annual cost required to pay off the capital cost of the equipment, the annual cost to replace the equipment in the system and the annual cost required to carry out maintenance on the plant equipment. As such, the total annualised cost for the proposed HEFC system was 793 USD.

The total production costs and revenue generated per year over the lifetime of the plant are given in Table 5.9. Plant production costs are the cost associated with the operation of the HEFC system. Despite the fact that negligible costs were assumed for seawater and the electricity consumed in the PEME, the production costs took into account the costs due to patents and royalties, insurance, sales and distribution and research and development. Research and development and insurance formed the bulk cost the production costs due to the continuous developments in PEME and PEMFC technology.

The total revenue generated per year is comprised of the revenue generated from the sale of electricity and freshwater produced. It should be noted that the selling price of electricity and water was assumed to be competitive to the prices in the market. As such, the total revenue generated over the lifetime of the plant was calculated as 30 614 USD.

In the discounted cash flow analysis, the revenue, depreciation, total production, profit before tax, tax and profit after tax were used to determine the financial position of the system. The discounted cash flow describes the current value of an asset, by considering the projected cash flows. The loss in the value of the assets in the HEFC system over time is described as the depreciation. In this model, depreciation per year was calculated using the straight-line. It is dependent on the capital cost of the asset and service life of the asset. The depreciation cost of 441.7 USD was distributed uniformly across the lifetime of the HEFC system. Furthermore, it is worth noting that in this instance depreciation considered the fixed capital investment, as well as the costs required to replace the PEME and PEMFC.

Table 5.9: Production Costs and Revenue Generated Over Plant Life

Year	Total Production Costs (USD)	Total Revenue Generated (USD)
1	146.2	720.0
2	158.2	820.5
3	164.8	875.6
4	171.8	935.0
5	179.4	998.1
6	187.4	1 065
7	196.0	1 137
8	205.1	1 214
9	214.9	1 296
10	225.3	1 384
11	236.5	1 477
12	248.4	1 577
13	261.1	1 683
14	274.6	1 797
15	289.1	1 918
16	304.5	2 047
17	321.0	2 186
18	338.6	2 333
19	357.4	2 491
20	377.4	2 659
Total		30 614

Table 5.10: Cash Flow Results

Year	PBT	Tax Payable	PAT	PATPD	Cash flow	Discount Factor	Present Value
1	132.1	37.00	95.15	536.8	-256.3	1.000	-256.3
2	220.6	61.78	158.9	600.5	-192.6	0.937	-180.4
3	269.4	75.44	194.0	635.7	-157.5	0.878	-138.2
4	321.5	90.02	231.5	673.1	-120.0	0.822	-98.62
5	377.1	105.6	271.5	713.2	-79.95	0.770	-61.57
6	436.4	122.2	314.2	755.9	-37.23	0.721	-26.85
7	499.8	139.9	359.8	801.5	8.381	0.676	5.664
8	567.4	158.9	408.5	850.2	57.07	0.633	36.13
9	639.6	179.1	460.5	902.1	109.0	0.593	64.66
10	716.6	200.7	516.0	957.6	164.6	0.556	91.39
11	798.9	223.7	575.2	1 017	223.7	0.520	116.4
12	886.7	248.3	638.4	1 080	287.0	0.487	139.9
13	980.4	274.5	705.9	1 148	354.5	0.457	161.9
14	1 080	302.5	777.9	1 220	426.5	0.428	182.4
15	1 187	332.4	854.8	1 297	503.4	0.401	201.7
16	1 301	364.4	936.9	1 379	585.5	0.375	219.8
17	1 423	398.5	1025	1 466	673.1	0.352	236.7
18	1 553	434.8	1118	1 560	766.7	0.329	252.6
19	1 692	473.7	1218	1 660	866.6	0.309	267.4
20	1 840	515.1	1325	1 766	973.2	0.289	281.3

Table 5.11: Techno-Economic Results

Total annualised cost (USD)	793.1
Internal rate of return (%)	16.3
Discount factor (%)	6.75
Payback period (years)	3.94
Net present value (USD)	1 496

The net present value (NPV) over a plant life of 20 years is positive indicating that the system generates enough income to compensate for all business risk. Thus, indicating the success of the venture. A discounted cash flow analysis was conducted to consolidate the economic evaluation and the payback period was found to be 3.94 years. This is considered a good payback period as generally, a chemical plant design with a payback period of fewer than 5 years is accepted as being feasible (Sinnott, Coulson and Richardson, 2005). Subsequently, the system proves to provide an environmental benefit in addition to its financial prospects. Additionally, the internal rate of return was calculated as 16.3%, therefore, indicating the that the system is economically viable .

5.10 References

Abdin, Z., Webb, C.J. and Gray, E.M.A. (2016) "PEM fuel cell model and simulation in Matlab–Simulink based on physical parameters," *Energy*, 116, pp. 1131–1144. doi:10.1016/j.energy.2016.10.033.

Badea, G.E. *et al.* (2007) "Hydrogen generation by electrolysis of seawater," *Fascicle of Management and Technological Engineering*, VI(XVI).

Colella, W.G. *et al.* (2014) *Techno-economic analysis of PEM electrolysis for hydrogen production*. Colorado. Available at: https://www.energy.gov/sites/prod/files/2014/08/f18/fcto_2014_electrolytic_h2_wkshp_colella1.pdf.

Han, B. *et al.* (2015) "Electrochemical performance modeling of a proton exchange membrane electrolyzer cell for hydrogen energy," *International Journal of Hydrogen Energy*, 40(22), pp. 7006–7016. doi:10.1016/j.ijhydene.2015.03.164.

IRENA (2020) *Renewable power generation costs in 2019*, *International Renewable Energy Agency*. Abu Dhabi: International Renewable Enery Agency. doi:10.1007/SpringerReference_7300.

Shimpalee, S. and van Zee, J.W. (2007) "Numerical studies on rib & channel dimension of flow-field on PEMFC performance," *International Journal of Hydrogen Energy*, 32(7), pp. 842–856. doi:10.1016/j.ijhydene.2006.11.032.

Sinnott, R.K., Coulson, J.M. and Richardson, J.F. (2005) "Coulson and Richardson's: Chemical Engineering Design," in *Coulson and Richardson's Chemical Engineering*. Fourth. Oxford: Elsevier Butterworth-Heinemann.

Strielkowski, W. (2020) "Renewable energy sources, power markets, and smart grids," in *Social Impacts of Smart Grids*. 1st edn. Elsevier Inc., pp. 97–151. doi:10.1016/b978-0-12-817770-9.00004-3.

Thomas, D. (2018) *Cost Reduction Potential for Electrolyser Technology, EY P2G Platform*. Berlin. Available at:

https://www.humsterlandenergie.nl/resources/LInks-duurzaam/Linkpagina/20180619_Hydrogenics_EU-P2G-Platform_for-distribution.pdf (Accessed: September 15, 2018).

Züttel, A. *et al.* (2010) "Hydrogen: the future energy carrier," *Philosophical Transactions of the Royal Society: Mathematical, Physical and Engineering Sciences*, 368(1923), pp. 3329–3342. doi:10.1098/rsta.2010.0113.

CHAPTER 6

Recommendations and Conclusions

6.1 Introduction

In this chapter, the implications, shortcomings and possible improvements to the mathematical model of the HEFC system are discussed. Additionally, future work that may be done to the HEFC is proposed. Finally, a summary of the dissertation is given in the conclusion.

6.2 Implications and Shortcomings

The concept of the HEFC system was to provide a cleaner alternative process to desalination plants and power conversion systems, as opposed to using conventional power generation and freshwater methods. By incorporating the HEFC system into background processes that require both power and water for operation, the quantity of fresh feed water and input energy required by the system will be reduced. Since the proposed system does not contain any storage facilities, the power and freshwater produced are ideal for background processes that are operated continuously.

Notably, since seawater was used to produce H_2 and O_2 in the electrolyser and seawater contains many salts dissolved in water, deposition of magnesium hydroxide and calcium carbonate on the cathode will occur. This will inhibit the transfer of ions from the anode to the cathode and reduce the hydrogen production rate, as well as the electrolyser efficiency.

Therefore, to eliminate precipitation build-up regular removal of precipitation deposits need to be implemented into the maintenance and cleaning schedule of the plant.

Secondly, corrosion is also another limiting factor which needs to be considered to ensure that the electrolyser operates at optimal efficiency. Platinum and nickel electrodes which have properties of being highly corrosion resistant will need to be used to protect the electrodes. Alternatively, other compatible electrodes which are corrosion resistant and cost-effective may be used.

The proposed mathematical formulation of the HEFC system in Chapter 3 is based on many simplifying assumptions and contains variables that are difficult to measure in a physical system. Through the development of a mathematical model, the feasibility and viability of the system may be determined quickly and cost-effectively. In addition, given that the PEME and PEMFC were initially modelled as separate units, and the presence of mathematical models for seawater electrolysis is limited, an experimental study of the system will need to be conducted to validate the results obtained from the model. This will also give an indication of whether the HEFC is practical and that the parameters used describe the physical system appropriately.

Furthermore, as the world becomes more technologically advanced, solvers and computers with greater computing power are frequently being developed to find an optimal solution in a shorter timeframe. However, licenses for many of these solvers are expensive and, in some cases, proprietary. As a result, it is recommended that other solvers and modelling packages which use improved solution algorithms, are easily accessible, and cost-effective be explored.

Some additional limitations associated with the HEFC model include:

(i) Cross-permeation of H_2 and O_2 was not taken into account, as the system was modelled as a one-dimensional model.

(ii) This model does not consider the operating costs of renewable power consumed. This may be considered as an extension of this work whereby the objective function is comprised of economic constraints and variables.

(iii) It should be noted that the power consumed by auxiliary units such as pumps, compressors and heat exchangers were not taken into account.

(iv) The proposed system was conducted on PEMEs and PEMFCs. Therefore, investigations on the optimal performance of other types of electrolysers and fuel cells were not considered.

6.3 Future Work

The proposed HEFC system addresses the water and energy crisis affecting many countries globally such as South Africa, where either water, energy or both water and energy are constrained. The system does not contain any storage equipment. It is, therefore, recommended that storage be incorporated into the proposed system to provide power and water when required to eliminate the intermittency issues associated with renewable energy. Additionally, by incorporating storage into the model the H_2 produced may be extracted for other applications such as, for use in H_2 fuel cell vehicles or to produce chemicals.

This work modelled the HEFC system as a one-dimensional model whereby cross-permeation of hydrogen and oxygen was not taken into account. As such, it is recommended that two-dimensional and three-dimensional models be formulated to understand the effect of cross-permeation on the performance of the system, as well as efficiency.

Additionally, the model formulation of the seawater electrolyser was developed based on the parameters sourced from literature. It is not clear whether these parameters explicitly describe the seawater electrolysis operation under the conditions that were found to be optimal. Therefore, it is recommended that an experiment study be conducted on the entire system, but particularly the seawater electrolyser.

Furthermore, it should be noted that the power consumed by auxiliary units such as pumps, compressors and heat exchangers were not considered. As a result, it is recommended that the power consumed by these units be taken into account, as it will directly affect the power conversion efficiency.

6.4 Conclusion

This work addresses the water crisis and energy trilemma that is affecting many countries globally. The proposed system models a hybrid electrolyser-fuel cell system to produce H_2 and freshwater from seawater. The proposed system may be used promote clean energy conversion systems and alleviate the strain on freshwater. The objective of this study was to:

(i) Highlight the importance of utilising hydrogen as a renewable energy storage mechanism

(ii) Model and optimise a hybrid electrolyser/fuel cell system to produce power and freshwater from seawater

(iii) Determine the techno-economic feasibility and viability of the system

(iv) Determine the optimal performance and design conditions that maximises power conversion efficiency.

As such, a one-dimensional, mathematical model operated under steady-state, continuous, isothermal, and isobaric conditions was developed for a HEFC system. The HEFC system was operated under atmospheric pressure and may be integrated into a background process (utility system) to provide supplementary power. The hybrid system was modelled and optimised as an NLP problem in GAMS/BARON to maximise power conversion efficiency.

The electrolyser stack was validated and was found to be in fair agreement with results obtained from literature. The H_2 fuel cell was validated with the model developed by Abdin, et al. (2016) and was found to be in good agreement with those results. However, the proposed system had a higher output voltage due to the optimisation of the PEMFC.

The results indicated that the optimal number of electrolysers and fuel cells required to produce 1 kW of power was 1 cell in the electrolyser stack, and 12 cells in the fuel cell stack. According to the model results, 48.2 % of the seawater fed to the electrolyser was recovered as freshwater in the fuel cell. The hybrid system shows potential as being an efficient seawater purification system which releases nearly 0% carbon emissions into the atmosphere. Additionally, it is environmentally friendly in its handling, production, and use.

The model also determined the optimal operating conditions in terms of temperature, current density, electrode thickness and humidity, as well as the performance of the system through the activation overpotential, diffusion overpotential, ohmic overpotential and the open-circuit voltage. Activation overpotential was found to be the main contributor towards voltage losses in the electrolyser sub-system and fuel cell subsystem, whereas the concentration overpotential was found to have no effect on the electrolyser stack and the fuel cell stack.

As an energy conversion system, 41.2 % power conversion efficiency was achieved. This indicates that the system shows promise of decentralising the production of electricity from fossil fuels, addressing the energy trilemma without straining freshwater bodies, and providing clean supplementary power to background processes.

Furthermore, in addition to its environmental benefits, the HEFC system is economically viable presenting a positive net present value, 3.94-year payback period over a 20-year plant life and a 16.3% internal rate of return.

The overall perspective of this work was to illustrate the optimal design of a HEFC system to produce H_2 and freshwater from seawater, as well as the viability of the system. The results from the mathematical model provide insight into the efficiency and performance of the system and can provide a better understanding of seawater electrolysis and the proposed hybrid system.

APPENDIX

GAMS MODEL

APPENDIX A: SET

```
Set
        c_e     Cells in electrolyser stack  /c_e1/

        c_f     Cells in fuel cell stack /c_f1*c_f12/

        s       Substances      /W,H,O/

        d       Critical values /Tc,Pc,Mm/

        a       Seawater density constants /a1,a2,a3,a4/

        g       Constants within seawater density constants/g1,g2,g3/

        N       Number of years/1,2,3,4,5,6,7,8,9,10,11,12,13,14,15,16,17,18,19,20/;
```

APPENDIX B: Parameters

B1. General HEFC System Parameters

Parameters

R	Universal gas	/8.314/
T_ref	Reference temperature in K	/298.15/
P_ref	Reference pressure assumed 1 atm	/0.101325/
F	Faraday's constant	/96485/
deltaa	Feasibility factor	/0.000001/
K_darcy	Water permeability coefficient inside the membrane	/0.00000000000000000158/
rho_m	Density of dry membrane (kg per m3)	/2000/
wt_W	Water molar mass (kg per mol)	/0.018016/
wt_m	Dry equivalent weight of membrane (kg per mol)	/1.1/
E	Porosity of electrodes	/0.3/
E_p	Percolation threshold	/0.11/
alpha	Empirical coefficient	/0.785/
Z	Number of electrons transferred	/2/
a_e	Empirical coefficient for a	/0.000364/
b_e	Empirical coefficient for b	/2.334/

*Seawater Density Constants

Table T1(a,g) Constants required for calculating seawater density

	g1	g2	g3
a1	4.032219	0.115313	0.000326
a2	-0.108199	0.001571	0.000423
a3	-0.012247	0.00174	0.000009
a4	0.000692	0.000087	0.000053 ;

*Water, Hydrogen and Water Critical Values

Table T2(s,d) Critical values for substances in electrolytic cell

	Tc	Pc	Mm
W	647.3	22.119248	0.018
H	33.3	1.29696	0.002
O	154.4	5.035852	0.032 ;

B2. Electrolyser Parameters

N_SWin	Seawater inlet flowrate (mol/s)	/0.01/
io_ae	Cathode exchange current density (A/m^3)	/900/
io_ae	Anode exchange current density (A/m^3)	/13/
alpha_ae	Electrolyser Anode charge transfer coefficient	/0.5/
alpha_ce	Electrolyser Cathode charge transfer coefficient	/0.5/
delta_me	Electrolyser Membrane thickness (m)	/0.000178/
D_we	Diffusion coefficient of water inside the membrane	/0.000000000128/
P_e `	Electrolyser pressure (MPa)	/0.101325/
n_e	Number of cell stacks in the electrolyser	/1/
sal	Salinity (parts per thousand)	/35/

B3. Fuel Cell Parameters

n_f	Number of cell stacks in the fuel cell	/12/
io_af	Anode exchange current density (A/m^3)	/2000/
io_cf	Cathode exchange current density (A/m^3)	/200/
alpha_af	Anode charge transfer coefficient	/0.5/
alpha_cf	Cathode charge transfer coefficient	/1/
delta_mf	Membrane thickness in m	/0.000178/
D_wf	Diffusion coefficient of water inside the membrane	/0.000000000128/
P_f	Fuel cell pressure (MPa)	/0.101325/

B4. Economic Factors

Direct Cost Factors

SCF_e	Electrolyser stack cost factor	/0.38/
SCF_f	Fuel cell stack cost factor	/0.38/
BOPCF_e	Electrolyser balance of plant cost factor	/0.62/
BOPCF_f	Fuel cell balance of plant cost factor	/0.62/
GMCF_ce	Electrolyser cathode gas management cost factor	/0.06/
GMCF_cf	Fuel cell cathode gas management cost factor	/0.02/
GMCF_ae	Electrolyser anode gas management cost factor	/0.02/
GMCF_af	Fuel cell anode gas management cost factor	/0.06/
WDCF_e	Electrolyser water delivery system cost factor	/0.05/
WDCF_f	Fuel cell water delivery system cost factor	/0.05/
TMCF_e	Electrolyser thermal management cost factor	/0.05/
TMCF_f	Fuel cell thermal management cost factor	/0.05/
PECF_e	Electrolyser power electronics cost factor	/0.26/
PECF_f	Fuel cell power electronics cost factor	/0.26/
CSCF_e	Electrolyser control and sensors cost factor	/0.06/
CSCF_f	Fuel cell control and sensors cost factor	/0.06/
MBOPCF_e	Electrolyser mechanical BOP capital cost factor	/0.05/
MBOPCF_f	Fuel cell mechanical BOP capital cost factor	/0.05/
ODCF_e	Electrolyser other direct costs cost factor	/0.02/
ODCF_f	Fuel cell other direct costs cost factor	/0.02/
ALCF_e	Electrolyser Assembly labour cost for factor	/0.05/
ALCF_f	fuel cell assembly labour cost for factor	/0.05/
LCF	Land capital cost	/0.04/
Inst_F	The cost of installing Equipment	/0.1/

*Indirect capital cost

CCF	Construction or site preparation factor	/0.02/
EDCF	Engineering and design factor	/0.08/
PCCF	Project contingency factor	/0.15/
LCCF	Legal and contractor cost factor	/0.15/

Other Economic Parameters and Rates

WCI	Working capital index	/0.2/
AI	Annual interest rate	/0.0675/
IR	Inflation rate	/0.045/
MCF_e	Electrolyser maintenance cost factor	/0.025/
MCF_f	Fuel cell maintenance cost factor	/0.025/
PL	Project lifetime	/20/
Op_hours	Operating hours per year	/8000/
Year	Purchase year	/2019/
TR	Tax rate in South Africa	/0.28/
Zar_doll	Rand to dollar exchange rate (16 December 2019)	/14.37/
Eur_doll	Euro to dollar exchange rate (16 December 2019)	/1.11/
water_cost	Cost of water in rand per kilo litre	/42.19/
elec_cost	Cost of electricity in USD per kilowatt hour (2018)	/0.09/;

APPENDIX C: Variables

C1. Positive Variables

V_oe	Reversible voltage in electrolyser
V_ocve	Open circuit voltage in the electrolyser(V)
V_ohme	Ohmic overpotential in the electrolyser(V)
V_acte	Activation overpotential in the electrolyser(V)
V_actae	Anode activation overpotential in the electrolyser(V)
V_actce	Cathode activation overpotential in the electrolyser(V)
V_e	Total electrolyser voltage(V)
CU_e	Current in electrolyser(A)
i_e	Current density in the electrolyser (A/m^2)
n_He	Hydrogen molar flux in the electrolyser
n_Oe	Oxygen molar flux in the electrolyser
n_Wane	Water molar flux at anode in the electrolyser
n_Wcate	Water molar flux at cathode in the electrolyser
N_Wcons	Molar flowrate of water consumed in the electrolyser (mol per second)
N_Hprod	Molar flowrate of hydrogen produced in the electrolyser (mol per second)
N_Oprod	Molar flowrate of oxygen produced in the electrolyser (mol per second)
N_Wme	Molar flowrate of water through membrane in the electrolyser (mol per second)
N_Weoe	Molar flowrate due to electro-osmotic drag mol in the electrolyser (mol per second)
N_Wpee	Molar flowrate due to pressure effect in the electrolyser (mol per second)

N_Woutae(c_e)	Molar flowrate of water out of anode electrolyser anode (mol per second)
N_Woutce(c_e)	Molar flowrate of water out of the cathode in the electrolyser
N_Winae(c_e)	Molar flowrate of water entering electrolyser anode (mol per second)
N_Woute(c_e)	Molar flowrate of water leaving the electrolyser (mol per second)
N_Woutsyse	Total Molar flowrate of water leaving the electrolyser (mol per second)
N_Houtce(c_e)	Molar flowrate of hydrogen leaving the cathode of the fuel cell (mol per second)
N_Houte(c_e)	Molar flowrate of hydrogen leaving the fuel cell (mol per second)
N_Houtsyse	Molar flowrate of hydrogen leaving the electrolyser system (mol per second)
N_Ooutae(c_e)	Molar flowrate of oxygen leaving the anode of the fuel cell (mol per second)
N_Ooute(c_e)	Molar flowrate of oxygen leaving the fuel cell (mol per second)
N_Ooutsyse	Molar flowrate of oxygen leaving the electrolyser system (mol per second)
M_Wcons	Mass flowrate of water consumed (kg per hour)
M_Hprod	Mass flowrate of hydrogen produced (kg per hour)
M_Oprod	Mass flowrate of oxygen produced (kg per hour)
M_SWin	Mass flowrate of seawater entering the electrolyser
M_Woutsyse	Total mass flowrate of water leaving the electrolyser (mol per second)
M_Houtsyse	Total mass flowrate of hydrogen leaving the electrolyser (mol per second)
M_Ooutsyse	Total mass flowrate of oxygen leaving the electrolyser (mol per second)
CW_mecate	Water concentration at cathode side of membrane in the electrolyser (mol per m3)
CW_meane	Water concentration at anode side of membrane in the electrolyser (mol per m3)

CO_me	Oxygen concentration at the electrode and membrane interface (mol per m3)
CH_me	Hydrogen concentration at the electrode and membrane interface (mol per m3)
CO_moe	Oxygen concentration at the electrode and membrane interface at reference (mol per m3)
CH_moe	Hydrogen concentration at the electrode and membrane interface at reference (mol per m3)
CO_che	Oxygen concentration at the channel in the electrolyser (mol per m3)
CH_che	Hydrogen concentration at the channel in the electrolyser (mol per m3)
CO_choe	Oxygen concentration at reference conditions at the channel (mol per m3)
CH_choe	Hydrogen concentration at reference conditions at the channel in the electrolyser (mol per m3)
delta_eae	Anode electrode thickness in the electrolyser (m)
yH_che	Hydrogen molar fraction at channel in the electrolyser
yO_che	Oxygen molar fraction at channel in the electrolyser
delta_ece	Cathode electrode thickness in the electrolyser (m)
D_effOWe	Diffusion coefficient of a water-oxygen substance mixture in the electrolyser (m2 per second)
D_OWe	Oxygen-water diffusion coefficient in the electrolyser (m2 per second)
D_HWe	Hydrogen-water diffusion coefficient in the electrolyser (m2 per second)
D_effHWe	Diffusion coefficient of a water-hydrogen substance mixture in the electrolyser
xa_e	Anode current density ratio in the electrolyser
xc_e	Cathode current density ratio in the electrolyser
n_de	Electrolyser Coefficient due to electro-osmotic drag
n_d	electrostatic drag coefficient in fuel cell

Mm_OW	Molar mass for water and oxygen in the electrolyser
Pc_OW	Critical pressure for water and oxygen in the electrolyser
Tc_OW	Critical temperature for water and oxygen in the electrolyser
Tr_OWe	Temperature ratio for water and oxygen in the electrolyser
Mm_HW	Molar mass for water and oxygen in the electrolyser
Pc_HW	Critical pressure for water and oxygen in the electrolyser
Tc_HW	Critical temperature for water and oxygen in the electrolyser
Tr_HWe	Temperature ratio for water and oxygen in the electrolyser
theta_me	Membrane conductivity in the electrolyser
Power_cons	Power in kW in the electrolyser
lamda_ae	Water content at anode of electrolyser
lamda_ce	water content at cathode of electrolyser
lamda_e	Degree of humidification in the electrolyser
RA_e	Reaction area in the electrolyser
RA_f	Reaction area in the fuel cell
P_ae	Anode operating pressure in the electrolyser(atm)
P_ce	Cathode operating pressure in (atm)
p_he	Electrolyser partial pressure of hydrogen in the electrolyser(atm)
p_oe	Electrolyser partial pressure of oxygen in the electrolyser(atm)
p_we	Electrolyser partial pressure of water in the electrolyser(atm)
T_e	Electrolyser temperature (K)
T_ec	Temperature of the electrolyser in degrees Celsius (C)
T_ae	Electrolyser anode Operating Temperature (K)
T_ce	Electrolyser Cathode Operating Temperature (K)

P_de	Electrolyser pressure difference between anode and the cathode (MPa)
PsatV1e	Electrolyser saturated vapor pressure (MPa)
PsatVe	Electrolyser vapor pressure (MPa)
V_of	Fuel cell reversible voltage (V)
V_ocvf	Fuel cell open circuit voltage (V)
V_f	Fuel cell total fuel cell voltage (V)
V_difff	Fuel cell diffusion overpotential (V)
V_diffaf	Fuel cell anode diffusion overpotential (V)
V_diffcf	Fuel cell cathode diffusion overpotential (V)
V_ohmf	Fuel cell ohmic overpotential (V)
V_actf	Fuel cell activation overpotential (V)
V_actaf	Fuel cell anode activation overpotential (V)
V_actcf	Fuel cell cathode activation overpotential (V)
CU_f	Fuel cell current (A)
i_f	Fuel cell current density (A per meter squared)
n_Hf	Fuel cell hydrogen molar flux
n_Of	Fuel cell oxygen molar flux
n_Wanf	Fuel cell water molar flux at anode
n_Wcatf	Fuel cell water molar flux at cathode
N_Hinf(c_f)	Fuel cell molar flowrate of hydrogen entering (mol per second)
N_Oinf(c_f)	Molar flowrate of oxygen entering the fuel cell (mol/s)
N_Houtf(c_f)	Molar flowrate of hydrogen leaving the fuel cell (mol/s)
N_Ooutf(c_f)	Molar flowrate of oxygen leaving the fuel cell (mol/s)

N_Woutf(c_f)	Molar flowrate of water leaving the fuel cell (mol/s)
N_Wprod	Molar flowrate of water consumed (mol/s)
N_Hcons	Molar flowrate of hydrogen produced (mol/s)
N_Ocons	Molar flowrate of oxygen produced (mol/s)
N_Houtsysf	Total molar flowrate of hydrogen leaving (mol/s)
N_Ooutsysf	Total molar flowrate of oxygen leaving (mol/s)
N_Wmf	Molar flowrate of water through membrane in the fuel cell (mol/s)
N_Weof	Molar flowrate due to electro-osmotic drag in the fuel cell(mol/s)
N_Wpef	Molar flowrate due to pressure effect in the fuel cell (mol/s)
N_Woutaf	Molar flowrate of water out of anode in the fuel cell (mol/s)
N_Winaf	Molar flowrate of water entering anode in the fuel cell (mol/s)
N_Woutaf	Molar flowrate of water leaving anode in the fuel cell (mol/s)
N_Woutcf	Molar flowrate of water out of the cathode in the fuel cell (mol/s)
N_Winf	Molar flowrate of fresh water entering the fuel cell (mol/s)
N_Woutf	Molar flowrate of fresh water leaving the fuel cell (mol/s)
N_Woutsysf	Total molar flowrate of water leaving the fuel cell system (mol/s)
M_Wprod	Mass flowrate of water consumed (kg/hr)
M_Hcons	Mass flowrate of hydrogen produced (kg/hr)
M_Ocons	Mass flowrate of oxygen produced (kg/hr)
M_Houtsysf	Total mass flowrate of hydrogen leaving fuel cell system (kg/s)
M_Ooutsysf	Total mass flowrate of oxygen leaving fuel cell system (kg/s)
M_Woutsysf	Total mass flowrate of water leaving fuel cell system (kg/s)
CW_mecatf	Water concentration at cathode-membrane interface of the fuel cell (mol/m^3)
CW_meanf	Water concentration at anode-membrane interface of the fuel cell (mol/m^3)
CO_mf	Oxygen concentration at the electrode- membrane interface in the fuel cell (mol/m3)

CH_mf	Hydrogen concentration at the electrode-membrane interface of the fuel cell (mol/ m^3)
CO_mof	Oxygen concentration at the electrode-membrane interface at reference conditions of the fuel cell (mol /m^3)
CH_mof	Hydrogen concentration at the electrode-membrane interface at reference conditions of the fuel cell (mol /m^3)
CO_chf	Oxygen concentration at the fuel cell channel (mol/ m^3)
CH_chf	Hydrogen concentration at the fuel cell channel (mol/ m^3)
CO_chof	Oxygen concentration at reference conditions at the fuel cell channel (mol/ m^3)
CH_chof	Hydrogen concentration at reference conditions at the fuel cell channel (mol/ m^3)
CW_Chanf	Concentration of water at the fuel cell channel (mol/ m^3)
CW_Chcatf	Concentration of water at the fuel cell channel (mol/ m^3)
delta_eaf	Fuel cell anode electrode thickness (m)
yH_chf	Hydrogen molar fraction at fuel cell channel
yO_chf	Oxygen molar fraction at fuel cell channel
delta_ecf	Fuel cell cathode electrode thickness (m)
D_effOWf	Fuel cell effective diffusion coefficient of a water-oxygen substance mixture (m^2/s)
D_effHWf	Fuel cell effective diffusion coefficient of a water-hydrogen substance mixture (m^2/s)
D_OWf	Fuel cell oxygen-water diffusion coefficient (m^2/s)
D_HWf	Fuel cell hydrogen-water diffusion coefficient (m^2/s)
Mm_OWf	Molar mass for water and oxygen
xa_f	Fuel cell anode current density ratio
xc_f	Fuel cell cathode current density ratio in the fuel cell

Tr_OWf	Temperature ratio for water and oxygen in the fuel cell
Tr_HWf	Temperature ratio for water and hydrogen in the fuel cell
theta_mf	Membrane conductivity in the fuel cell
Power_prod	Power produced in kW
lamda_af	Fuel cell water content at anode
lamda_cf	Fuel cell water content at cathode
lamda_f	Fuel cell degree of humidification (mol water per mol SO3-)
P_aF	Fuel cell anode operating pressure (MPa)
P_cF	Fuel cell cathode operating pressure (MPa)
P_df	Fuel cell pressure difference between anode and the cathode (MPa)
p_hf	Fuel cell partial pressure of hydrogen (MPa)
p_of	Fuel cell partial pressure of oxygen (MPa)
p_wf	Fuel cell partial pressure of water (MPa)
PsatV1f	Fuel cell saturated vapor pressure (MPa)
PsatVf	Fuel cell saturated vapor pressure (MPa)
T_f	Fuel cell temperature (K)
T_fc	Fuel cell cathode temperature in Celsius (C)
T_af	Fuel cell anode temperature (K)
T_cf	Cathode operating temperature in the fuel cell(K)
yW_mecate	Electrolyser water molar composition at cathode-membrane interface (mol/m^3)
yW_meane	Electrolyser water molar composition at anode-membrane interface (mol/m^3)
yW_mecatf	Fuel cell water molar composition at cathode-membrane interface (mol/m^3)
yW_meanf	Fuel cell water molar composition at anode-membrane interface (mol/m^3)

Power_Eff	Power efficiency of the system
Water_eff	Water efficiency for the hybrid system
System_eff	Efficiency of the system
V_esys	Electrolyser system voltage (V)
V_fsys	Fuel cell system voltage (V)

Electrolyser Sizing Variables

w_GDL_ea	Electrolyser gas diffusion layer width (m)
w_GDL_ec	Electrolyser gas diffusion layer width (m)
w_CL_ea	Electrolyser catalyst layer width (m)
w_CL_ec	Electrolyser catalyst layer width(m)
w_channel_ea	Electrolyser channel width(m)
w_channel_ec	Electrolyser channel width(m)
w_CC_ea	Electrolyser current collector width (m)
w_CC_ec	Electrolyser current collector width (m)
h_GDL_e	Electrolyser gas diffusion layer height(m)
h_CL_e	Electrolyser catalyst layer height(m)
h_channel_e	Electrolyser channel height(m)
l_GDL_e	Electrolyser gas diffusion layer(m)
l_CL_e	Electrolyser catalyst layer length(m)
l_channel_e	Electrolyser channel length(m)
T_w_ce	Total cathode width of one cell in the electrolyser (m)
T_w_ae	Total anode width of one cell in the electrolyser (m)
T_w_e	Total width of one cell in the electrolyser (m)
T_h_e	Total height of one cell in the electrolyser (m)
T_l_e	Total length of one cell in the electrolyser (m)

*Fuel Cell Sizing *

w_GDL_fa	Fuel cell gas diffusion layer width (m)
w_GDL_fc	Fuel cell gas diffusion layer width (m)
w_CL_fa	Fuel cell catalyst layer width (m)
w_CL_fc	Fuel cell catalyst layer width (m)
w_channel_fa	Fuel cell channel width (m)
w_channel_fc	Fuel cell channel width (m)
w_CC_fa	Fuel cell current collector width (m)
w_CC_fc	Fuel cell current collector width (m)
h_GDL_f	Fuel cell gas diffusion layer height (m)
h_CL_f	Fuel cell catalyst layer height (m)
h_channel_f	Fuel cell channel height (m)
l_GDL_f	Fuel cell gas diffusion layer (m)
l_CL_f	Fuel cell catalyst layer length (m)
l_channel_f	Fuel cell channel length (m)
T_w_cf	Total cathode width of one cell in the fuel cell (m)
T_w_af	Total anode width of one cell in the fuel cell (m)
T_w_f	Total width of one cell in the fuel cell (m)
T_h_f	Total height of one cell in the fuel cell (m)
T_l_f	Total length of one cell in the fuel cell (m)

Direct Capital Cost

Cap_DC_e	Electrolyser direct capital cost ($)
Cap_DC_f	Fuel cell direct capital cost ($)
Cap_DC	Total direct capital cost ($)
SCap_DC_e	Electrolyser stack capital cost ($)
SCap_DC_f	Fuel cell stack capital cost ($)
BOPCap_DC_e	Electrolyser balance of plant cost ($)
BOPCap_DC_f	Fuel cell balance of plant cost ($)
CM_DC_e	Electrolyser cathode gas management cost ($)
CM_DC_f	Fuel cell cathode gas management cost ($)
AM_DC_e	Electrolyser anode gas management cost ($)
AM_DC_f	Fuel cell anode gas management cost ($)
WD_DC_e	Electrolyser water reactant delivery cost ($)
WD_DC_f	Fuel cell water reactant delivery cost ($)
TM_DC_e	Electrolyser thermal management system cost ($)
TM_DC_f	Fuel cell thermal management system cost ($)
PE_DC_e	Electrolyser power electronics cost ($)
PE_DC_f	Fuel cell power electronics ($)
CS_DC_e	Electrolyser controls and sensors cost ($)
CS_DC_f	Fuel cell controls and sensors cost ($)
MBOP_DC_e	Electrolyser mechanical BOP capital cost ($)
MBOP_DC_f	Fuel cell mechanical BOP cost ($)
OD_DC_e	Electrolyser other direct capital cost ($)
OD_DC_f	Fuel cell other direct capital cost ($)
AL_DC_e	Electrolyser assembly labour cost for electrolyser ($)
AL_DC_f	Fuel cell assembly labour cost ($)
Land	Direct land cost ($)

Installation cost

Cap_IC_e	Electrolyser capital installation cost ($)
Cap_IC_f	Fuel cell capital installation cost ($)
Cap_IC	Total capital installation cost ($)
SCap_IC_e	Electrolyser stack capital installation cost ($)
SCap_IC_f	Fuel cell stack capital installation cost ($)
BOPCap_IC_e	Electrolyser balance of plant capital installation cost ($)
BOPCap_IC_f	Fuel cell balance of plant capital installation cost ($)
CM_IC_e	Electrolyser cathode gas management installation cost ($)
CM_IC_f	Fuel cell cathode gas management installation cost ($)
AM_IC_e	Electrolyser anode gas management installation cost ($)
AM_IC_f	Fuel cell anode gas management installation cost ($)
WD_IC_e	Electrolyser water reactant delivery installation cost ($)
WD_IC_f	Fuel cell water reactant delivery installation cost ($)
TM_IC_e	Electrolyser thermal management system installation cost ($)
TM_IC_f	Fuel cell thermal management system installation cost ($)
PE_IC_e	Electrolyser power electronics installation cost ($)
PE_IC_f	Fuel cell power electronics installation cost ($)
CS_IC_e	Electrolyser controls and sensors installation cost ($)
CS_IC_f	Fuel cell controls and sensors installation cost ($)
MBOP_IC_e	Electrolyser mechanical BOP installation cost ($)
MBOP_IC_f	Fuel cell mechanical BOP installation cost ($)
OD_IC_e	Electrolyser other direct installation cost ($)
OD_IC_f	Fuel cell other direct installation cost ($)
AL_IC_e	Electrolyser assembly labour installation cost ($)
AL_IC_f	Fuel cell assembly labour installation cost ($)

*Total installed cost of equipment

Dcap_Tcost_e	Total electrolyser direct capital cost ($)
DCap_Tcost_f	Total fuel cell direct capital installation cost for PEM fuel cell ($)
DCap_Tcost	Total direct capital installation cost ($)
SCap_Tcost_e	Total electrolyser capital stack cost ($)
SCap_Tcost_f	Total fuel cell capital stack cost ($)
BOPCap_Tcost_e	Total electrolyser balance of plant capital cost ($)
BOPCap_Tcost_f	Total fuel cell balance of plant capital cost ($)
CM_Tcost_e	Total electrolyser cathode gas management cost ($)
CM_Tcost_f	Total fuel cell cathode gas management cost ($)
AM_Tcost_e	Total electrolyser anode gas management cost ($)
AM_Tcost_f	Total fuel cell anode gas management cost ($)
WD_Tcost_e	Total electrolyser water reactant delivery cost ($)
WD_Tcost_f	Total fuel cell water reactant delivery cost ($)
TM_Tcost_e	Total electrolyser thermal management system cost ($)
TM_Tcost_f	Total fuel cell thermal management system cost ($)
PE_Tcost_e	Total electrolyser power electronics cost ($)
PE_Tcost_f	Total fuel cell power electronics cost ($)
CS_Tcost_e	Total electrolyser controls and sensors cost ($)
CS_Tcost_f	Total fuel cell controls and sensors cost ($)
MBOP_Tcost_e	Total electrolyser mechanical BOP cost ($)
MBOP_Tcost_f	Total fuel cell mechanical BOP cost ($)
OD_Tcost_e	Total electrolyser other direct cost ($)
OD_Tcost_f	Total fuel cell other direct cost ($)
AL_Tcost_e	Total electrolyser assembly labour cost ($)
AL_Tcost_f	Total fuel cell assembly labour cost ($)
TD_cost	Total direct capital cost ($)

Indirect costs

C_cost	Construction cost ($)
ED_cost	Engineering and design costs ($)
PC_cost	Project contingency costs ($)
LC_fees	Legal and contractor fees ($)
TI_cost	Total indirect capital cost ($)

*Fixed investment capital

FCI	Fixed investment capital ($)

*Working Capital

Work_cap	Working capital required ($)

Replacement cost

Rep_cost_e	Electrolyser replacement cost ($)
Rep_cost_f	Fuel cell replacement cost for the fuel cell ($)
Rep_cost	Total replacement cost ($)
Rep_Icost	Installation cost for replacement equipment ($)
Rep_Tcost	Total installed replacement cost ($)

*Maintenance cost

Main_cost_e	Electrolyser maintenance cost ($)
Main_cost_f	Fuel cell maintenance cost ($)
Main_cost	Total maintenance cost ($)

*Revenue

Rev(N)	Revenue generated in Nth year ($)
Tot_Rev	Total revenue generated in the plant ($)
Elec_sale	Revenue generated from electricity ($)
water_sale ``	Revenue generated from sale of fresh water ($)

*Production costs

PR_cost	Patents and royalties factor cost ($)
LTR_Cost	Local rates and taxes ($)
I_Cost	Insurance cost ($)
DS_cost	Distribution and selling ($)
RD_cost	Research and development ($)
TP_cost	Total production cost ($)
PR_factor	Patents and royalties' factor
I_factor	Insurance factor
DS_factor	Distribution and Selling factor
RD_factor	Research and development factor

Annualised Capital Cost

Acap_cost	Annualised capital cost ($)
Arep_cost	Annualised replacement cost ($)
Amain_cost	Annualized maintenance cost ($)
DF(N) `	Discount factor for the plant
TAC	Total annualised cost ($)
Dep	Depreciation ($)
PBP ``	Payback period;

C2. Free Variables

Free variable	
V_oce	Voltage as a function of temperature (V)
N_Wdde	Molar flowrate due to concentration gradient in the electrolyser (mol/s)
DA	Seawater density constant A
DB	Seawater density constant B
DA1	Seawater density calculation for A1
DA2	Seawater density calculation for A2
DA3	Seawater density calculation for A3
DA4	Seawater density calculation for A4
F3	Seawater density calculation for F3
F4	Seawater density calculation for F4
Rho_FW	Freshwater density (kg/m^3)
Rho_sw	Overall Seawater density (kg/m^3)
mu_A	Seawater viscosity constant A
mu_B	Seawater viscosity constant B
mu_r	Viscosity value R
mu_wr	Viscosity of wr
mu_sw1	Viscosity of seawater (Pa.s)
mu_sw	Viscosity of seawater (MPa.s)
N_Wddf	Molar flowrate due to concentration gradient in the fuel cell (mol/s)
V_diffe	Diffusion overpotential in the electrolyser(V)
V_diffae	Anode Diffusion overpotential in the electrolyser(V)
V_diffce	Cathode Diffusion overpotential in the electrolyser(V)

AW_ae	Water activity at the anode of electrolyser
AW_ce	Water Activity at the cathode of the electrolyser
AW_af	Fuel cell water activity at the anode
AW_cf	Fuel cell water activity at the cathode
mu_fw1	Viscosity of freshwater as a function of Temperature (Pa.s)
mu_fw2	Viscosity of freshwater as a function of Temperature (MPa.s)
PBT	Profit before tax ($)
PAT	Profit after tax ($)
Tax	Tax paid ($)
PATPD	Profit after tax plus depreciation ($)
Cash	Cash flow ($)
PV	Present value ($)
NPV	Net present value ($)
Obj	Objective function;

APPENDIX D: List of Equations

D. Seawater Electrolyser Model Equation

e1 Current calculation

*Open circuit voltage

e2_1 Reversible voltage calculation

e2_2 Voltage as a function of temperature calculation

e2_3 Open circuit voltage calculation

*Activation Overpotential

e3_1 Anode current density ratio calculation

e3_2 Anode activation overpotential calculation

e3_3 Cathode current density ratio calculation

e3_4 Cathode activation overpotential calculation

e3_5 Total activation overpotential calculation

*Mass flows inside the cell

e4_1 Molar of water consumed calculation

e4_2 Mass of water consumed calculation

e5_1 Molar flowrate of hydrogen produced per second calculation

e5_2 Mass flowrate of hydrogen produced per hour calculation

e6_1 Molar flowrate of oxygen produced per second calculation

e6_2 Mass flowrate of oxygen produced per hour calculation

*Seawater density calculations

e7_1 Calculating A in density calculation

e7_2 Calculating B in density calculation

e7_3 Calculating A1 in density calculation

e7_4 Calculating A2 in density calculation

e7_5 Calculating A3 in density calculation

e7_6 Calculating A4 in density calculation

e7_8 Calculating F4 in density calculation

e7_9 Calculating overall seawater density

*Seawater viscosity calculations

e8_1 Seawater viscosity constant A calculation

e8_2 Seawater viscosity constant B calculation

e8_3 Relative viscosity calculation

e8_4 Viscosity of pure water at electrolyser temperature calculation

e8_5 Dynamic viscosity of seawater calculation

e8_6 Dynamic viscosity of seawater conversion calculation

*Molar flux calculations

e9_1 Electrolyser water molar flux at anode calculation

e9_2 Electrolyser water molar flux of water at cathode calculation

e10_1 Electrolyser hydrogen molar flux calculation

e10_2 Electrolyser oxygen molar flux calculation

*Concentration of anode and cathode calculation

e11_1 Mole fraction of water at the anode-membrane interface of electrolyser calculation

e11_2 Mole fraction of water at the cathode- membrane interface of electrolyser calculation

e11_3 Electrolyser saturated vapor pressure in pascals calculation

e11_4 Electrolyser saturated vapor pressure in megapascals calculation

e11_5 Electrolyser anode water activity calculation

e11_6 Electrolyser cathode water activity calculation

e11_7 Electrolyser anode-membrane humidity calculation

e11_8 Electrolyser cathode-membrane humidity calculation

e11_9 Concentration of water in anode -membrane interface of the electrode

e11_10 Concentration of water in cathode-membrane interface calculation

e11_11 Membrane water humidity calculation

*Mass flow in membrane

e12 Electrolyser molar flowrate due to concentration gradient calculation

e13_ 1 Electrolyser electro-osmotic drag coefficient as a function of membrane humidification calculation

e13_2 Electrolyser molar flowrate due to electro-osmotic drag calculation

e14_1 Electrolyser pressure difference between anode and cathode calculation

e14_2 Electrolyser molar flowrate due to pressure difference calculation

e15 Electrolyser net flowrate of water through the membrane calculation

*Water mass balance

e16_1(c_e) Total molar flowrate of water entering the first cell of the electrolyser calculation

e16_2(c_e) Molar flowrate of water leaving the anode of the first cell of the electrolyser

e16_3(c_e) Molar flowrate if the water leaving the cathode of the first cell of the electrolyser

e16_4(c_e) Molar flowrate of water leaving the first cell of the electrolyser calculation

e16_5(c_e) Total molar flowrate of water entering the anode of the electrolyser

e16_6(c_e) Molar flowrate of water leaving the anode of the electrolyser calculation

e16_7(c_e) Molar flowrate if the water leaving the cathode of the electrolyser calculation

e16_8(c_e) Molar flowrate of water leaving the electrolyser calculation

e16_9 Total water leaving the electrolyser stack calculation

e16_10 Total mass flowrate of water leaving the electrolyser stack calculation

e16_11 Total mass flowrate of seawater entering the electrolyser calculation

*Hydrogen mass balance

e17_1 Molar flowrate of hydrogen produced calculation

e17_2 Molar flowrate of hydrogen out the electrolyser calculation

e17_3 Total molar flowrate of hydrogen produced in the electrolyser system calculation

e17_4 Total mass flowrate of hydrogen produced in the electrolyser system calculation

*Oxygen Mass Balance

e18_1(c_e) Molar flowrate of oxygen produced in the electrolyser calculation

e18_2(c_e) Molar flowrate of oxygen out the electrolyser calculation

e18_3 Total molar flowrate of oxygen leaving the electrolyser calculation

e18_4 Total mass flowrate of oxygen leaving the electrolyser calculation

*Diffusion Overpotential

e19_1 Critical temperature for water and oxygen calculation

e19_2 Temperature ratio in Deff calculation for water and oxygen calculation

e19_3 Critical pressure for water and oxygen calculation

e19_4 Molar mass calculation for water and oxygen calculation

e19_5 Electrolyser diffusion coefficient for water and oxygen calculation

e20_1 Critical temperature for water and hydrogen calculation

e20_2 Temperature ratio in Deff calculation for water and hydrogen calculation

e20_3 Critical pressure for water and hydrogen calculation

e21_1 Molar mass calculation for water and hydrogen calculation

e21_2 Electrolyser diffusion coefficient for water and hydrogen calculation

e22 Electrolyser effective diffusion coefficient for water and oxygen calculation

e23 Electrolyser effective diffusion coefficient for water and hydrogen calculation

e24_1 Electrolyser molar fraction of hydrogen in channel calculation

e24_2 Electrolyser molar fraction of oxygen in channel calculation

e25_1 Electrolyser concentration of hydrogen in channel calculation

e25_2 Electrolyser concentration of oxygen in channel calculation

e26_1 Electrolyser concentration of hydrogen in membrane-electrode interface calculation

e26_2 Electrolyser concentration of oxygen in membrane-electrode interface calculation

e27_1 Electrolyser concentration of hydrogen at reference conditions in channel calculation

e27_2 Electrolyser concentration of oxygen at reference conditions in channel calculation

e28_1 Electrolyser concentration of H_2 at reference conditions in membrane-electrode interface

e28_2 Electrolyser concentration of O_2 at reference conditions in membrane-electrode interface

e29_1 Electrolyser anode diffusion overpotential calculation

e29_2 Electrolyser cathode diffusion overpotential calculation

e29_3 Electrolyser diffusion overpotential calculation

*Ohmic overpotential

e30 Electrolyser membrane conductivity calculation

e31 Electrolyser ohmic overpotential calculation

Total cell voltage

e32_1 Total voltage in a electrolyser cell calculation

e32_2 Total electrolyser system voltage calculation

*Power calculation

e33 Electrolyser power consumed calculation

D2. Fuel Cell Model Equations

FUEL CELL MODEL

e34 Fuel cell current calculation

Open circuit voltage

e35 Fuel cell open circuit calculation

*Activation Overpotential

e36_1 Fuel cell anode current density ratio calculation

e36_2 Fuel cell anode activation overpotential calculation

e36_3 Fuel cell cathode current density ratio calculation

e36_4 Fuel cell cathode activation overpotential calculation

e36_5 Fuel cell total activation overpotential calculation

*Mass flows inside the cell

e37_1 Molar of water consumed in the fuel cell calculation

e37_2 Mass of water consumed in the fuel cell calculation

e38_1 Molar flowrate of hydrogen produced in the fuel cell calculation

e38_2 Mass flowrate of hydrogen produced in the fuel cell calculation

e39_1 Molar flowrate of oxygen produced in the fuel cell calculation

e39_2 Mass flowrate of oxygen produced in the fuel cell calculation

*Temperature of water in degrees Celsius

e40 Converting temperature from kelvins to degrees Celsius calculation

*Water density calculation

e41 Density of freshwater as a function of temperature in the fuel cell calculation

*Water viscosity =

e42_1 Viscosity of freshwater as a function of temperature in Pa.s in the fuel cell calculation

e42_2 Viscosity of freshwater as a function of temperature in MPa.s in the fuel cell calculation

*Hydrogen mass balance

e43_1(c_f) Molar flowrate of hydrogen entering the first fuel cell calculation

e43_2(c_f) Fuel cell molar flowrate of hydrogen leaving first fuel cell calculation

e43_3(c_f) Fuel cell molar flowrate of hydrogen entering N+1 cell calculation

e43_4(c_f) Fuel cell molar flowrate of hydrogen leaving N+1 cell calculation

e43_5(c_f) Total molar flowrate of hydrogen leaving the fuel cell system calculation

e43_6 Total mass flowrate of hydrogen leaving the fuel cell system calculation

*Oxygen mass balance

e44_1(c_f) Molar flowrate of oxygen entering the first fuel cell calculation

e44_2(c_f) Fuel cell molar flowrate of oxygen leaving first fuel cell calculation

e44_3(c_f) Fuel cell molar flowrate of oxygen entering N+1 cell calculation

e44_4(c_f) Fuel cell molar flowrate of oxygen leaving N+1 cell calculation

e44_5(c_f) Total molar flowrate of oxygen leaving the fuel cell system calculation

e44_6 Total mass flowrate of oxygen leaving the fuel cell system calculation

*Molar flux in fuel cell

e45_1 Fuel cell Molar flux at anode calculation

e45_2 Fuel cell Molar flux of water at cathode calculation

e46_1 Fuel cell Hydrogen molar flux

e46_2 Fuel cell Oxygen molar flux

*Molar flux in fuel cell

e45_1 Fuel cell molar flux of water at the anode calculation

e45_2 Fuel cell molar flux of water at cathode calculation

e46_1 Fuel cell hydrogen molar flux calculation

e46_2 Fuel cell Oxygen molar flux calculation

e47_1 Mole fraction of water at the anode of fuel cell calculation

e47_2 Mole fraction of water at the cathode of fuel cell calculation

e47_3 Fuel cell saturated vapor pressure calculation in pascals calculation

e47_4 Fuel cell saturated vapor pressure calculation in megapascals calculation

e47_5 Activity of water in the fuel cell anode calculation

e47_6 Activity of the water in the fuel cell cathode calculation

e47_7 Water content in the anode of the fuel cell calculation

e47_8 Water content in the cathode of the fuel cell calculation

e47_9 Concentration of water in anode-membrane interface of the fuel cell calculation

e47_10 Concentration of water in cathode-membrane interface of the fuel cell calculation

e47_11 Water content in the membrane of the fuel cell calculation

e48 Concentration of water in anode-membrane interface of the electrode

e49 Fuel cell Molar flowrate due to electro-osmotic drag calculation

e50_1 Pressure difference between anode and cathode

e50_2 Fuel cell Molar flowrate due to pressure effect calculation

e51 Fuel cell Net flowrate of water through the membrane

*Water balance

e52_1(c_f) Fuel cell molar flowrate of water leaving the anode calculation

e52_2(c_f) Molar flowrate of water leaving the fuel cell cathode calculation

e52_3 Total molar flowrate of water leaving the fuel cell system

e52_4 Total mass flowrate of water leaving the fuel cell system

*Diffusion overpotential

e53 Fuel cell temperature ratio in D_{eff} calculation for water and oxygen calculation

e54 Fuel cell diffusion coefficient for water and oxygen calculation

e55 Fuel cell temperature ratio in D_{eff} calculation for water and hydrogen calculation

e56 Fuel cell diffusion coefficient for water and hydrogen calculation

e57_1 Fuel cell effective diffusion coefficient for water and oxygen calculation

e57_2 Fuel cell effective diffusion coefficient for water and oxygen calculation

e58_1 Fuel cell molar fraction of hydrogen in the channel calculation

e58_2 Fuel cell molar fraction of oxygen in the channel calculation

e59_1 Fuel cell concentration of hydrogen in the channel calculation

e59_2 Fuel cell concentration of oxygen in the channel calculation

e60_1 Fuel cell concentration of hydrogen in the membrane-electrode interface calculation

e60_2 Fuel cell concentration of oxygen in the membrane-electrode interface calculation

e61_1 Fuel cell concentration of hydrogen at reference conditions in the channel calculation

e61_2 Fuel cell concentration of oxygen at reference conditions in the channel calculation

e62_1 Fuel cell Concentration of H_2 at reference conditions in the membrane-electrode interface

e62_2 Fuel cell concentration of O_2 at reference conditions in the membrane -electrode interface

e63_1 Fuel cell Anode diffusion overpotential calculation

e63_2 Fuel cell cathode diffusion overpotential calculation

e63_3 Total fuel cell diffusion overpotential calculation

*Ohmic overpotential

e64 Membrane conductivity in the fuel cell calculation

e65 Ohmic overpotential in the fuel cell calculation

Total cell voltage

e66_1 Total voltage in a cell of the fuel cell calculation

e66_2 Total voltage in the fuel cell system calculation

*Power calculation

e67 Calculating power consumed in kW

*Efficiency calculation

e68 Power efficiency calculation

e69 Water recovery rate calculation

D3. Sizing Equations

*Sizing the electrolyse and the fuel cell

e70_1 Cathode electrode thickness of the electrolyser calculation

e70_2 Anode electrode thickness of the electrolyser calculation

e70_3 Catalyst layer length of the electrolyser calculation

e70_4 Catalyst layer height of the electrolyser calculation

e70_5 Gas diffusion layer length of the electrolyser calculation

e70_6 Gas diffusion layer height of the electrolyser calculation

e70_7 Channel length of the electrolyser calculation

e70_8 Channel height of the electrolyser calculation

e71_1	Cathode electrode thickness of the fuel cell calculation
e71_2	Anode electrode thickness of the fuel cell calculation
e71_3	Catalyst layer length of the fuel cell calculation
e71_4	Catalyst layer height of the fuel cell calculation
e71_5	Gas diffusion layer length of the fuel cell calculation
e71_6	Gas diffusion layer length height of the fuel cell calculation
e71_7	Channel length of the fuel cell calculation
e71_8	Channel height of the fuel cell calculation
e72_1	Total width of cathode in the electrolyser calculation
e72_2	Total width of anode in the electrolyser calculation
e72_3	Total width of the electrolyser calculation
e72_4	Total length of the electrolyser calculation
e72_5	Total height of the electrolyser calculation
e73_1	Total width of cathode in the fuel cell calculation
e73_2	Total width of anode in the fuel cell calculation
e73_3	Total width of the fuel cell calculation
e73_4	Total length of the fuel cell calculation
e73_5	Total height of the fuel cell calculation

D4. Economic Evaluation Equations

Capital cost

e74_1	Direct capital cost for PEM electrolyser calculation
e74_2	Direct capital cost for PEM fuel cell calculation
e74_3	Total direct capital cost calculation
e74_4	Stack capital cost for the electrolyser calculation
e74_5	Stack capital cost for the fuel cell calculation
e74_6	BOP capital cost for the electrolyser calculation
e74_7	BOP capital cost for the fuel cell calculation
e74_8	Cathode gas management for the electrolyser calculation
e74_9	Cathode gas management for the fuel cell calculation
e74_10	Anode gas management for the electrolyser calculation
e74_11	Anode gas management for the fuel cell calculation
e74_12	Water delivery management system capital cost for the electrolyser calculation
e74_13	Water delivery management system capital cost for the fuel cell calculation
e74_14	Thermal management system capital cost for the electrolyser calculation
e74_15	Thermal management system capital cost for the fuel cell calculation
e74_16	Power electronics management system capital cost for the electrolyser calculation
e74_17	Power electronics management system capital cost for the fuel cell calculation
e74_18	Control and sensors management system capital cost for the electrolyser calculation
e74_19	Control and sensors management system capital cost for the fuel cell calculation
e74_20	Mechanical BOP capital cost for electrolyser calculation
e74_21	Mechanical BOP capital cost for fuel cell calculation
e74_22	Other direct capital cost for electrolyser calculation
e74_23	Other direct capital cost for fuel cell calculation
e74_24	Assembly labour capital cost for electrolyser calculation
e74_25	Assembly labour capital cost for fuel cell calculation
e74_26	Capital cost of land calculation

Installation costs

e75_1	Installed direct capital cost for PEM electrolyser calculation
e75_2	Installed direct capital cost for PEM fuel cell calculation
e75_3	Installed direct capital cost calculation
e75_4	Installed stack capital cost for the electrolyser calculation
e75_5	Installed stack capital cost for the fuel cell calculation
e75_6	Installed BOP capital cost for the electrolyser calculation
e75_7	Installed BOP capital cost for the fuel cell calculation
e75_8	Installed cathode gas management cost for the electrolyser calculation
e75_9	Installed cathode gas management cost for the fuel cell calculation
e75_10	Installed anode gas management cost for the electrolyser calculation
e75_11	Installed anode gas management cost for the fuel cell calculation
e75_12	Installed water delivery management system cost for the electrolyser calculation
e75_13	Installed water delivery management system cost for the fuel cell calculation
e75_14	Installed thermal management system cost for the electrolyser calculation
e75_15	Installed thermal management system cost for the fuel cell calculation
e75_16	Installed power electronics management system cost for the electrolyser calculation
e75_17	Installed power electronics management system cost for the fuel cell calculation
e75_18	Installed control and sensors management system cost for the electrolyser calculation
e75_19	Installed control and sensors management system cost for the fuel cell calculation
e75_20	Installed mechanical BOP capital cost for electrolyser calculation
e75_21	Installed mechanical BOP capital cost for fuel cell calculation
e75_22	Installed other direct capital cost for the electrolyser calculation
e75_23	Installed other direct capital cost for the fuel cell calculation
e75_24	Installed assembly labour capital cost for the electrolyser calculation
e75_25	Installed assembly labour capital cost for the fuel cell calculation

Total equipment cost including installation

e76_1 Total direct capital cost for PEM electrolyser calculation

e76_2 Total direct capital cost for PEM fuel cell calculation

e76_3 Total direct capital cost calculation

e76_4 Total stack capital cost for the electrolyser calculation

e76_5 Total stack capital cost for the fuel cell calculation

e76_6 Total BOP capital cost for the electrolyser calculation

e76_7 Total BOP capital cost for the fuel cell calculation

e76_8 Total cathode gas management cost for the electrolyser calculation

e76_9 Total cathode gas management cost for the fuel cell calculation

e76_10 Total anode gas management cost for the electrolyser calculation

e76_11 Total anode gas management cost for the fuel cell calculation

e76_12 Total water delivery management system cost for the electrolyser calculation

e76_13 Total water delivery management system cost for the fuel cell calculation

e76_14 Total thermal management system cost for the electrolyser calculation

e76_15 Total thermal management system cost for the fuel cell calculation

e76_16 Total power electronics management system cost for the electrolyser calculation

e76_17 Total power electronics management system cost for the fuel cell calculation

e76_18 Total control and sensors management system cost for the electrolyser calculation

e76_19 Total control and sensors management system cost for the fuel cell calculation

e76_20 Total mechanical BOP capital cost for electrolyser calculation

e76_21 Total mechanical BOP capital cost for fuel cell calculation

e76_22 Total other direct capital cost for the electrolyser calculation

e76_23 Total other direct capital cost for the fuel cell calculation

e76_24 Total assembly labour capital cost for the electrolyser calculation

e76_25 Total assembly labour capital cost for the fuel cell calculation

e76_26 Total direct capital cost calculation

*Indirect Capital cost

e77_1	Construction site costs
e77_2	Engineering and design cost calculation
e77_3	Project contingency cost calculation
e77_4	Legal and contractor fee calculation
e77_5	Total indirect capital costs calculation

*Total Fixed Investment cost

e78	Fixed investment capital calculation

*Working Capital

e79	Working capital required calculation

*Replacement cost

e80_1	Replacement cost for the electrolyser calculation
e80_2	Replacement cost for the fuel cell calculation
e80_3	Total replacement cost calculation
e80_4	Total replacement installation cost calculation
e80_5	Total installed replacement cost calculation

*Maintenance cost

e81_1	Maintenance cost for the electrolyser calculation
e81_2	Maintenance cost for the fuel cell calculation
e81_3	Total Maintenance cost calculation

*Discount factor

e82(N) Discount factor for each year calculation

*Revenue

e83_1 Revenue generated from sale of freshwater calculation

e83_2 Revenue generated from sale of electricity calculation

e83_3(N) Total revenue generated from sale of products in the first-year calculation

e83_4(N) Revenue generated after the first-year calculation

e83_5 Total revenue generated from the plant calculation

*Other production cost

e84_1(N) Patents and royalties cost calculation

e84_2 Insurance costs calculation

e84_3(N) Distribution and selling costs calculation

e84_4(N) Research and development costs for the first-year calculation

e84_5(N) Total production costs for each year calculation

*Annualised costs

e85_1 Annualised capital cost calculation

e85_2 Annualised replacement cost calculation

e85_3 Annualised maintenance cost calculation

e85_4(N) Total annualised cost for each year calculation

*Cash flow calculations

e86(N) Depreciation for each year calculation

e87(N) Profit before tax for each year calculation

e88(N) Tax payable for each year calculation

e89(N) Profit after tax for each year calculation

e90(N) Profit after tax plus depreciation for each year calculation

e91(N) Cash flow for each year calculation

Net present value

e92 Present value for each year calculation

e93 Net present value calculation

*Payback period

e94 Payback period calculation

*Objective function

e95 Objective function to minimise power consumed and maximise power produced

APPENDIX E: Model

E1. Seawater Electrolyser Model

Current

e1 CU_e=e=i_e*RA_e;

Open circuit voltage

e2_1 V_oe=e=1.229-0.0009*(T_e-T_ref);

e2_2 V_oce=e=((R*T_e)/(z*F))*(log(p_he+deltaa)+0.5*log(p_oe+deltaa)- log(p_we+deltaa));

e2_3.. V_ocve=e=V_oe+V_oce;

*Activation Overpotential

e3_1 xa_e*2*io_ae=e=i_e;

e3_2 V_actae*(alpha_ae*F)=e=(R*T_e)*log(xa_e+((xa_e**2)+1)**(0.5));

e3_3 xc_e*2*io_ce=e=i_e;

e3_4 V_actce*(alpha_ce*F)=e=(R*T_e)*log(xc_e+((xc_e**2)+1)**(0.5));

e3_5 V_acte=e=V_actae+V_actce;

*Mass flows inside the cell

e4_1 N_Wcons=e=(CU_e)/(2*F);

e4_2 M_Wcons=e=N_Wcons*T2('W','Mm')*3600;

e5_1 N_Hprod=e=(CU_e)/(2*F);

e5_2 M_Hprod=e=N_Hprod*T2('H','Mm')*3600;

e6_1 N_Oprod=e=(CU_e)/(4*F);

e6_2 M_Oprod=e=N_Oprod*T2('O','Mm')*3600;

Seawater density calculations

e7_1 DA=e=(2*(T_e-273.15)-200)/160;

e7_2 2*sal-150)/150=e=DB;

e7_3 (0.5*T1('a1','g1'))+(DB*T1('a1','g2'))+(T1('a1','g3')* (2*power(DB,2)-1))=e=DA1;

e7_4 (0.5*T1('a2','g1'))+(DB*T1('a2','g2'))-(T1('a2','g3')* (2*power(DB,2)-1))=e=DA2;

e7_5 (0.5*T1('a3','g1'))+(DB*T1('a3','g2'))-(T1('a3','g3')* (2*power(DB,2)-1))=e=DA3;

e7_6 (0.5*T1('a4','g1'))-(DB*T1('a4','g2'))-(T1('a4','g3')* (2*Power(DB,2)-1))=e=DA4;

e7_7 (2*power(DA,2)-1)=e=F3;

e7_8 4*power(DA,3)-(3*DA))=e=F4;

e7_9 ((DA1*0.5)+(DA2*DA)+(DA3*F3)+(DA4*F4))*1000=e=rho_sw;

Seawater Viscosity calculation

e8_1 0.001474+(0.000015*(T_e-273.15))-0.00000003927*power ((T_e-273.15),2)=e=mu_A;

e8_2 0.000010734-(0.000000085*(T_e-273.15))+0.000000000223*power ((T_e-272.15),2)=e=mu_B;

e8_3 1+mu_A*sal+mu_B*(sal**2)=e=mu_r;

e8_4 (139.18+(T_e-273.15))*log(mu_wr+deltaa)=e=-3.79418*(139.18+ (T_e-273.15))+604.129;

e8_5 mu_wr*mu_r=e=mu_sw1*1000;

e8_6 mu_sw=e=mu_sw1*0.000001;

*Molar flux calculations

e9_1 n_Wane*RA_e=e=N_Wcons+N_Wme;

e9_2 n_Wcate*RA_e=e=N_Wme;

e10_1 n_He*RA_e=e=N_Hprod;

e10_2 n_Oe*RA_e=e=N_Oprod;

*Concentration of water in the anode-membrane and cathode-membrane interface

e11_1 yW_meane*(n_Wane+n_Oe)=e=n_Wane;

e11_2 yW_mecate*(n_Wcate+n_He)=e=n_Wcate;

e11_3 T_e*(log(PsatV1e+deltaa)-log(611+deltaa))=e=19.65*(T_e-273.15);

e11_4 PsatVe=e=PsatV1e/(1000000);

e11_5 AW_ae*PsatVe=e=yW_meane*P_e;

e11_6. AW_ce*PsatVe=e=yW_mecate*P_e;

e11_7 lamda_ae=e=14+1.4*(AW_ae-1);

e11_8 lamda_ce=e=0.043+(17.81*AW_ce)-(39.85*((AW_ce)**2))+(36*((AW_ce)**3));

e11_9 CW_meane=e=(rho_m/wt_m)*lamda_ae;

e11_10 CW_mecate=e=(rho_m/wt_m)*lamda_ce;

e11_11 lamda_e*2=e=lamda_ae+lamda_ce;

*Mass flow in membrane

e12 N_Wdde=e=(RA_e*D_we*(CW_mecate-CW_meane))/delta_me;

e13_1 n_de=e=(2.5/22)*lamda_e;

e13_2 N_Weoe=e=(n_de*Cu_e)/F;

e14_1 P_de=e=P_ae-P_ce;

e14_2 N_Wpee*mu_sw=e=(RA_e*rho_SW*K_darcy*P_de)/(wt_W*delta_me);

e15 N_Wme=e=N_Wdde+N_Weoe-N_Wpee;

*Water mass balance

e16_1(c_e)$(ord(c_e)=1) N_SWin=e=N_Winae(c_e);

e16_2(c_e)$(ord(c_e)=1) N_Woutae(c_e)=e= N_Winae(c_e)-N_Wcons-N_Wme;

e16_3(c_e)$(ord(c_e)=1) N_WOutce(c_e)=e=N_Wme;

e16_4(c_e)$(ord(c_e)=1) N_Woute(c_e)=e=N_Woutae(c_e)+N_Woutce(c_e);

e16_5(c_e)$(ord(c_e)>1) N_Winae(c_e) =e=N_Woute(c_e-1);

e16_6(c_e)$(ord(c_e)>1) N_Woutae(c_e)=e= N_Winae(c_e)-N_Wcons-N_Wme;

e16_7(c_e)$(ord(c_e)>1) N_WOutce(c_e)=e=N_Wme;

e16_8(c_e)$(ord(c_e)>1) N_Woute(c_e)=e=N_Woutae(c_e)+N_Woutce(c_e);

e16_9(c_e)$(ord(c_e)=card(c_e)) N_Woute(c_e)=e=N_Woutsyse;

e16_10 M_Woutsyse=e=N_Woutsyse*T2('W','Mm');

e16_11 M_SWin=e=N_SWin*T2('W','Mm');

*Hydrogen mass balance

e17_1(c_e) N_Houtce(c_e)=e=N_Hprod;

e17_2(c_e) N_Houte(c_e)=e=N_Houtce(c_e);

e17_3 N_Houtsyse=e=sum(c_e,N_Houte(c_e));

e17_4 M_Houtsyse=e=N_Houtsyse*T2('H','Mm');

*Oxygen mass balance

e18_1(c_e) N_Ooutae(c_e)=e=N_Oprod;

e18_2(c_e) N_Ooute(c_e)=e=N_Ooutae(c_e);

e18_3 N_Ooutsyse=e=sum(c_e,N_Ooute(c_e));

e18_4 M_Ooutsyse=e=N_Ooutsyse*T2('O','Mm');

*Diffusion overpotential

e19_1 Tc_OW=e= T2('W','Tc')*T2('O','Tc');

e19_2 Tr_OWe*(Tc_OW**0.5)=e=T_e;

e19_3 Pc_OW=e=T2('W','Pc')*T2('O','Pc');

e19_4 Mm_OW=e=(1/T2('W','Mm'))+(1/T2('O','Mm'));

e19_5
D_OWe*P_e=e=(a_e*(Tr_OWe**b_e)*(Pc_OW**(1/3))*(Tc_OW**(5/12))*(Mm_OW**(0.5)));

e20_1 Tc_HW=e= T2('W','Tc')*T2('H','Tc');

e20_2 Tr_HWe*(Tc_HW**0.5)=e=T_e;

e20_3 Pc_HW=e=T2('W','Pc')*T2('H','Pc');

e21_1 Mm_HW=e=(1/T2('W','Mm'))+(1/T2('H','Mm'));

e21_2 D_HWe*P_e=e=(a_e*(Tr_HWe**b_e)*(Pc_HW**(1/3))*(Tc_HW**(5/12))*
(Mm_HW**(0.5)));

e22 D_effOWe=e=D_OWe*E*((E-E_p)/(1-E_p))**alpha;

e23 D_effHWe=e=D_HWe*E*((E-E_p)/(1-E_p))**alpha;

e24_1 yH_che*(n_He+n_Wcate)=e=n_He;

e24_2 yO_che*(n_Oe+n_Wane)=e=n_Oe;

e25_1 CH_che*T_ce=e=P_ce*yH_che/(R);

e25_2 CO_che*T_ae=e=P_ae*yO_che/(R);

e26_1 CH_me*D_effHWe=e=CH_che*D_effHWe+delta_ece*n_He;

e26_2 CO_me*D_effOWe=e=CO_che*D_effOWe+delta_eae*n_Oe;

e27_1 CH_choe=e=P_ref*yH_che/(R*T_ref);

e27_2 CO_choe=e=P_ref*yO_che/(R*T_ref);

e28_1 CH_moe*D_effHWe=e=CH_choe*D_effHWe+delta_ece*n_He;

e28_2 CO_moe*D_effOWe=e=CO_choe*D_effOWe+delta_eae*n_Oe;

e29_1 V_diffae=e=((R*T_ae)/(4*F))*(log(CO_me+deltaa)-log(CO_moe+deltaa));

e29_2 V_diffce=e=((R*T_ce)/(2*F))*(log(CH_me+deltaa)-log(CH_moe+deltaa));

e29_3 V_diffe=e=V_diffae+ V_diffce;

*Ohmic overpotential

e30 T_e*log(theta_me+deltaa)-T_e*log(0.5139*lamda_e-0.326)=e=1268* ((T_e/303)-1);

e31 V_ohme*theta_me=e=(delta_me*i_e);

Total cell voltage

e32_1 V_e=e= V_ocve+V_acte+V_diffe+V_ohme;

e32_2 V_esys=e=V_e*n_e;

*Power consumed in electrolyser

e33 Power_cons=e=(V_esys*Cu_e)/(1000);

E2. Fuel Cell Model

```
*FUEL CELL MODEL*

    *Current*
        e34     CU_f=e=i_f*RA_f;

    *Open circuit voltage*

        e35     V_ocvf*P_f=e=1.229*P_f-
                0.0009*P_f*(T_f-298)+(R*T_f/(z*F))*P_f*(log(p_hf+deltaa)+
                0.5*log(p_of+deltaa)-log(p_wf+deltaa));

    *Activation Overpotential

        e36_1   xa_f*2*io_af=e=i_f;

        e36_2   V_actaf=e=((R*T_f)/(alpha_af*F))*(log(i_f+deltaa)-log(io_af+deltaa));

        e36_3   xc_f*2*io_cf=e=i_f;

        e36_4   V_actcf=e=((R*T_f)/(alpha_cf*F))*(log(i_f+deltaa)-log(io_cf+deltaa));

        e36_5   V_actf=e=V_actaf+V_actcf;

    *Mass flows inside the cell

        e37_1   N_Wprod=e=(CU_f)/(2*F);

        e37_2    M_Wprod=e=N_Wprod*T2('W','Mm')*3600;

        e38_1   N_Hcons=e=(CU_f)/(2*F);

        e38_2   M_Hcons=e=N_Hcons*T2('H','Mm')*3600;

        e39_1   N_Ocons=e=(CU_f)/(4*F);

        e39_2   M_Ocons=e=N_Ocons*T2('O','Mm')*3600;


*Temperature of the fuel cell in degree celcius

        e40     T_fc=e=T_f-273.15;
```

*Water density calculation

e41 Rho_FW*(1+0.016897850*T_fc)=e=999.83952+16.945176*T_fc-
0.0079870401*Power(T_fc,2)-0.000046170461*Power(T_fc,3)+
0.00000010556302*Power(T_fc,4)-0.00000000028054253*power(T_fc,5);

*Water viscosity calculation

e42_1 mu_fw1=e=system.exp(log(0.00002414)+(247.8/(T_f-140))*log(10));

e42_2 mu_fw2=e=mu_fw1*0.000001;

*Hydrogen mass balance

e43_1(c_f)$(ord(c_f)=1 N_Houtsyse=e=N_Hinf(c_f);

e43_2(c_f)$(ord(c_f)=1) N_Houtf(c_f)=e=N_Hinf(c_f)-N_Hcons;

e43_3(c_f)$(ord(c_f)>1) N_Hinf(c_f)=e=N_Houtf(c_f-1);

e43_4(c_f)$(ord(c_f)>1) N_Houtf(c_f)=e=N_Hinf(c_f)-N_Hcons;

e43_5(c_f)$(ord(c_f)=card(c_f)) N_Houtf(c_f)=e=N_Houtsysf;

e43_6 .. M_Houtsysf=e=N_Houtsysf*T2('H','Mm');

*Oxygen mass balance

e44_1(c_f)$(ord(c_f)=1) N_Ooutsyse=e=N_Oinf(c_f);

e44_2(c_f)$(ord(c_f)=1) N_Ooutf(c_f)=e=N_Oinf(c_f)-N_Ocons;

e44_3(c_f)$(ord(c_f)>1) N_Oinf(c_f)=e=N_Ooutf(c_f-1);

e44_4(c_f)$(ord(c_f)>1) N_Ooutf(c_f)=e=N_Oinf(c_f)-N_Ocons;

e44_5(c_f)$(ord(c_f)=card(c_f) N_Ooutf(c_f)=e=N_Ooutsysf;

e44_6 M_Ooutsysf=e=N_Ooutsysf*T2('O','Mm');

*Molar flux in fuel cell

e45_1 n_Wanf*RA_f=e=N_Wmf;

e45_2 n_Wcatf*RA_f=e=N_Wprod-N_wmf;

e46_1 n_Hf*RA_f=e=N_Hcons;

e46_2 n_Of*RA_f=e=N_Ocons;

e47_1 yW_meanf*(n_Wanf+n_hf)=e=n_Wanf;

e47_2 yW_mecatf*(n_Wcatf+n_of)=e=n_Wcatf;

e47_3 T_f*(log(PsatV1f+deltaa)-log(611+deltaa))=e=19.65*(T_f-273.15);

e47_4 PsatVf=e=PsatV1f/(1000000);

e47_5 AW_af*PsatVf=e=yW_meanf*P_f;

e47_6 AW_cf*PsatVf=e=yW_mecatf*P_f;

e47_7 lamda_af=e=0.043+(17.81*AW_af)-(39.85*((AW_af)**2))+(36*((AW_af)**3));

e47_8 lamda_cf=e=14+1.4*(AW_cf-1);

e47_9 CW_meanf*D_effHWf=e=(((rho_fw*T_af)/T2('W','Mm'))*D_effHWf)-(delta_eaf*n_Wanf);

e47_10 CW_mecatf*D_effOWf=e=(((rho_fw*T_cf)/T2('W','Mm'))*D_effOWf)+(delta_ecf*n_Wcatf);

e47_11 lamda_f*2=e=lamda_af+lamda_cf;

*Mass flow in the membrane

e48 N_Wddf=e=(RA_f*D_wf*(CW_mecatf-CW_meanf))/delta_mf;

e49 N_Weof=e=(n_d*Cu_f)/F;

e50_1 P_df=e=P_cf-P_af;

e50_2 N_Wpef*mu_fw2=e=(RA_f*rho_FW*K_darcy*P_df)/(wt_W*delta_mf);

e51 N_Wmf=e=N_Weof-N_Wddf-N_Wpef;

*Water mass balance

e52_1(c_f)N_Woutaf(c_f)=e=N_wmf;

e52_2(c_f) N_Woutcf(c_f)=e=N_Wprod-N_Wmf;

e52_3 N_Woutsysf=e=(N_Wprod*n_f);

e52_4 M_Woutsysf=e=N_Woutsysf*T2('W','Mm');

*Diffusion Overpotential

e53 Tr_OWf*(Tc_OW**0.5)=e=T_f;

e54 D_OWf*P_f=e=(a_e*(Tr_OWf**b_e)*(Pc_OW**(1/3))*(Tc_OW**(5/12))*(Mm_OW**(0.5)));

e55 Tr_HWf*(Tc_HW**0.5)=e=T_f;

e56 D_HWf*P_f=e=(a_e*(Tr_HWf**b_e)*(Pc_HW**(1/3))*(Tc_HW**(5/12))*(Mm_HW**(0.5)));

e57_1 D_effOWf=e=D_OWf*E*((E-E_p)/(1-E_p))**alpha;

e57_2 D_effHWf=e=D_HWf*E*((E-E_p)/(1-E_p))**alpha;

e58_1 yH_chf*(n_Hf+n_Wanf)=e=n_Hf;

e58_2 yO_chf*(n_Of+n_Wcatf)=e=n_Of;

e59_1 CH_chf*T_af=e=P_af*yH_chf/(R);

e59_2 CO_chf*T_cf=e=P_cf*yO_chf/(R);

e60_1 CH_mf*D_effHWf=e=CH_chf*D_effHWf+delta_eaf*n_Hf;

e60_2 CO_mf*D_effOWf=e=CO_chf*D_effOWf+delta_ecf*n_Of;

e61_1 CH_chof=e=P_ref*yH_chf/(R*T_ref);

e61_2 CO_chof=e=P_ref*yO_chf/(R*T_ref);

e62_1 CH_mof*D_effHWf=e=CH_chof*D_effHWf+delta_eaf*n_Hf;

e62_2 CO_mof*D_effOWf=e=CO_chof*D_effOWf+delta_ecf*n_Of;

e63_1 V_diffcf=e=((R*T_cf)/(4*F))*(log(CO_mf+deltaa)-log(CO_mof+deltaa));

e63_2. V_diffaf=e=((R*T_af)/(2*F))*(log(CH_mf+deltaa)-log(CH_mof+deltaa));

e63_3 V_difff=e=V_diffaf+ V_diffcf;

*Ohmic overpotential

e64 T_f*log(theta_mf+deltaa)-T_f*log(0.5139*lamda_f-0.326+deltaa)=e=1268*((T_f/303)-1);

e65 V_ohmf*(theta_mf)=e=(delta_mf*i_f);

Total cell voltage

e66_1 V_f=e= V_ocvf-V_actf-V_difff-V_ohmf;

e66_2 V_fsys=e=V_f*n_f;

*Power

e67 Power_prod=e=(V_fsys*Cu_f)/(1000);

*Efficiency Calculations

e68 Power_Eff*Power_cons=e=Power_prod*100*system_eff;

e69 Water_eff*N_SWin=e=(N_Wprod*n_f)*100;

Geometric sizing of the electrolyser and the fuel cell

e70_1 delta_ece=e=w_GDL_ec+w_CL_ec;

e70_2 delta_eae=e=w_GDL_ea+w_CL_ea;

e70_3 l_CL_e=e=sqrt(RA_e);

e70_4 h_CL_e=e=sqrt(RA_e);

e70_5 l_GDL_e=e=l_CL_e;

e70_6 h_GDL_e=e=h_CL_e;

e70_7 l_channel_e=e=1.2*l_GDL_e;

e70_8 h_channel_e=e=1.2*h_GDL_e;

e71_1 delta_ecf=e=w_GDL_fc+w_CL_fc;

e71_2 delta_eaf=e=w_GDL_fa+w_CL_fa;

e71_3 l_CL_f=e=sqrt(RA_f);

e71_4 h_CL_f=e=sqrt(RA_f);

e71_5 l_GDL_f=e=l_CL_f;

e71_6 h_GDL_f=e=h_CL_f;

e71_7 l_channel_f=e=1.2*l_GDL_f;

e71_8 h_channel_f=e=1.2*h_GDL_f;

e72_1 T_w_ce=e=delta_ece+w_CC_ec+w_channel_ec;

e72_2 T_w_ae=e=delta_eae+w_CC_ea+w_channel_ea;

e72_3 T_w_e=e=T_w_ce+T_w_ae;

e72_4 T_l_e=e=l_channel_e;

e72_5 T_h_e=e=h_channel_e;

e72_1 T_w_ce=e=delta_ece+w_CC_ec+w_channel_ec;

e72_2 T_w_ae=e=delta_eae+w_CC_ea+w_channel_ea;

e73_3 T_w_f=e=T_w_cf+T_w_af;

e73_4 T_l_f=e=l_channel_f;

e73_5 T_h_f=e=h_channel_f;

E3. Economic Evaluation

*Direct capital cost

e74_1 Cap_DC_e=e=(4.6*power(year,2)-18658.2*year+18920787)*power_cons*Eur_doll;

e74_2 Cap_DC_f=e=(4.6*power(year,2)-18658.2*year+18920787)*power_prod*Eur_doll;

e74_3 Cap_DC=e=Cap_DC_e+Cap_DC_f;

e74_4 SCap_DC_e=e=Cap_DC_e*SCF_e;

e74_5. SCap_DC_f=e=Cap_DC_f*SCF_f;

e74_6 BOPCap_DC_e=e=Cap_DC_e*BOPCF_e;

e74_7 BOPCap_DC_f=e=Cap_DC_f*BOPCF_f;

e74_8 CM_DC_e=e=Cap_DC_e*GMCF_ce;

e74_9 CM_DC_f=e=Cap_DC_f*GMCF_cf;

e74_10 AM_DC_e=e=Cap_DC_e*GMCF_ae;

e74_11 AM_DC_f=e=Cap_DC_f*GMCF_af;

e74_12 WD_DC_e=e=Cap_DC_e*WDCF_e;

e74_13 WD_DC_f=e=Cap_DC_f*WDCF_f;

e74_14 TM_DC_e=e=Cap_DC_e*TMCF_e;

e74_15 TM_DC_f=e=Cap_DC_f*TMCF_f;

e74_16 PE_DC_e=e=Cap_DC_e* PECF_e;

e74_17 PE_DC_f=e=Cap_DC_f* PECF_f;

e74_18 CS_DC_e=e=Cap_DC_e* CSCF_e;

e74_19 CS_DC_f=e=Cap_DC_f* CSCF_f;

e74_20 MBOP_DC_e=e=Cap_DC_e*MBOPCF_e;

e74_21 MBOP_DC_f=e=Cap_DC_f*MBOPCF_f;

e74_22 OD_DC_e=e=Cap_DC_e*ODCF_e;

e74_23 OD_DC_f=e=Cap_DC_f*ODCF_f;

e74_24 AL_DC_e=e=Cap_DC_e*ALCF_e;

e74_25 AL_DC_f=e=Cap_DC_f*ALCF_f;

e74_26 Land=e=LCF*Cap_DC;

Direct Installation Cost

e75_1 Cap_IC_e=e=Cap_DC_e*Inst_F;

e75_2 Cap_IC_f=e=Cap_DC_f*Inst_F;

e75_3 Cap_IC=e=Cap_DC*Inst_F;

e75_4 SCap_IC_e=e= SCap_DC_e*Inst_F;

e75_5 SCap_IC_f=e= SCap_DC_f*Inst_F;

e75_6 BOPCap_IC_e=e=BOPCap_DC_e*Inst_F;

e75_7 BOPCap_IC_f=e=BOPCap_DC_f*Inst_F;

e75_8 CM_IC_e=e=CM_DC_e*Inst_F;

e75_9 CM_IC_f=e=CM_DC_f*Inst_F;

e75_10 AM_IC_e=e=AM_DC_e*Inst_F;

e75_11 AM_IC_f=e=AM_DC_f*Inst_F;

e75_12 WD_IC_e=e=WD_DC_e*Inst_F;

e75_13 WD_IC_f=e=WD_DC_f*Inst_F;

e75_14 TM_IC_e=e=TM_DC_e*Inst_F;

e75_15 TM_IC_f=e=TM_DC_f*Inst_F;

e75_16 PE_IC_e=e=PE_DC_e*Inst_F;

e75_17 PE_IC_f=e=PE_DC_f*Inst_F;

e75_18 CS_IC_e=e=CS_DC_e*Inst_F;

e75_19 CS_IC_f=e=CS_DC_f*Inst_F;

e75_20 MBOP_IC_e=e=MBOP_DC_e*Inst_F;

e75_21 MBOP_IC_f=e=MBOP_DC_f*Inst_F;

e75_22 OD_IC_e=e=OD_DC_e*Inst_F;

e75_23 OD_IC_f=e=OD_DC_f*Inst_F;

e75_24 AL_IC_e=e=AL_DC_e*Inst_F;

e75_25 AL_IC_f=e=AL_DC_f*Inst_F;

*Total installed cost of equipment

e76_1 DCap_Tcost_e=e=Cap_DC_e+Cap_IC_e;

e76_2 DCap_Tcost_f=e=Cap_DC_f+Cap_IC_f;

e76_3 DCap_Tcost=e=Cap_DC+Cap_IC;

e76_4 SCap_Tcost_e=e= SCap_DC_e+SCap_IC_e;

e76_5 SCap_Tcost_f=e= SCap_DC_f+SCap_IC_f;

e76_6 BOPCap_Tcost_e=e=BOPCap_DC_e+BOPCap_IC_e;

e76_7 BOPCap_Tcost_f=e=BOPCap_DC_f+BOPCap_IC_f;

e76_8 CM_Tcost_e=e=CM_DC_e+CM_IC_e;

e76_9 CM_Tcost_f=e=CM_DC_f+CM_IC_f;

e76_10 AM_Tcost_e=e=AM_DC_e+AM_IC_e;

e76_11 AM_Tcost_f=e=AM_DC_f+AM_IC_f;

e76_12 WD_Tcost_e=e=WD_DC_e+WD_IC_e;

e76_13 WD_Tcost_f=e=WD_DC_f+WD_IC_f;

e76_14 TM_Tcost_e=e=TM_DC_e+TM_IC_e;

e76_15 TM_Tcost_f=e=TM_DC_f+TM_IC_f;

e76_16 PE_Tcost_e=e=PE_DC_e+PE_IC_e;

e76_17 PE_Tcost_f=e=PE_DC_f+PE_IC_f;

e76_18 CS_Tcost_e=e=CS_DC_e+CS_IC_e;

e76_19 CS_Tcost_f=e=CS_DC_f+CS_IC_f;

e76_20 MBOP_Tcost_e=e=MBOP_DC_e+MBOP_IC_e;

e76_21 MBOP_Tcost_f=e=MBOP_DC_f+MBOP_IC_f;

e76_22 OD_Tcost_e=e=OD_DC_e+OD_IC_e;

e76_23 OD_Tcost_f=e=OD_DC_f+OD_IC_f;

e76_24 AL_Tcost_e=e=AL_DC_e+AL_IC_e;

e76_25 AL_Tcost_f=e=AL_DC_f+AL_IC_f;

e76_26 TD_cost=e=DCap_Tcost+Land;

Indirect Cost

e77_1 C_cost=e=CCF*TD_cost;

e77_2 ED_cost=e=EDCF*DCap_Tcost;

e77_3 PC_cost=e=PCCF*TD_cost;

e77_4 LC_fees=e=LCCF*TD_cost;

e77_5 TI_cost=e=C_cost+ED_cost+PC_cost+LC_fees;

Fixed investment capital

e78 FCI=e=TD_cost+TI_cost;

Working Capital

e79 Work_cap=e=FCI*WCI;

Replacement cost

e80_1 Rep_cost_e=e=(4.6*power((year+10),2)-18658.2*(year+10)+18920787)*power_cons*Eur_doll;

e80_2 Rep_cost_f=e=(4.6*power((year+10),2)-18658.2*(year+10)+18920787)*power_prod*Eur_doll;

e80_3 Rep_cost=e=Rep_cost_e+Rep_cost_f;

e80_4 Rep_Icost=e=(Rep_cost_e*Inst_F)+(Rep_cost_f*Inst_F);

e80_5 Rep_Tcost=e=Rep_cost+Rep_Icost;

*Maintenance cost

e81_1 Main_cost_e=e=Cap_DC_e*MCF_e;

e81_2 Main_cost_f=e=Cap_DC_f*MCF_f;

e81_3 Main_cost=e=main_cost_e+main_cost_f;

```
*Discount Factor*

        e82(N)    DF(N)*((1+AI)**(ord(N)-1))=e=1;

*Revenue

        e83_1     Water_sale*1000*Zar_doll=e=M_Woutsysf*water_cost*Op_hours;

        e83_2     elec_sale=e=elec_cost*power_prod*Op_hours;

        e83_3(N) $(ord(N)=1)Rev(N)=e=Water_sale+Elec_sale;

        e83_4(N)$(ord(N)>1)..Rev(N)=e=(Water_sale+Elec_sale)*((1+AI)**ord(N));

        e83_5     Tot_Rev=e=Sum(N,Rev(N));

*Production costs

        e84_1(N) PR_cost(N)=e=PR_factor*Rev(N);

        e84_2     I_cost=e=I_factor*FCI;

        e84_3(N) DS_cost(N)=e=DS_factor*Rev(N);

        e84_4(N) RD_cost(N)=e=RD_factor*Rev(N);

        e84_5(N) TP_cost(N)=e=(PR_cost(N)+I_cost+DS_cost(N)+RD_cost(N));


*Annualized Costs*

        e85_1     Acap_cost*(((AI+1)**PL)-1)=e=(FCI*AI)*((AI+1)**PL);

        e85_2     Arep_cost*PL=e=Rep_Tcost;

        e85_3     Amain_cost=e=Cap_DC*0.025;

        e85_4(N) TAC(N)=e=Acap_cost+Arep_cost+Amain_cost;

*Cashflow calculations

        e86(N)..  Dep(N)*PL=e=FCI+Rep_Tcost;

        e87(N)..  PBT(N)=E=Rev(N)-TP_cost(N)-Dep(N);

        e88(N)..  Tax(N)=e=PBT(N)*TR;

        e89(N)..  PAT(N)=e=PBT(N)-Tax(N);

        e90(N)..  PATPD(N)=e=PAT(N)+Dep(N);

        e91(N)..  Cash(N)=e=PATPD(N)-TAC(N);
```

```
*Net present value
        e92(N)..  PV(N)=e=DF(N)*Cash(N);

        e93..     NPV=e=sum(N,PV(N));

*Payback Period
        e94       PBP*Tot_Rev=e=FCI*PL;

*Objective function

        e95..     Obj=e=Power_eff;

*Bounds*
        b1..      T_ce=e=T_e;

        b2..      T_ae=e=T_ce;

        b3..      P_ae=e=P_e;

        b4..      P_ce=e=P_e;

        b5..      p_we=e=P_e;

        b6..      p_he=e=p_we;

        b7..      p_oe=e=P_we;

        b8..      T_cf=e=T_f;

        b9..      T_af=e=T_cf;

        b10..     P_cf=e=P_f;

        b11..     P_af=e=P_cf;

        b12..     p_wF=e=P_f;

        b13..     p_hf=e=p_f;

        b14..     p_of=e=p_f;

        b15..     M_SWin=e=M_Woutsyse+M_Houtsyse+M_Ooutsyse;

        b16       (c_f)$(ord(c_f)=1)..M_Woutsysf+M_Houtsysf+M_Ooutsysf=e=

                  (N_Hinf(c_f)*T2('H','Mm'))+(N_Oinf(c_f)*T2('O','Mm'));

        b17..     M_Swin=e=M_Woutsyse+M_Woutsysf;
```

APPENDIX F: Upper and Lower Bounds

T_e.lo=298.15;

T_e.up=363.15;

T_f.lo=298.15;

T_f.up=363.15;

i_e.lo=10000;

i_e.up=50000;

lamda_e.up=25;

lamda_e.lo=14;

lamda_f.up=25;

lamda_f.lo=14;

V_e.lo=2.1;

V_e.up=6;

n_d.lo=0.2;

AW_ae.lo=1;

AW_ae.up=3;

AW_ce.lo=0;

AW_ce.up=1;

AW_af.lo=0;

AW_af.up=1;

AW_cf.lo=1;

AW_cf.up=3;

delta_eae.up=0.00625;

delta_eae.lo=0.00005;

delta_ece.up=0.00625;

delta_ece.lo=0.00005;

delta_eaf.up=0.00625;

delta_eaf.lo=0.00005;

delta_ecf.up=0.00625;

delta_ecf.lo=0.00005;

w_channel_ec.up=0.00125;

w_channel_ec.lo=0.001;

w_channel_ea.up=0.00125;

w_channel_ea.lo=0.001;

w_channel_fc.up=0.00125;

w_channel_fc.lo=0.001;

w_channel_fa.up=0.00125;

w_channel_fa.lo=0.001;

w_GDL_ec.up=0.0003;

w_GDL_ec.lo=0.00021;

w_GDL_ea.up=0.0003;

w_GDL_ea.lo=0.00021;

w_GDL_fc.up=0.0003;

w_GDL_fc.lo=0.00021;

w_GDL_fa.up=0.0003;

w_GDL_fa.lo=0.00021;

w_CL_ec.up=0.00002;

w_CL_ec.lo=0.00001;

w_CL_ea.up=0.00002;

w_CL_ea.lo=0.00001;

```
w_CL_fc.up=0.00002;

w_CL_fc.lo=0.00001;

w_CL_fa.up=0.00002;

w_CL_fa.lo=0.00001;

w_CC_ea.fx=0.001;

w_CC_ec.fx=0.001;

w_CC_fa.fx=0.001;

w_CC_fc.fx=0.001;

ra_f.lo=0.005;

ra_f.up=0.04;

ra_e.lo=0.005;

ra_e.up=0.04;

PR_factor.lo=0.01;

PR_factor.up=0.05;

I_factor.fx=0.01;

DS_factor.lo=0;

DS_factor.up=0.07;

DS_factor.fx=0.03;

RD_factor.lo=0.02;

RD_factor.up=0.05;

RD_factor.fx=0.05;

power_prod.fx=1;

system_eff.lo=0.67;

system_eff.up=0.82;
```

```
Model HEFC_Model/all/;

Option NLP=baron;

OPTION RESLIM = 28600;

Option optcr = 0.0001;

Option optca = 0.001;

Solve HEFC_Model_12 using NLP maximizing Obj
```